Óbuda University

PhD Thesis

Further development and novel applications of the Robust Fixed Point Transformation-based adaptive control

Krisztián Kósi

Supervisor:
Prof. Dr. habil József Kázmér Tar DSc.

Doctoral School of Applied Informatics and Applied Mathematics

Budapest, 20th Aug. 2015

Members of the Comprehensive Examination Committee:

Members of the Defense Committee:

Day of the defense:

CONTENTS

ACKNOWLEDGEMENT

CHAPTER 1

INTRODUCTION

Iterative techniques as numerical methods are widely used for finding the solutions to typically non-linear problems for which normally no closed-form analytical solutions exist. The classical Newton-Raphson algorithm that was developed in the 17th century [1] obtained wide attention even in our days (e.g. [2, 3, 4]). It is a *root finding algorithm* in which the original task is transformed to a *fixed point problem* that is solved via iteration. The convergence properties of such iterative sequences were systematically studied by Stefan Banach in 1922 in his *Fixed Point Theorem* [5]. Techniques for speeding up the convergence of iterative sequences were also introduced in the 20th century (e.g. [6, 7]).

Robotics is a typical subject area in which strongly nonlinear systems have to be controlled. The method of *Iterative Learning Control (ILC)* applied in robotics was at first announced in English by Arimoto in 1984 [8]. It also obtained various applications *whenever the task of the robot is to repeatedly reproduce a typical motion* (e.g. [9], [10], [11]). By the application of the concept of *motor primitives* similar approach was recently applied by Deniša et al. in [12].

In a wider context in robotics i.e. when the robot has to precisely track a *nominal motion* that is not periodic the classical adaptive control approaches normally use Lyapunov's 2nd or "direct" method that originally was developed for the investigation of the stability of motion of nonlinear systems in the last decade of the 19th century [13]. In the sixties of the past century his work was translated to English [14] and became the mathematical basis in nonlinear adaptive control design. *Its great advantage is that even in the lack of the existence of closed analytical solutions of the equations of motion various stability definitions can be proved for the controlled motion without knowing its other details.* The classic examples as the *Adaptive Inverse Dynamics Controller (AIDC)*, the *Adaptive Slotine-Li Controller (ASLC)* [15, 16] as well as the *Model Reference Adaptive Controllers (MRAC)* (e.g. [17, 18, 19]) were designed by the us of various Lyapunov functions.

In spite of its great advantages this design technology has some drawbacks. At first it is a "complicated" method often burdened by mathematical difficulties. It is easy to see that these mathematical difficulties mainly originate from affording certain "unnecessary luxuries" as follows: the method often guarantees *global stability* that is practically too much: in the practice both the unknown external disturbances and the model parameter uncertainties are *bounded* therefore it is not compulsory to guarantee stability for arbitrarily big model errors, disturbances, and initial states e.g. [20]; the majority of the so designed controllers does not sharply distinguish between the physical role of the *kinematic* and the *dynamic* details: sometimes force terms are directly fed back without using the dynamic model of the system that results in complicated proofs. Furthermore, the method tries to satisfy *satisfactory conditions* instead *necessary* ones that practically also is "too much"; the solutions normally contain a great number of more or less arbitrary parameters; their optimal setting may need the application of

complicated evolutionary technologies (e.g. [21, 22]).

In order to avoid the mathematical complications related to the Lyapunov function-based design techniques, as alternative approach, iterative solutions were introduced in adaptive control of robots and other nonlinear systems that have to follow in general non-periodic nominal motion with the significant main characteristic features as follows: a) by applying "sterile distinction" between the role of *kinematics* and *dynamics* purely kinematic formulation of the desired tracking error damping was prescribed; b) the necessary control forces (or other control signals in the case of phenomenologically different physical systems) were calculated on the basis of an available approximate and even incomplete dynamic model; c) by observing the actual response of the controlled system and comparing this response with the model-based expectation the input of the approximate model was iteratively deformed to better approximate the kinematically prescribed *"desired response"*; d) the iteration was generated by a fixed point transformation; e) the need for global stability was generally given up.

In [23] and certain related publications transformations based on simple geometric interpretation were introduced and their applicability for various physical systems were clarified. In 2009 one of these transformations, the *"Robust Fixed Point Transformations (RFPT)"* were found to be especially efficient [24]. The method contained only a single kinematic and only three adaptive control parameters and found numerous potential applications e.g. adaptive optimal dynamic control for nonholonomic systems [25], quasi-stationary control approach in adaptive emission control of freeway traffic [26], etc.

1.1 Outline of the Main Problems in my Research

In my research, the goal was to improve the stability and usability of the nonlinear adaptive controllers. I chose the Robust Fixed Point Transformation (RFPT)-based iterative solutions instead of the Lyapunov function-based technique for the basis of the research, which was developed by J. K. Tar in 2009 [24]. In my thesis new contributions related to this new technique are considered. Accordingly, this research had the logical structure as follows:

1. The original investigations related to the method announced in [24] were restricted to the operation of the controller in the convergent regime. The methods that were elaborated for tuning one of the adaptive control parameters in [27, 28] essentially were restricted to and effective within the convergent regime that was determined by the *local properties* of the fixed point transformation and the response function near the useful fixed point. In [29] the appearance of small fluctuations of the control signal was observed and reduced in the case of a SISO system. No systematic investigations were done to reveal what happens if the controller leaves this regime for MIMO systems. These investigations were initiated by me at first for a 2DOF system [A. 1], later for a 3DOF one [A. 2], and for a chemical system using Brusselator model [A. 3], [A. 4], [A. 5]. It turned out that these controllers produce bounded chaotic motion outside of the region of convergence. By the use of affine approximation of the response functions I systematically studied this motion. It turned out that the main features of this motion depend on the global properties of the function that realizes the fixed point transformation and also depends on the properties of the system's response function. I also invented a novel method to extend SISO Robust Fixed Point Transformation method for MIMO systems.

2. Using the results of the investigation of chaos formation, I realized that at appropriate adaptive control parameter setting continuous increase of the tuned parameter at first produces monotonic convergence with increasing convergence speed, then, before skipping into the chaotic regime, it yields non-monotonic convergence with decreasing speed of convergence. I referred to this phenomenon as "precursor oscillations". I introduced a novel method to stabilize the control system by using a model-independent observer for the precursor oscillations in the parameter tuning process [A. 6], [A. 7].

3. To improve the usability of the original Robust Fixed Point Transformation method, I suggested a truncated linear sigmoid function to replace its original main component with a practically simpler realization. I also introduced a tuning method for it [A. 8],[A. 9].

4. I combined the RFPT-based technique with the application of the classical Luenberger observer for cases in which the system's state cannot fully and directly measured [A. 10].

2.1   Brief Introduction for the RFPT-based Method

The great majority of control literature applies Lyapunov's 2nd method ([13], [14]) for designing *globally stable adaptive* controllers for both linear and nonlinear systems when the available system models are imprecise and the presence of unknown external perturbations is expected. While the design of *model based predictive controllers* on the basis of Lyapunov's technique is relatively easy, the adaptive ones can be designed in a complicated manner is which numerous control parameters can arbitrarily set and the subtle details of trajectory tracking are not well revealed. Both "simple adaptive" as well as "*Model Reference Adaptive Controllers (MRAC)*" can be designed in this manner (examples from the early nineties of the past century to our days are [15], [16], [17], [30], [18], [31], [19], [32], [33], [34]). Regarding the details of trajectory tracking as well as finding the appropriate Lyapunov function itself evolutionary methods can be applied, too [21].

Though Lyapunov's method has the great virtue that it normally guarantees *global stability*, it also has certain drawbacks as follows:

- The primary intent of the designer of the controller may be to impose precise restrictions on the tracking error relaxation as the controller "learns" or tunes itself. However, these details are not in the focus of the design and they can be revealed only by numerical computations.

- Normally the Lyapunov function may contain *ample number of arbitrary adaptive control parameters* (mainly among the matrix elements of positive definite symmetric matrices). The global stability can be guaranteed for various settings that have significant effects on the details of the controlled motion. For determining the practically satisfactory setting some optimization can be done even by the use of the means of *evolutionary computations* (e.g., [35], [22]) that normally may mean high computational burden.

- Though it is easy to understand the mathematical essence of Lyapunov's method, its particular applications require very good skills on behalf of the designer.

- The method is built up on *rather satisfactory than necessary conditions*, consequently it normally requires *"too much"*, i.e., it works with more than necessary stipulations.

- These stipulations mainly originate from *formal considerations* and do not allow the method to become "versatile enough". For instance, it was recently shown that slight modification of the parameter tuning rules of the "classic" *Adaptive Inverse Dynamics Controller* and the *Slotine-Li*

Adaptive Controller, due to which the tuning rules were not deduced from a Lyapunov function it became possible to combine a modern adaptive technique with the classic parameter learning methods [36], [37].

To evade the above difficulties, an alternative adaptive design method, the *Robust Fixed Point Transformations* (RFPT)-based design was introduced [24]. Realizing that though global stability (if it is guaranteed) is an advantage but from practical point of view it is "too much" (the modern robust controllers are designed for bounded/limited uncertainties e.g. [20]), insisting on it is not necessary if the prices are increased computational costs and further complications in the design, alternative solutions were initiated in [23] and the related publications. This method applies a particular iterative learning control in which the iterative sequence is obtained by the use of a contractive map in a Banach Space and it converges on the basis of Banach's *Fixed Point Theorem* [5]. Furthermore it places into the focus the realization of a prescribed trajectory tracking error relaxation. In its simplest form it only needs 3 adaptive parameters that can be fixed for many applications. It can guarantee only a bounded basin of convergence that may be left by the system. If it is necessary for maintaining the convergence, one of its parameters can be adaptively tuned by various manners (e.g., [27], [28]). With the introduction of these tuning rules only a few new parameters are introduced that have well identified roles. This design has the advantage that it does not need any precise initial model of the system under control. It can do with a very approximate model: without trying to "amend" this model it adaptively deforms its input via observing the behavior of the controlled system. It can well compensate the simultaneous effects of modeling errors and unknown, directly not observable external disturbances. (Since no model improvement happens, this control permanently needs fresh observations and cannot promise asymptotic stability.)

The most successful version was based on the application of the "*Robust Fixed Point Transformations (RFPT)*" [24] for the applicability of which it was assumed that the controlled *system's response* (e.g. acceleration in Classical Mechanics) to the primary controlling physical agent (e.g. torque or force components) is directly *observable*. (This condition normally is satisfied e.g. in robotics). In this case, by the use of an *approximate system model* the necessary force or other control action for a purely kinematically calculated "*desired response*" r^{Des} can be estimated and exerted on the controlled system that produces the observed response r. In this manner a "*response function*" $f(r^{Des},\ldots)$ can be introduced that is not known analytically but can be identified as pairs of known input and output values. The symbol "$\ldots$" stands for the other arguments of f that partly describe the actual state of the system and the variables of the environmental interactions.

The essence of RFPT is to generate a *contractive map G* by the use of which instead of directly applying r^{Des} an *iterative control sequence* defined as $r_{n+1} = G\left(r_n, f(r_n), r_{n+1}^{Des}\right)$ is generated in a *linear, normed, complete metric space* (Banach space). Due to the completeness of the space this sequence has to converge to some $r_\star$ that is a *fixed point* of G: $r_\star = G\left(r_\star, f(r_\star), r_{n+1}^{Des}\right)$. If G is so constructed that $f(r_\star) = r_{n+1}^{Des}$ this sequence yields the solution of the control task. In [24] the following function was introduced for *Single Input - Single Output (SISO)* systems:

$$G\left(r_n, f(r_n), r_{n+1}^{Des}\right) :=$$
$$(r_n + K_c)\left(1 + B_c \sigma\left(A_c\left[f(r_n) - r_{n+1}^{Des}\right]\right)\right) - K_c \tag{2.1}$$

with a monotone increasing smooth sigmoid function $\sigma(x) \in (-1, +1)$ also satisfying the requirements $\sigma(0) = 0$ and $\frac{d\sigma(x)}{dx}|_{x=0} = 1$, $B_c = \pm 1$, and K_c and A_c are adaptive control parameters. Since f and therefore G are related to certain derivatives of the state variable of the controlled system normally r^{Des} varies slowly and its other variables denoted by "$\ldots$" can be regarded as parameters. The original idea in [24] concentrated only on the condition of the derivative of G in $r_\star$ in (2.2)

$$\left.\frac{dG\left(r_n, f(r_n), r_{n+1}^{Des}\right)}{dr_n}\right|_{r_n=r_\star} =$$
$$= 1 + (r_\star + K_c)B_c A_c \left.\frac{df}{dr_n}\right|_{r_n=r_\star} \tag{2.2}$$

to achieve $-1 < \left.\frac{dG\left(r_n, f(r_n), r_{n+1}^{Des}\right)}{dr_n}\right|_{r_n=r_\star} < 1$ that is needed for the contractivity of the map near $r_\star$. For this purpose estimations were made for the order of magnitude of the occurring response r (e.g. by simulations made by approximate models and simple PID controllers), then simply some big coefficient $K \gg |r|$, and depending on the sign of $\frac{df}{dr_n}$ a constant $B_c = \pm 1$, and a little positive parameter A_c were set. For "*Multiple Input - Multiple Output (MIMO)*" systems a modification of (2.1) was introduced as

$$\vec{h} := \vec{f}(\vec{r}_n) - \vec{r}^{Des}, \quad \vec{e} := \vec{h}/\|\vec{h}\|,$$
$$\tilde{B} = B_c \sigma(A_c\|\vec{h}\|) \tag{2.3}$$
$$\vec{r}_{n+1} = (1 + \tilde{B})\vec{r}_n + \tilde{B}K_c\vec{e}$$

that simply corresponds to a scaling in the direction of the response error $\vec{h} := \vec{f}(\vec{r}_n) - \vec{r}^{Des}$.

It was found that for several applications a constant settings for $\{K_c, A_c, B_c\}$ can work well. The RFPT-based method was found to be also applicable for designing new types of MRAC controllers (e.g. [38]). For applications for which this constant settings did not work, to keep the occurring responses in the vicinity of $r_\star$ two different tuning approaches were invented for the parameter A_c at fixed K_c and B_c ([27], [28]).

The behavior of the controller outside of the region of convergence was first investigated in In [29] in connection with the control of a van der Pol oscillator. Strong chattering was observed that was found to be similar to that of the *Variable Structure /Sliding Mode (VS/SM)* controllers (e.g. [39], [40], [41]) that slowly approached the nominal trajectory with good precision. Similar behavior was observed in the case of MIMO system in [A. 1]. In [A. 6] a systematic investigation revealed that depending on the nature of $\frac{df}{dr_n}$ by increasing A_c from zero at first *monotone*, than *non-monotone, oscillating convergence* that was called "*precursor oscillations*" in [A. 6] can be guaranteed in $r_n \to r_\star$ before the *bounded chattering* at higher A_c occurred. On this basis a *model-independent observer* was designed to monitor the oscillations in $\{r_n\}$ to keep the controller in the convergent region.

2.2 Early Parameter Tuning in the RFPT-based Method

Though the conditions of convergence were detailed in [24] it worths noting that, as it can well be seen in (3.25), the properties of the partial differential $\frac{\partial \vec{f}(\vec{r}_n)}{\partial \vec{r}_n}$ certainly influence the convergence of the method since it considerably influences the formation of the control sequences through $\frac{\partial \vec{r}_{n+1}}{\partial \vec{r}_n}$. Actually this quantity can be used for deciding if the choice $B_c = 1$ or $B_c = -1$ can be taken, as well as for deciding the proper range for $|K_c|$. In the particular examples considered instead of computing the components of the matrix $\frac{\partial \vec{f}(\vec{r}_n)}{\partial \vec{r}_n}$ the more easily computable scalar product $[\vec{f}(\vec{r}_n) - \vec{f}(\vec{r}_{n-1})]^T [\vec{r}_n - \vec{r}_{n-1}]$ was *observed* for determining the controllability of the given stage of the process.
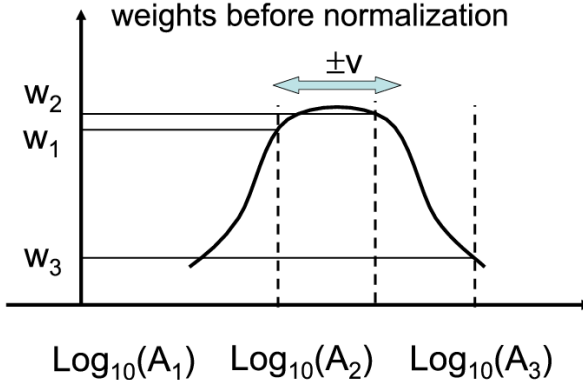
Figure 2.1: Explanation of "fuzzy grid" used for fine tuning of the adaptive control parameters $\{A_{c_i}\}$ first introduced in [42] and completed by rigidly shifting the whole grid

For developing *observers* the properties of the series given in (2.4) is utilized by the use of which *forgetting filters* can be constructed for the discrete *time-sequence of physical quantities* $\{z(t-s)|s = 0,\ldots,\infty\}$ as $\bar{z}(t) = (1-\beta)\sum_{s=0}^{\infty}\beta^s z(t-s)$ in which $s = 0$ corresponds to the present instant, and the higher values pertain to the past (also used e.g. in [42]). The old, rather "obsolete" information is forgotten faster for smaller $0 < \beta < 1$ values. For constant $z(i) \equiv z$ evidently $\bar{z} = z$ therefore (2.4) acts as a noise filter, too, that is able to average out fluctuations. From technical point of view the realization of this filter is very easy: a quantity $\hat{z}(t)$ can be stored in a buffer and in each control cycle the refreshing operation $\hat{z}(t+1) := \beta\hat{z}(t) + z(t+1)$, $\bar{z}(t) = (1-\beta)\hat{z}(t)$ can be applied.

$$\Sigma := \sum_{s=0}^{\infty} \beta^s = \frac{1}{1-\beta} < \infty \text{ if } |\beta| < 1 \tag{2.4}$$

2.3 Fractional Derivatives

Though the idea of the fractional integrals and derivatives is as old sa that of the integer order ones (in 1695. L'Hospital asked Leibniz about the meaning of $D^n y$ if $n = \frac{1}{2}$ [43]), in the development of natural sciences the integer order differentiation and integral calculus played the prime role till the first third of the 20th century (Gemant about 1930) when it was used for describing viscoelastic phenomena. (In the development of Classical Mechanics Galilei observed the fundamental significance of the acceleration according to which the theory has been formalized in a variation principle using a Lagrangian that contained integer order derivatives of the state variable. Since Classical Mechanics served as a prototype for other physical theories this trend was deterministic for a long while. The mathematicians continuously worked on the development of this theory during the 19th century, too.) In connection with the description of physical systems of long term memory it became clear that the integer order description suffers from the need of very high order derivatives requiring a lot of data describing the initial condition. It was found that this difficulty can be elegantly evaded by fitting only a few parameters of a fractional order model [liquid-porous wall interaction, earthquake models, classical masses coupled by springs, etc. [43]]. Another problem with the use of the integer order derivatives consists in their sensitivity to measurement noises: the higher the order of derivation is the more sensitive the result is. The fractional order derivatives can be defined for functions that does not have integer order ones, furthermore their inherent memory make them promising tools for noise filtering applications.

2.4   Order Reduction Techniques

If a mechanical system is driven by permanent magnet DC motors then for a prescribed acceleration the mechanical components' acceleration or deceleration needs driving force or torque signals. In these motors the necessary torque is proportional to the actual current of the coils. Due to the inductivity of the electric subsystem this current cannot be abruptly changed: only the first time-derivative of this current can be set by the control voltage. Consequently, only the 3rd time-derivatives of the generalized coordinates of the mechanical system can be immediately be set, that is the order of the control task is 3. If we insist on the use of a 2nd order controller we also need some order reduction technique.

Whenever we wish to control the motion of big systems consisting of numerous dynamically coupled subsystems the application of certain order reduction for the model practically is inevitable since a very high order practically would not be handled [44]. The basic idea of the methods that were already elaborated for the LTI systems is very simple. Instead of using the "time-picture" these systems can easily be handled in the "frequency-picture" by using the concept of the *"transfer function"*. Normally these transfer functions consist of fractional expressions made of polynomials. The effects of these polynomials in the inverse Fourier transformation can easily be estimated if the excitation of the system is described by the elements of function class $\mathcal{D}$, by the use of the *"Residuum Theorem"*. The Fourier transform of these functions do not contain any singularity in the complex plain $\mathbb{C}$, and converge to 0 in the infinity. This convergence is faster than that of the function $\frac{1}{|\omega|^n}$, $\forall n \in \mathbb{N}$. Therefore the integral of the inverse Fourier transform taken along a contour that comes from $-\infty$ and goes to ∞ can be "completed" by the contribution of a semicircle that is zero. (According to the requirement of causality this semicircle must be located on the upper half of the complex plain. According to [45] it can be stated that this function class can widely be used for modeling practically occurring excitations.)

This "completion" results in an integral along a closed curve for the evaluation of which the Residuum Theorem can be applied. It means that only the contributions of the poles of the transfer function have to be summarized. These contributions are weighted in the sum by the values of the polynomials in the numerators of the fractional expressions and by the values of the Fourier transform of the excitation signal in the poles [46, 47]. If the excitation functions are modeled by the elements of the class $\mathcal{D}$ ([45], [46, 47]), due to their fast decrease in the infinity it can be stated that only the contribution of those poles are significant in the vicinity of which the Fourier transform of the excitation signal has considerable absolute value. The contribution of the other poles can be neglected. The neglected poles can be eliminated by appropriately decreasing the orders of the polynomials in the fractional expressions.

A possible systematic method for constructing the new polynomials originates from the PhD theses by Padé in 1892 [48]. It is well known that a polynomial of finite order always diverges if $|\omega| \to \infty$. Therefore, if we wish to work with Taylor series, near the border of the region of convergence numerous terms must be taken into account for appropriate precision. This fact makes the use of the Taylor series inconvenient in many cases. The application of the fractional expressions of polynomials may be more convenient since they do not diverge in the range in which their approximate only very imprecisely. The basic idea is very simple: let us make the first few terms of the Taylor series of the functions to be approximated and the approximating fractional expressions identical in the center of the frequency region that has practical significance (*"moment matching"* [49, 44, 50]). The method can well be used in the case of fractional order models (e.g. [51]).

Returning to the use of the time-picture for the description of the Linear Time Invariant (LTI) systems, it is well known that the general solution of the initial problem task $x \in \mathbb{R}^n$, $x(t_0) = x_0$ for the LTI system (5.2) is

$$\dot{x} = Ax + bu \ ,$$
$$x(t) = \exp\left(A(t - t_0)\right)x_0 + \qquad\qquad (2.5)$$
$$\int_{t_0}^{t} \exp\left(A(t - \xi)\right)Bu(\xi)d\xi \ .$$

Due to the Cayley-Hamilton theorem in the matrix exponential in (5.2) the linearly independent columns of the resulting matrix may be only the elements of the set $\{B, AB, A^2B, \ldots, A^{n-1}B\}$. If our system is stable the term $\exp\left(A(t - t_0)\right) x_0$ – that is independent of the control signal– converges to zero, consequently the subset of the possible states that is reachable by the controller is spanned by this set (Krylov -base). For the application of Padé's method the relationship between the moments and the Krylov base has to be clarified. In 1950 Kornél Lánczos [52] elaborated an algorithm for the construction of a system of basis vectors that is more specific to this need than the original Krylov base. In 1951 Arnoldi invented a more stable algorithm for the same purpose [53].

In the case of nonlinear systems a popular technique is the linearization [44] that can be used for treating the motion of a systems that is restricted to the vicinity of an equilibrium point. For starting point it takes the linearized approximation of the original model in the equilibrium point. The method can be improved by taking into account the higher order terms (e.g. [54, 55]). In general it can be stated that the current methods concentrate on the "augmented application" of the essentially linear approaches (e.g. *"Proper Orthogonal Decomposition" (POD)* [56]), or on the isolation of the nonlinearities and reduction of the linear parts in their vicinity (e.g. [57, 58])).

INVESTIGATION OF THE ROBUST FIXED POINT TRANSFORMATION BASED CONTROLLER OUTSIDE OF THE REGION OF CONVERGENCE

3.1 Investigation of Chaos formation

The investigation of chaos formation has to concentrate on the whole possible control region since divergent behavior may happen whenever the system leaves the vicinity of the attractive fixed point that can guarantee the desired convergent operation of the controller. In the case of the control of a SISO system the response function of which can be approximated by an *affine model* for the control signal $r \in \mathbb{R}$ the following ranges are of especial interest:

1. the range in which the sigmoid function in the equations (3.1) saturates at the vale of +1: in this case $G(r)$ can be approximated as $G(x) \approx 2r + K$,

2. the vicinity of the fixed point $r = -K$,

3. the interval between the two fixed points $-K$ and r_* $(f(r_*) = r^d)$, and

4. the saturation range of the sigmoid at -1 resulting in $G(r) \approx -K$.

Figure 3.15 explains the reason, why the controller cannot suffer fatal crash. The limits are $y = 2r + K$, $-K$.

$$G(r, f(r_{extr_1}), r^d) := (r + K) \times 2 - K = 2r + K$$
$$G(r, f(r_{extr_2}), r^d) := -K$$

(3.1)
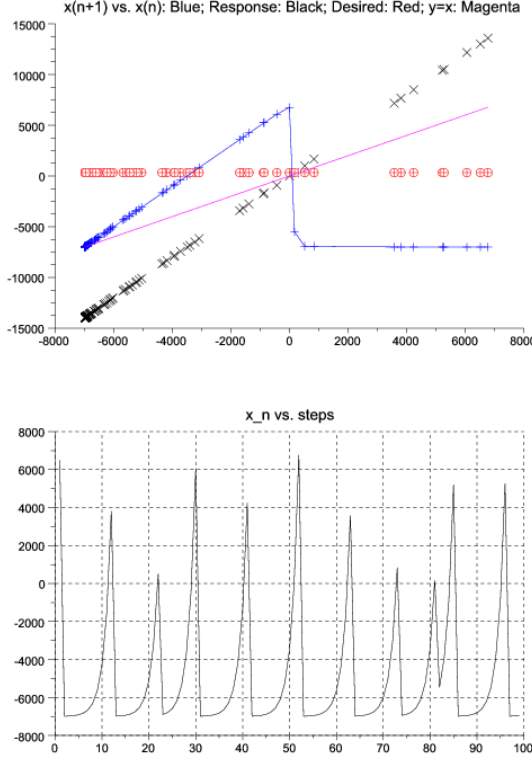
Figure 3.1: Schematic figure explaining the formation of chaos for a 1 DOF system [A. 1]

3.1.1 Simulations for the Chaotic Regime of a 2 DOF System

The system consists of two mass-points coupled by nonlinear damped springs in vertical direction. The model parameters are: $m_1 = 20\,kg$, $m_2 = 30\,kg$, $g = 9.81\,m/s^2$, $L_1 = 0.4\,m$, $L_2 = 0.8\,m$, $k_1 = 120\,N/m$, $k_2 = 200\,N/m$, $b_1 = 0.6\,Ns/m$, and $b_2 = 0.4\,Ns/m$. The rough model parameters are: $\tilde{m}_1 = 40\,kg$, $\tilde{m}_2 = 40\,kg$, $\tilde{g} = 11\,m/s^2$, $\tilde{L}_1 = 0.3\,m$, $\tilde{L}_2 = 0.3\,m$, $\tilde{k}_1 = 260\,N/m$, $\tilde{k}_2 = 260\,N/m$, $\tilde{b}_1 = 1\,Ns/m$, and $\tilde{b}_2 = 1\,Ns/m$ [A. 1].

The model is described by the equations of motion as follows:

$$
\begin{aligned}
m_1(\ddot{q}_1 - g) + k_1 \cdot (q_1 - L_1)^3 - \\
k_2 \cdot (q_2 - q_1 - L_2)^3 + b_1 \dot{q}_1 = Q_1 \\
m_2(\ddot{q}_2 - g) + k_2 \cdot (q_2 - q_1 - L_2)^3 + b_2 \dot{q}_2 = Q_2
\end{aligned}
\tag{3.2}
$$

The rough model is represented by similar but little bit different equations of motion:

$$
\begin{aligned}
\tilde{m}_1(\ddot{q}_1 - \tilde{g}) + \tilde{k}_1 \cdot \left(q_1 - \tilde{L}_1\right)^5 - \\
\tilde{k}_2 \cdot \left(q_2 - q_1 - \tilde{L}_2\right)^5 + \tilde{b}_1 \dot{q}_1 = Q_1 \\
\tilde{m}_2(\ddot{q}_2 - \tilde{g}) + \tilde{k}_2 \cdot \left(q_2 - q_1 - \tilde{L}_2\right)^5 + \tilde{b}_2 \dot{q}_2 = Q_2
\end{aligned}
\tag{3.3}
$$

The kinematically prescribed trajectory tracking is given as:

$$
\begin{aligned}
\ddot{q}_i^d(t) := \ddot{q}_i^N(t) + 3\Lambda^2 \left(q_i^N(t) - q_i(t)\right) + \\
+ 3\Lambda \left(\dot{q}_i^N(t) - \dot{q}_i(t)\right) + \\
+ \Lambda^3 \int_0^t \left(q_i^N(\tau) - q_i(\tau)\right) d\tau
\end{aligned}
\tag{3.4}
$$

The control parameters are: $B = -1$, $K = 10^6$, and $A_i \in \{10^{-7.5}, 10^{-6.5}, 10^{-5.5}\}$ [A. 1].
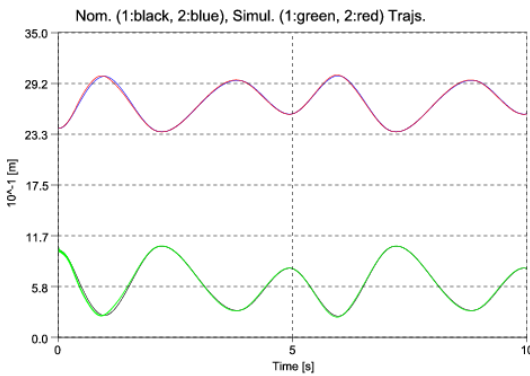
Figure 3.2: Trajectory tracking of the adaptive RFPT-based controller in its nonconvergent regime [A. 1]
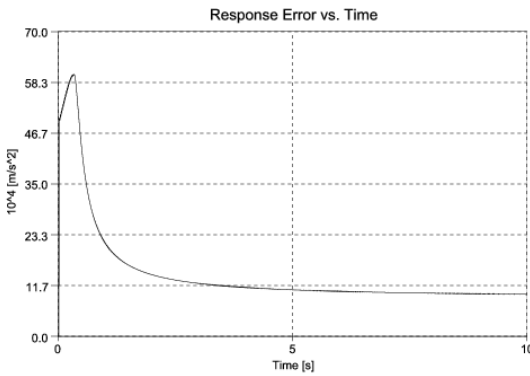
Figure 3.3: The response error of the adaptive RFPT-based controller in its nonconvergent regime [A. 1]
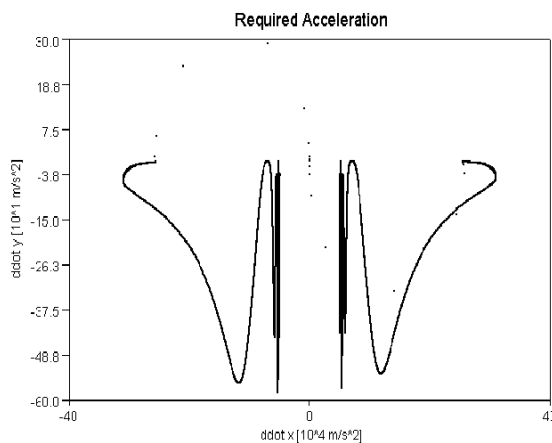
Figure 3.4: The strange attractor of the adaptively deformed *"required responses"* $r_n := \ddot{q}^{Req}(n)$ ($x := \ddot{q}_1^{Req}$, $y := \ddot{q}_2^{Req}$) of the adaptive RFPT-based controller in its nonconvergent regime for 10^4 control cycles [A. 1]
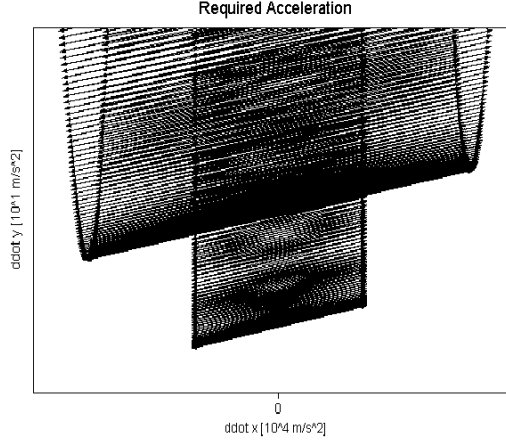
Figure 3.5: Excerpt (the lower part of Fig. 3.4) of the strange attractor of the adaptively deformed *"required responses"* $r_n := \ddot{q}^{Req}(n)$ ($x := \ddot{q}_1^{Req}$, $y := \ddot{q}_2^{Req}$) of the adaptive RFPT-based controller in its nonconvergent regime for 10^4 control cycle: arrows denote the sequence of the consecutive points [A. 1]
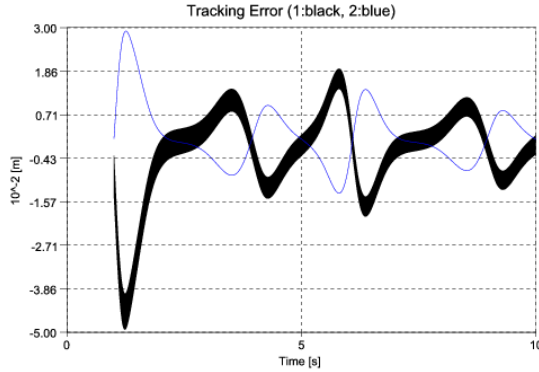
Figure 3.6: The tracking error of the adaptive RFPT-based controller in its non-convergent regime [A. 1]

Figure 3.2 shows that in spite of the chaotic behavior of the control signal the trajectory tracking is acceptable, and the response error decreases in time (Figure 3.3). The chaotic behavior are clearly revealed by Figures 3.4 and 3.5. The connections of the arrows have considerable distances in Figure 3.5. It means strong chattering. The tracking error, in a non-convergent regime of the Robust Fixed Point-based adaptive controller, is shown in Figure 3.6. In subsection 3.1.2, a simple chattering reduction method will be shown.

3.1.2 Chaos Reduction by Smoothing

In the SISO case [29], the amplitude of the observed small vibrations in the control signal was essentially determined by parameter K. For that case, necessarily a big number was chosen for parameter K. In order to reduce these vibrations a sigmoid function was introduced for limiting the control signal so that instead of r^{Req} the limited signal $r_{red}^{Req} = K_s \sigma\left(\frac{r^{Req}}{K_s}\right)$ was chosen with parameter $0 < K_s \ll |K|$. The reason was that for "small r^{Req}" (i.e. for $|r^{Req}| \ll |K|$) no further deformation was necessary, so $r_{red}^{Req} \approx r^{Req}$ was guaranteed, and only the higher values (i.e. signals in the order of magnitude of K_s) were deformed/limited. Using that idea for a MIMO system with chattering reduction, the following equation can be written (3.5).

$$\vec{h} := \vec{f}(\vec{r}_n) - \vec{r}^d, \quad \vec{e} := \vec{h}/\|\vec{h}\|,$$
$$\tilde{B} = B\sigma(A\|\vec{h}\|)$$
$$\vec{r}_{n+1} = (1 + \tilde{B})\vec{r}_n + K_s\sigma\left(\frac{\tilde{B}K}{K_s}\right)\vec{e}. \tag{3.5}$$

In the reduction the sigmoid function $\sigma(x) = \frac{x}{1+|x|}$ was applied.

In the forthcoming simulations $K_s = 15 \ll K = 10^6$ was chosen in the control of the system defined in (3.2) and its rough model given in (3.3). Both Figs. 3.6 and 3.7 reveal that the chattering concerned only the component $\ddot{q}_1^{Req}$ and that the chattering reduction considerably improved the trajectory tracking precision. Figures 3.8 and 3.9 provide convincing proof that the significantly reduced chattering must be practically tolerable since it results in smooth phase trajectory and only small relative fluctuation in the driving forces.
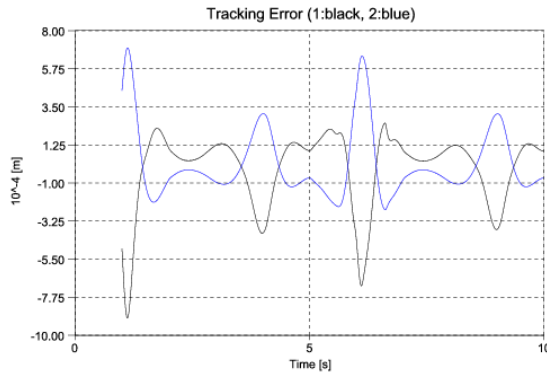
Figure 3.7: The tracking error of the adaptive RFPT-based controller in its nonconvergent regime with chattering reduction by $K_s = 15\,m/s^2$ [A. 1]
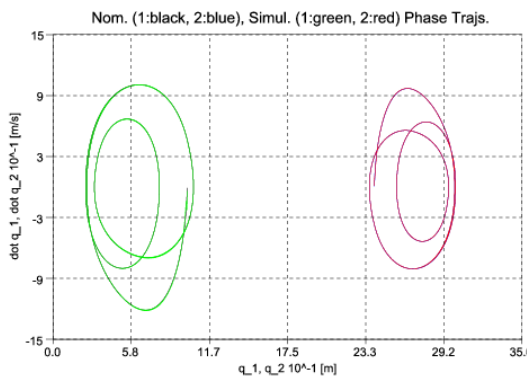
Figure 3.8: The phase trajectory tracking of the adaptive RFPT-based controller in its nonconvergent regime with chattering reduction by $K_s = 15\,m/s^2$ [A. 1]
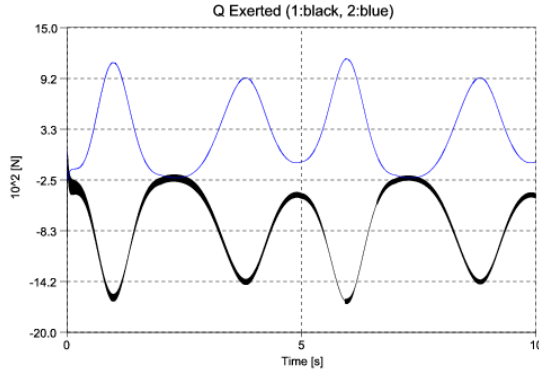
Figure 3.9: The driving forces of the adaptive RFPT-based controller in its nonconvergent regime with chattering reduction by $K_s = 15\,m/s^2$ [A. 1]
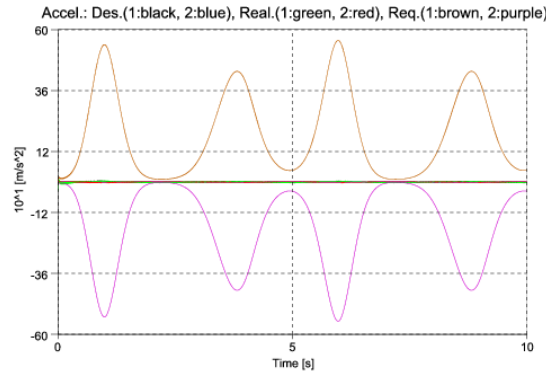
Figure 3.10: The "*desired*", "*realized*", and "*required*" accelerations of the adaptive RFPT-based controller in its nonconvergent regime with chattering reduction by $K_s = 15\,m/s^2$ [A. 1]
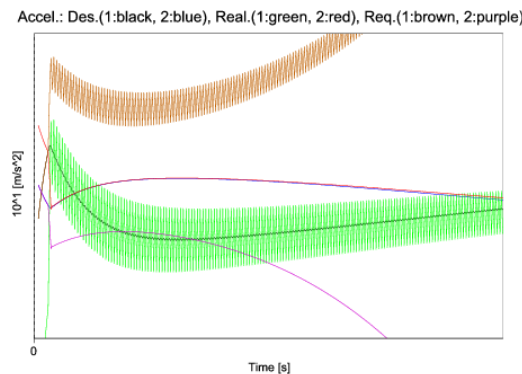
Figure 3.11: The "*desired*", "*realized*", and "*required*" accelerations of the adaptive RFPT-based controller in its nonconvergent regime with chattering reduction by $K_s = 15\,m/s^2$ (zoomed in excerpt) [A. 1]
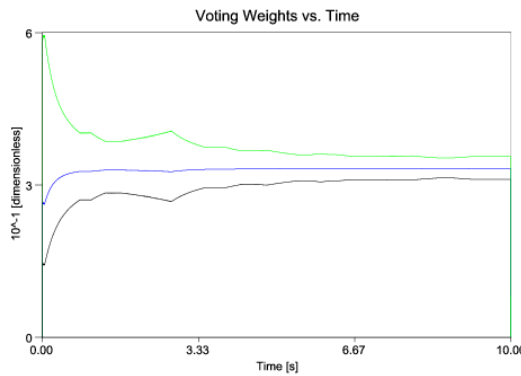
Figure 3.12: The voting weights for $A_1 = 10^{-7.5}$ (black line), $A_2 = 10^{-6.5}$ (blue line), and $A_3 = 10^{-5.5}$ (green line) of the adaptive tuning [A. 1]
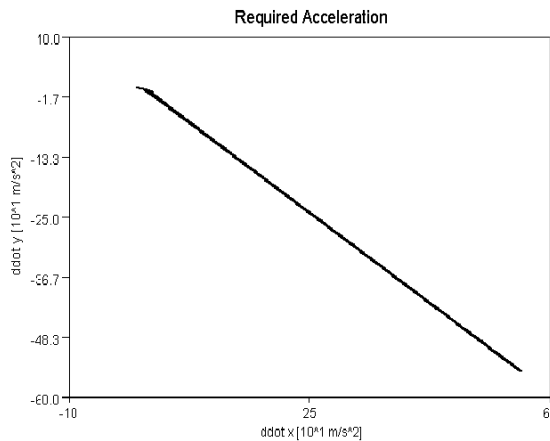
Figure 3.13: The strange attractor of the adaptively deformed *"required responses"* $r_n := \ddot{q}^{Req}(n)$ ($x := \ddot{q}_1^{Req}$, $y := \ddot{q}_2^{Req}$) of the adaptive RFPT-based controller in its nonconvergent regime for 10^4 control cycles with chattering reduction by $K_s = 15\,m/s^2$ [A. 1]
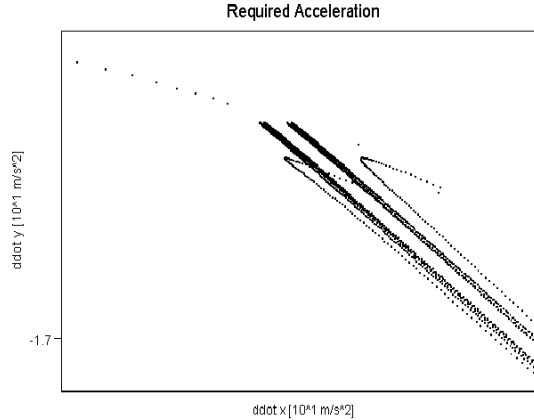
Figure 3.14: The strange attractor of the adaptively deformed *"required responses"* $r_n := \ddot{q}^{Req}(n)$ ($x := \ddot{q}_1^{Req}$, $y := \ddot{q}_2^{Req}$) of the adaptive RFPT-based controller in its nonconvergent regime for 10^4 control cycles with chattering reduction by $K_s = 15\,m/s^2$ (zoomed excerpt) [A. 1]

Figure 3.11 is a zoomed version of Figure 3.10. Those figures shows that in spite of the fact that there are little fluctuations present, the controller maintained its adaptive nature even in the non-convergence regime.

Figure 3.13 shows that the result practically becomes free of any chaos. Figure 3.14 shows the "fine structure" of this little "remnant chaos". [A. 1]

3.1.3   A 3 DOF System

In the previous subsection it was shown that chaotic behavior can be handled with simple smoothing. In the following part it will be investigated in the case of a 3 DOF system.

The motion equations for the 3DOF system is (4.1), and its schematic picture is shown in Figure 3.15. The *generalized coordinates* of the 3 DOF system are [A. 2]:

- q_1 (rad): rotation angle of the beam,

- q_2 (rad): rotation angle of the hamper at the top of the beam,

- q_3 (m): linear displacement of the cart's body.

The *dynamic parameters* are:

- m is the mass of the body, in top of the beam (kg)

- M is the mass of the body of the "car" (kg)

- L is the length of the beam (m)

- Θ is the moment of inertia of the hamper with respect to its own mass center point ($kg \cdot m^2$)

The *generalized forces* to be exerted by the controller are:

- Q_1 ($N \cdot m$): torque at axle 1;

- Q_2 ($N \cdot m$): torque at axle 2;

- Q_3 (N): force pushing the cart in the lateral direction,

furthermore g represents the gravitational acceleration. This model is just a rough initial model of the system. It is assumed that the hamper's mass center point is located on its axle [A. 2].

For the RFPT method it is satisfactory to have some rough approximation of the dynamic parameters. Whenever the RFPT is applied for designing a "*Model Reference Adaptive Controller (MRAC)*", also significant difference can be between the actual system's parameters and that of the Reference Model to be imitated by the controlled system [59]. In the simulations carried out the MRAC solution was investigated with *actual system parameters* as $M = 30\,kg$ $m = 10\,kg$ $L = 2\,m$,$\Theta = 20\,kg \cdot m^2$, $g = 10\,m/s^2$, while *the reference model* had the dynamic parameters as $\hat{M} = 60\,kg$ $\hat{m} = 20\,kg$ $\hat{L} = 2.5\,m$ (also having effects on the dynamic behavior), $\hat{\Theta} = 50\,kg \cdot m^2$, and $\hat{g} = 8\,m/s^2$. In the simulations it was assumed that the system's response was observable as a noisy signal. (In contrast to the other methods using various model-based estimators as Kalman filters, no any special assumption was necessary for the statistical nature of this observation noise, apart from the zero mean.) [A. 2]

$$
\begin{bmatrix}
(mL^2 + \Theta) & \Theta & mL\cos(q_1) \\
\Theta & \Theta & 0 \\
mL\cos(q_1) & 0 & (m+M)
\end{bmatrix}
\begin{bmatrix}
\ddot{q}_1 \\
\ddot{q}_2 \\
\ddot{q}_3
\end{bmatrix} +
$$
$$
+
\begin{bmatrix}
-mLg\sin(q_1) \\
0 \\
-mL\sin(q_1)\dot{q}_1{}^2
\end{bmatrix}
=
\begin{bmatrix}
Q_1 \\
Q_2 \\
Q_3
\end{bmatrix}
\tag{3.6}
$$
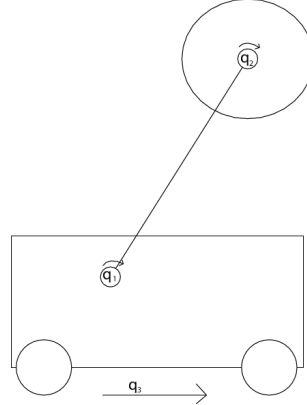
Figure 3.15: Sketch of the model used for the computation [A. 2]

3.1.4 Simulation Results and Chaos Patterns

In the simulations the following control parameter settings were used: $K_s = 600$, $K_c = 7000$, $B_c = -1$, and A_c was adaptively tuned in the case of necessity. Figures 3.36 and 3.17 display the trajectories and the phase trajectories of the controlled system revealing that the tracking in both spaces remained smooth and precise. Figure 3.18 reveals that besides the considerable parameter differences between the actual and the reference models significant observation disturbances were assumed. According to Figs. 3.19, 3.20, and 3.21 it can be stated that quite significant adaptive deformation was necessary for the imitation of the reference model but all the occurring accelerations are very close to each other that testifies the success of the adaptive controller. Figure 3.21 reveals the details of the adaptation mechanism showing that the *reference* and the *recalculated* values are in each other's close vicinity, i.e. the "*illusion*" to be created by the MRAC controller was successful, too. Figure 3.20 displays an excerpt of Fig. 3.21 that clearly shows that the *reference* and the *recalculated* values (i.e. the cyan–yellow, the red–dark blue, and the magenta–light blue pairs) are closely in each other's vicinity. The tracking

errors are displayed in Fig. 3.22. Figures 3.23-3.25 reveal the formation of the very much curbed chaos pattern in the exerted control forces.[A. 2]
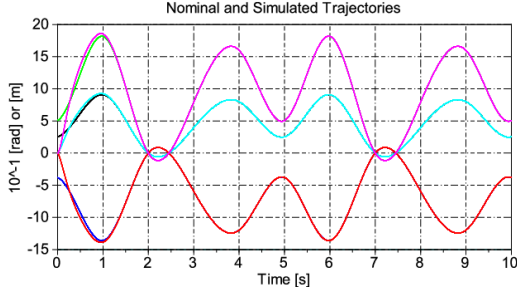
Figure 3.16: The nominal (q_1: black, q_2: blue, q_3: green lines) and the simulated trajectories (q_1: cyan, q_2: red, q_3: magenta lines) [A. 2]
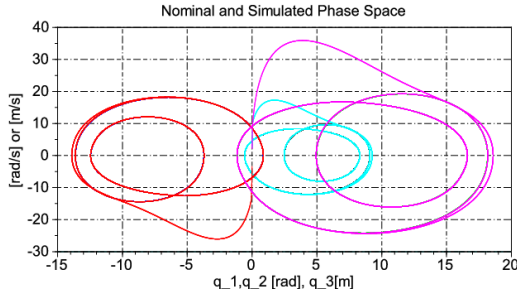
Figure 3.17: The nominal (q_1: black, q_2: blue, q_3: green lines) and simulated (q_1: cyan, q_2: red, q_3: magenta lines) phase trajectories [A. 2]
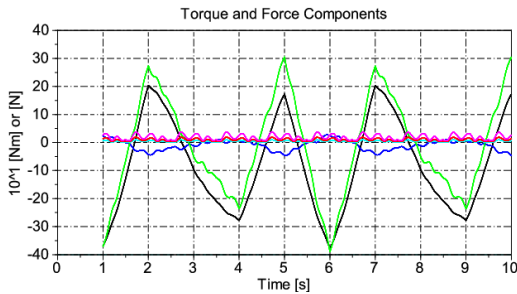
Figure 3.18: The exerted control torques (Q_1: black, Q_2: blue, Q_3: green lines), and the noisy disturbance forces (Q_1: cyan, Q_2: red, Q_3: magenta lines) [A. 2]
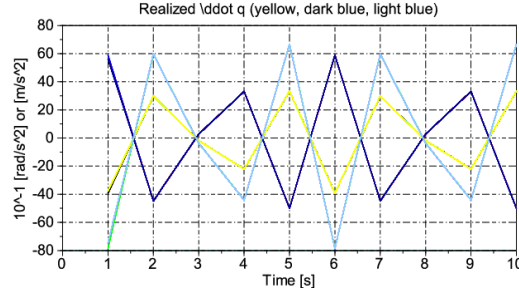
Figure 3.19: The second time-derivatives of the generalized coordinates (realized: $\ddot{q}_1$: yellow, $\ddot{q}_2$: dark blue, $\ddot{q}_3$: light blue, kinematically desired: $\ddot{q}_1$: cyan, $\ddot{q}_2$: red, $\ddot{q}_3$: magenta, nominal: $\ddot{q}_1$: black, $\ddot{q}_2$: blue, $\ddot{q}_3$: green lines) [A. 2]
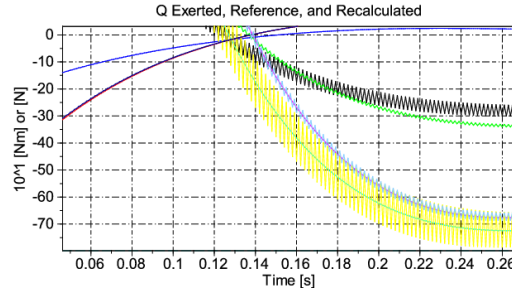
Figure 3.20: The *exerted* (Q_1: black, Q_2: blue, Q_3: green lines), the *recalculated* (Q_1: yellow, Q_2: dark blue, Q_3: light blue lines), and the *reference* (Q_1: cyan, Q_2: red, Q_3: magenta lines) (zoomed excerpt) [A. 2]
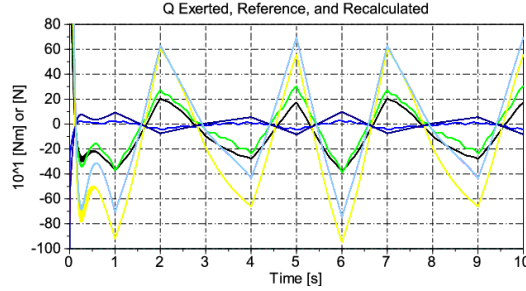
Figure 3.21: The *exerted* (Q_1: black, Q_2: blue, Q_3: green lines), the *recalculated* (Q_1: yellow, Q_2: dark blue, Q_3: light blue lines), and the *reference* (Q_1: cyan, Q_2: red, Q_3: magenta lines) [A. 2]

[A. 2]
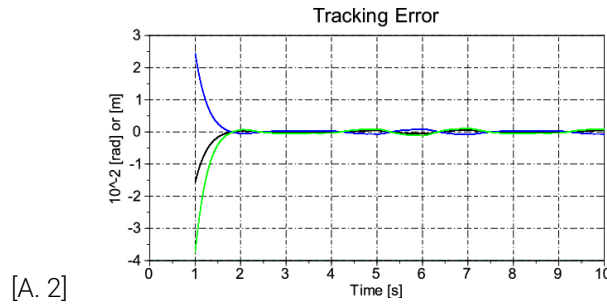
Figure 3.22: The trajectory tracking error (q_1: black, q_2: blue, q_3: green lines) [A. 2]
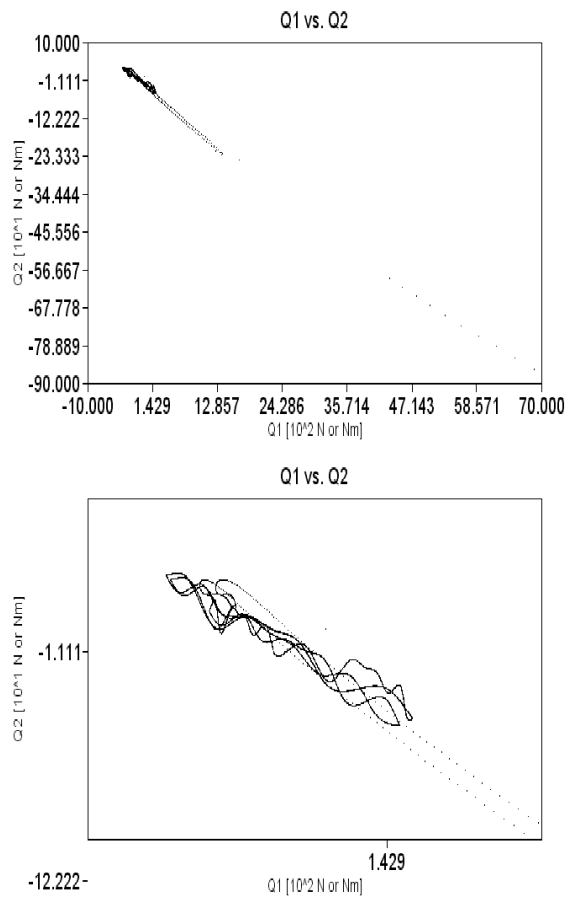
Figure 3.23: The projection of the generalized forces on the Q_1 - Q_2 plane with zoomed excerpts [A. 2]
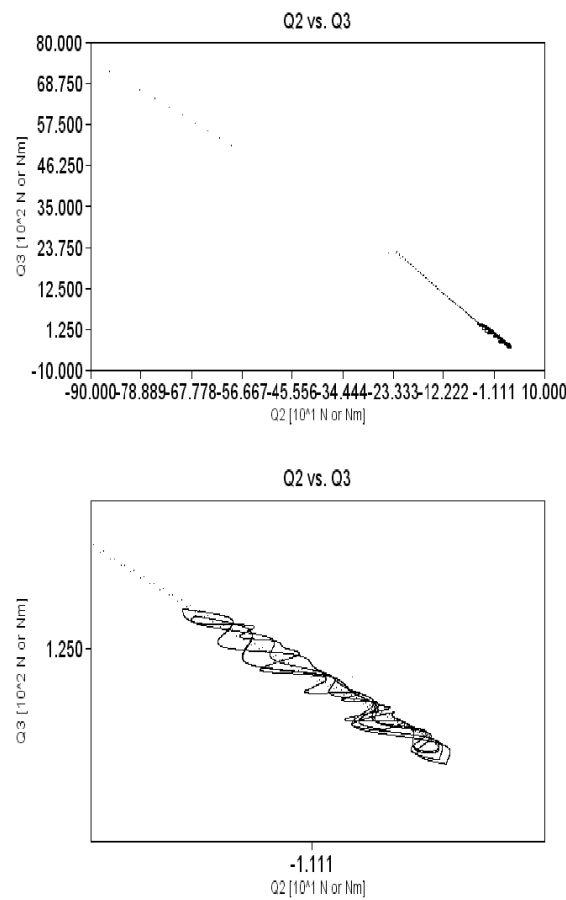
Figure 3.24: The projection of the generalized forces on the Q_2 - Q_3 plane with zoomed excerpts [A. 2]
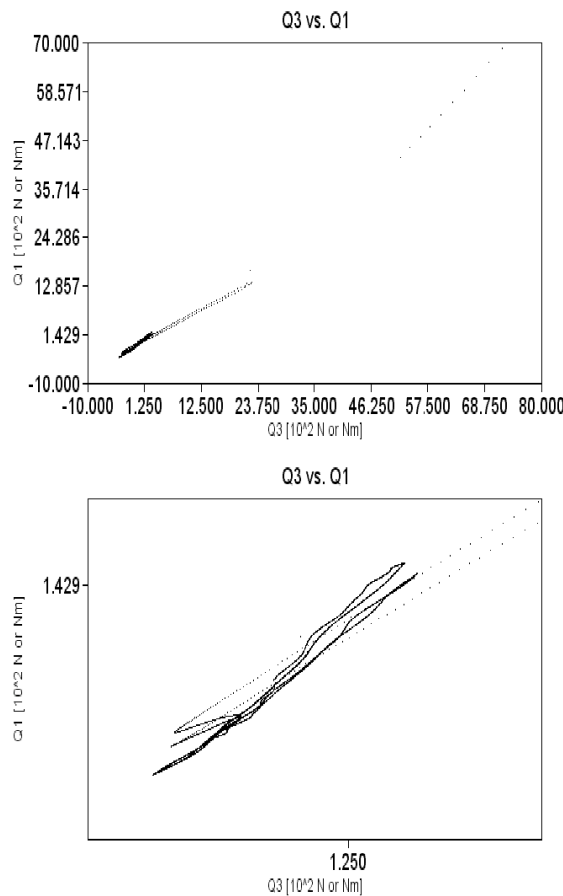
Figure 3.25: The projection of the generalized forces on the Q_3 - Q_1 plane with zoomed excerpts [A. 2]

3.2 Investigating Asymmetries in Chemical Systems

3.2.1 Challenges in Controlling Chemical Systems

Controlling Chemical Systems usually could be harder that of Classical Mechanical Systems. The usual problems can be summarized as follows:

1. Normally in Classical Mechanical Systems the control torque or force components can have positive and negative values. In contrast to that the control actions in chemical systems correspond to adding dense reagents into tank reactor therefore they can have only positive values. It is impossible to extract pure components from the mixture that could correspond to negative control actions. Therefore the action must be cut at zero whenever negative values would be desired by the controller. During such sessions the system remains without efficient control.

2. In Classical Mechanics the velocity can be positive and negative. In chemical systems negative concentrations do not have physical interpretation. Normally the analytical equations do not contain these restrictions and from purely mathematical point of view they could be applied by the controller even when not having physical relevance.

3. In the useful model the original equations have to be completed by these restrictions. If the concentration reaches zero its time derivative cannot be negative. Consequently it is dangerous to

use big feedback terms because they may cause big concentrations of certain reagents which cannot be decreased quickly in the following session of the control process.

4. Normally the various components cannot be separately controlled. When a dense reagent is added to the system it automatically dilutes the other components while increases the concentration of the desired one. I referred to this effect as *input coupling*. In the great majority of the literature this effect is completely neglected. I systematically investigated its effect in the structure of the possible control strategies.

5. The structure of the RFPT-based adaptive method naturally allows the use of various derivatives for the control of various order or relative order physical systems. It is well known that the higher order derivatives are very noise-sensitive expressions. The idea naturally arose to use non-integer order ones for the purpose of adaptive control. The fractional order derivatives correspond to long system memory therefore their use can be interpreted as the application of certain noise filtering effect. A natural expectation also arose that due to the use of longer internal memory the cycle time of the adaptive controllers may be increased by the use of fractional order derivatives in the learning process. This would have practical significance whenever the cycle time of the available sensor is limited. The idea was investigated by simulations in the case of a chemical process.

During former investigations it was also observed that leaving the region of convergence not necessarily leads to the decay of the adaptive control. It trajectory tracking can remain precise at the cost of the appearance of big chattering in the control signal. In [29] simple method was successfully suggested for the reduction of this chattering. [A. 3].

3.2.2 The Particular Paradigms Under Consideration

The investigated system was the famous *Brusselator Model of the Belousov-Zhabotinskii Reaction* developed by Prigogine and Lefever in 1968 [60].

3.2.3 RFPT-based Adaptive Control of the Brusselator Model

The portmanteau "*Brusselator*" introduced by J.J. Tyson in 1976 in [61] refers to the *Brussels School of Thermodynamics* in which the first model of *chemical oscillations* were mathematically expounded. In [62] the reactions described by (3.9) were used with assumedly constant A and $B\,mole/L$ concentrations. In the present paper its modification (3.10) is applied with the assumption that in a stirred reactor vessel of volume V during a small time-interval δt, δN_A ingress of the very dense reagent A of negligible volume is introduced that does not observably dilute the other reagents in the vessel. Similar assumption was made for reagent B that led to *decoupled control signals* as $u_A := \frac{\delta N_A}{V\delta t} \geq 0$ and $u_B := \frac{\delta N_B}{V\delta t} \geq 0$ of dimension $\frac{mole}{L\cdot s}$. Since the molecules X, Y, D and E are produced of A and B in this approach replenishment of components A and B must be satisfactory for control purposes. Since the time-derivatives of the first two equations of (3.10) contained $\dot{A}$ and $\dot{B}$ a 2nd order PID-type control was designed for the *desired* $\ddot{X}^d$ and $\ddot{Y}^d$ values (exactly of the same form that was considered in the case of the coupled springs) that so provided the *desired* $\dot{A}^d$ and $\dot{B}^d$ by the use of which u_A and u_B were determined from the last two equations according to the available model [A. 3].

In the forthcoming simulations the *exact parameters* were assumed to be $k_1 = 1$, $k_2 = 1$, $k_3 = 1$, and $k_4 = 1$ while *the approximate ones used by the controller* were $\tilde{k}_1 = 0.8$, $\tilde{k}_2 = 0.9$, $\tilde{k}_3 = 0.7$, and $\tilde{k}_4 = 0.6$ of appropriate physical dimensions that comply with (3.10). The simulations made for $\Lambda = 6/s$ for the non-adaptive simple PID controller for large amplitude ($0.5\,\frac{mole}{L}$) oscillation in the nominal trajectory of frequency $\omega = 3/s$ provided nice trajectory tracking but in it the *physically not interpretable* $u_A < 0$, $u_B < 0$, $A < 0$, $B < 0$ quantities also occurred. For getting rid of the physically not interpretable sessions (3.10) were completed with truncations for the negative values. This lead to completely unapplicable PID

control that allowed fast rate of increase in certain concentrations with considerable positive ingress rates, however, since the extraction of pure reactants were impossible the decreasing phases were left without active control with long $u_A \equiv 0$ and $u_B \equiv 0$ sessions. *These asymmetries are the main barriers of the available control speed.* On this reason the fast transients of the iterative learning that were not critical in the case of the mechanical system were carefully avoided in the case of the chemical reaction by setting the *cycle time of the controller* $10\,ms$ and the discrete time-resolution of the Euler integration to $1\,ms$. Furthermore nominal trajectory of considerably smaller amplitude $H = 0.05\frac{mole}{L}$ was considered for which the common PID controller provided useful results (Fig. 3.26). The results obtained for the adaptive counterpart of the controller for the same nominal motion are given in Fig. 3.27 for the *adaptive parameter settings* $K_c = 600$, $K_s = 5\frac{mole}{L\cdot s^2}$, $B_c = -1$, and $A_c \in \{1.67, 5.27, 16.67, 52.70, 166.67, 527.05\} \times 10^{-5}\ \frac{L\cdot s^2}{mole}$. The adaptivity was switched on at $t = 5\,s$ when the rough initial transients were already damped by the common PID controller and further refinement of the tracking properties became actual. The improvement in the tracking precision in the stabilized stage of the motion is evident [A. 3].

$$A \to^{k_1} X, B + X \to^{k_2} Y + D,$$
$$2X + Y \to^{k_3} 3X, X \to^{k_4} E. \tag{3.7}$$

$$\dot{X} = k_1 A - k_2 BX + k_3 X^2 Y - k_4 X,$$
$$\dot{Y} = k_2 BX - k_3 X^2 Y,$$
$$\dot{A} = -k_1 A + u_A, \dot{B} = -k_2 BX + u_B. \tag{3.8}$$
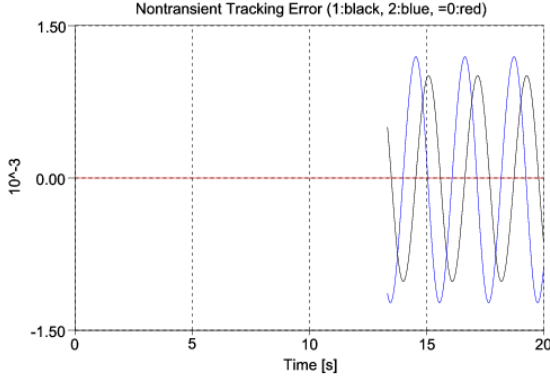
Figure 3.26: Tracking error of the simple non-adaptive PID controller in the non-transient stage (for X: black and green lines, for Y: blue and red lines) [A. 3]
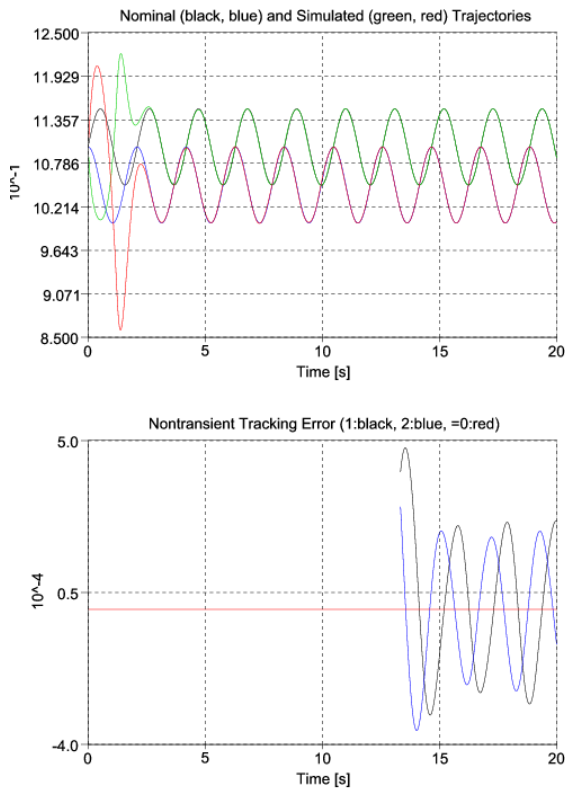
Figure 3.27: Tracking of the adaptive controller (for X: black and green lines, for Y: blue and red lines) [A. 3]

Figure 3.28 reveals the details of the adaptation mechanism [A. 3].
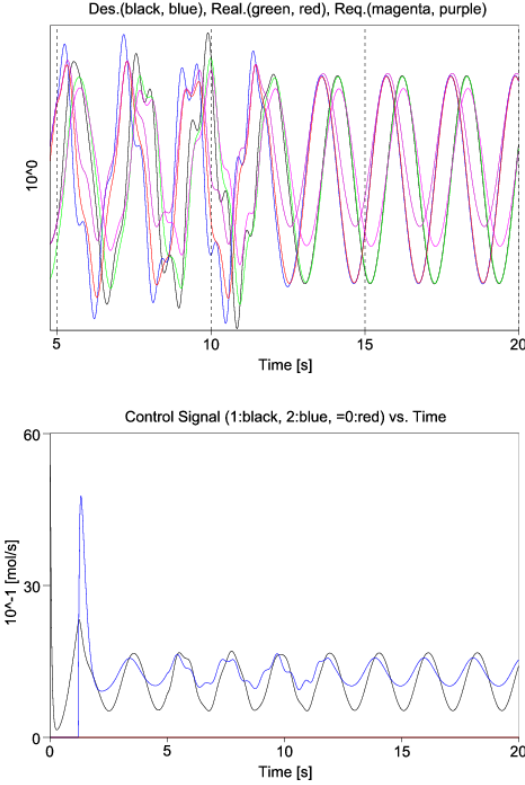
Figure 3.28: The *"desired"* ($\ddot{X}$: black, $\ddot{Y}$: blue), adaptively deformed *"required"*($\ddot{X}$: magenta, $\ddot{Y}$: purple), and the *realized* ($\ddot{X}$: green, $\ddot{Y}$: red) signals of the adaptive controller, and the control signals (u_A: black, u_B: blue) [A. 3]

3.2.4   Input Coupling in the Control of the Brusselator Model

In [62] the reactions described by (3.9) were used with assumedly constant A and B $\left[\frac{mole}{L}\right]$ concentrations. (No any mechanism was detailed regarding the question how to keep these concentrations constant [A. 4].)

$$A \to^{k_1} X, B + X \to^{k_2} Y + D,$$
$$2X + Y \to^{k_3} 3X, X \to^{k_4} E \tag{3.9}$$

that leads to the reaction equations as follows:

$$\dot{X} = k_1 A - k_2 BX + k_3 X^2 Y - k_4 X$$
$$\dot{Y} = k_2 BX - k_3 X^2 Y$$
$$\dot{A} = -k_1 A,$$
$$\dot{B} = -k_2 BX \tag{3.10}$$

in which k_1, k_2, k_3 and k_4 are assumed to be constants. Presently we assume that the active volume of the CSTR is V [L], the actual concentrations of the reagents are A, B, X, Y, and at the inlets of reagents A and B the available concentrations are ρ_A, and ρ_B $\left[\frac{mole}{L}\right]$, respectively. We also assume that the volumes are additive that (in the case of not very great concentrations) may be reasonable. We should like to simultaneously produce the nominal $X^{Nom}(t)$ and $Y^{Nom}(t)$ concentrations by adding the reagents A and B into the reaction vessel, and if necessary, by egressing some amount of solution from the tank. If the controller so operates that during time δt δw_A [L] of reagent A and δw_B [L] of reagent B are pumped into the well stirred tank, furthermore δV [L] mixture is egressed at the outlet the appropriate mole numbers and full volume after time δt will be as follows [A. 4]:

$$
\begin{aligned}
N_A(t+\delta t) &\approx V(t)A(t) + \delta N_A^\star + \rho_A \delta w_A - A(t)\delta V \\
N_B(t+\delta t) &\approx V(t)B(t) + \delta N_B^\star + \rho_B \delta w_B - B(t)\delta V \\
N_X(t+\delta t) &\approx V(t)X(t) + \delta N_X^\star - X(t)\delta V \\
N_Y(t+\delta t) &\approx V(t)Y(t) + \delta N_Y^\star - Y(t)\delta V \\
V(t+\delta t) &\approx V(t) + \delta w_A + \delta w_B - \delta V,
\end{aligned}
\tag{3.11}
$$

in which $\delta N_A^\star$, $\delta N_B^\star$, $\delta N_X^\star$ and $\delta N_Y^\star$ denote the variation in the mole numbers due to the chemical reactions that are not accompanied by volume modification. Consequently the new concentrations will be [A. 4]

$$
\begin{aligned}
A(t+\delta t) &:= \frac{N_A(t+\delta t)}{V(t+\delta t)} \approx \\
&\approx \frac{V(t)A(t) + \delta N_A^\star + \rho_A \delta w_A - A(t)\delta V}{V(t) + \delta w_A + \delta w_B - \delta V} \\
B(t+\delta t) &:= \frac{N_B(t+\delta t)}{V(t+\delta t)} \approx \\
&\approx \frac{V(t)B(t) + \delta N_B^\star + \rho_B \delta w_B - B(t)\delta V}{V(t) + \delta w_A + \delta w_B - \delta V} \\
X(t+\delta t) &:= \frac{N_X(t+\delta t)}{V(t+\delta t)} \approx \\
&\approx \frac{V(t)X(t) + \delta N_X^\star - X(t)\delta V}{V(t) + \delta w_A + \delta w_B - \delta V} \\
Y(t+\delta t) &:= \frac{N_Y(t+\delta t)}{V(t+\delta t)} \approx \\
&\approx \frac{V(t)Y(t) + \delta N_Y^\star - Y(t)\delta V}{V(t) + \delta w_A + \delta w_B - \delta V}.
\end{aligned}
\tag{3.12}
$$

By dividing the denominators and the numerators by the actual full volume $V(t)$ we obtain that [A. 4]

$$
\begin{aligned}
A(t+\delta t) &\approx \frac{A(t) + \frac{\delta N_A^\star}{V(t)} + \frac{\rho_A}{V(t)}\delta w_A - A(t)\frac{\delta V}{V(t)}}{1 + \frac{\delta w_A}{V(t)} + \frac{\delta w_B}{V(t)} - \frac{\delta V}{V(t)}} \\
B(t+\delta t) &\approx \frac{B(t) + \frac{\delta N_B^\star}{V(t)} + \frac{\rho_B}{V(t)}\delta w_B - B(t)\frac{\delta V}{V(t)}}{1 + \frac{\delta w_A}{V(t)} + \frac{\delta w_B}{V(t)} - \frac{\delta V}{V(t)}} \\
X(t+\delta t) &\approx \frac{X(t) + \frac{\delta N_X^\star}{V(t)} - X(t)\frac{\delta V}{V(t)}}{1 + \frac{\delta w_A}{V(t)} + \frac{\delta w_B}{V(t)} - \frac{\delta V}{V(t)}} \\
Y(t+\delta t) &\approx \frac{Y(t) + \frac{\delta N_Y^\star}{V(t)} - Y(t)\frac{\delta V}{V(t)}}{1 + \frac{\delta w_A}{V(t)} + \frac{\delta w_B}{V(t)} - \frac{\delta V}{V(t)}}.
\end{aligned}
\tag{3.13}
$$

Utilizing that the modifications are infinitesimally small the approximation $\frac{1}{1+\varepsilon} \approx 1 - \varepsilon$ can be applied and in (3.13) the higher order terms can be neglected that results in [A. 4]

$$
\begin{aligned}
A(t+\delta t) &\approx A(t) + \frac{\delta N_A^\star}{V(t)} + \frac{\rho_A}{V(t)}\delta w_A - \\
&\quad - A(t)\frac{\delta w_A}{V(t)} - A(t)\frac{\delta w_B}{V(t)} \\
B(t+\delta t) &\approx B(t) + \frac{\delta N_B^\star}{V(t)} + \frac{\rho_B}{V(t)}\delta w_B - \\
&\quad - B(t)\frac{\delta w_A}{V(t)} - B(t)\frac{\delta w_B}{V(t)} \\
X(t+\delta t) &\approx X(t) + \frac{\delta N_X^\star}{V(t)} - X(t)\frac{\delta w_A}{V(t)} - X(t)\frac{\delta w_B}{V(t)} \\
Y(t+\delta t) &\approx Y(t) + \frac{\delta N_Y^\star}{V(t)} - Y(t)\frac{\delta w_A}{V(t)} - Y(t)\frac{\delta w_B}{V(t)},
\end{aligned}
\tag{3.14}
$$

suggesting that

$$\dot{A}(t) = \frac{\delta N_A^\star}{V(t)\delta t} + \frac{\rho_A}{V(t)}W_A - \frac{A(t)}{V(t)}W_A - \frac{A(t)}{V(t)}W_B$$
$$\dot{B}(t) = \frac{\delta N_B^\star}{V(t)\delta t} + \frac{\rho_B}{V(t)}W_B - \frac{B(t)}{V(t)}W_A - \frac{B(t)}{V(t)}W_B$$
$$\dot{X}(t) = \frac{\delta N_X^\star}{V(t)\delta t} - \frac{X(t)}{V(t)}W_A - \frac{X(t)}{V(t)}W_B \tag{3.15}$$
$$\dot{Y}(t) = \frac{\delta N_Y^\star}{V(t)\delta t} - \frac{Y(t)}{V(t)}W_A - \frac{Y(t)}{V(t)}W_B$$
$$\dot{V} = W_A + W_B - W.$$

in which the well interpreted control quantities as $W_A := \frac{\delta w_A}{\delta t}$, $W_B := \frac{\delta w_B}{\delta t}$, and $W := \frac{\delta V}{\delta t}$ of the dimension $\left[\frac{L}{s}\right]$ have been introduced [A. 4].

In the special case of $W_A = 0$, $W_B = 0$, and $W = 0$, equation (3.15) must result in (3.10) therefore we can identify the term $\frac{\delta N_A^\star}{V(t)\delta t}$ and its similar counterparts in (3.15), and obtain the equations as [A. 4]

$$\dot{A}(t) = -k_1 A + \frac{\rho_A - A(t)}{V(t)}W_A - \frac{A(t)}{V(t)}W_B$$
$$\dot{B}(t) = -k_2 BX + \frac{\rho_B - B(t)}{V(t)}W_B - \frac{B(t)}{V(t)}W_A$$
$$\dot{X}(t) = k_1 A - k_2 BX + k_3 X^2 Y - k_4 X -$$
$$- \frac{X(t)}{V(t)}(W_A + W_B) \tag{3.16}$$
$$\dot{Y}(t) = k_2 BX - k_3 X^2 Y - \frac{Y(t)}{V(t)}(W_A + W_B)$$
$$\dot{V} = W_A + W_B - W$$

in which both the effects of the chemical reactions and that of the ingression of the reagents and egression of the mixture are taken into account. Equation (3.16) satisfies the *qualitative expectations* as follows [A. 4]:

1. The ingress of each reagent has immediate effect on the concentration of all the other components: its additional volume dilutes the other components.

2. In contrast to the previous approximation in [A. 3] this more sophisticated model allows both increasing the concentration and dilution of a particular component depending on the difference as e.g. $(\rho_A - A)$: if $\rho_A > A$ increasing concentration is caused by the ingress of reagent A, otherwise dilution happens.

3. The egression rate W does not have any effect on the concentrations. This is reasonable in the case of a CSTR removes components from the tank reactor according to their concentrations. It influences only the full volume of the liquid in the tank.

4. It is guaranteed that if $A = 0$ then $\dot{A} \geq 0$; if $B = 0$ then $\dot{B} \geq 0$; if $X = 0$ then $\dot{X} \geq 0$, and if $Y = 0$ then $\dot{Y} \geq 0$. Therefore the cuts in the derivatives that were essential in [A. 3] now will not have essential effects: they can be kept in the simulation program but they are expected to play some role if some little numerical errors happen at low concentrations.

Now let us consider the control issues. Since the volume of the reactor tank is finite, according to (3.16) it is expedient to introduce the rule $W = W_A + W_B$, i.e. $\dot{V} = 0$, $V = const$. It can be observed that though W_A and W_B explicitly are present in $\dot{X}$ and $\dot{Y}$ in (3.16), only the sum $W_A + W_B$ is present in these equations, i.e. if we try to arbitrarily prescribe $\dot{X}$ and $\dot{Y}$ these two equations generally yield contradictory conditions for $(W_A + W_B)$. Consequently $\dot{X}$ and $\dot{Y}$ cannot be arbitrarily prescribed. We have to consider a higher order controller in which $\ddot{X}$ and $\ddot{Y}$ can be prescribed by deriving the appropriate equations in (3.16). In this derivative the sum $(\dot{W}_A + \dot{W}_B)$ will occur that also cannot be directly set due to the same contradiction. However, $\dot{A}$ and $\dot{B}$ will also occur in the derivatives that can be substituted from the first two equations of (3.16) to obtain two equations in which $(\dot{W}_A + \dot{W}_B)$, W_A, and W_B occur. Since $\ddot{X}$ contains $\dot{X}$ and $\ddot{Y}$ contains $\dot{Y}$, quadratic equations are expected for W_A, and W_B. Fortunately these

equations have particular form that allows their solution in closed analytical form. This is convenient when $\dot{A}$ and $\dot{B}$ are substituted into $\ddot{X}$ and $\ddot{Y}$. Assume that we have a digital controller that provides *constant* $W_A = const.$, $W_B = const.$ control signals during the control cycles within which we can utilize the simplification that $\dot{W}_A = 0$ and $\dot{W}_B = 0$ during the controller's cycle time. If these signals have only very sharp jumps at the boundaries of the discrete control cycles these derivatives can be considered to be identically zero. Observing that typical quantities occur more than one times in the equations by the introduction of the notations $\alpha := \frac{k_1A-k_2BX+2k_3X^2Y-k_4X}{V}$, $\beta := \frac{-k_2B+2k_3XY-k_4}{V}$, and $\gamma := \frac{k_2B-2k_3XY}{V}$ the following expressions can be obtained [A. 4]:

$$\begin{aligned}
\ddot{X} = W_A\left[k_1\tfrac{\rho_A-A}{V} + k_2\tfrac{BX}{V} - \alpha - \beta X\right] + \\
+ W_B\left[-k_1\tfrac{A}{V} - k_2X\tfrac{\rho_B-B}{V} - \alpha - \beta X\right] \\
- k_1^2A + k_2^2BX^2 + V\beta(V\alpha - k_3x^2Y) + \\
+ k_3X^2(k_2BX - k_3X^2Y) \\
+ \tfrac{X}{V^2}(W_A + W_B)^2
\end{aligned} \tag{3.17}$$

$$\begin{aligned}
\ddot{Y} = W_A\left[-k_2\tfrac{BX}{V} - 2\gamma X\right] + \\
+ W_B\left[k_2X\tfrac{\rho_B-B}{V} - 2\gamma X\right] \\
- k_2^2BX^2 + V\gamma(V\alpha - k_3X^2Y) - \\
- k_3X^3(V\gamma + k_3XY) + \tfrac{Y}{V^2}(W_A + W_B)^2.
\end{aligned} \tag{3.18}$$

Equations (3.17) and (3.18) have a relatively simple structure since since they allow to eliminate the only quadratic term in W_A and W_B, i.e. $(W_A + W_B)^2$ from $\ddot{X}Y - \ddot{Y}X$, therefore a linear relationship can be obtained between W_A and W_B [A. 4]:

$$\ddot{X}Y - \ddot{Y}X - \hat{c} = \hat{a}W_A + \hat{b}W_B \tag{3.19}$$

where

$$\begin{aligned}
\hat{a} := Y\left[k_1\tfrac{\rho_A-A}{V} + k_2\tfrac{BX}{V} - \alpha - \beta X\right] - \\
- X\left[-k_2\tfrac{BX}{V} - 2\gamma X\right], \\
\hat{b} := Y\left[-k_1\tfrac{A}{V} - k_2X\tfrac{\rho_B-B}{V} - \alpha - \beta X\right], \\
\hat{c} := Y\left[-k_1^2A + k_2^2BX^2 + V\beta(V\alpha - k_3X^2Y)\right] + \\
+ Y\left[k_3X^3(V\gamma + k_3XY)\right] + k_2^2BX^3 - \\
- V\gamma(V\alpha - k_3X^2Y)X + k_3X^4(V\gamma + k_3XY).
\end{aligned} \tag{3.20}$$

By the use of (3.19) W_B can be expressed as a linear function of W_A as $\breve{a} := \frac{\hat{a}}{\hat{b}}$, $\breve{c} := \frac{\ddot{X}Y-\ddot{Y}X-\hat{c}}{\hat{b}}$ [A. 4]:

$$\begin{aligned}
\ddot{Y} = W_A\left[-k_2\tfrac{BX}{V} - 2\gamma X - \breve{a}(k_2X\tfrac{\rho_B-B}{V} - 2\gamma X)\right] + \\
+ \breve{c}(k_2X\tfrac{\rho_B-B}{V} - 2\gamma X) - k_2^2BX^2 + \\
+ V\gamma(V\alpha - k_3X^2Y) - \\
- k_3X^3(V\gamma + k_3XY) + \tfrac{Y}{V^2}\left((1-\breve{a})W_A + \breve{c}^2\right)^2.
\end{aligned} \tag{3.21}$$

and it can be substituted into the simpler equation (3.18) to obtain a 2nd order equation for W_A [A. 4]:

$$0 = \tilde{a}W_A^2 + \tilde{b}W_A + \tilde{c}, \quad W_A = \frac{-\tilde{b} + \sqrt{\tilde{b}^2 - 4\tilde{a}\tilde{c}}}{2\tilde{a}}, \tag{3.22}$$

with

$$\tilde{a} := \frac{Y(1-\breve{a})^2}{V^2},$$
$$\tilde{b} := \frac{2Y(1-\breve{a})\breve{c}}{V^2} - k - 2\frac{bx}{V} - 2\gamma X -$$
$$-\breve{a}(k_2 X \frac{\rho_B - B}{V} - 2\gamma X),$$
$$\tilde{c} := +\breve{c}(k_2 X \frac{\rho_B - B}{V} - 2\gamma X) - k_2^2 B X^2 +$$
$$+V\gamma(V\alpha - k_3 X^2 Y)$$
$$-k_3 X^3 (V\gamma + k_3 XY) + \frac{Y\breve{c}^2}{V^2} - \ddot{Y}.$$

(3.23)

In the solution instead of the formally possible terms $\pm\sqrt{(..)}$ we intentionally have kept only the positive one in the hope of obtaining better realizable (possibly positive) W_A solution [A. 4].

3.2.5 Application of the RPFPT-based Technique for this Chemical System

The idea of the application of RFPTs in adaptive control was detailed in various contexts in e.g. [24], [42], [63]. Here we have room only for a very concentrated briefing. Assume, that in our case we *kinematically design* some trajectory tracking error relaxation, in out case for the 2nd time-derivatives of the concentrations that directly can be manipulated by the control signals W_A and W_B according to the equations (3.17)-(3.23). A PID-type trajectory tracking with an error converging to zero is prescribed by (3.24) with a parameter $\Lambda > 0$ in which *desired 2nd time-derivatives* are given [A. 4].

$$\ddot{X}^d := \ddot{X}^N + 3\Lambda(X^N - X) + 3\Lambda^2(X^N - X) +$$
$$+\Lambda^3 \int_0^t \left(X^N(\xi) - X(\xi)\right) d\xi$$
$$\ddot{Y}^d := \ddot{Y}^N + 3\Lambda(Y^N - Y) + 3\Lambda^2(Y^N - Y) +$$
$$+\Lambda^3 \int_0^t \left(Y^N(\xi) - Y(\xi)\right) d\xi$$

(3.24)

Assume that instead of the *exact model parameters* k_1, k_2, k_3, k_4, their approximations $\tilde{k}_1$, $\tilde{k}_2$, $\tilde{k}_3$, and $\tilde{k}_4$ are available. By writing these approximate values into the model described by (3.17)-(3.23) the controller computes some W_A and W_B control signals that produces the *observable system answers* according to (3.17) and (3.18) in which the exact parameter values have to be taken into account. Du to modeling errors evidently $\ddot{X}^d \neq \ddot{X}$, $\ddot{Y}^d \neq \ddot{Y}$. Instead of trying to tune the parameters $\tilde{k}_1$, $\tilde{k}_2$, $\tilde{k}_3$, and $\tilde{k}_4$ the RFPT-based approach brings about a sequence of control signals $\{W_A(n), W_B(n)\}$ that converges to the *solution of the control task* $W_A^\star$ and $W_B^\star$ for which the $\ddot{X}_\star^d = \ddot{X}$, $\ddot{Y}_\star^d = \ddot{Y}$ are well approximated. If the observed system response in the controller's cycle n is denoted by f_n, the deformed kinematically prescribed values for which the inaccurate model computes the control signals for which f_n is observed are denoted by r_n, and the desired response at cycle n are denoted by r_n^d the sequence is generated as [A. 4]

$$\vec{h}_{n+1} := \vec{f}(\vec{r}_n) - \vec{r}_{n+1}^d, \vec{e}_{n+1} := \vec{h}_{n+1}/\|\vec{h}_{n+1}\|,$$
$$\tilde{B}_{n+1} = B_c \sigma(A_c \|\vec{h}_{n+1}\|),$$
$$\vec{r}_{n+1} = (1 + \tilde{B}_{n+1})\vec{r}_n + K_s \sigma\left(\frac{\tilde{B}_{n+1} K_c}{K_s}\right)\vec{e}_{n+1}$$

(3.25)

in which $\sigma(x)$ *a sigmoid function varying between* ± 1 *also satisfying the restriction that* $\sigma(0) = 0$, *and* $\frac{d\sigma}{dx}|_{x=0} = 1$, and K_c, K_s, A_c, and $B_c = \pm 1$ are the *adaptive control parameters*. It is evident that $(X_\star^d, Y_\star^d)$ is the fixed point of the function in (3.25). If this function is made contractive by properly manipulating the parameters K_c, A_c, and B_c the iterative sequence generated by this function converges to the solution of the controller's task. In the sequel simulation results will be presented for demonstrating the applicability of this method for the controlled Brusselator model developed in the previous section [A. 4].

3.2.6 Simulation Results for the Input Coupling Approach

In the simulations according to [62] the exact parameter values were assumed to be $k_1 = 1$, $k_2 = 1$, $k_3 = 1$, and $k_4 = 1$. The approximate values were $\tilde{k}_1 = 0.8$, $\tilde{k}_2 = 0.9$, $\tilde{k}_3 = 0.7$, and $\tilde{k}_4 = 0.6$. The initial concentrations in the tank were $A(0) = 0$, $B(0) = 0$, $X(0) = 0.5$, and $Y(0) = 0.2 \left[\frac{mole}{L}\right]$. In (3.24) a small value $\Lambda = 1/s$ was applied for slowly varying nominal trajectory. The *cycle-time of the controller* was $0.025\,s$. These parameters were selected on the basis of simulations published in [A. 3] to achieve realizable control signals. The simulations were made the SCILAB software with internal Euler integration of $1\,ms$ discrete time-resolution. In the simulations real solutions were obtained to (3.22) in both the simple PID case and in the adaptive control, too. Figures 3.29 and 3.30 reveal that the non-adaptive controller works well in a stable manner [A. 4].
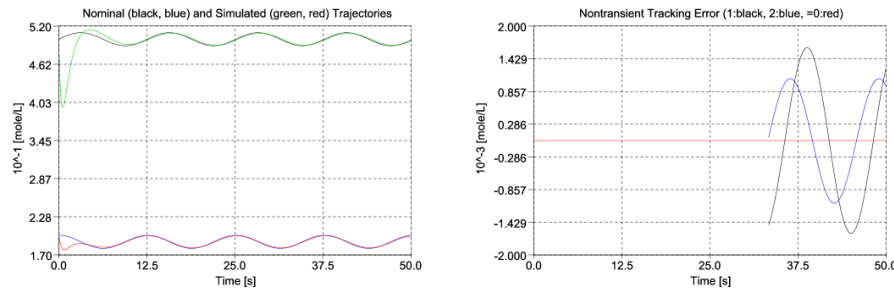
Figure 3.29: Trajectory tracking and tracking error of the simple non-adaptive PID controller in the non-transient stage (for X: black and green lines, for Y: blue and red lines) [A. 4]
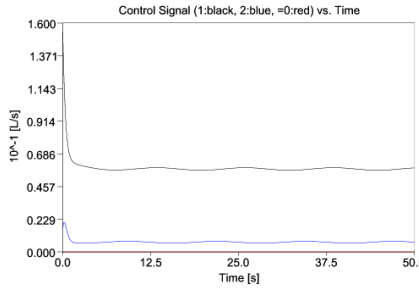
Figure 3.30: The control signals for the simple non-adaptive PID controller (for W_A: black line, for W_B: blue line) [A. 4]

The adaptive counterparts of Figs. 3.29 and 3.30 with the adaptive control parameters $K_c = 225$, $K_s = 10 \left[\frac{mole}{L \cdot s^2}\right]$, $B_c = -1$ and $A_{c_i} \in \{0.0000444, 0.0001405, 0.0004444, 0.0014055, \quad 0.0044444, 0.0140546\}$ $\left[\frac{L \cdot s^2}{mole}\right]$ of which a weighted "next element of iteration" was calculated according to the method detailed in [42] are given as Figs. 3.31 and 3.32 that reveal an improvement in the tracking error and show the transients in the control signals when the adaptivity is switched on at $t = 2.5\,s$. Figure 3.33 also well reveals the transients generated by switching on the adaptivity as well the success of the adaptive deformation: the "*desired*" and "*realized*" curves are in each other's close vicinity and significantly differ from the adaptively deformed "*required*" ones [A. 4].
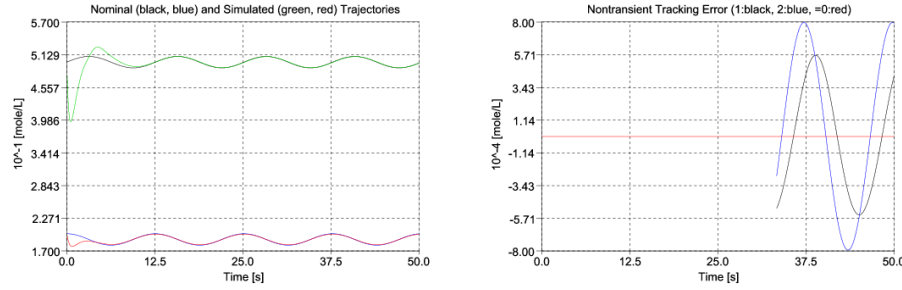
Figure 3.31: Trajectory tracking and tracking error of the adaptive controller in the non-transient stage (for X: black and green lines, for Y: blue and red lines) [A. 4]
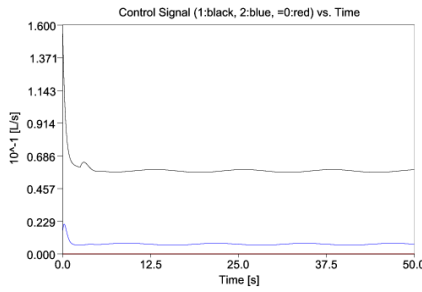
Figure 3.32: The control signals for the adaptive controller (for W_A: black line, for W_B: blue line) [A. 4]
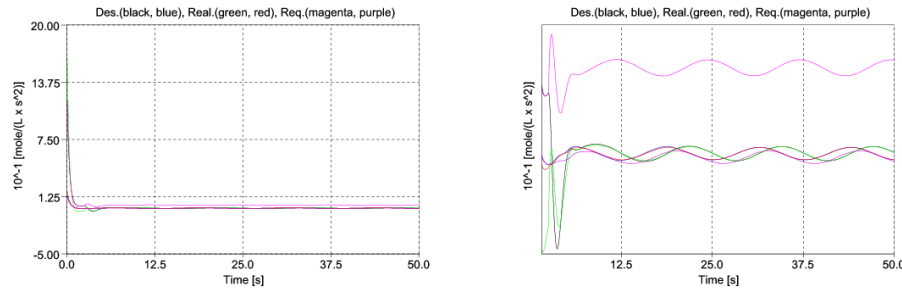
Figure 3.33: The "*desired*" ($\ddot{X}$: black, $\ddot{Y}$: blue), adaptively deformed "*required*"($\ddot{X}$: magenta, $\ddot{Y}$: purple), and the *realized* ($\ddot{X}$: green, $\ddot{Y}$: red) signals of the adaptive controller [A. 4]

3.2.7 The RFPT Method for the Brusselator Model using Fractional Order Derivatives

In the here presented application the basic idea of using fractional order derivatives stemmed from the observation that due to the input coupling effect of adding reactants into a tank reactor required a 2nd order control for the Brusselator model [A. 4] due to which the control system became noise-sensitive and required fast response, i.e. very short cycle time for the controller. It was theoretically expected that by the use of the noise filtering nature of the fractional order derivatives these advantageous properties could be used for increasing the necessary sampling time of the controller. Since this application was based on the use of an iterative adaptive controller in which machine learning happened via Robust Fixed Point Transformations that create the actual control value by observing the system's response for the past signal this adaptive approach also has some memory. After switching on adaptivity normally a

short, transient learning phase can be observed in which both monotonic and fluctuating approaching of the fixed point (that is the solution of the control task) may happen Figs. 3.34, and 3.35. It can be expected that the memory of the fractional order derivative does not seriously concern the learning abilities of the controller if it works in the monotonic regime, however, in the fluctuating mode the memory of the fractional order derivatives can keep in the system of the transient fluctuation of iterative learning and may act in unfortunate manner. In the simulations published in this paper it was found that within certain limits the use of fractional derivatives had good and useful action. It worths noting that in our approach the finite Taylor series expansion of the z-transform of the fractional order derivatives was applied that corresponded to the use of input signals with different delay times that were integer multiples of the cycle time of the controller [A. 5].
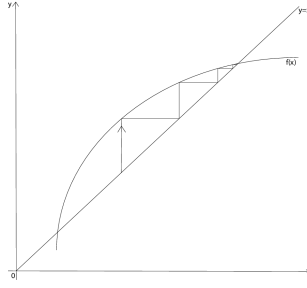
Figure 3.34: Schematic picture explaining a possible operation of the algorithm that iteratively approaches the fixed point: the case of a monotone sequence that helps noise reduction and may be combined with the long term memory properties of the fractional order derivatives [A. 5]
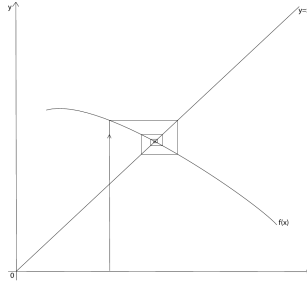
Figure 3.35: Schematic picture explaining a possible operation of the algorithm that iteratively approaches the fixed point: the case of a non-monotone sequence that fluctuates around the fixed point and may not be combined with the long term memory properties of the fractional order derivatives: the long memory may save or conserve the transient fluctuation of the RFPT-based iterative learning that may cease to be a transient effect [A. 5]

The fractional derivatives are represented by the Taylor series of the Z transform as $(1 - z^{-1})^{0.8} \approx 1 - 0.8z^{-1} - 0.08z^{-2} - 0.032z^{-3} - 0.0176z^{-4} - 0.011264z^{-5} + O(z^{-6})$, where z^{-n} corresponds to the signal of n step delay in a digital controller [64]. These delays are applied for the error signal according a following formula (3.26) [A. 5]:

$$\ddot{S} = \ddot{S}_N + 3\lambda^{1.2}[(S_N - S_S) - \tfrac{4}{5}(S_N(1) - S_S(1)) -$$
$$- \tfrac{2}{25}(S_N(2) - S_S(2)) - \tfrac{4}{125}(S_N(3) - S_S(3)) -$$
$$- \tfrac{11}{625}(S_N(4) - S_S(4)) - \tfrac{176}{15625}$$
$$(S_N(5) - S_S(5))]/dt^{0.8} + 3(\lambda^2)(S_N - S_S) + \lambda^3 err_{int}$$

(3.26)

For the convergence of the RFPT-based iterative learning sequence only the limitation of the absolute value of the derivative of the response function is prescribed in the close vicinity of the fixed point.

The derivative itself may be either positive or negative as in Figs. 3.34, and 3.35. However, these *local properties* depend on the *global shape of the nonlinear function* applied in the RFPT. Consequently, besides concerning the monotonic or fluctuating approach of the fixed point the aftermaths of leaving the region of convergence may be significantly different, too. This subject area needs more detailed investigations in the future [A. 5].

3.2.8   Simulation Results for the Use of the Fractional Derivatives

The control parameters for the simulation were: $K = 150, B = -1$, $A_{step} = 0.5$, $A_{centr} = -2,954$, $A(i)_{min} = log10(A_{centr}) - int(\frac{A_{step}}{2})$, $A_{ctrl}(i+1,1) = 10^{(A(i)_{min}+A_{step}i)}$, where $i : samplecycle$. One of the goals in the simulations was the reduction of the sampling time. Two cases were investigated, the difference between them was in the sampling time. In the first case the sampling time was 0.08s, in the second case it was 0.05s. The *trajectories* seem to be precise, in both cases approximately the same result was obtained Fig. 3.36. In the first case in the 2nd *time derivatives of the concentrations* fluctuation appeared and grew up to around $3 \times 10^{-1} \frac{mol}{L \cdot s^2}$ in the second half of the time-frame, but the controller eliminated it, the zoomed Figs shows that effect Fig. 3.37. In the second case there are two places, where the fluctuations grew up. The controller could control it, and reduced both of them (Fig. 3.38). The *correlation buffer* shows where can the controller adaptively handle the reactions. It is approximately same for both cases (Fig. 3.39). If the value is 1 on the buffer, the controller can work adaptively. *Densities* show the concentrations of reagents A and B in the tank. In the first case, in the second half of the time-frame, small fluctuations appeared in correlation with the chattering in the control signals. (Fig. 3.40 and 3.44). In the second case there are three places, where small fluctuations appeared in correlation with the chattering in the control signals (Fig. 3.41 and 3.45). The *voting weights* weight the proposals generated by the different A_c values for the next cycle (Fig. 3.42 - 3.43). The *control signals* show the way, how the controller try to handle the reactions. In the first case, the zoomed figure shows the input coupling effects, where the cut below 0 can be observed, too (Fig 3.44 - 3.45). In the figures of the *nontransient tracking error* is cut off the big initial transients are hidden in order to reveal the fine structure of the graphs of the errors (great initial transients can be seen in the diagrams describing the trajectory tracking) (Fig 3.46 - 3.47) [A. 5].
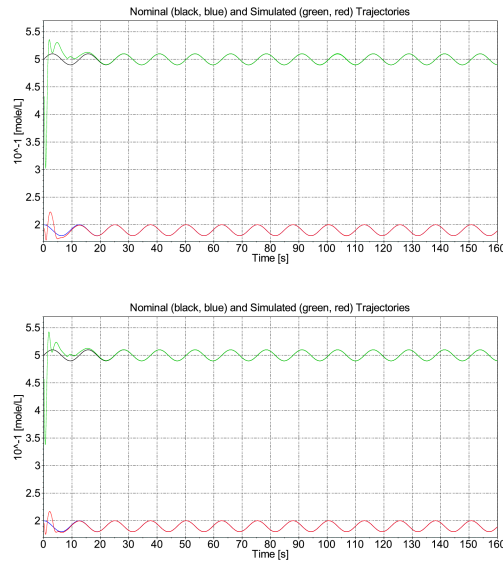
Figure 3.36: Trajectories for both cases (in the first chart the sampling time was 0.08*s*, in the second one it was 0.05*s*): the nominal ("A" input concentrations: black lines, "B" input concentrations: blue lines) and the simulated ("A" input concentrations: green lines, "B" input concentrations: red lines) [A. 5]
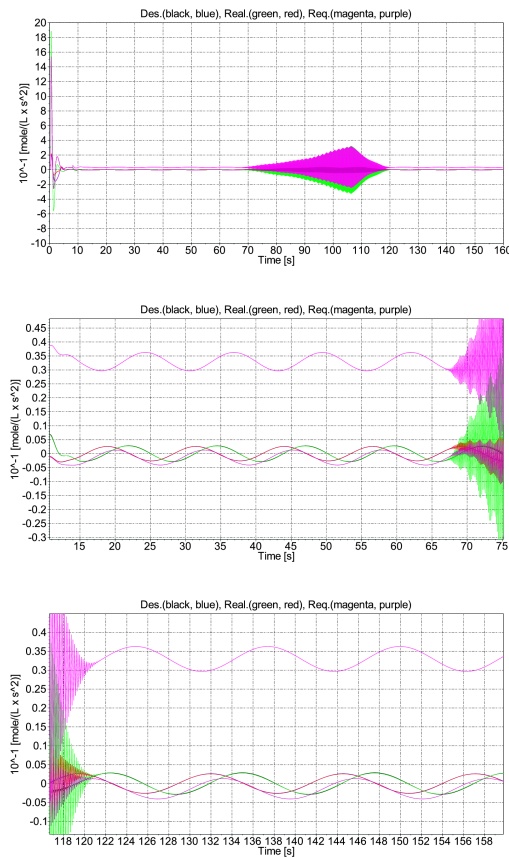
Figure 3.37: 2*nd* time derivatives of the concentrations in first case, where the sampling time was 0.08*s*. The first chart is the full picture, the second and third display zoomed excerpts, Desired ("A" input concentrations: black line, "B" input concentrations: blue line), Realized ("A" input concentrations: green line, "B" input concentrations: red line), Requested ("A" input concentrations: magenta line, "B" input concentrations: purple line) [A. 5]
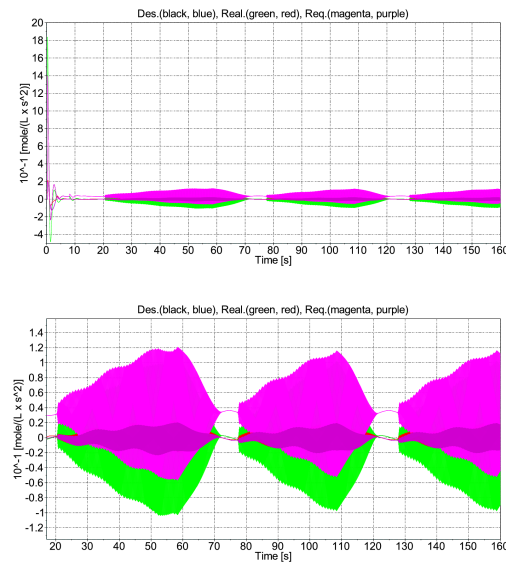
Figure 3.38: *2nd* time derivatives of the concentrations in second case, where the sampling time was 0.05*s*. The first chart is the full picture, the second displays zoomed excerpts, Desired ("A" input concentrations: black line, "B" input concentrations: blue line), Realized ("A" input concentrations: green line, "B" input concentrations: red line), Requested ("A" input concentrations: magenta line, "B" input concentrations: purple line) [A. 5]
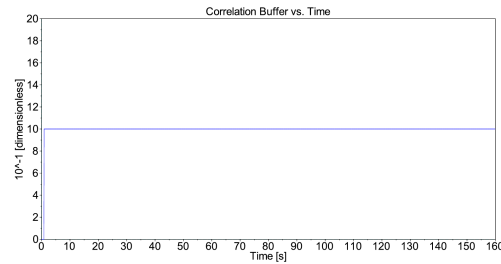
Figure 3.39: Correlation Buffer, which shows that the adaptivity worked during the whole session. [A. 5]
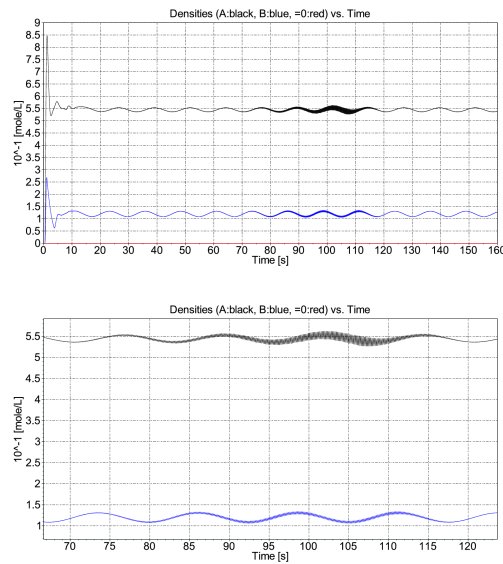
Figure 3.40: Densities of the concentrations for the first case, where the sampling time was 0.08*s*: ("A" input concentrations: black line, "B" input concentrations: blue line, "0": red line) [A. 5]
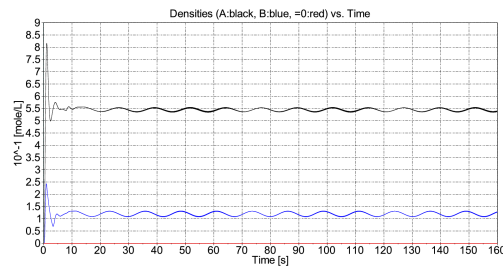
Figure 3.41: Densities of the concentrations for the second case, where the sampling time was 0.05*s*: ("A" input concentrations: black line, "B" input concentrations: blue line, "0": red line) [A. 5]
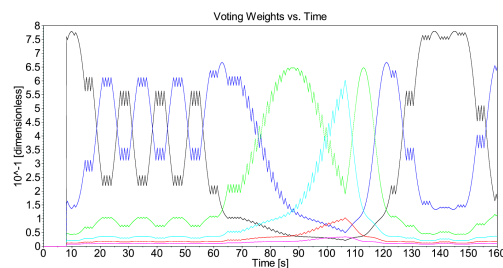
Figure 3.42: Voting Weights, for the first case, where the sampling time was 0.08*s*: (1: black, 2: blue, 3: green, 4: cyan, 5: red, 6: magenta lines) [A. 5]
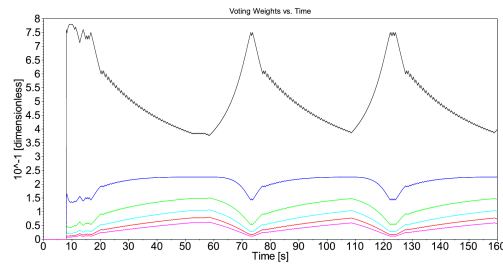
Figure 3.43: Voting Weights, for the second case, where the sampling time was 0.05*s*: (1: black, 2: blue, 3: green, 4: cyan, 5: red, 6: magenta lines) [A. 5]
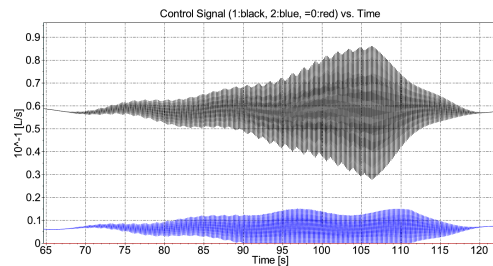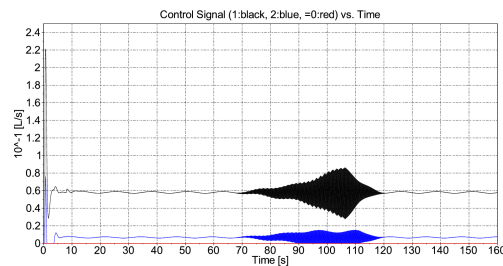
Figure 3.44: Control Signals for the first case, where the sampling time was 0.08*s*: ("A" input: black line, "B" input: blue, "0": red line) [A. 5]
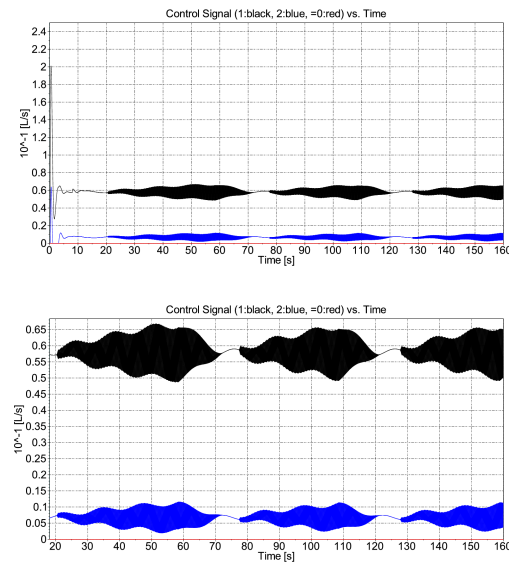
Figure 3.45: Control Signals for the second case, where the sampling time was 0.05*s*: ("A" input: black line, "B" input: blue line, "0": red line) [A. 5]
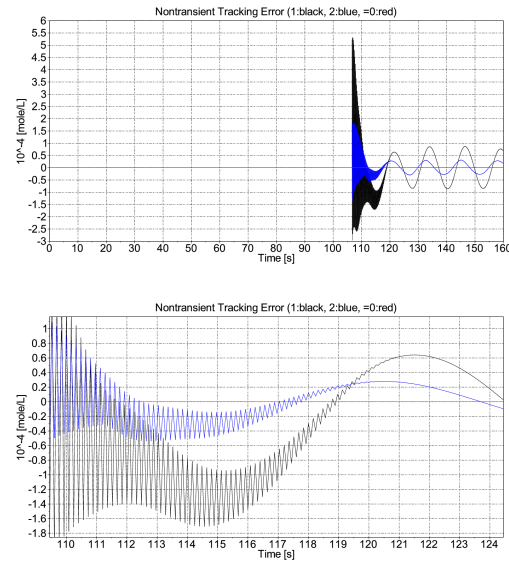
Figure 3.46: Nontransient Tracking Error for the first case, where the sampling time was 0.08*s*: (X: black line, Y: blue line, "0": red line) [A. 5]
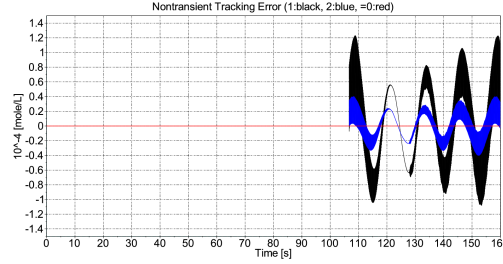
Figure 3.47: Nontransient Tracking Error for the second case, where the sampling time was 0.05*s*: (X: black line, Y: blue line, "0": red line) [A. 5]

3.3 Improvement of Extension from SISO to MIMO in RFPT-based Systems

3.3.1 Systematic Extension of the RFPT-based Method from SISO to MIMO Systems

The original SISO Robust Fixed Point Transformation method [24] has three control parameters as $A \in \mathbb{R}$, $K \in \mathbb{R}$, $B = \pm 1$, and a sigmoid function with the properties $\sigma(0) = 0$, $\frac{d\sigma}{dx}\big|_{x=0} = 1$.

The orignal structure is:

$$G(r) \overset{def}{=} (r + K)\Big[1 + B\sigma\Big(A\big(f(r) - r^d\big)\Big)\Big] - K \quad \text{that is:} \tag{3.27a}$$

$$G(r) = r\Big(1 + B\sigma\Big(A(f - r^d)\Big)\Big) + KB\sigma\Big(A(f - r^d)\Big) \;. \tag{3.27b}$$

This type of function has two fixed points. One of them is $-K$ and the another one is equal to $r_\star$, where $f(r_\star) = r^d$. The MIMO version of this formula was constructed in [65] as

$$G_s = r_s\Big(1 + B\sigma\Big(A\|f - r^d\|\Big)\Big) + KB\sigma\Big(A\|f - r^d\|\Big)e_s \tag{3.28}$$

where $e_s \overset{def}{=} \dfrac{f_s - r_s^d}{\sqrt{\sum_l (f_l - r_l^d)^2}}$ is a unit vector, that determines the direction of the system's response error. Let $\tilde{B} \overset{def}{=} B\sigma\Big(A\|f - r^d\|\Big)$.

$$G_s = r_s\Big(1 + \tilde{B}\Big) + K\tilde{B}e_s \;. \tag{3.29}$$

For proving the contractivity of function G its partial derivatives according to variable r have to be investigated:

$$\frac{\partial G_s}{\partial r_u} = \delta_{su}(1 + \tilde{B}) + r_s\frac{\partial \tilde{B}}{\partial r_u} + Ke_s\frac{\partial \tilde{B}}{\partial r_u} + K\tilde{B}\frac{\partial e_s}{\partial r_u} \;, \tag{3.30}$$

where

$$\frac{\partial e_s}{\partial r_u} = \frac{1}{\sqrt{\sum_w (f_w - r_w^d)^2}}\frac{\partial f_s}{\partial r_u} - \frac{\big(f_s - r_s^d\big)\sum_l\big(f_l - r_l^d\big)}{\Big(\sum_w (f_w - r_w^d)^2\Big)^{\frac{3}{2}}}\frac{\partial f_l}{\partial r_u} \;, \tag{3.31}$$

let $h_s \overset{def}{=} f_s - r_s^d$ denotes the response error. It can be written in vector form that:

$$\frac{\partial e}{\partial r} = \frac{1}{\|h\|}\left(\frac{\partial f}{\partial r} - ee^T\frac{\partial f}{\partial r}\right) \ . \tag{3.32}$$

Similarly

$$\frac{\partial \tilde{B}}{\partial r_u} = B\sigma' A\frac{\partial\sqrt{\sum_w(f_w - r_w^d)^2}}{\partial r_u} = B\sigma' A\frac{\sum_l(f_l - r_l^d)^2}{\sqrt{\sum_w(f_w - r_w^d)^2}}\frac{\partial f_l}{\partial r_u} \ , \tag{3.33}$$

where σ' is the derivative of function $\sigma(x)$. Equation (3.33) in vector form is:

$$\frac{\partial \tilde{B}}{\partial r} = BA\sigma'e^T\frac{\partial f}{\partial r} \ . \tag{3.34}$$

The (3.30) equation in vector form is:

$$\frac{\partial \tilde{G}}{\partial r} = \left(1 + \tilde{B}\right)I + (r + Ke)BA\sigma'e^T\frac{\partial f}{\partial r} + \frac{K\tilde{B}}{\|h\|}\left[I - ee^T\right]\frac{\partial f}{\partial r} \ . \tag{3.35}$$

In the fixed point the vector e cannot be defined because $\|h\| = 0$, but (3.35) can be defined with its own limit value: because of the properties of the $\sigma(x)$ function $\frac{\tilde{B}}{\|h\|} \to BA$, $\tilde{B} = 0$, $\sigma'(0) = 1$, (3.35) therefore (3.35) can be written as

$$\frac{\partial \tilde{G}}{\partial r} = I + rBAe^T\frac{\partial f}{\partial r} + KBAee^T\frac{\partial f}{\partial r} + KBA\frac{\partial f}{\partial r} - KBAee^T\frac{\partial f}{\partial r} \ , \tag{3.36}$$

i.e.

$$\frac{\partial \tilde{G}}{\partial r} = I + BA\left(re^T + K\right)\frac{\partial f}{\partial r} \ . \tag{3.37}$$

The contractivity of this matrix may be guaranteed for a wide class of physical systems since we have an additional term to the unit matrix. This addition contains the control parameter A as a multiplication factor that can be made small enough. For instance is $\frac{\partial f}{\partial r}$ symmetric positive definite or negative definite the contractivity can be achieved. For instance, in the case of fully driven Classical Mechanical systems the inertia matrix is symmetric positive definite. Regarding the cases in which this partial derivative contains symmetric and skew symmetric parts the Jordan canonical form may be used for further studies.

3.3.2 More simple extension from SISO to MIMO systems in the RFPT-based adaptive control

In the 3.3.1 section's sigmoid function ($\sigma(x) : \mathbb{R} \mapsto \mathbb{R}$) will be used.

$$H(x) = x\left[1 + B\sigma(x)\right] + KB\sigma(x) \ , \tag{3.38}$$

where $x = 0$ is the fixed point, because $H(0) = 0$. In SISO case, can be used the following function to generate iteration:

$$G(r) \stackrel{def}{=} r + H\left(A(f - r^d)\right) = r + A(f - r^d)\left[1 + B\sigma\left(A(f - r^d)\right)\right] + KB\sigma\left(A\left(f - r^d\right)\right) \ . \tag{3.39}$$

It is trivial that if $f(r_\star) = r^d$, then $G(r_\star) = r_\star$. The derivative of that function:

$$\frac{\mathrm{d}G}{\mathrm{d}r} = 1 + A\frac{\mathrm{d}f}{\mathrm{d}r}\left[1 + B\sigma\left(A(f - r^d)\right)\right] + A(f - r^d)B\sigma' A\frac{\mathrm{d}f}{\mathrm{d}r} + KBA\sigma'\frac{\mathrm{d}f}{\mathrm{d}r} \ , \tag{3.40}$$

which has a following value in the fixed point:

$$\frac{\mathrm{d}G}{\mathrm{d}r} = 1 + A(1 + KB)\frac{\mathrm{d}f}{\mathrm{d}r} \quad . \tag{3.41}$$

To satisfy the $\left|\frac{\mathrm{d}G}{\mathrm{d}r}\right| < 1$ condition, which guarantees the convergence into the fixed point, it can be achieved by choosing a properly small value for control parameter A.

This transformation can be simplified. Usually in the practical setup $|x| \ll |K|$, therefore the expression

$$H(x) = x + KB\sigma(x) \tag{3.42}$$

can be tried, which leads to the following function:

$$G(r) \stackrel{def}{=} r + H\left(A(f - r^d)\right) = r + A(f - r^d) + KB\sigma\left(A\left(f - r^d\right)\right) \quad , \tag{3.43}$$

furthermore

$$\frac{\mathrm{d}G}{\mathrm{d}r} = 1 + A\frac{\mathrm{d}f}{\mathrm{d}r} + KBA\sigma'\frac{\mathrm{d}f}{\mathrm{d}r} \quad , \tag{3.44}$$

which leads to the result of the equation (3.41).

This can be extend to MIMO case in the following way:

$$\tilde{G}(r) \stackrel{def}{=} r + \left[A\|f - r^d\| + KB\sigma\left(A\|f - r^d\|\right)\right]e \quad , \tag{3.45}$$

where $e \stackrel{def}{=} \frac{f - r^d}{\|f - r^d\|}$. The partial derivatives are $\frac{\partial\sqrt{\sum_l(f_l - r_l^d)^2}}{\partial r_u} = \frac{2\sum_l(f_l - r_l^d)}{2\sqrt{\sum_w(f_w - r_w^d)^2}}\frac{\partial f_l}{\partial r_u} = e^T\frac{\partial f}{\partial r}$:

$$\frac{\partial G_s}{\partial r_u} = \delta_{su} + A(1 + \sigma'KB)e_s\sum_l e_l\frac{\partial f_l}{\partial r_u} \quad , \tag{3.46}$$

which in vector form in the fixed point:

$$\frac{\partial G}{\partial r} = I + A(1 + KB)ee^T\frac{\partial f}{\partial r} \quad . \tag{3.47}$$

Regarding the contractivity of this function similar considerations can be applied as in the previous case.

CHAPTER 4

IMPROVEMENT OF THE STABILITY OF THE RFPT-BASED ADAPTIVE CONTROL

4.1 Improved parameter tuning: "Precursor Oscillations"

A detailed analysis reveals that the following cases may happen: *a) monotone convergence to the solution of the control task $r_\star$, b) non-monotone convergence to the solution of the control task $r_\star$ c) chaotic behavior in a bounded region, d) divergence to infinity, f) convergence to the trivial fixed point of G i.e. to $-K_c$.* These cases are not "isolated ones" but follow each other in a well traceable order. [A. 6]

This statement will be demonstrated for an *affine approximation* of $f(r) = ar+b$ with $a, b = 1$ that corresponds to the $\frac{df}{dr} > 0$ case. A "P-type" tracking feedback prescribed as $r_n^{Des} = r_n^{Nom} + \Lambda \left(r_n^{Nom} - f_n \right)$ with $\Lambda = 0.9$ and constant $r^{Nom} = 5$ nominal signal was considered. The settings $K_c = -6$ ("*big negative*") and $B_c = 1$ produces the mentioned sequence: if $A_c = 0$ (2.1) evidently is an identity transformation. For "*very small*" $A_c = 0.2$ *monotone convergence* to the solution $r_\star = 4$ was obtained according to Fig. 4.1. Via increasing A_c to 0.4 ("*medium value*") the derivative of G turns into small negative number that yields fluctuating convergence to $r_\star$ (Fig. 4.2). Finally for "*great*" $A_c = 2$ bounded chaotic chattering can be observed in Fig. 4.3. Figure 4.4 also illustrates/expounds the formation of this chaotic motion [A. 6].

It worths noting that the $r_{ini} \ll -K_c$ initial condition guarantees the reliable operation of the controller. Divergence to the infinity happens only at the other side of the repulsive trivial fixed point when $r > -K_c$. In the next section simulations will be presented that exemplify the use of the appearance of the "precursor fluctuations" in tuning A_c [A. 6].
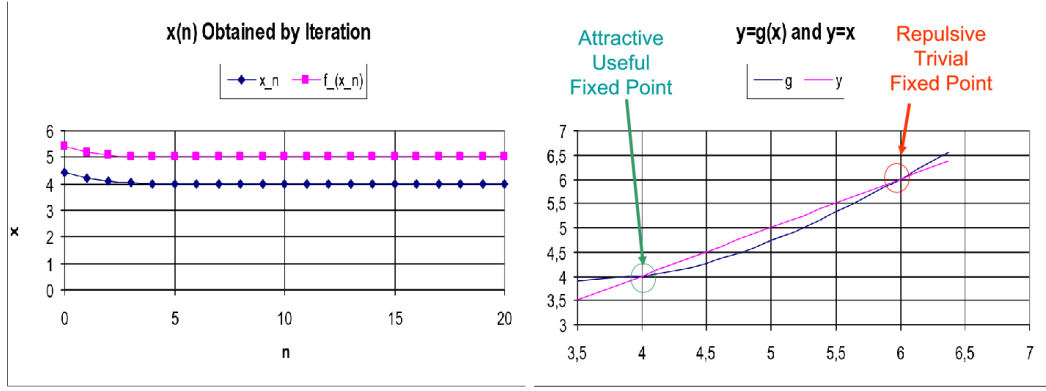
Figure 4.1: Monotone convergent iteration to $r_\star$ for "small" $A_c = 0.2$ (it can well be identified that the trivial fixed point at $r = -K_c$ is repulsive while the nontrivial one is attractive and yields acceptable solution) [A. 6]
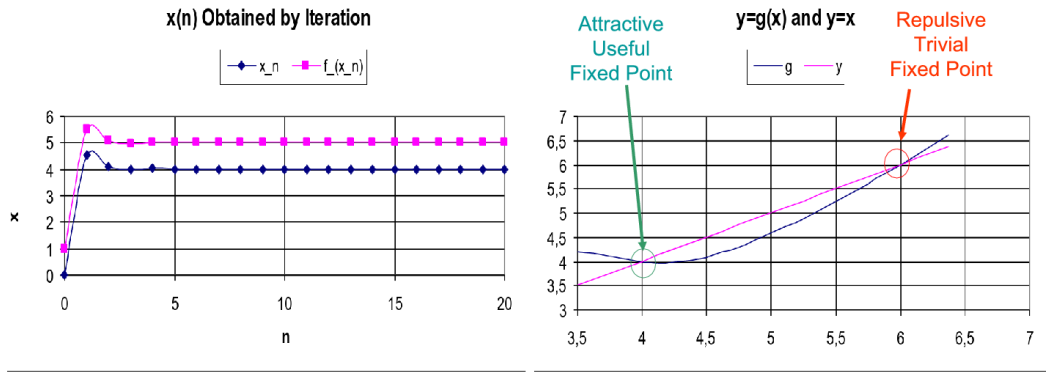
Figure 4.2: Non-monotone convergent iteration to $r_\star$ for "medium" $A_c = 0.4$ (it can well be identified that the trivial fixed point at $r = -K_c$ is repulsive while the nontrivial one is still attractive and yields acceptable solution) [A. 6]
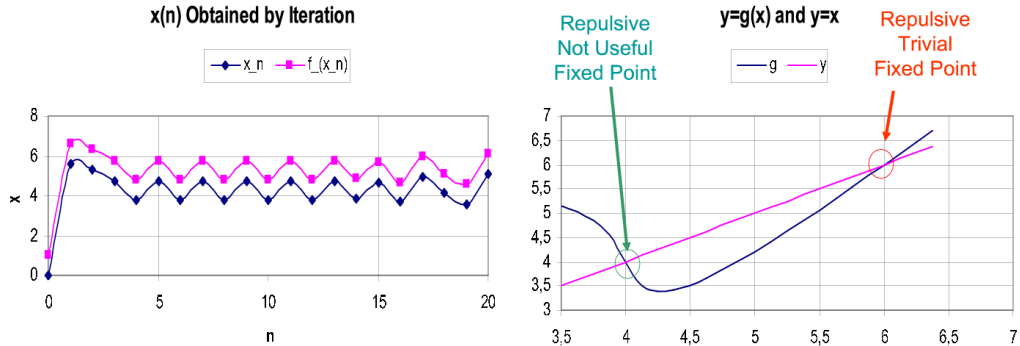
Figure 4.3: Chaotic chattering for "great" $A_c = 2$ [A. 6]
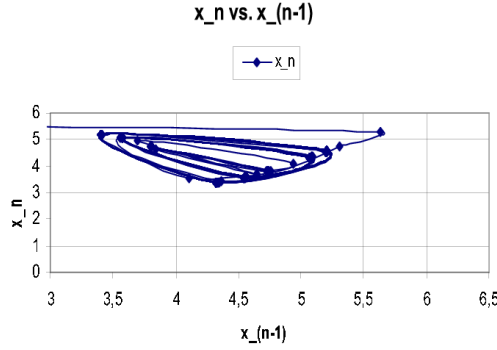
Figure 4.4: Formation of the chaotic chattering for the "great" setting $A_c = 2$ (it can well be identified that both fixed points are repulsive that guarantees finite control signals of order of magnitude of K_c) [A. 6]

4.1.1   The RFPT-based MRAC Controller for a 2 DoF TORA System

The "*TORA*" (*Translational Oscillations with an Eccentric Rotational Proof Mass Actuator*) system was considered as a simplified model of a dual-spin spacecraft with mass imbalance in the literature. It served as a "benchmark problem" for controller design in [66]. In [67] it was controlled by a cascade and a passivity based controller. In [68] for example the "*Tensor Product Form*" of the system model was applied to develop a model-based controller. For our purposes its 2 DoF variant was considered that consisted of a cart, a pendulum (practically a beam) and a dial that can be rotated around an axle attached to the end of the beam. Its equations of motion are given in (4.1). This seemingly 3 DoF system was made 2 DoF indirectly driven one by setting $Q_3 \equiv 0$ and trying to control the motion of axles $q_2 \, [rad]$ and $q_3 \, [m]$ by properly setting $Q_1 \, [N \times m]$ and $Q_2 \, [N \times m]$ [A. 6].

$$
\begin{bmatrix} (mL^2 + \Theta) & \Theta & mL\cos(q_1) \\ \Theta & \Theta & 0 \\ mL\cos(q_1) & 0 & (m+M) \end{bmatrix} \begin{bmatrix} \ddot{q}_1 \\ \ddot{q}_2 \\ \ddot{q}_3 \end{bmatrix} +
$$
$$
+ \begin{bmatrix} -mLg\sin(q_1) \\ 0 \\ -mL\sin(q_1)\dot{q}_1^{\,2} \end{bmatrix} = \begin{bmatrix} Q_1 \\ Q_2 \\ Q_3 \end{bmatrix}
$$

(4.1)

with the dynamic parameters as follows: $m = 20 \, [kg]$ (the mass of the dial), $M = 30 \, [kg]$ (the mass of the body of the cart, $L = 2 \, [m]$ (the length of the beam), and $\Theta = 20 \, [kg \times m^2]$ (the momentum of inertia of the dial with respect to its own mass center point). Utilizing that $Q_3 \equiv 0$ the last equation of (4.1) determines $\ddot{q}_1$ in (4.2) [A. 6]

$$
\ddot{q}_1 = \frac{mL\sin(q_1)\dot{q}_1^{\,2} - (m+M)\ddot{q}_3}{mL\cos(q_1)}
$$

(4.2)

that can be substituted into the first two equations of (4.1) to calculate the necessary Q_1 and Q_2 torque components in (4.3).

$$
\begin{bmatrix} -\frac{(mL^2+\Theta)(m+M)}{mL\cos(q_1)} + mL\cos(q_1) & \Theta \\ -\frac{(m+M)\Theta}{mL\cos(q_1)} & \Theta \end{bmatrix} \begin{bmatrix} \ddot{q}_3 \\ \ddot{q}_2 \end{bmatrix} +
$$
$$
\begin{bmatrix} \frac{(mL^2+\Theta)mL\sin(q_1)\dot{q}_1^{\,2}}{mL\cos(q_1)} - mLg\sin(q_1) \\ 0 \end{bmatrix} = \begin{bmatrix} Q_1 \\ Q_2 \end{bmatrix}
$$

(4.3)

that is considerably different to that of the directly driven Classical Mechanical systems: certain elements of the "inertia matrix" and the additional terms are singular and may contain infinite elements if $\cos(q_1) = 0$. The aim of the MRAC controller in our case was to simplify the dynamics given in (4.3) *for an external control loop* as a 2 DoF *reference model* described by (4.4) [A. 6].

$$\Theta_{ref} \ddot{q}_2 = Q_2, \quad -\left(M_{ref} + m_{ref}\right) \ddot{q}_3 = Q_1. \tag{4.4}$$

with the parameters $m_{ref} = 15\,[kg]$, $M_{ref} = 25\,[kg]$, and $\Theta_{ref} = 16\,[kg \times m^2]$ for nominal motion that avoids the configurations in which $\cos(q_1)$ approaches 0. The details of how to develop MRAC controllers by the use of RFPT were described in details e.g. in [38]. In the sequel we give only simulation results that exemplify how can the "precursor" oscillations be utilized for guaranteeing stable tuning for A_c [A. 6].

4.1.1.1   The Tuned RFPT-based MRAC Controller

In the simulations the $\ddot{q}_i^{Des} = \ddot{q}_i^{Nom} + 3\Lambda^2(q_i^{Nom} - q_i) + 3\Lambda(\dot{q}_i^{Nom} - \dot{q}_i) + \Lambda^3 \int_0^t \left(q_i^{Nom}(\tau) - q_i(\tau)\right) d\tau$ with $\Lambda = 10/s$ *kinematic tracking* was prescribed for $i = 2, 3$. The actively driven axle q_1 started from the "not dangerous" $q_1 = 0$ initial position. A digital controller was assumed to yield constant torque for cycle time of $\Delta t = 1\,ms$. In the *adaptive case* the adaptive control parameters were set as follows: $\{K_c = -10^4, B_c = 1\}$ *or* $\{K_c = 10^4, B_c = -1\}$ for yielding the appropriate precursor phenomenon, and $A_{c_{ini}} = 10^{-7}$ were chosen. For tuning A_c an *asymmetric rule* was applied that cautiously increases its value if no "*precursor oscillations*" are observed but causes fast decrease if the oscillations appear as

$$\dot{A}_c = \begin{cases} v_+ \ if \ \hat{F}_n - F_{thr} \geq 0 \ and \ A_c \leq A_{c_{ini}} \\ -c_v v_+ \ if \ \hat{F}_n - F_{thr} < 0 \ or \ A_c \geq A_{c_{max}} \end{cases} \tag{4.5}$$

with $v_+ = 10^{-4}$, $c_v = 3$, $F_{thr} = 10^{-4}$, and $A_{c_{max}} = 10 A_{c_{ini}}$. The $\hat{F}_n$ values were calculated by a "*forgetting integral*" that served as a *model-independent observer* in the following manner: the *scalar products* $F(t_n) := [\vec{Q}(t_n) - \vec{Q}(t_n - \Delta t)]^T [\vec{Q}(t_n - \Delta t) - \vec{Q}(t_n - 2\Delta t)]$ in general can be used for *monitoring the precursor of chattering* since its positive value pertains to definite *modification of the control force* "approximately in the same direction" while negative value reveals a significant fluctuation in the direction of the force between the subsequent control cycles. (The scalar product $\vec{Q}(t_n)^T \vec{Q}(t_n - \Delta t)$ could reveal only a rough chattering.) The forgetting integral with the output $\hat{F}_n := (1 - \beta) \sum_{s=0}^n \beta^s F_{n-s}$ with $\beta = 0.1$ and threshold value F_{thr} is able to filter out single changes in the direction of the forces that normally occur only in certain points of a smooth variation [A. 6].

4.1.1.2   Simulations for Big Negative K_c and $B_c = 1$

In Fig. 4.5 the movement of the axles in the adaptive case are described for a nominal trajectory converging from zero to a third order spline function of time. In Fig. 4.6 the trajectory tracking errors are described for *non-adaptive* and the *adaptive* controllers [A. 6].
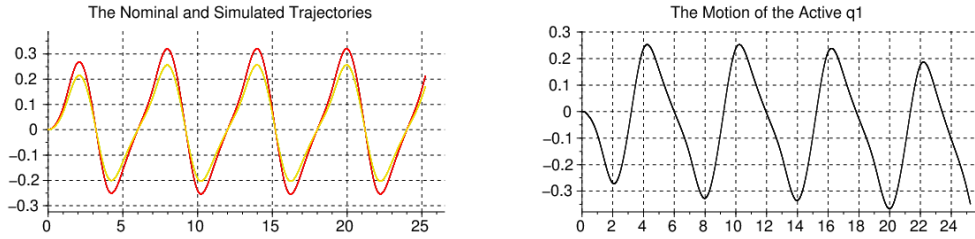
Figure 4.5: Trajectory tracking of the *adaptive controller* [q_2 [rad]: black, q_3 [m]: green, q_2^{Nom} [rad]: red, q_3^{Nom} [m]: ochre lines] (LHS), and the motion of the actively driven axis [q_1 : [rad] vs. time in [s] units (RHS)] [A. 6]
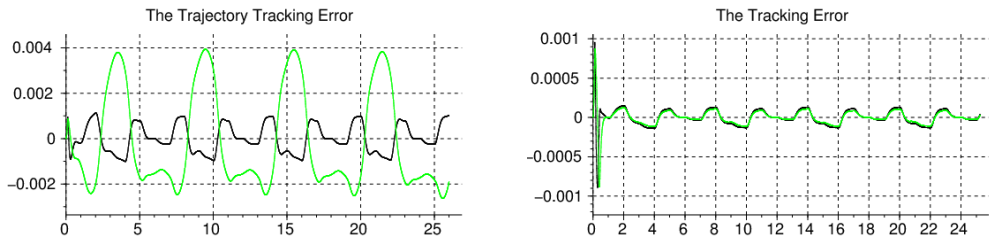
Figure 4.6: Trajectory tracking errors of the *non-adaptive controller* (LHS) and the *adaptive one* (RHS) [q_2 [rad]: black, q_3 [m]: green lines vs. time in [s] units] [A. 6]

Figure 4.7 reveals the control forces that have the following definitions: the "*desired forces*" with super-script "Des" denote the force needs of the *reference model* calculated by the external control loop using the *kinematically prescribed tracking error relaxation* and the *dynamic model of the reference system* given in (4.4). The "*exerted*" forces are calculated by the internal loop of the MRAC controller that has double responsibility: a) guaranteeing precise trajectory tracking, and b) generating the illusion to the external loop that the reference model well describes the controlled system (the "MRAC illusion"). The "recalculated forces" marked by the superscript "Rec" means *the force need of the reference model* at the realized response of the controlled system in its actual state. It is evident that the controller well generated the MRAC illusion since the "recalculated" forces are in the vicinity of the "desired ones" while both of them considerably differ from the adaptively deformed, realized control forces actually exerted. Figure 4.8 displays zoomed excerpts of the force diagram of the adaptive controller. In the diagram little fluctuations in the control signal in certain segments can well be observed. These fluctuations are related to the tuned value of A_c depicted in Fig. 4.9. By the use of the time axis of the diagrams it can well be seen that the appearance of the the little fluctuations in the control signal are related to the too great values of A_c and that the fast decrease in A_c makes them cease quickly [A. 6].
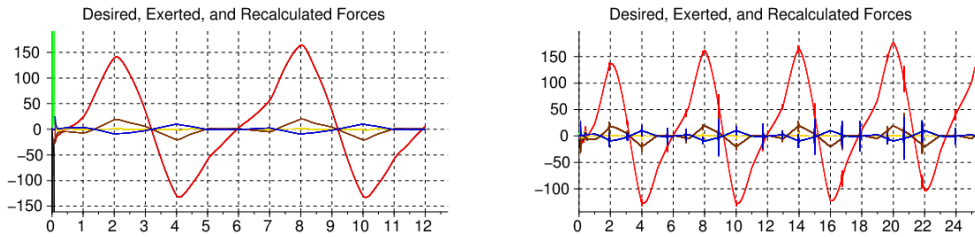
Figure 4.7: The *generalized forces* for the *non-adaptive* (LHS) and the *adaptive* (RHS) cases versus time in [s] units [Q_1^{Des}: black, $Q_1^{Exerted}$: red, Q_1^{Rec}: brown, and Q_2^{Des}: green, $Q_2^{Exerted}$: ochre, Q_2^{Rec}: dark blue lines in [$N \times m$] units] [A. 6]
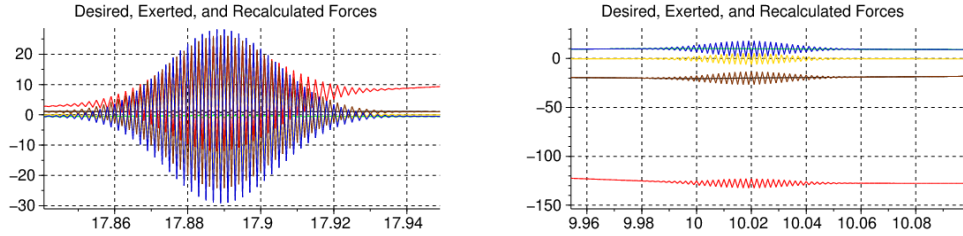
Figure 4.8: Detailed excerpts of the *generalized forces* of the *adaptive controller* versus time in $[s]$ units $[Q_1^{Des}$: black, $Q_1^{Exerted}$: red, Q_1^{Rec}: brown, and Q_2^{Des}: green, $Q_2^{Exerted}$: ochre, Q_2^{Rec}: dark blue lines in $[N \times m]$ units] [A. 6]
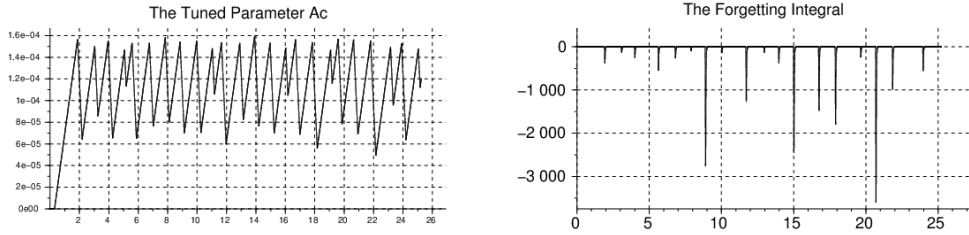
Figure 4.9: Variation of A_c vs. time in $[s]$ units (LHS) and the time-dependence of the forgetting integral (RHS) [A. 6]

4.1.1.3   Simulations for Big Positive K_c and $B_c = -1$

These alternative settings also produce observable and useful "precursor oscillations" for the same nominal motion. Figure 4.10 reveals precise trajectory and smooth and precise phase trajectory tracking. According to Fig. 4.11 it can be stated that similar and efficient parameter tuning happened as in the case of the original settings $\{K_c = -10^4, B_c = 1\}$. In the diagram of the generalized forces (Fig. 4.12) similar precursor oscillations can be observed, too [A. 6].
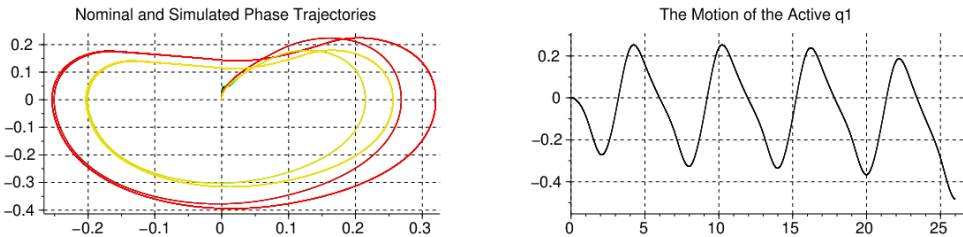
Figure 4.10: The phase trajectories $[q_2\ [rad]$: black, $q_3\ [m]$: green, $q_2^{Nom}\ [rad]$: red, $q_3^{Nom}\ [m]$: ochre lines] (LHS) and the trajectory tracking errors of the *adaptive controller* using the alternative parameter settings (RHS) $[q_2\ [rad]$: black, $q_3\ [m]$: green lines vs. time in $[s]$ units] [A. 6]
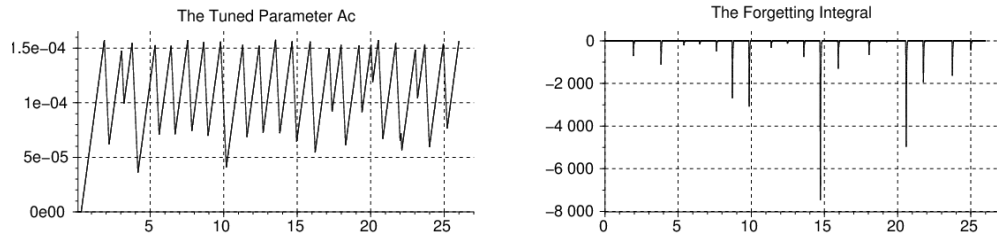
Figure 4.11: Variation of A_c vs. time in $[s]$ units (LHS) and the time-dependence of the forgetting integral (RHS) using the alternative parameter settings [A. 6]
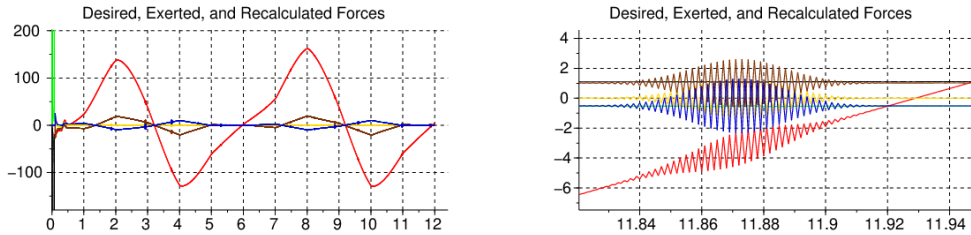
Figure 4.12: The chart of the *generalized forces* of the *adaptive controller* at the alternative parameter settings versus time in $[s]$ units and its detailed excerpts [Q_1^{Des}: black, $Q_1^{Exerted}$: red, Q_1^{Rec}: brown, and Q_2^{Des}: green, $Q_2^{Exerted}$: ochre, Q_2^{Rec}: dark blue lines in $[N \times m]$ units] [A. 6]

4.2 The Global Behavior of the Bounded RFPT

As in [A. 6] let us approximate the *response function* f with an *affine* formula as $f(r) = \alpha r + \beta$ with $\alpha = 1$ and $\beta = 1$. Regarding the derivative $\frac{df}{dr}$ only α has significance. As in [A. 6] a "P-type" tracking feedback prescribed as $r_n^{Des} = r_n^{Nom} + \Lambda\left(r_n^{Nom} - f_n\right)$ with $\Lambda = 0.9$ and constant $r^{Nom} = 5$ nominal signal was considered with $K_s = 10$, $K_c = \pm 1000$, $B_c = \pm 1$, and various $0 < A_c$ parameter settings [A. 7].

For $\frac{df}{dr} > 0$ the simultaneous settings for a big $A_c = 10^{-2}$, $K_c > 0$ and $B_c = 1$ or $K_c < 0$ and $B_c = -1$ are "dangerous". Figure 4.13 reveals the global shape of the bounded RFPT transformation in this case. It is evident that some *attractive fixed points* at $-K_s <\approx r_\star^{(1)}$ and $K_s >\approx r_\star^{(2)}$ with flat adaptive mapping. In Fig. 4.14 an example for the convergence to $\approx -K_s$ is provided [A. 7].
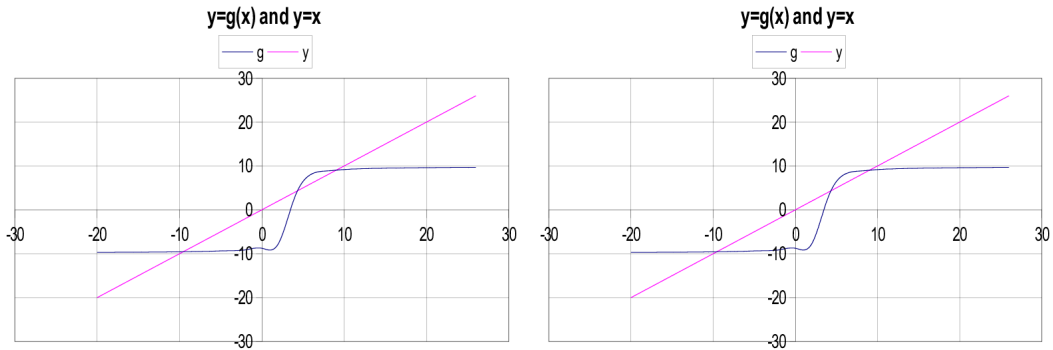
Figure 4.13: The global shape of the bounded RFPT in the "dangerous situations" for $\frac{df}{dr} > 0$ systems: K_c big positive, $B_c = 1$ (LHS) and K_c big negative and $B_c = -1$ (RHS) (in each case $A_c = 10^{-2}$ was "big") [A. 7]
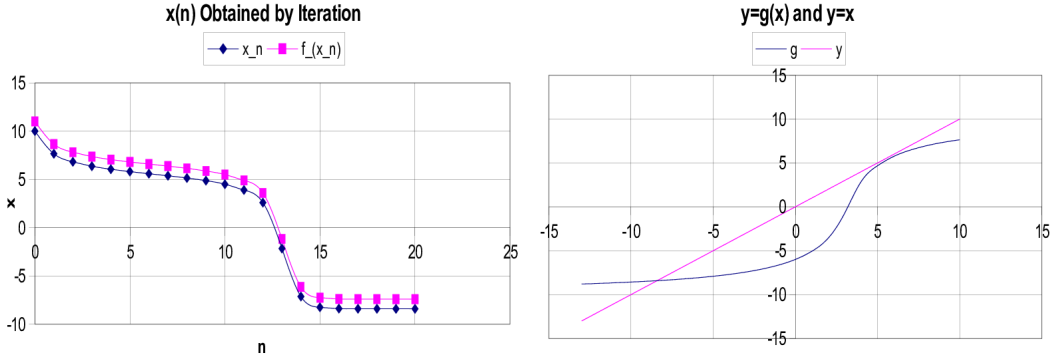
Figure 4.14: The convergence to near $-K_s$ for $\frac{df}{dr} > 0$ systems: K_c big positive, $B_c = 1$ and $A_c = 2 \times 10^{-3}$ ("moderate" value) [A. 7]

For cases providing "*emerging*" or "*precursor oscillations*" in the control signal r_n at first the *monotone* convergence for $r_n \to r\star$ is exemplified by Figs. 4.15, , and 4.17 belonging to "*small*" $A_c = 10^{-4}$ value. (Due to the small value of β in the affine model the appropriate figures are very similar to each other.) [A. 7]
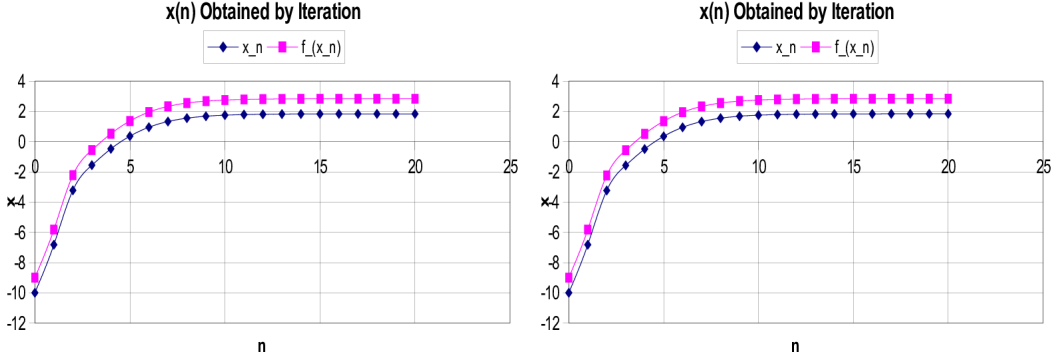
Figure 4.15: Monotone convergence for $\frac{df}{dr} > 0$ systems: $K_c = -1000$, $B_c = 1$ (LHS) and $K_c = 1000$, $B_c = -1$ (RHS) (in each case $A_c = 10^{-4}$ was "small") [A. 7]
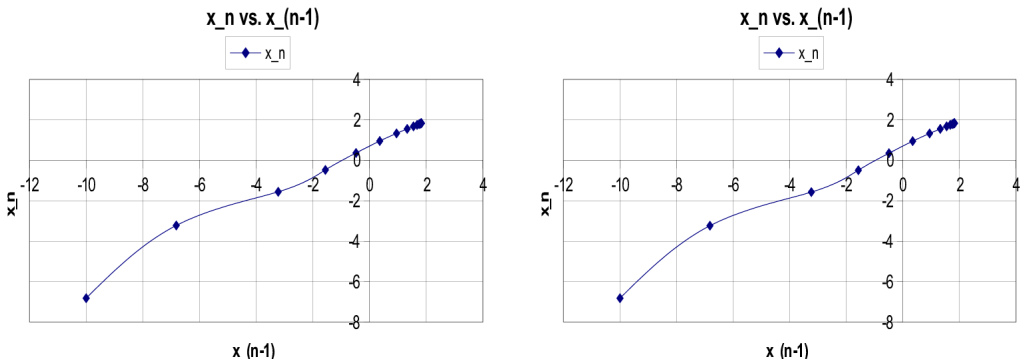
Figure 4.16: Phase trajectory of the monotone convergence for $\frac{df}{dr} > 0$ systems: $K_c = -1000$, $B_c = 1$ (LHS) and $K_c = 1000$, $B_c = -1$ (RHS) (in each case $A_c = 10^{-4}$ was "small") [A. 7]
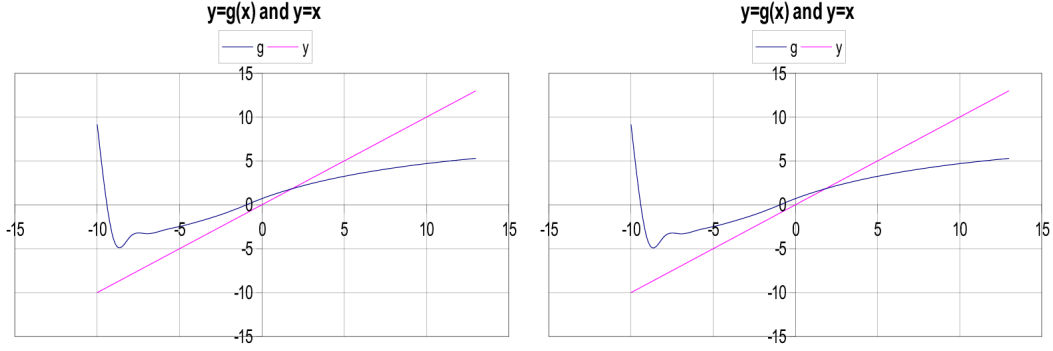
Figure 4.17: Function shapes for the monotone convergence for $\frac{df}{dr} > 0$ systems: $K_c = -1000, B_c = 1$ (LHS) and $K_c = 1000, B_c = -1$ (RHS) (in each case $A_c = 10^{-4}$ was "small") [A. 7]

Further increase in A_c results in emerging oscillations in the control signal but the controller remains convergent (Figs. 4.18, 4.19, and 4.20) [A. 7].
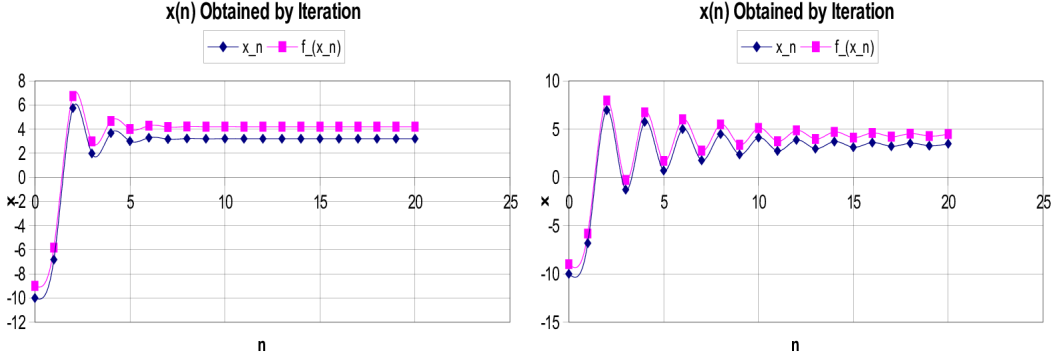
Figure 4.18: Non-monotone convergence for $\frac{df}{dr} > 0$ systems: $K_c = -1000, B_c = 1, A_c = 10^{-3}$ (LHS) and $K_c = 1000, B_c = -1, A_c = 1.5 \times 10^{-3}$ (RHS) [A. 7]
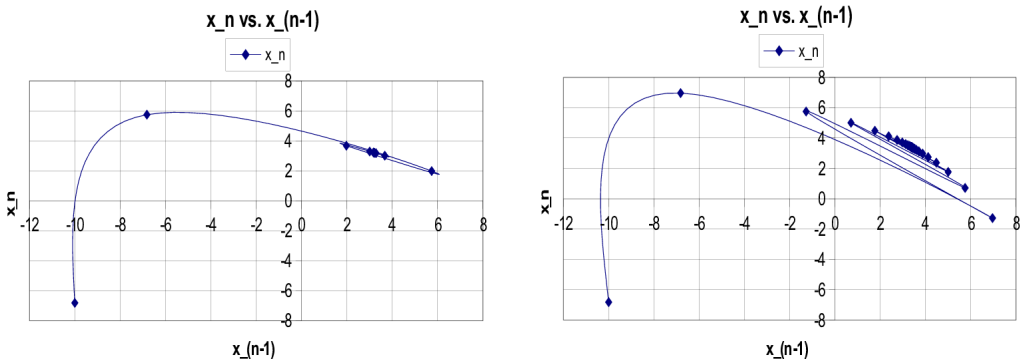
Figure 4.19: Phase trajectory of the monotone convergence for $\frac{df}{dr} > 0$ systems: $K_c = -1000, B_c = 1$, $A_c = 10^{-3}$ (LHS) and $K_c = 1000, B_c = -1, A_c = 1.5 \times 10^{-3}$ (RHS) [A. 7]
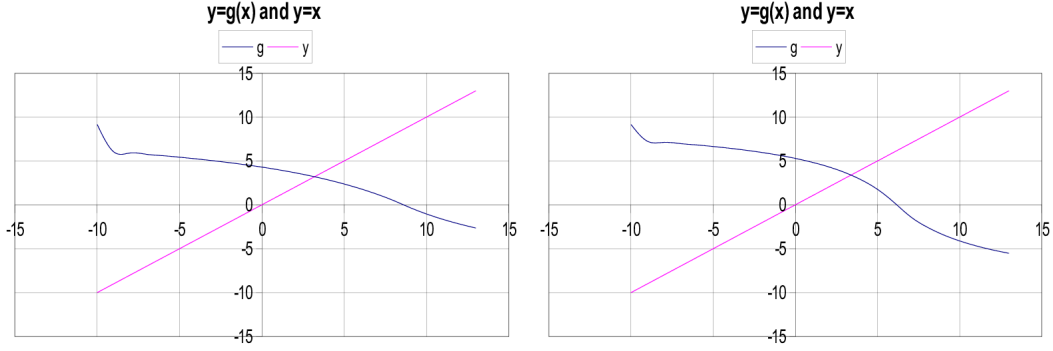
Figure 4.20: Function shapes for the monotone convergence for $\frac{df}{dr} > 0$ systems: $K_c = -1000$, $B_c = 1$, $A_c = 10^{-3}$ (LHS) and $K_c = 1000$, $B_c = -1$, $A_c = 1.5 \times 10^{-3}$ (RHS) [A. 7]

Further increase in A_c will again result in *bounded chattering* (Figs. 4.21, 4.22, and 4.23) [A. 7].
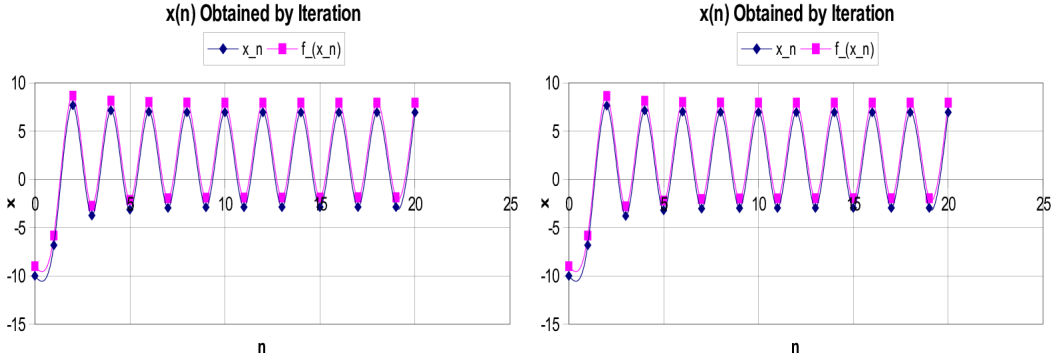
Figure 4.21: Bounded chattering for $\frac{df}{dr} > 0$ systems: $K_c = -1000$, $B_c = 1$, $A_c = 2 \times 10^{-3}$ (LHS) and $K_c = 1000$, $B_c = -1$, $A_c = 2 \times 10^{-3}$ (RHS) [A. 7]
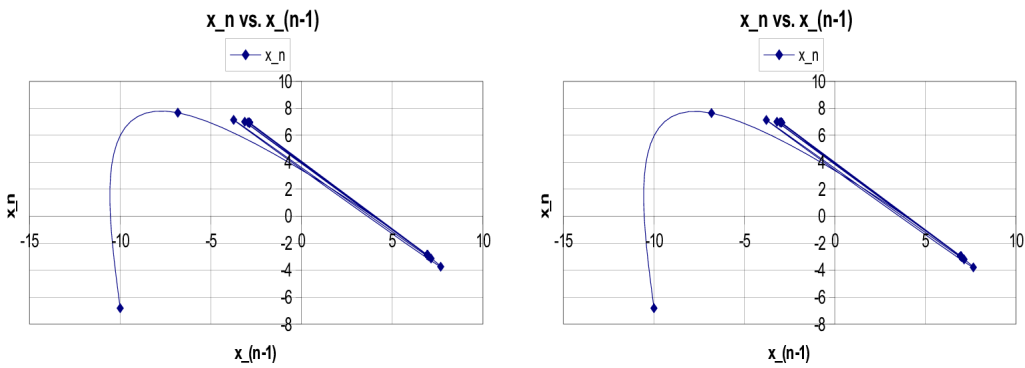
Figure 4.22: Phase trajectory of the bounded chattering for $\frac{df}{dr} > 0$ systems: $K_c = -1000$, $B_c = 1$, $A_c = 2 \times 10^{-3}$ (LHS) and $K_c = 1000$, $B_c = -1$, $A_c = 2 \times 10^{-3}$ (RHS) [A. 7]
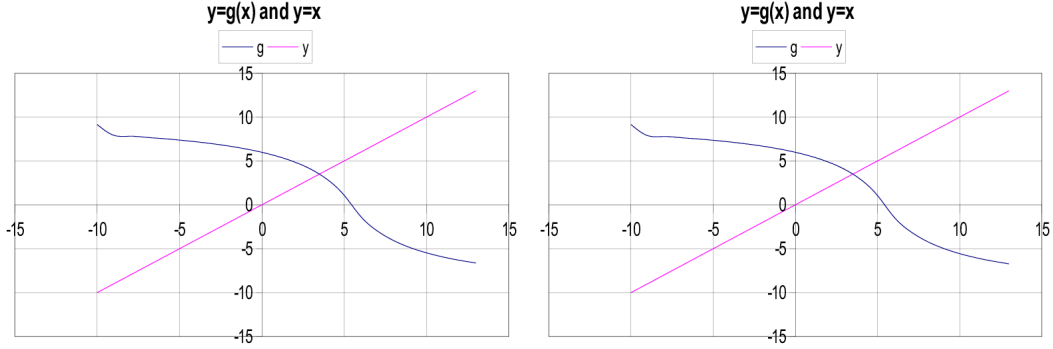
Figure 4.23: Function shapes for the bounded chattering for $\frac{df}{dr} > 0$ systems: $K_c = -1000$, $B_c = 1$, $A_c = 2 \times 10^{-3}$ (LHS) and $K_c = 1000$, $B_c = -1$, $A_c = 2 \times 10^{-3}$ (RHS) [A. 7]

It can clearly be seen that the limitation by the parameter $0 < K_s \ll |K_c|$ conserves the formation of emerging fluctuation in the control signal r_n. In the case of a digital controller working in control cycles for a $0 < \tilde{\beta} < 1$ *"forgetting factor"* the quantity yielding positive contribution for monotone variation and negative one for fluctuating signals

$$B_{n+1} = \tilde{\beta} B_n + (r_{n-2} - r_{n-1})(r_{n-1} - r_n) \tag{4.6}$$

easily can be observed and utilized for properly tuning A_c. The tuning process can be initiated from a small initial value and A_c can be kept slowly increasing until B_n approaches a small positive B_{thr} *threshold value*. Following that it can be kept decreasing until B_n becomes greater than B_{thr}. In the sequel simulations will be presented that reveal the applicability of this approach for a strongly nonlinear 1 DoF physical system [A. 7].

4.3   Simulations for a 1 DoF Nonlinear System

The system model applied is a combination of the van der Pol oscillator [69] and a nonlinear spring of limited force described by the equation [A. 7]

$$m\ddot{q} + k\tanh\left(\frac{q}{w}\right) + b\left(q^2 - d\right)\dot{q} = F \tag{4.7}$$

with $k = 1$, $b = 2$, $m = 5$, $w = 5$, $d = 2$, and F denotes the control force. The *approximate model* of this system was a common damped spring as

$$\hat{m}\ddot{q} + \hat{k}q + \hat{b}\dot{q} = F \tag{4.8}$$

with the parameters $\hat{m} = 1$, $\hat{b} = 20$, $\hat{k} = 10$. The kinematically prescribed trajectory tracking was $\ddot{q}^{Des} = \ddot{q}^N + 2\Lambda\left(\dot{q}^N - \dot{q}\right) + \Lambda^2\left(q^N - q\right)$ with $\Lambda = 6/s$. The adaptive control parameters were as follows: $B_c = 1$, $K_c = -2000$, $K_s = 100$, $\tilde{\beta} = 0.5$, the cycle time was 1 ms. A_c was either kept constant or kept tuned according to the rule [A. 7]:

$$A_c(n+1) = \begin{cases} A_c(n) - 3\Delta A_c \ if \ B(n) \leq B_{thr} \\ A_c(n) + \Delta A_c \ otherwise \end{cases} \tag{4.9}$$

with $\Delta Ac = 10^{-6}$ and $B_{thr} = 10^{-2}$. Figure 4.24 well exemplifies the effects of introducing adaptivity. In the phase trajectories belonging to the fixed $A_c = 5 \times 10^{-3}$ value the traces of certain fluctuations can be revealed. In Fig. 4.25 these oscillations can be well observed in details in the case of the fixed A_c value.

It can well be seen that the *adaptively deformed* signal (blue line in the graphs) is drastically different to the *desired* one (black line), and the *realized* signal (red line) is in the close vicinity of the desired values. Furthermore, tuning of A_c considerably reduced the fluctuation in the applied (deformed) signal. Figure 4.26 reveals that A_c really adaptively varied and the tracking error remained moderate [A. 7].
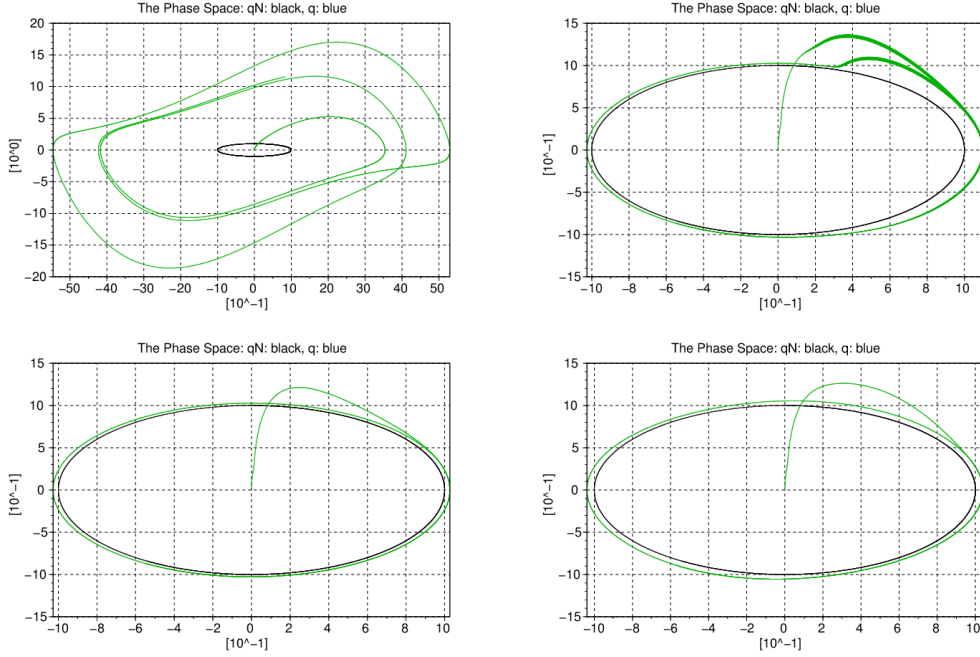
Figure 4.24: The phase trajectories for the *non-adaptive motion* (upper left), the adaptive motion with fixed $A_c = 5 \times 10^{-3}$ without any limitation by K_s (upper right), the effect of limitation with $K_s = 100$ without tuning (lower left), and the limitation with $K_s = 100$ and simultaneous tuning of A_c (lower right) [A. 7]
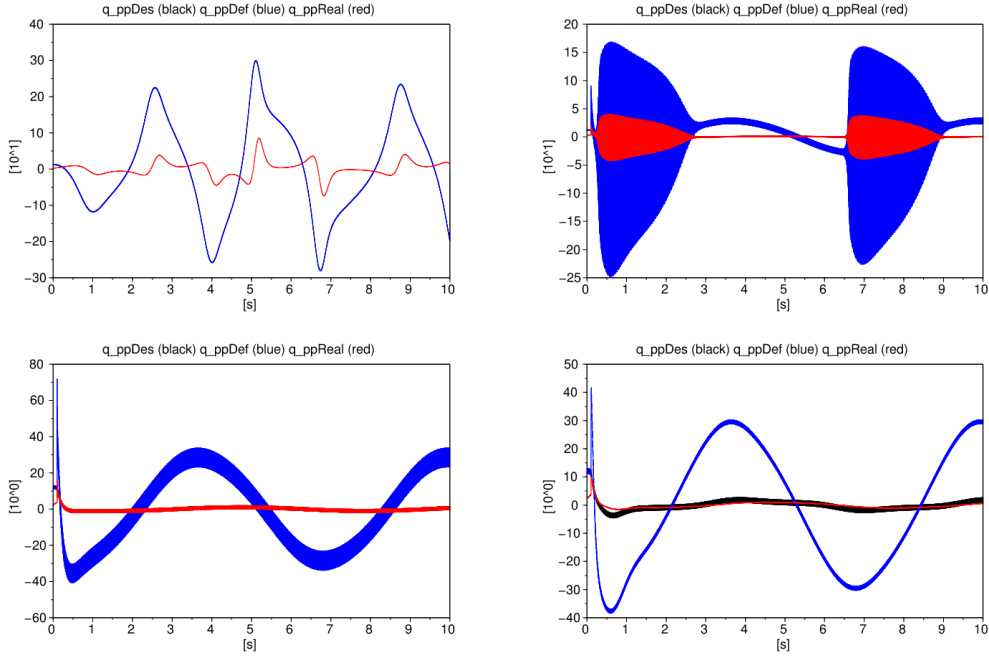
Figure 4.25: The kinematically calculated "*desired*", the *adaptively deformed*, and the *realized $\ddot{q}$* signal for the *non-adaptive motion* (upper left), the adaptive motion with fixed $A_c = 5 \times 10^{-3}$ without any limitation by K_s (upper right), the effect of limitation with $K_s = 100$ without tuning (lower left), and the limitation with $K_s = 100$ and simultaneous tuning of A_c (lower right) [A. 7]
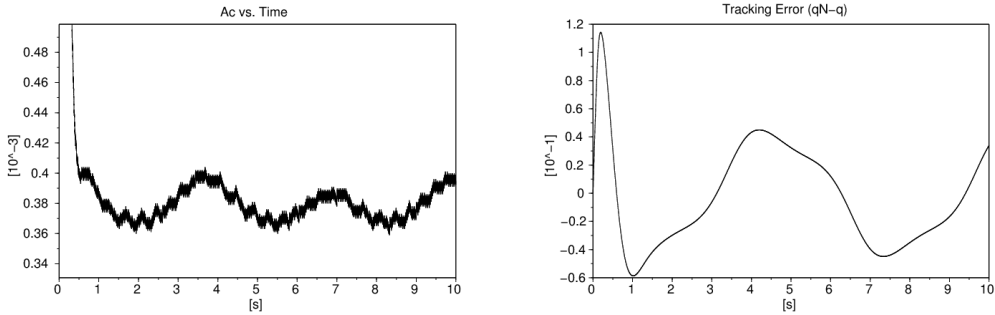
Figure 4.26: The variation of the tuned A_c parameter and the trajectory tracking error in the case of limitation with $K_s = 100$ [A. 7]

MODIFICATIONS FOR THE ORIGINAL RFPT BASED CONTROL

5.1 Tuning of the applied sigmoid function

5.1.1 The Sigmoid Function

The sigmoid function must produce output between ± 1 with the restrictions that $\sigma(0) = 0$, $\frac{d\sigma}{dx}|_{x=0} = 1$ [70]. For sigmoid function now the following construction was used (5.1) [A. 8]:

$$\sigma := \begin{cases} -1 \ if \ x < -\varepsilon \\ \frac{x}{\varepsilon}; if \ -\varepsilon \leq x \leq \varepsilon \\ 1 \ if \ x > \varepsilon \end{cases} \tag{5.1}$$

This choice differs from the originally used sigmoids that the restriction $\frac{d\sigma}{dx}|_{x=0} = 1$ not necessarily is met. In this manner the width of the unsaturated region is not uniquely determined by parameter A_c so the introduction of this new parameter ε introduces new possibilities in the design [A. 8].

5.1.2 Fine Tuning Results

The results are compared with the previous ones taken from subsection 3.1.4 [A. 1] (the model of the system is same as used in that subsection), where $\sigma(x) := \frac{x}{1+|x|}$ was in use. If $\varepsilon = 1$ the function in (5.1) produces results that are very similar to that obtained by the original sigmoid function. In the here presented simulations the option $\varepsilon = 2.4$ was chosen. Finding a balance between smoothness and precision, parameter $\varepsilon = 1.6$ was chosen. The trajectories were approximately the same, just small differences are in the that look like that of the original case the original case was a bit more precise Fig. 5.1,5.2 [A. 8].
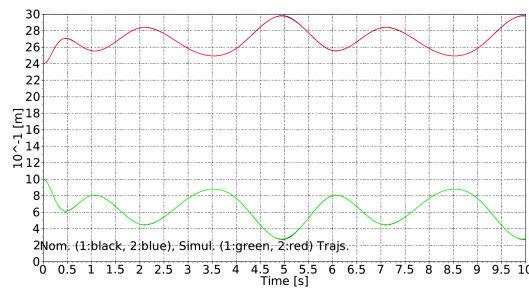
Figure 5.1: Trajectories for the truncated linear system ($\varepsilon = 2.4$) [A. 8]
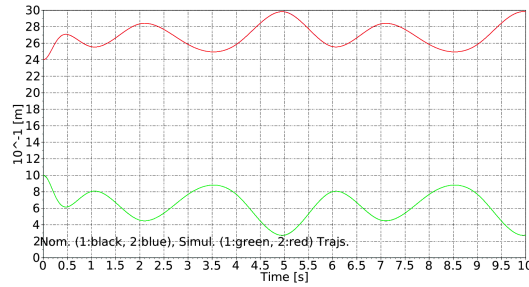
Figure 5.2: Trajectories for the original case, taken from [A. 1]

It can be noted that the *phase trajectories* are a bit better in the original case.
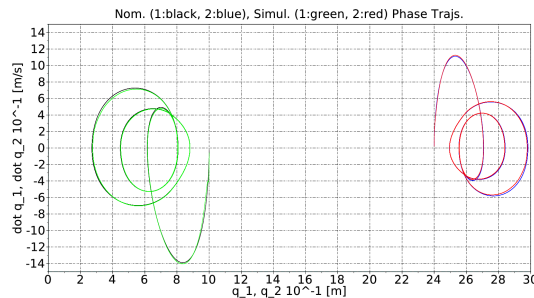
Figure 5.3: Phase trajectories for the truncated linear system ($\varepsilon = 2.4$)
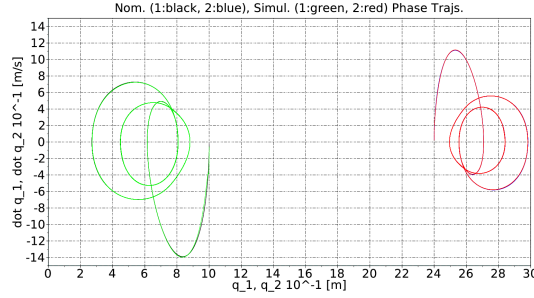
Figure 5.4: Phase trajectories for the original case, taken from [A. 1]

The exerted force was approximately the same for both the $\varepsilon = 2.4$ and the original case, because the same masses were moved along almost the same paths.
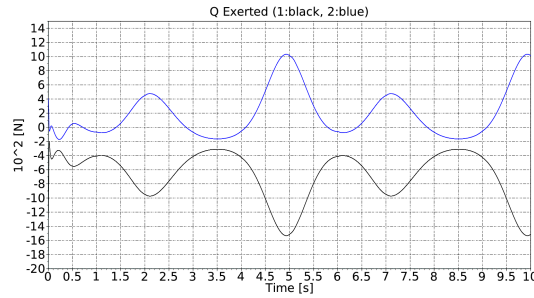
Figure 5.5: Exerted force (Q) for the truncated linear system ($\varepsilon = 2.4$) [A. 8]
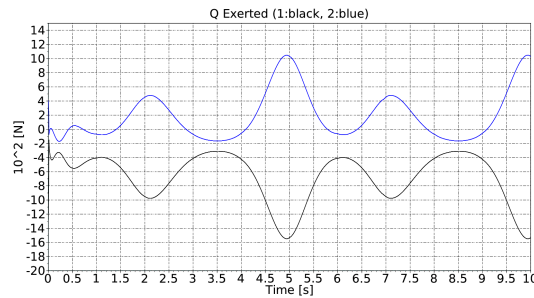
Figure 5.6: Exerted force (Q) for the original case, taken from [A. 1]

The accelerations of the original system were a bit more precise then that belonging to the truncated linear function with $\varepsilon = 2.4$.
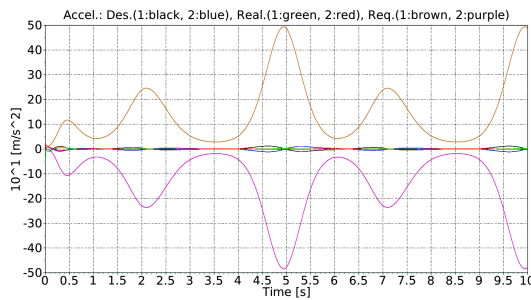
Figure 5.7: Accelerations for the truncated linear system ($\varepsilon = 2.4$) [A. 8]
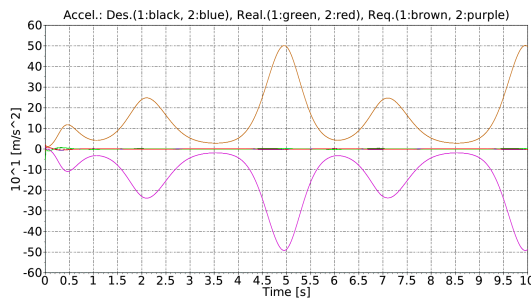
Figure 5.8: Accelerations for the original case, taken from [A. 1]
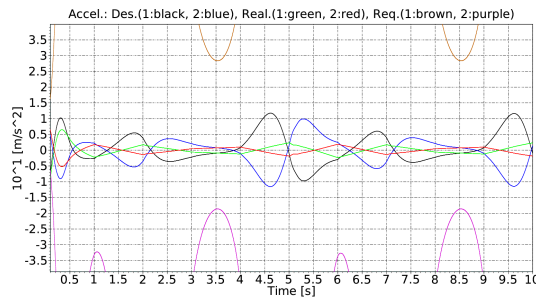
Figure 5.9: Accelerations for the truncated linear system (zoomed) ($\varepsilon = 2.4$) [A. 8]
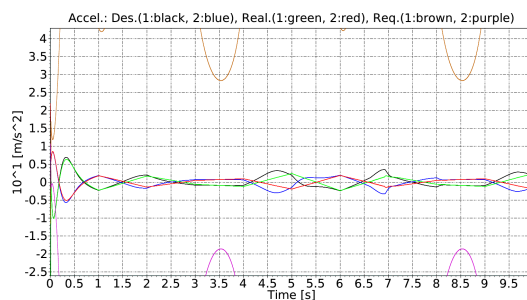
Figure 5.10: Accelerations for the original case (zoomed), taken from [A. 1]

The tracking error was smaller in the original system than that of the truncated linear system, but it was acceptable difference for that case.
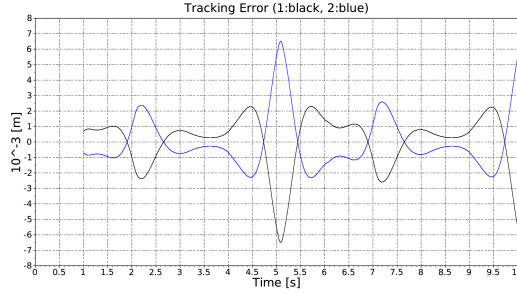
Figure 5.11: Tracking error for the truncated linear system ($\varepsilon = 2.4$) [A. 8]

In the simulations the kinematically designed trajectory tracking policy was deduced from the prescription
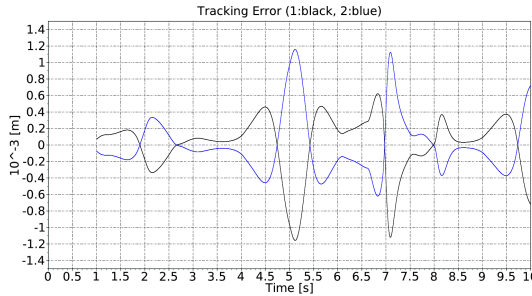
Figure 5.12: Tracking error for the original case, taken from [A. 1]

The variation of the *voting weights* were much more smoother in the case of the truncated linear system than in the original case. It means that the controller works much smoother [A. 8].
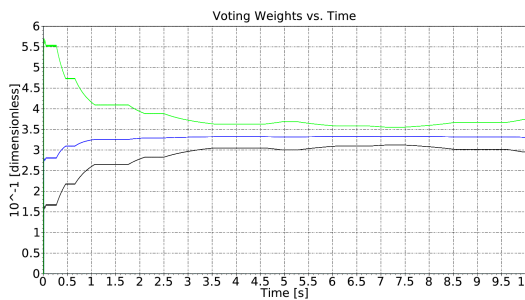
Figure 5.13: Voting weights for the truncated linear system ($\varepsilon = 2.4$) [A. 8]
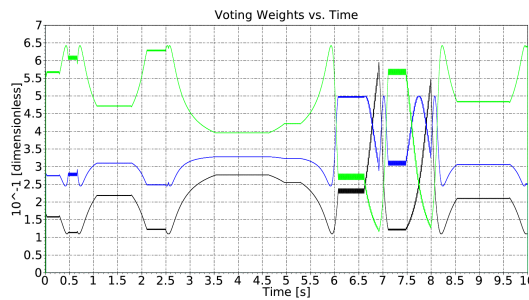
Figure 5.14: Voting weights for the original case, taken from [A. 1]

The response error is better in the original system, but the difference is in the acceptable range.
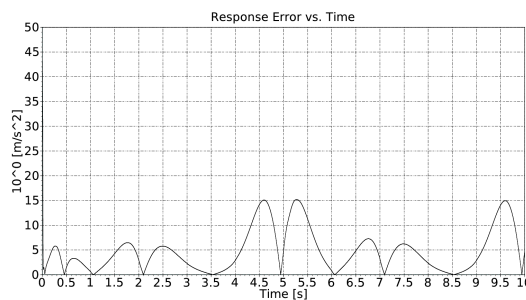
Figure 5.15: Response error for the truncated linear system ($\varepsilon = 2.4$) [A. 8]
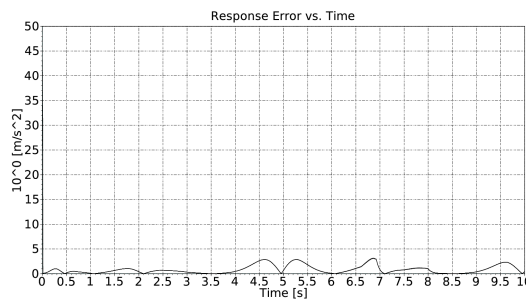
Figure 5.16: Response error for the original case, taken from [A. 1]

The "*Required Accelerations*" (i.e. the adaptively distorted ones) were approximately same for both cases.
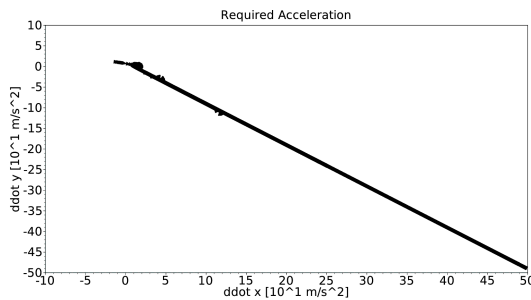
Figure 5.17: The "Required Acceleration" for the truncated linear system ($\varepsilon = 2.4$) [A. 8]
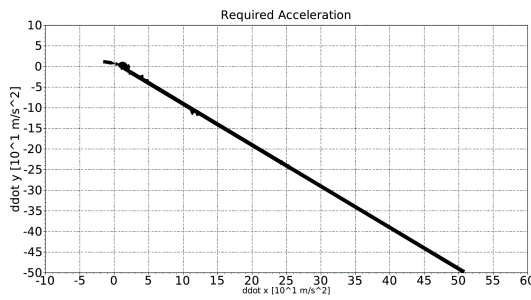
Figure 5.18: The "Required Acceleration" for the original case, taken from [A. 1]

The response error was higher than in the original case, but it is less when truncated linear sigmoid function with parameter $\varepsilon = 2.4$ applied.
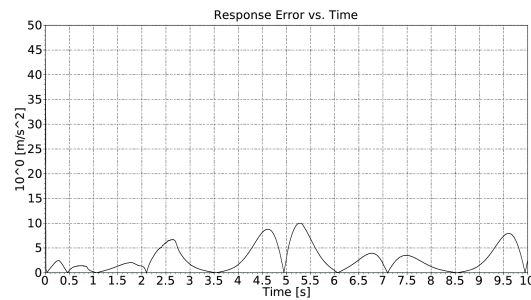
Figure 5.19: Response error for the truncated linear system ($\varepsilon = 1.6$) [A. 8]

The tracking error was higher than in the original case, but it was less when truncated linear sigmoid function with parameter $\varepsilon = 2.4$ was applied.
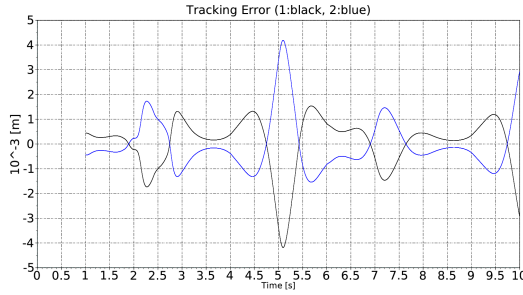
Figure 5.20: Tracking error for the truncated linear system ($\varepsilon = 1.6$) [A. 8]

The variation of the voting weights was much smoother than in the original case, but the truncated linear function with parameter $\varepsilon = 2.4$ yielded smoother result.
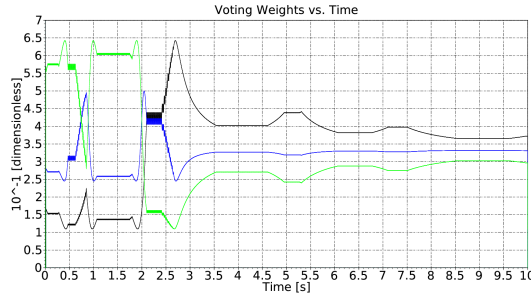
Figure 5.21: Voting weights for the truncated linear system ($\varepsilon = 1.6$) [A. 8]

The results show that by sacrificing some precision a controller can be obtained that works smoother than the original one [A. 8].

5.1.3   Simulation for TORA system using Fine Tuning method

The model of the TORA system was described in subsection 4.1.1.

In the simulations the kinematically designed trajectory tracking policy was deduced from the prescription resulting in a PID-type trajectory tracking with $\Lambda = 10\frac{m}{s}$ [A. 9].

In Figs. 5.22-5.25 the results obtained by the non-adaptive controller are described. It worths noting that in the non-adaptive case no any adaptive deformation exists therefore the "desired" and the "exerted" torque values are exactly the same. On this reason in Fig. 5.24 the black line is exactly covered by the red one, and the green one is hidden by the ocher line [A. 9].

The adaptive settings was $K_c = 10^4$, $B_c = -1$, $A_c ini = 10^{-7}$. The initial parameters was $v_+ = 10^{-4}$, $F_t hr = 0.0001$, $c_v = 6$ and $\beta = 0.1$. Since the figure of the trajectory tracking does not reveal observable details the results obtained for the operation of the adaptive MRAC controller are described in Figs. 5.26-5.32Comparison of Figs. 5.23 and 5.26immediately reveals the significant improvement in the trajectory tracking. According to Figs. 5.24 and 5.27it can be stated that the necessary torque signals were of the same order of magnitude in the adaptive and the non-adaptive cases, however, the adaptive case worked with smaller signals and in Fig. 5.27 the formation of the "precursor oscillations" can well be identified in coincidence with the negative values of the forgetting integral. (Certain excerpts are better described in Fig.5.30.) The motion of the actively driven axle shows only little differences (Figs. 5.25 and 5.31) . The disappearance of the precursor oscillations is also in coincidence with the fast reduction of the tuned parameter Ac (consider Figs. 5.28 and 5.31) [A. 9].

The formation of the "MRAC illusion" can well be traced in Fig. 5.29that reveals the control torques in the interval that contains the instant in which the adaptation was switched on (at t=0.2 s): the "desired" and the "adaptively deformed" lines that are identical in the non-adaptive session are splitted at this moment and the "recalculated" lines well approach the "desired" ones and considerably differ from the "exerted" ones in the adaptive session [A. 9].

To make a comparison the simulations were made for the same setting for the originally used sigmoid function $\sigma(x) \overset{def}{=} \frac{x}{1+|x|}$. The results are given in Figs. 5.33 and 5.34 that are the counterparts of Figs. 5.26 and 5.27 . No significant differences can be revealed between the appropriate charts.as it can be seen in Figs. 5.32 and 5.35 [A. 9].
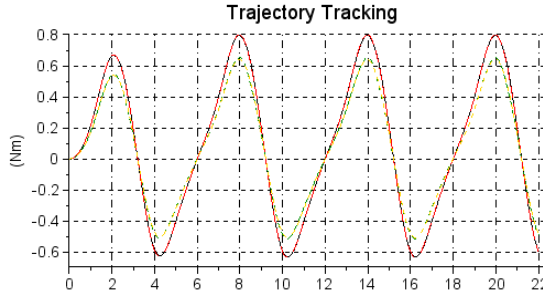
Figure 5.22: The trajectory tracking of the non-adaptive controller using the reference model: [$q_2(rad)$: black solid, $q_3(m)$: green dashed, $q_2^{Nom}(rad)$: red dash dot, $q_3^{Nom}(m)$: ocher long dashdot lines]. [A. 9]
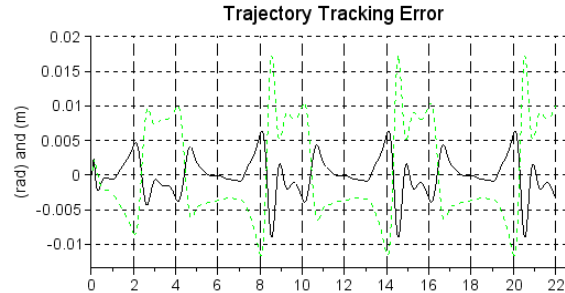
Figure 5.23: The trajectory tracking error of the non-adaptive controller using the reference model: [$q_2(rad)$: black solid, $q_3(m)$: green dashed lines]. [A. 9]
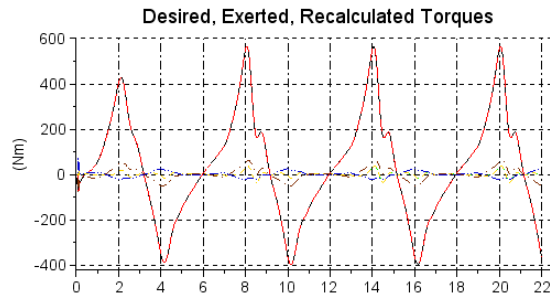
Figure 5.24: The generalized forces for the non-adaptive controller versus time in s units [Q_1^{Des}: black solid, $Q_1^{Exerted}$: red dash dot, Q_1^{Rec}: brown bigdash dot, and Q_2^{Des}: green dashed, $Q_2^{Exerted}$: ocher long dash dot, Q_2^{Rec} : dark blue bigdash longdash lines in Nm units]. [A. 9]
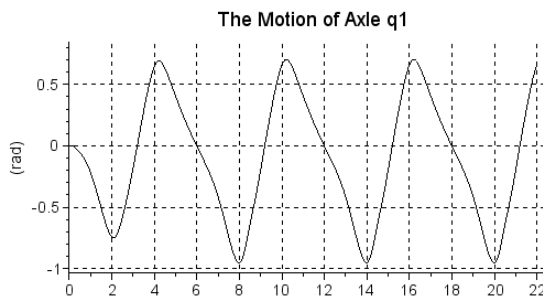
Figure 5.25: The motion of the actively driven axis $[q_1 : rad]$ vs. time in s units. [A. 9]
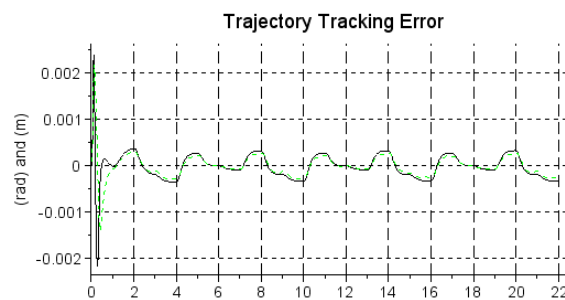
Figure 5.26: The trajectory tracking error of the adaptive MRAC controller using the reference model: $[q_2(rad)$: black solid, $q_3(m)$: green dashed lines]. [A. 9]
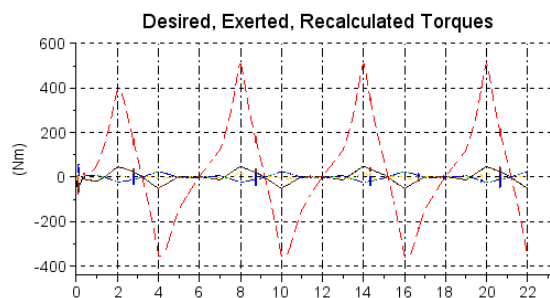
Figure 5.27: The generalized forces for the adaptive MRAC controller versus time in s units $[Q_1^{Des}$: black solid, $Q_1^{Exerted}$: red dash dot, Q_1^{Rec} : brown bigdash dot, and Q_2^{Des} : green dashed, $Q_2^{Exerted}$: ocher long dash dot, Q_2^{Rec} : dark blue bigdash longdash lines in Nm units]. [A. 9]
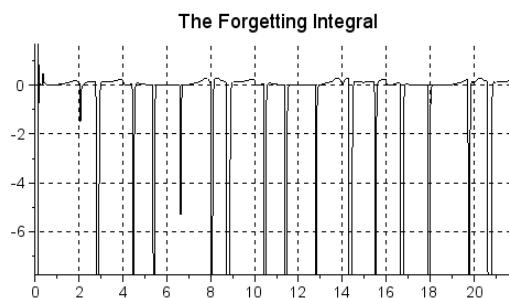
Figure 5.28: The forgetting integral for the adaptive MRAC controller. [A. 9]
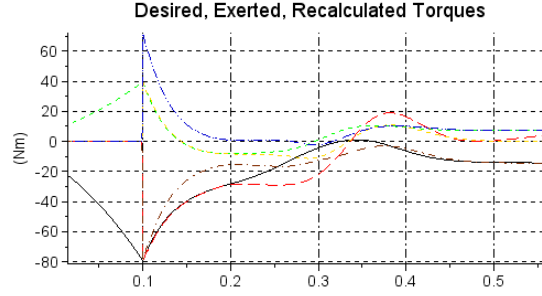
Figure 5.29: The generalized forces for the adaptive MRAC controller versus time in s units when the adaptivity is turned on at $t = 0.2$ [Q_1^{Des} : black solid, $Q_1^{Exerted}$: red dash dot, Q_1^{Rec} : brown bigdash dot, and Q_2^{Des} : green dashed, $Q_2^{Exerted}$: ocher long dash dot, Q_2^{Rec} : dark blue bigdash longdash lines in Nm units]. [A. 9]
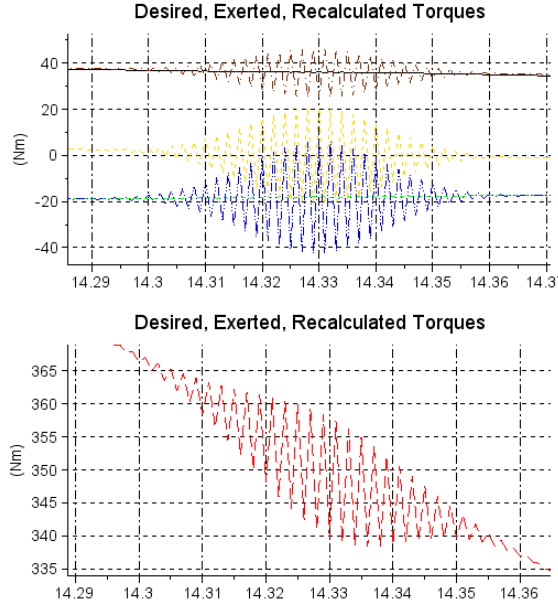
Figure 5.30: The generalized forces for the adaptive MRAC controller versus time in s units: zoomed excerpt exemplifying the details of formation of the "precursor oscillations" about $t = 14.33s$ [Q_1^{Des} : black solid, $Q_1^{Exerted}$: red dash dot, Q_1^{Rec} : brown bigdash dot, and Q_2^{Des} : green dashed, $Q_2^{Exerted}$: ocher long dash dot, Q_2^{Rec} : dark blue bigdash longdash lines in Nm units]. [A. 9]
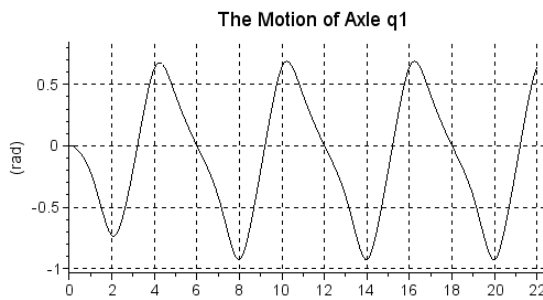
Figure 5.31: The motion of the actively driven axis in the case of the adaptive MRAC controller [q_1 : rad] vs. time in s units. [A. 9]
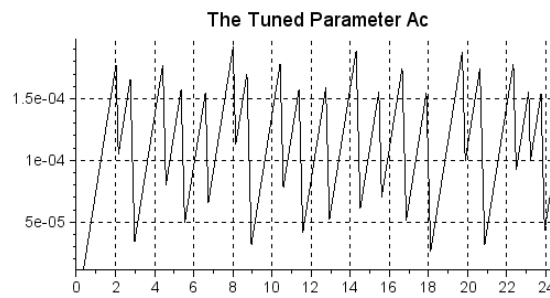
Figure 5.32: The tuned parameter A_c in the case of the adaptive MRAC controller vs. time in s units. [A. 9]
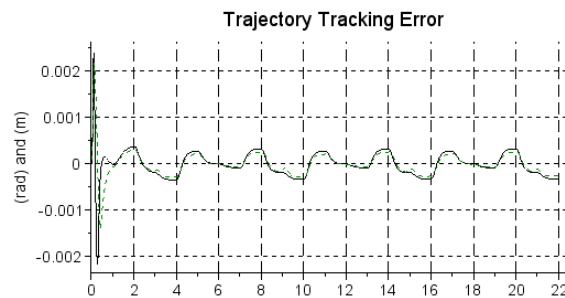
Figure 5.33: The trajectory tracking error of the adaptive MRAC controller using the reference model and the original sigmoid function: [$q_2(rad)$: black solid, $q_3(m)$: green dashed lines]. [A. 9]
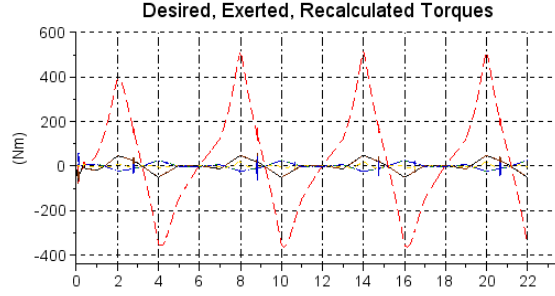
Figure 5.34: The generalized forces for the adaptive MRAC controller using the original sigmoid function versus time in s units [Q_1^{Des} : black solid, $Q_1^{Exerted}$: red dash dot, Q_1^{Rec} : brown bigdash dot, and Q_2^{Des} : green dashed, $Q_2^{Exerted}$: ocher long dash dot, Q_2^{Rec} : dark blue bigdash longdash lines in Nm units]. [A. 9]
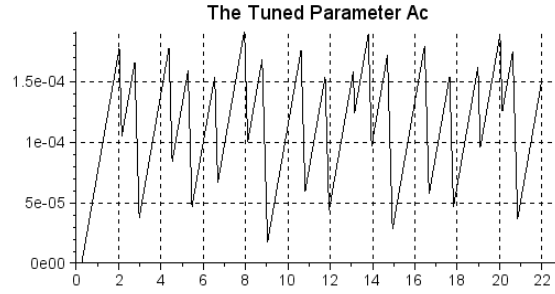
Figure 5.35: The tuned parameter A_c in the case of the adaptive MRAC controller vs. time in s units with the original sigmoid function. [A. 9]

5.2 Combination with the Luenberger observer

The simple LTI described in Isidori's book on nonlinear control systems [71] starts with the investigation of the "*Linear Time-Invariant (LTI)*" systems of the form

$$\dot{x} = Ax + Bu,$$
$$y = Cx$$
(5.2)

in which A is a constant real matrix of size $n \times n$, B is also a constant real matrix of size $n \times m$ ($0 \leq m \leq n$), u of size $m \times 1$ is the array of the control signals, and C is a constant real matrix of size $k \times n$ ($k \leq n$), and y is the *directly measurable quantity* (it is assumed that the components of x are not immediately observable. The possession of the "system model" means that we have exact information on matrices A, B, and C. If these matrices have explicit time-dependence through the parameters of the system we have "*Linear Parameter Varying (LPV)*" systems. If these matrices also depend on time through certain components of the state variable x the system is categorized as "*Quasi-Linear Parameter-Varying (qLPV)*". This latter concept was found to be very fruitable since with the combination of the "*Tensor Product (TP)*" model and the "*Higher Order Singular Value Decomposition (HOSVD)*" it allowed the utilization of the results obtained for linear controllers via solving linear matrix inequalities (e.g. [72], [68]) [A. 10].

Our model is a *nonlinear oscillator* having the exact equations of motion as [A. 10]

$$\ddot{q} = -kq - b\dot{q} - c\dot{q}^2 + u$$
(5.3)

in which $k > 0$ is a spring stiffness constant, $b > 0$ describes viscous friction, and $c > 0$ corresponds to the coefficient of the drag force while moving in e.g. air or water. This latter term makes the system's dynamics nonlinear. For the controller design the linear approximation of (6.14) is applied as [A. 10]

$$\ddot{q} = -kq - b\dot{q} + u \qquad (5.4)$$

for which a linear design is possible as follows. The formal state-space model can be constructed by the introduction of the state variable $x := [x_1, x_2]^T = [q, \dot{q}]^T$ leading to the reformulation of the *approximate model* as [A. 10]

$$\begin{bmatrix} \dot{x}_1 \\ \dot{x}_2 \end{bmatrix} = \begin{bmatrix} 0 & 1 \\ -k & -b \end{bmatrix} \begin{bmatrix} x_1 \\ x_2 \end{bmatrix} + \begin{bmatrix} 0 \\ 1 \end{bmatrix} u \qquad (5.5)$$

that corresponds to (5.2) with $A = \begin{bmatrix} 0 & 1 \\ -k & -b \end{bmatrix}$ and $B = \begin{bmatrix} 0 \\ 1 \end{bmatrix}$ and a one dimensional control signal $u \in \mathfrak{Re}$. It is worthy of note that in the "*Adaptive Inverse Dynamics*" and the "*Adaptive Slotine-Li Robot Controller*" [15] a similar step is done with the aim of obtaining a Lyapunov equation that contains the appropriate matrix A [A. 10].

If the task is to trace a *nominal trajectory* $x^N(t) := [q^N(t), \dot{q}^N(t)]^T$, in the possession of the exact model and the state variable x the following feedback rule could be introduced: $Bu^N(t) := \dot{x}^N(t) - Ax^N(t)$ [A. 10]:

$$\begin{bmatrix} 0 \\ u^N \end{bmatrix} = \begin{bmatrix} \dot{x}_1^N \\ \dot{x}_2^N \end{bmatrix} - \begin{bmatrix} 0 & 1 \\ -k & -b \end{bmatrix} \begin{bmatrix} x_1^N \\ x_2^N \end{bmatrix} \qquad (5.6)$$

leading to $u^N = kx_1^N + bx_2^N$ without any contradiction since $\dot{x}_1^N = x_2^N$. This term can be completed by an *error-feedback* as $Bu(t) = Bu^N(t) + B[K_1, K_2](x^N(t) - x(t))$ in which K_1 and K_2 are *feedback gains* in $K := [K_1, K_2]$. In this manner the following equations of motion can be obtained [A. 10]:

$$\dot{x} = Ax + Bu^N + BK(x^N(t) - x(t)),$$
$$\dot{x}^N = Ax^N + Bu^N \Rightarrow \qquad (5.7)$$
$$\frac{d}{dt}(x^N - x) = (A - BK)(x^N - x)$$

with $A - BK = \begin{bmatrix} 0 & 1 \\ -k - K_1 & -b - K_2 \end{bmatrix}$. In this simple case the $x \to x^N$ convergence can be guaranteed by the simple method of *Pole Placement* i.e. by prescribing the spectrum of $A - BK$ in the following manner [A. 10]:

$$\det(A - BK - \lambda I) = (\lambda - \lambda_1)^2 \Rightarrow$$
$$\lambda^2 + \lambda(b + K_2) + k + K_1 = \lambda^2 - 2\lambda_1\lambda + \lambda_1^2 \qquad (5.8)$$

yielding $K_1 = \lambda_1^2 - k$ and $K_2 = -b - 2\lambda_1$ with $\mathfrak{Re} \ni \lambda_1 < 0$.

If we assume that only x_1 can directly be observed the $y = [1, 0][x_1, x_2]^T = x_1$ rule is valid with $C = [1, 0]$ in (5.2), i.e. we need one derivation as [A. 10]

$$\begin{bmatrix} y \\ \dot{y} \end{bmatrix} = \begin{bmatrix} [1, 0][x_1, x_2]^T \\ [1, 0][\dot{x}_1, \dot{x}_2]^T \end{bmatrix} = \begin{bmatrix} x_1 \\ \dot{x}_1 \end{bmatrix} = \begin{bmatrix} x_1 \\ x_2 \end{bmatrix} \qquad (5.9)$$

therefore our complete set of equations will be

$$\dot{x} = Ax + Bu^N + BK(x^N - \hat{x}),$$
$$\dot{\hat{x}} = A\hat{x} + Bu^N + BK(x^N - \hat{x}) + L(x - \hat{x}) \qquad (5.10)$$

since the feedback is realized instead of x by $\hat{x}$. For the *state estimation error* $e := x - \hat{x}$ this yields [A. 10]

$$\frac{d}{dt}e = Ae - Le = (A - L)e. \tag{5.11}$$

For the convergence $\hat{x} \to x$ the spectrum of $A - L$ must be properly set. Here L denotes the feedback gain of the *Luenberger Observer* [73] [A. 10].

If L is only a scalar then this spectrum is determined by the characteristic polynomial's roots that is by the solutions of the equation [A. 10]

$$\det \begin{bmatrix} -L - \mu & 1 \\ -k & -b - L - \mu \end{bmatrix} = 0 \tag{5.12}$$

yielding $\mu^2 + (b + 2L)\mu + L(b + l) + k = 0$, therefore $\mu_{1,2} = \frac{-b - 2L \pm \sqrt{(b+2L)^2 - 4L(b+L) - 4k}}{2}$, that is $\mu_{1,2} = \frac{-b - 2L \pm \sqrt{b^2 - 4k}}{2}$, so $\Re\mu_{1,2} < -L < 0$ if $L > 0$, therefore the $\hat{x} \to x$ convergence is granted for $L > 0$. In the sequel the operation of this control designed for the linear approximation of the model is investigated for the nonlinear system. It is expected that for small coefficient c it can work well but after transcending a limit for c the controller may become unstable. Before providing simulation results the adaptive completion of this controller by the use of the RFPT transformations [A. 10].

In the present context no complementary parameter tuning was necessary. In the "role" of the *desired response* $\ddot{q}$ that is the response of the approximate linear model was placed. The control signals were so deformed that the response of the nonlinear system well approximated that of the linear system. The nominal trajectory to be tracked was a third order spline function of time. The parameters were set as follows: $k = 100$, $b = 10$ for the model, $\lambda_1 = -12$, $L = 24$, $K_c = 10^6$, $B_c = -1$, $A_c = 10^{-6}$ [A. 10].

Figure 5.36 demonstrates the operation of the Luenberger observer in the non-adaptive control for the exactly linear case in which $c = 0$. It well corresponds to the theoretical expectations. Tis non-adaptive controller worked for $c = 3$ (Fig. 6.56) but for higher values of c it was found to be divergent (this corresponds to the limits of the linear design) [A. 10].
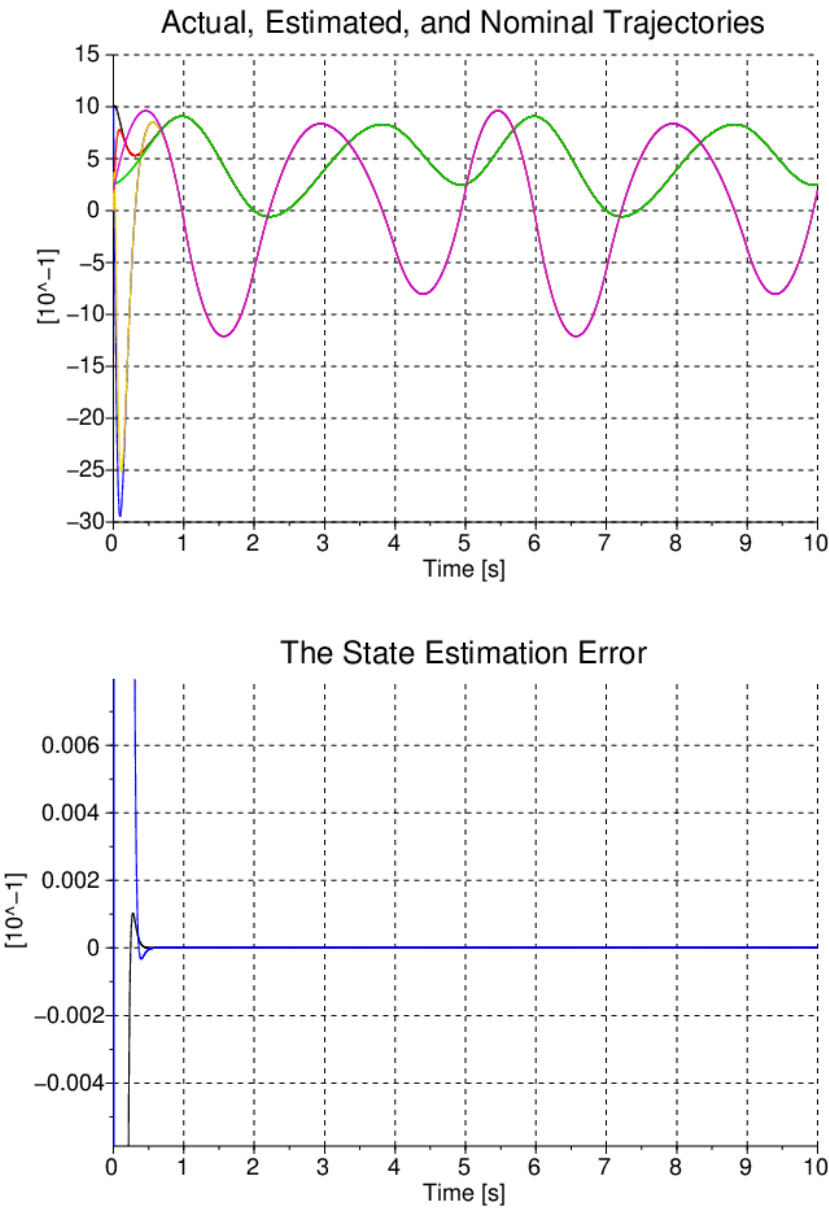
Figure 5.36: The operation of the non-adaptive Luenberger observer for the exactly linear system model: *trajectory tracking* (top: x_1: black, x_2: blue, $\hat{x}_1$: red, $\hat{x}_2$: ocher, x_1^N: green, x_2^N: purple lines) and the *state estimation error* (bottom) versus time in [s] units [A. 10]

Actual, Estimated, and Nominal Trajectories

The State Estimation Error
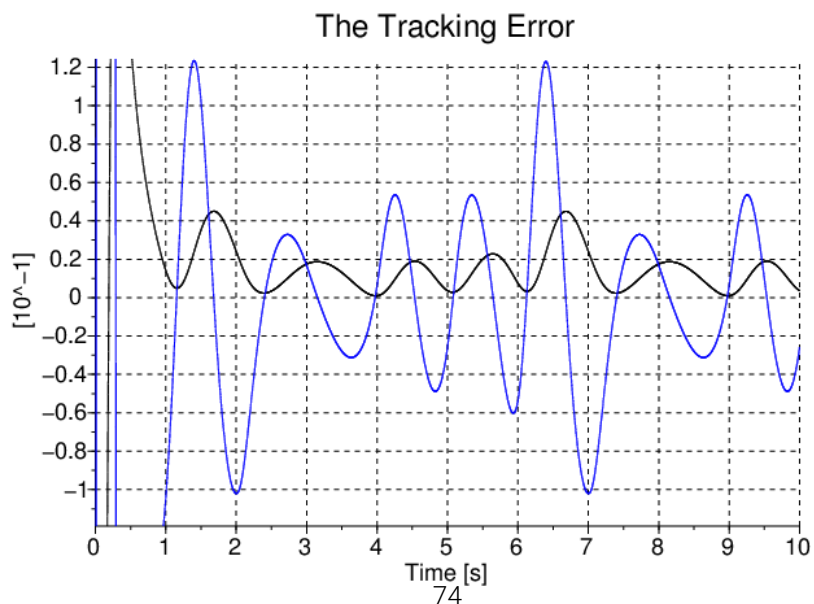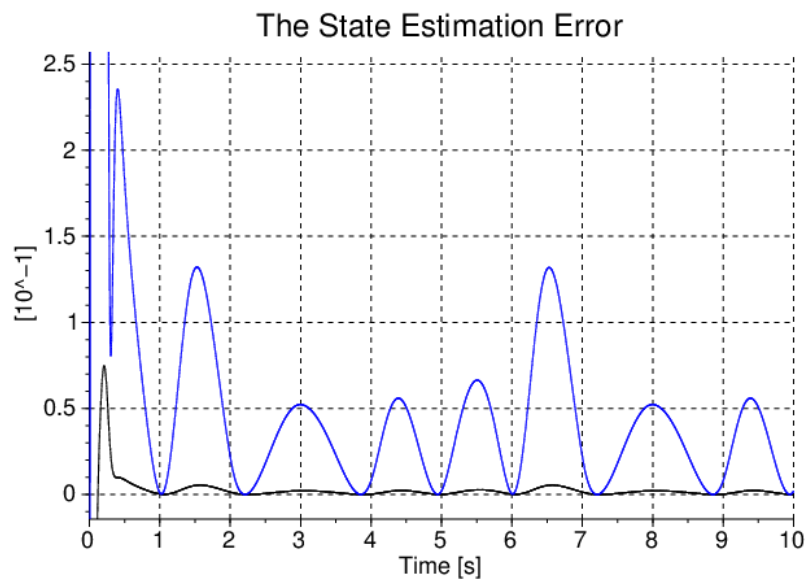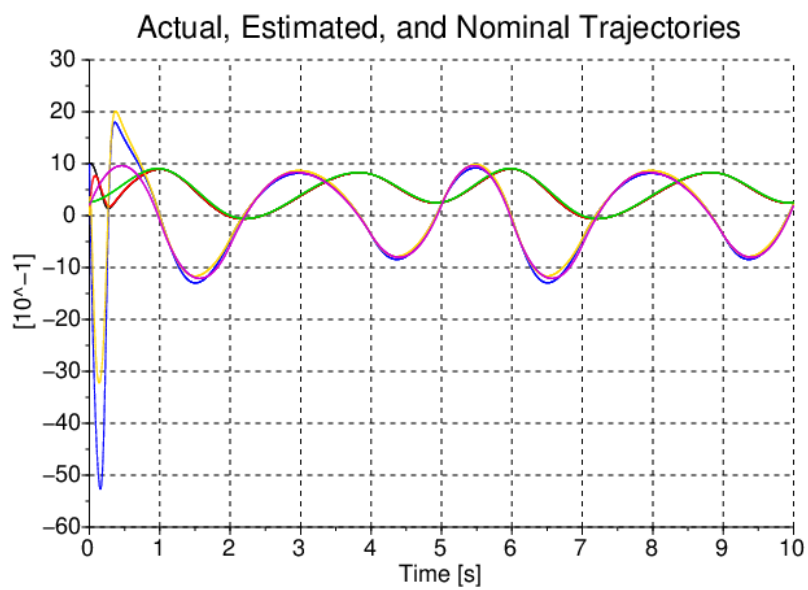
The Tracking Error

The adaptive counterpart of Fig. 6.56 is Fig. 5.38. The precision of the state estimation as well as that of the trajectory tracking were evidently improved [A. 10].

The State Estimation Error
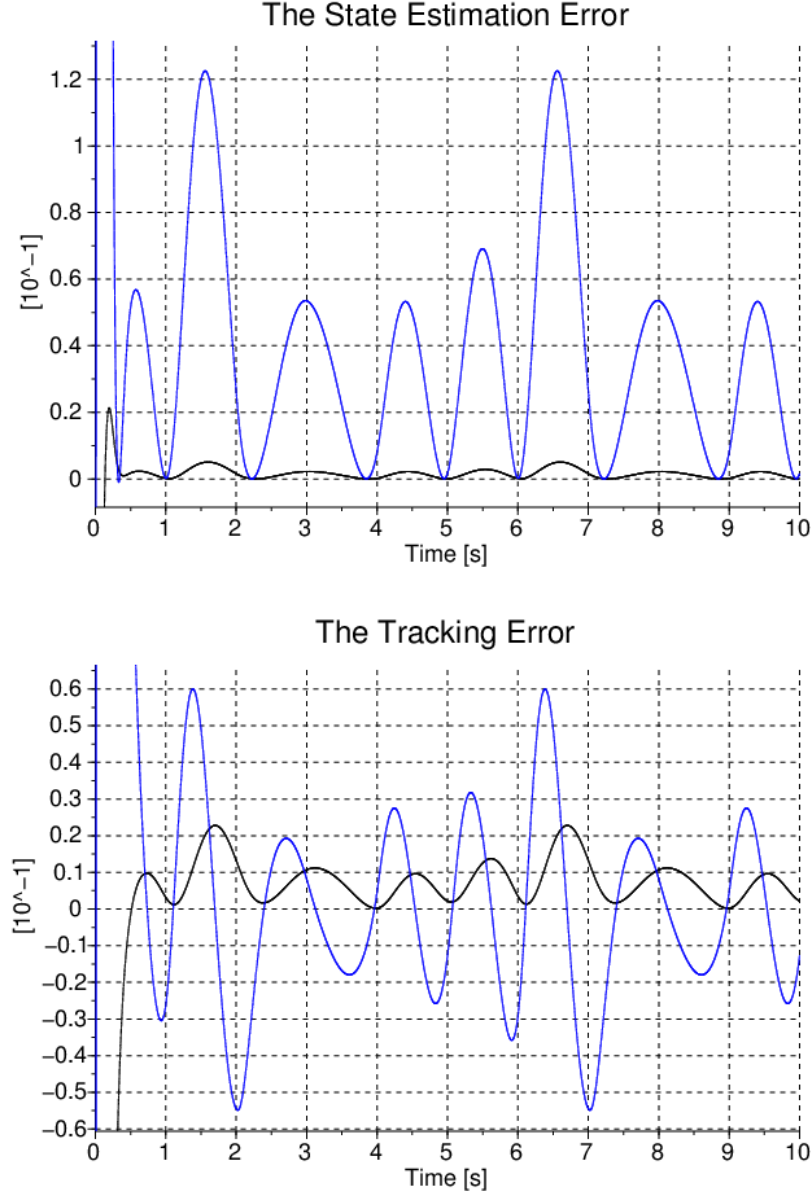
The Tracking Error

Figure 5.38: The operation of the adaptive Luenberger observer for the modeling inaccuracy belonging to $c = 3$: the state estimation error (top), and tracking error (bottom) [black line for x_1, and blue line for x_2] versus time in [s] units [A. 10]

The adaptive version was able to realize the control till $c = 6$ (Fig. 5.39). The differences between the adaptive and non-adaptive control signals for $c = 3$ and $c = 6$ are given in Fig. 5.40. In Fig. 5.41 the control signals are described. It is worthy of note that the relative differences are small. However, if the fact is taken into account that the integral of the control signal is accumulated in time the significance of this little difference can well be understood [A. 10].
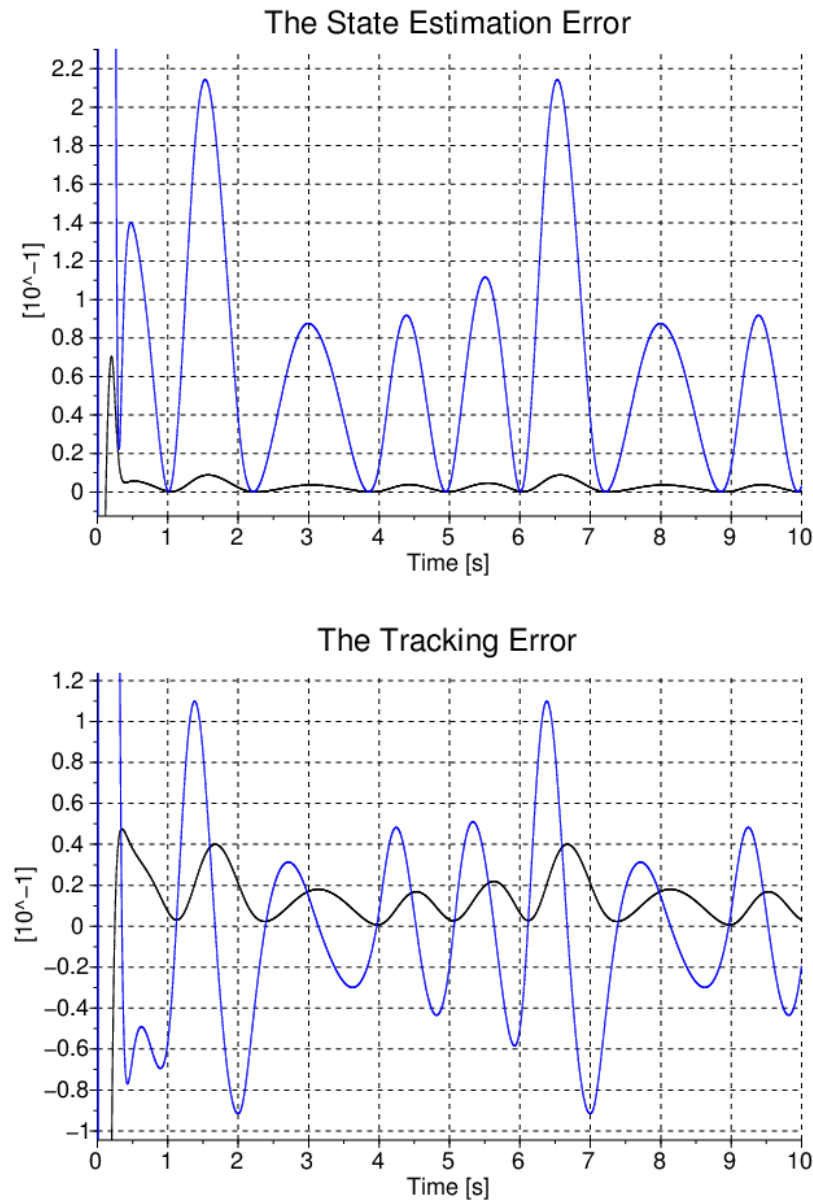
Figure 5.39: The operation of the adaptive Luenberger observer for the modeling inaccuracy belonging to $c = 6$: the state estimation error (top), and tracking error (bottom) [black line for x_1, and blue line for x_2] versus time in [s] units [A. 10]
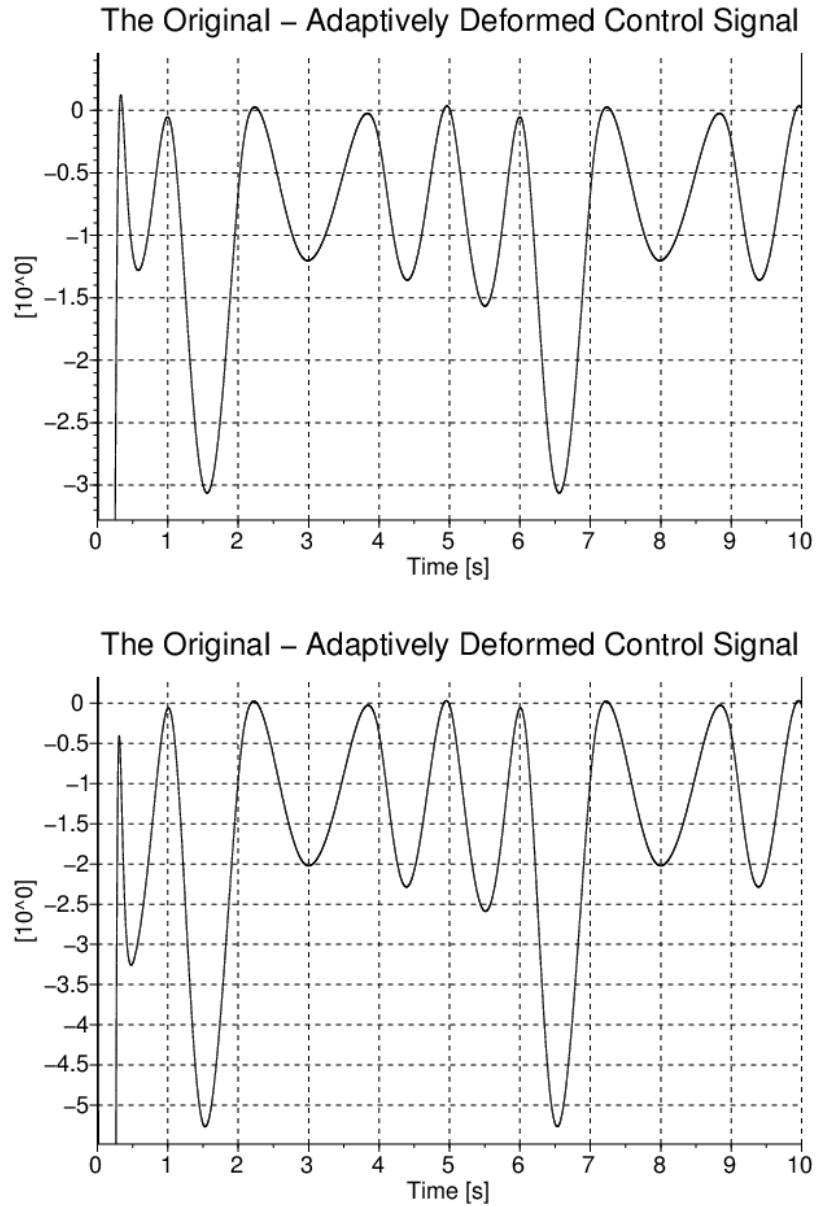
Figure 5.40: The difference between the non-adaptive (black line) and adaptive (blue line) control signals for $c = 3$ (top), and $c = 6$ (bottom) versus time in $[s]$ units [A. 10]
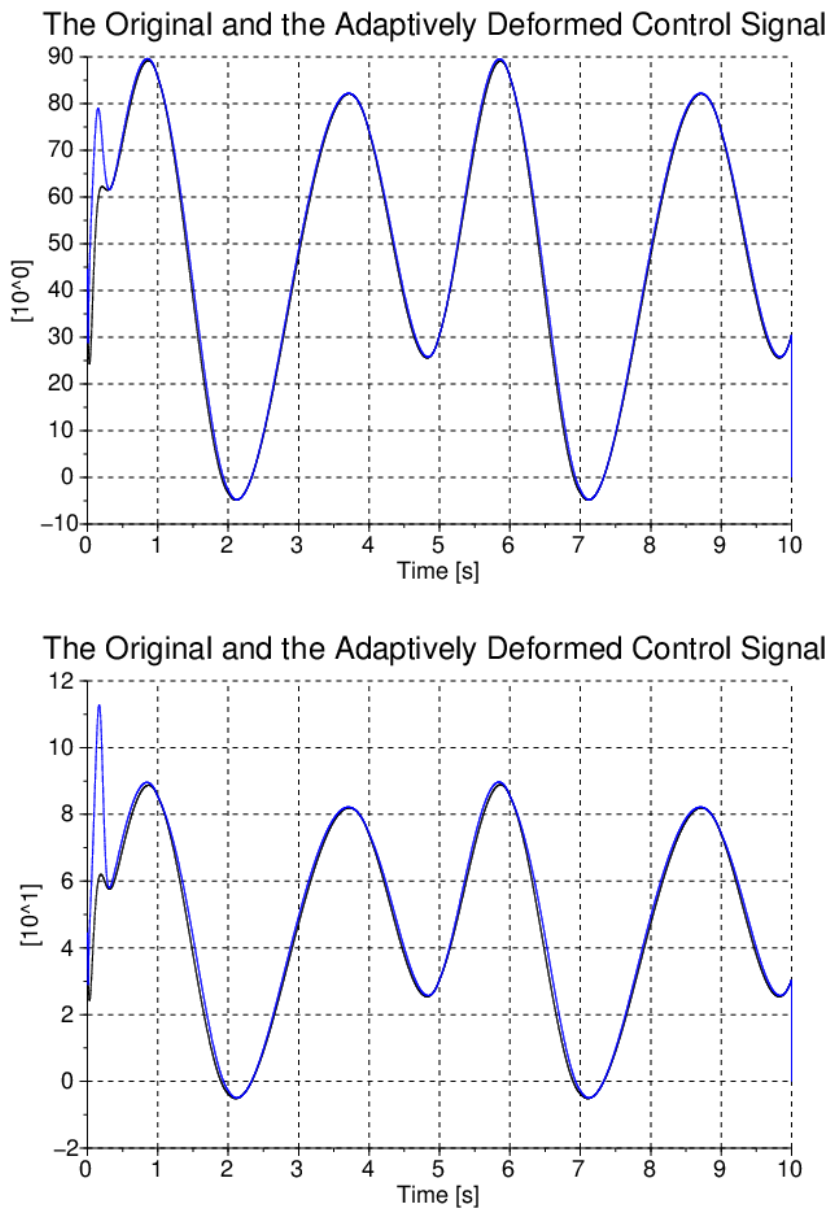
Figure 5.41: The non-adaptive (black line) and adaptive (blue line) control signals for $c = 3$ (top), and $c = 6$ (bottom) versus time in $[s]$ units [A. 10]

CHAPTER 6

NOVEL APPLICATIONS OF THE FIXED POINT TRANSFORMATION BASED ADAPTIVE CONTROLLERS

6.1 Applications in control of the small airplane motion and airplane components

6.1.1 Adaptive control of aeroelastic wing component

The schematic picture of the aeroelastic wing model is given Fig. 6.1 while its equations of motion are defined in Eq. 6.1 citePrime:2010. The parameters of the wing can be completed with that of the actuator system that results in certain "effective" values given in the following list: $m_h = 6.516[kg]$, $m_\alpha = 6.7[kg]$, $m_\beta = 0.537[kg]$ masses, $x_\alpha = 0.21$ (non-dimensional), $x_\beta = 0.233[m]$ distance values, $r_\beta = 0[m]$, $a = 0.673$ non-dimensional distance from the mid-chord to the elastic axis, $b = 0.1905[m]$ semi-chord of the wing, $I_\alpha = 0.126[kg \times m^2]$, $I_\beta = 10^5[kg \times m^2]$, $c_h = 27.43[N \times m \times s/rad]$ the plunge structural damping coefficient, $c_\alpha = 0.215[N \times m \times s/rad]$ the pitch structural damping coefficient, $c_{\beta servo} = 4.182 \times 10^4[N \times m \times s/rad]$ trailing-edge structural damping coefficient, $k_h = 2844[N/m]$ plunge structural spring constant, $k_{\beta servo} = 7.6608 \times 10^{-3}[N \times m/rad]$ spring constant, $ = 1.225[kg/m^3]$ air density, $C_{l\alpha} = 6.757$ the aerofoil coefficient of lift about the elastic axis, $C_{m\alpha eff} = 1.17$, $C_{l\beta} = 3.774$, $C_{m\beta eff} = 2.1$, aerofoil moment coefficients, $S = 0.5945[m]$, and $U = 14.1[m/s]$ free stream velocity. The $k_\alpha(\alpha)$ function describes some nonlinearity in the elastic deformation of the wing and it is given as $k_\alpha(\alpha) = 25.55103.19\alpha + 543.24\alpha^2$ [A. 12].
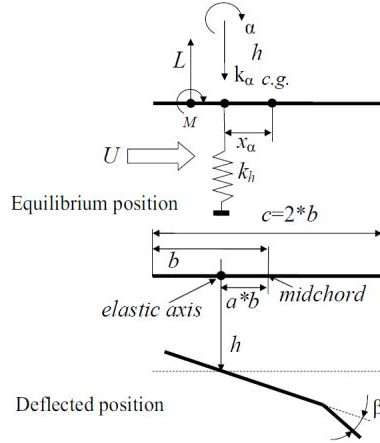
Figure 6.1: Schematic picture of the aeroelastic wing model (taken from [74])

$$
\begin{pmatrix}
m_h + m_\alpha + m_\beta & m_\alpha x_\alpha b + m_\beta x_\beta + m_\beta r_\beta & m_\beta r_\beta \\
m_\alpha x_\alpha b + m_\beta x_\beta + m_\beta r_\beta & I_\alpha + I_\beta + m_\beta r_\beta^2 + 2 x_\beta m_\beta r_\beta & I_\beta + x_\beta m_\beta r_\beta \\
m_\beta r_\beta & I_\beta + x_\beta m_\beta r_\beta & I_\beta
\end{pmatrix}
\begin{pmatrix} \ddot{h} \\ \ddot{\alpha} \\ \ddot{\beta} \end{pmatrix} +
$$

$$
+ \begin{pmatrix}
c_h + \rho b S C_{l\alpha} U & (0.5 - a) b \rho b S C_{l\alpha} U & 0 \\
-\rho b^2 S C_{m\alpha eff} U & c_\alpha - (0.5 - a) b \rho b^2 S C_{m\alpha eff} U & 0 \\
0 & 0 & c_{\beta servo}
\end{pmatrix}
\begin{pmatrix} \dot{h} \\ \dot{\alpha} \\ \dot{\beta} \end{pmatrix} +
$$

$$
+ \begin{pmatrix}
k_h & \rho b S C_{l\alpha} U^2 & \rho b S C_{l\beta} U^2 \\
0 & k_\alpha(\alpha) - \rho b^2 S C_{m\alpha eff} U^2 & -\rho b^2 S C_{m\beta eff} U^2 \\
0 & 0 & k_{\beta servo}
\end{pmatrix}
\begin{pmatrix} h \\ \alpha \\ \beta \end{pmatrix}
= \begin{pmatrix} 0 \\ 0 \\ k_{\beta servo} \end{pmatrix} u
\tag{6.1}
$$

For the development of a realistic controller we cannot use the exact structure of Eq. 6.1 with approximate parameters, since we cannot assume that besides $d^2\beta/dt^2$ the other accelerations as d^2h/dt^2 and $d^2\alpha/dt^2$ are also measurable since due to the (3,1) and (3,2) elements of the inertia matrix (the multiplier of d^2q/dt^2 in Eq. 6.1) their contribution appears in u. It may be a more realistic assumption that no any measurable information we have on h and α but we have information only on $\beta, d\beta/dt$, and $d^2\beta/dt^2$. This situation can simply be modeled if instead of Eq. 6.1 we use the even more rough approximation of the model as given in Eq. 6.2 [A. 11].

$$
\begin{pmatrix}
m_h + m_\alpha + m_\beta & m_\alpha x_\alpha b + m_\beta x_\beta + m_\beta r_\beta & m_\beta r_\beta \\
m_\alpha x_\alpha b + m_\beta x_\beta + m_\beta r_\beta & I_\alpha + I_\beta + m_\beta r_\beta^2 + 2 x_\beta m_\beta r_\beta & I_\beta + x_\beta m_\beta r_\beta \\
0 & 0 & I_\beta
\end{pmatrix}
\begin{pmatrix} \ddot{h} \\ \ddot{\alpha} \\ \ddot{\beta} \end{pmatrix} +
$$

$$
+ \begin{pmatrix}
c_h + \rho b S C_{l\alpha} U & (0.5 - a) b \rho b S C_{l\alpha} U & 0 \\
-\rho b^2 S C_{m\alpha eff} U & c_\alpha - (0.5 - a) b \rho b^2 S C_{m\alpha eff} U & 0 \\
0 & 0 & c_{\beta servo}
\end{pmatrix}
\begin{pmatrix} \dot{h} \\ \dot{\alpha} \\ \dot{\beta} \end{pmatrix} +
$$

$$
+ \begin{pmatrix}
k_h & \rho b S C_{l\alpha} U^2 & \rho b S C_{l\beta} U^2 \\
0 & k_\alpha(\alpha) - \rho b^2 S C_{m\alpha eff} U^2 & -\rho b^2 S C_{m\beta eff} U^2 \\
0 & 0 & k_{\beta servo}
\end{pmatrix}
\begin{pmatrix} h \\ \alpha \\ \beta \end{pmatrix}
= \begin{pmatrix} 0 \\ 0 \\ k_{\beta servo} \end{pmatrix} u
\tag{6.2}
$$

Formally the equations is the same, both for adaptive and MRAC cases, but the containing elements are different. In adaptive case the parameters $I_{\beta Approx} = 0.8 \times I_\beta, c_{\beta servo Approx} = 0.8 \times c_{\beta servo}, k_{\beta servo Approx} = k_{\beta servo}$ was chosen. In MRAC case $I_{\beta Ref} = 2 I_\beta, c_{\beta servo Ref} = 1.1 c_{\beta servo}, and k_{\beta servo Ref} = k_{\beta servo}$ was chosen.

The simulation parameters in adaptive case was: $P = 1000[1/s^2], I = 200[1/s^3]$ and $D = 0$ were

chosen with $B = 1, K = 10^6$, and $A = 1.25 \times 10^6$. The simulation parameters in MRAC case was: $P = 1000[1/s^2], I = 200[1/s^3]$ and $D = 0$ were chosen with $B = 1, K = 10^6$, and $A = 5 \times 10^7$

6.1.1.1 Simulation results

The RFPT case:
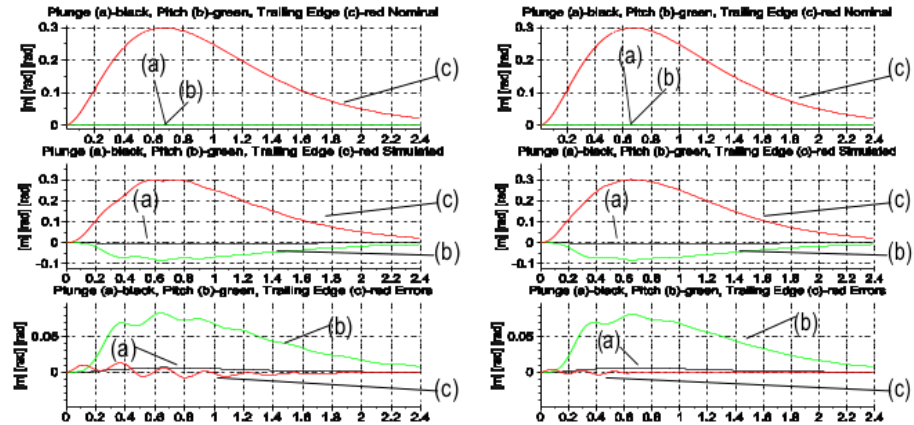
Figure 6.2: Trajectory tracking of a simple PI-type (proportional, integral feedback controller) without adaptation (LHS) and with RFPT-based iterative adaptive improvement (RHS): the nominal trajectories (upper charts), the simulated trajectories (middle charts), and the tracking error (lower charts) versus time in [s] [A. 11]
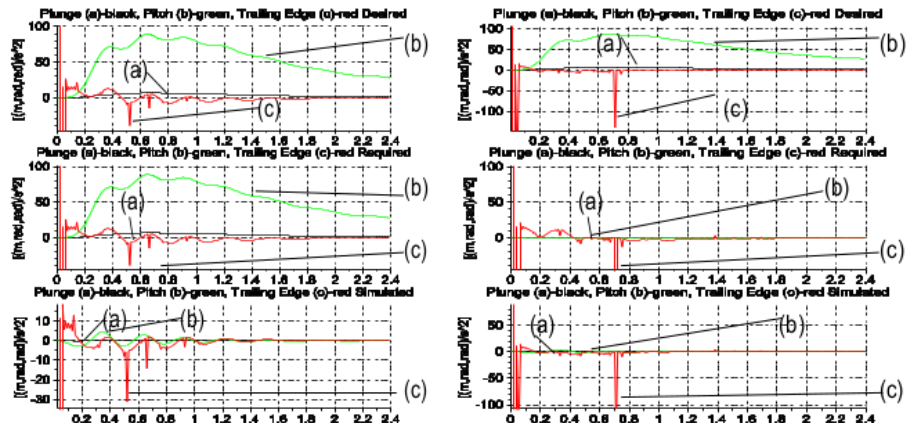
Figure 6.3: The second time-derivatives of a simple PI-type (proportional, integral feedback controller) without adaptation (LHS) and with RFPT-based iterative adaptive improvement (RHS): the desired values (upper charts), the adaptively deformed "required" values (middle charts), and the simulated values (lower charts) versus time in [s] [A. 11]
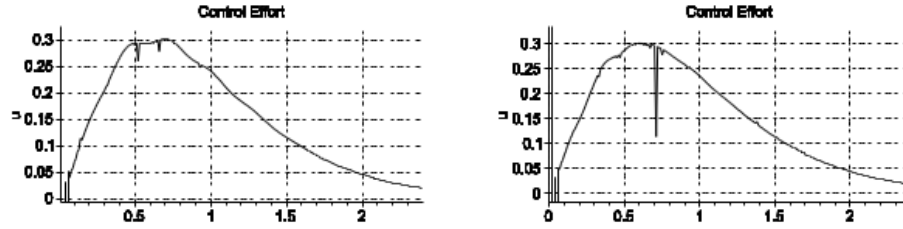
Figure 6.4: The control action versus time in [s] for a simple PI-type (proportional feedback controller) without adaptation (LHS) and with RFPT-based iterative adaptive improvement (RHS) [A. 11]
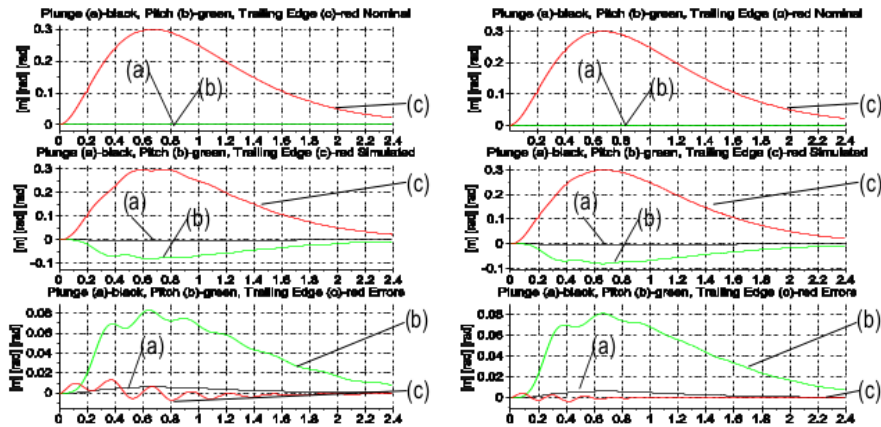
Figure 6.5: Trajectory tracking of a simple P-type (proportional feedback controller) without adaptation (LHS) and with RFPT-based iterative adaptive improvement (RHS) when it has information only on β : the nominal trajectories (upper charts), the simulated trajectories (middle charts), and the tracking error (lower charts) versus time in [s] [A. 11]
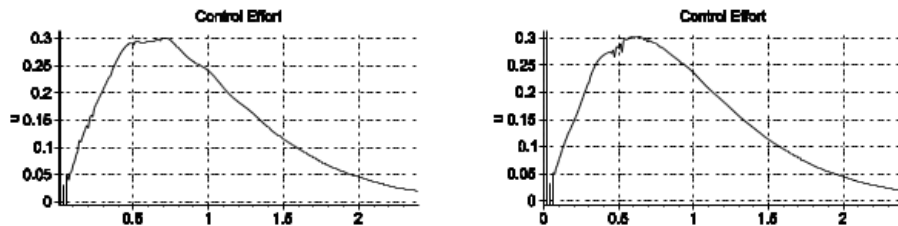
Figure 6.6: The control action versus time in [s] for a simple P-type (proportional feedback controller) without adaptation (LHS) and with RFPT-based iterative adaptive improvement (RHS) when it has information only on β [A. 11]

The appropriate simulation results are given in Figs. 6.2-6.4. In general it is expected that the small integrating contribution of the PI-type controllers well reduces the steady-state errors. In the non-adaptive version the tracking errors shows considerable fluctuation, however, in the adaptive version it can be observed that the swinging is better reduced and damped as in the non-adaptive version, furthermore, the center of swinging in the tracking error signal is shifted to zero while it remains in the negative region in the non-adaptive case [A. 11].

Figures 6.5 and 6.6 belong to the results of the P-type controller with the control parameters $P =$

$1000[1/s^2]$, $I = 0$ and $D = 0$, $B = 1$, $K = 10^6$, and $A = 1.25 \times 10^6$. It can well be seen that by dropping the integrated feedback no very significant differences occur, but in both cases the prescribed adaptive controller successfully reduced the swinging of $\beta(t)$ around $\beta^{Nom}(t)$ [A. 11].

The MRAC case:
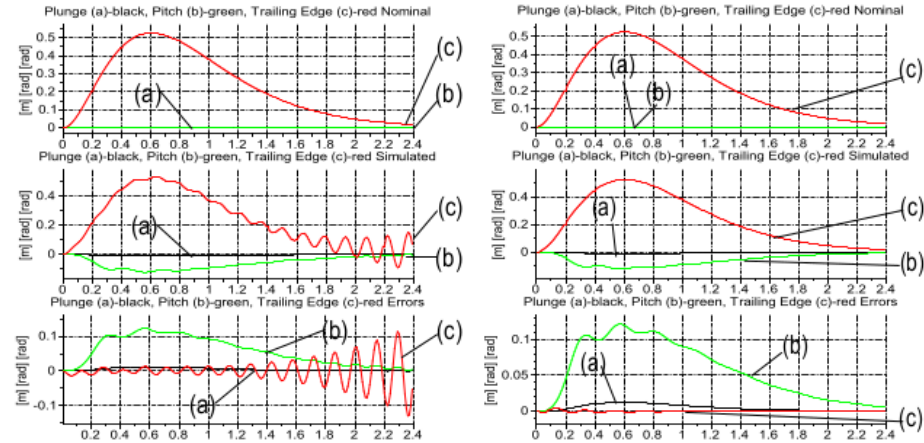
Figure 6.7: Trajectory tracking of a PI-type (proportional, and integral feedback controller) without adaptation (LHS) and with RFPT-based MRAC adaptive improvement (RHS): the nominal trajectories (upper charts), the simulated trajectories (middle charts), and the tracking error (lower charts) versus time in [s] [A. 12]
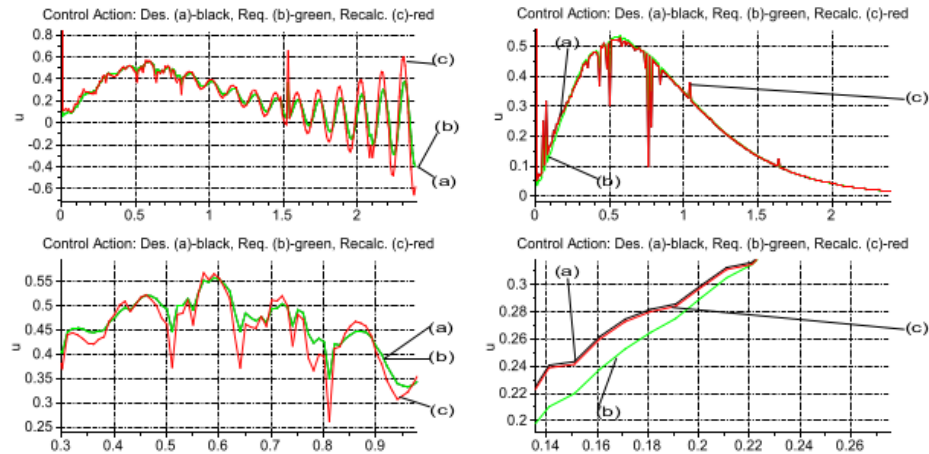
Figure 6.8: The control signals versus time in [s] of a PI-type (proportional, and integral feedback controller) without adaptation (LHS) and with RFPT-based MRAC adaptive improvement (RHS) (upper charts), and zoomed excerpts (lower charts) [A. 12]
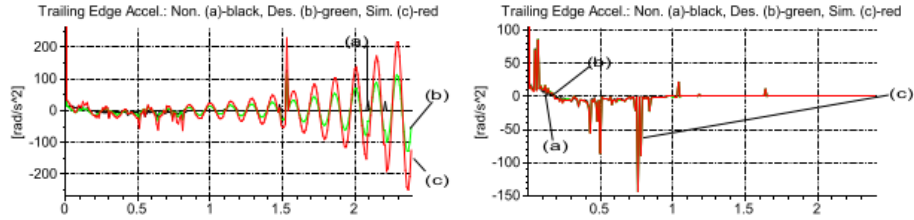
Figure 6.9: The $d^2\beta^{Nom}(t)/dt^2$ (black line), $d^2\beta^{Des}(t)/dt^2$ (green line), and $d^2\beta(t)/dt^2$ (simulated) (red line) signals versus time in [s] of a PI-type (proportional, and integral feedback controller) without adaptation (LHS) and with RFPT-based MRAC adaptive improvement (RHS) [A. 12]
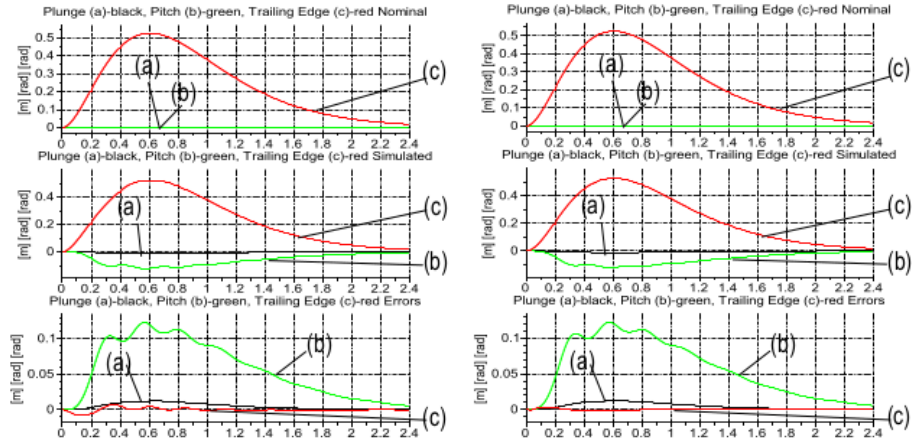
Figure 6.10: Trajectory tracking of a PID-type (proportional, integral, and derivative feedback controller) without adaptation (LHS) and with RFPT-based MRAC adaptive improvement (RHS): the nominal trajectories (upper charts), the simulated trajectories (middle charts), and the tracking error (lower charts) versus time in [s] [A. 12]
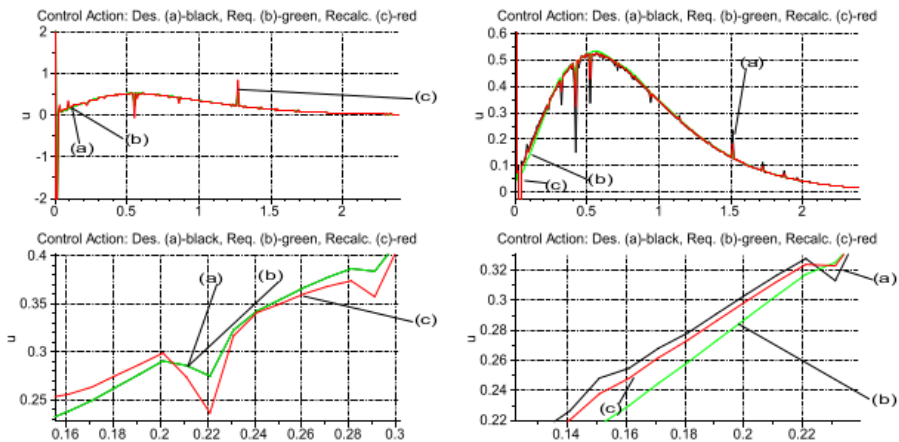
Figure 6.11: The control signals versus time in [s] of a PID-type (proportional, integral, and derivative feedback controller) without adaptation (LHS) and with RFPT-based MRAC adaptive improvement (RHS) (upper charts), and zoomed excerpts (lower charts) [A. 12]
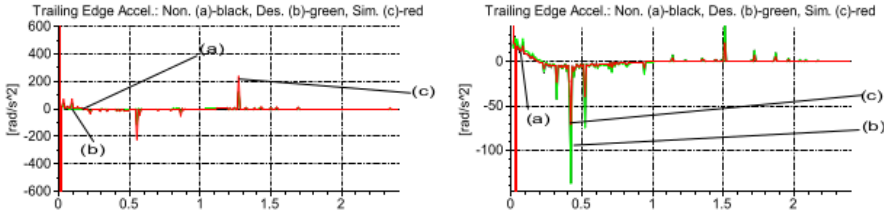
Figure 6.12: The $d^2\beta^{Nom}(t)/dt^2$ (black line), $d^2\beta^{Des}(t)/dt^2$ (green line), and $d^2\beta(t)/dt^2$ (simulated) (red line) signals versus time in [s] of a PID-type (proportional, integral, and derivative feedback controller) without adaptation (LHS) and with RFPT-based MRAC adaptive improvement (RHS) [A. 12]

Figure 6.7 well exemplifies that some swinging in $\beta(t)$ around $\beta^N(t)$ can be observed in both the adaptive and the non-adaptive cases, however, in the adaptive case this swinging is much better damped. The non-adaptive case now is unstable. The excitation of the coupled dynamic degrees of freedom can well be observed in the charts, too [A. 12].

To reveal the significance of adaptivity in Fig. 6.8 the control signals. In the non-adaptive case $u^{Req} \equiv u^{Des}$ therefore the black lines are exactly covered by the green ones, but in the adaptive solution the recalculated red lines are in the close vicinity of the desired black lines and significantly differ from the exerted green lines. This means that the dynamic illusion to be created by the MRAC controller works well: on the basis of purely kinematical considerations and using the reference model the external loop (before the adaptive deformation) calculates a control signal and obtains a realized response from the controlled system that really corresponds to this control action. (It is worthy of note that the jumps in the control signal are produced by the numerical integrator of SCILAB as it works with the time-grid in the integration [A. 12].

Their appearance and positions depend on the numerical integrator chosen, and they never appear if one applies "hand–made" Euler integration in a sequential program.) The precision of the MRAC illusion is very well revealed by Fig. 6.9 that compares the $d^2\beta^{Nom}(t)/dt^2$, $d^2\beta^{Des}(t)/dt^2$, and $d^2\beta(t)/dt^2$ (simulated) values. In the non-adaptive case very drastic PI-corrections are added to $d^2\beta^{Nom}(t)/dt^2$ that is the realized motion is far less smooth than the nominal one. In the adaptive case the three different lines are in each other's close vicinity that means that only very little PI corrections were needed in the kinematic error relaxation design [A. 12].

In the second set of simulations PID-type kinematic error relaxation was prescribed. It was observed that the appearance of the derivative term required far smaller feedback gains for a stable control than a simple PI-type relaxation. The error relaxation strategy $(d/dt + \Lambda)^3 \int [\beta^N(\tau) - \beta(\tau)]d\tau = 0$ was chosen with $\tau = 15[1/s]$ and $B = 1$, $K = 10^3$, and $A = 2.5 \times 10^4$ adaptive control parameters. It can be seen in Fig. 6.10 that adding the derivative term considerably improves the operation of the non- adaptive controller, and the adaptive improvement even better reduces the fluctuation of $\beta(t)$ around $\beta^N(t)$. According to Figs. 6.11 and 6.12 it can be stated that the MRAC illusion was almost perfect again [A. 12].

6.1.2 Control for a small airplane

6.1.2.1 The Linearized Small Airplane Model

The small model airplanes have relatively low velocity and fly with relatively small rotation speed. On this reason their linearized model is widely used for simulation investigations. In [75] a detailed model is given for MATLAB users. I the sequel this model will be used in SCILAB 5.4.0 and XCOS environment for simulations [A. 13].

The linearized model consists of two independent, not coupled subsystems both having the canonical form of LTI models as $\dot{x} = Ax + Bu_c$ with state variable x, state matrix A, control matrix B, and control

signal u_c. In the *longitudinal subsystem* the state variables are the velocities of the airplane with respect to the orientation of the frame rigidly attached to the airplane u, w, the rotational velocity q, the height of flight h, the Euler angle of the rotational pose θ, and the rotational speed of the propeller Ω with control signals *elevator* and *throttle* [A. 13]:

```
State vector: x = [u w q theta h Omega]
Input vector: uc = [elevator throttle]
State matrix: A =
-0.2197 +0.6002 -1.4882 -9.7967 -0.5820 -4.1204
22.4024 -0.6461 +0.4823 -4.5284 -4.7512 +0.0000
+0.0000 +0.0000 +1.0000 +0.0000 +0.0658 -0.9978
+0.0000 22.9997 32.1012 2.1170  +0.0000 +0.0000
-0.0001 +0.0009 +0.0000 +0.0000 +0.0000 -0.0295
+0.0108 +0.0000 -0.0084 +0.0000 +0.0000 -2.7813
Control matrix: B =
+00.3246 0
-02.1520 0
-29.8216 0
+00.0000 0
+00.0000 0
+00.0000 448.5357
```

The *lateral subsystem*'s state variables contain the third velocity component v, two rotational velocity components p, and r, and the remaining two Euler angles ϕ, and ψ, and the control signals as *aileron* and *rudder* as follows [A. 13]:

```
State vector: x = [v p r phi psi]
Input vector: uc = [aileron rudder]
State matrix: A =
-0.6373 1.5135   -22.9498 +9.7967 +0
-4.1919 -20.6283 9.9282   0       0
0.6798  -2.6757  -1.0377  0       0
0       1.0000   0.0659   -0.0000 0
0       0        1.0022   -0.0000 0
Control matrix: B =
-1.2510   3.1931
-109.8373 1.9763
-4.3307   -20.1754
 0        0
 0        0
```

The *observation matrices* in both cases contain satisfactory number of linearly independent columns therefore the responses of the subsystems, i.e. the $\dot{x}$ time-derivatives are assumed to be observable, i.e. our method based on the concept of the *response function* can be applied. It worths noting that this system is *strongly under-actuated* since for 11 state variables we have only 4 control signals. It can be also observed that the *throttle* signal has effect exceptionally on $\dot{\Omega}$ while $\dot{u}$ depends on Ω and *elevator* but $\dot{w}$ does not depend on Ω. For steering the airplane the direct control of the velocity components $\{u, w, v\}$ is certainly important for a pilot, and a possible independently steered quantity can be the rotational speed component r. By making the time-derivative of the 1st equation of the longitudinal subsystem instead of $\dot{\Omega}$ the *throttle* signal can be introduced therefore by using the 2nd equation $\ddot{u}^{Des}$, $\dot{w}^{Des}$ can be prescribed that (according to the available imprecise model) makes it possible to determine the *throttle* signal and the time-derivative of the *elevator* signal. The rough model of the lateral subsystem makes it possible to determine the *aileron* and *rudder* signals from $\dot{v}^{Des}$ and $\dot{r}^{Des}$, too. The adaptive deformation therefore can be applied for these four desired values while the actual $\ddot{u}$, $\dot{w}$, $\dot{v}$, and $\dot{r}$ values can be observed. The *elevator* signal can be integrated from an initial estimation according to its time-derivative determined by the desired values. The simulation results displayed and discussed in the next section are derived according to this approach [A. 13].

6.1.2.2 Simulation Results

Two kinds of simulations were made for this system. In the 1st step the effects of the *external perturbations* were investigated when the *model parameters* (denoted by the symbol $\hat{}$) were set as follows: $\hat{A}_{long} = 0.8A_{long}$, $\hat{A}_{lat} = 0.8A_{lat}$, $\hat{B}_{long} = 0.8B_{long}$, $\hat{B}_{lat} = 0.8B_{lat}$. In the 2nd one the *simultaneous effects of uneven parameter uncertainties* as $\hat{A}_{long} = 0.9A_{long}$, $\hat{B}_{long} = B_{long}$, and $\hat{A}_{lat} = 0.9A_{lat}$, $\hat{B}_{lat} = B_{lat}$, and the *external perturbations* were considered. According to the preliminary investigations in both cases the *longitudinal* subsystem worked well with a fixed $A_{c_{long}}$ value. The $A_{c_{lat}}$ value for the lateral subsystem was tuned. In both cases a simple PID-type kinematic tracking was prescribed as is given in (6.3) [A. 13].

$$\left(\Lambda + \tfrac{d}{dt}\right)^3 \int_{t_0}^t \left(u^{Nom}(\tau) - u(\tau)\right) d\tau = 0$$
$$\left(\Lambda + \tfrac{d}{dt}\right)^2 \int_{t_0}^t \left(w^{Nom}(\tau) - w(\tau)\right) d\tau = 0$$
$$\left(\Lambda + \tfrac{d}{dt}\right)^2 \int_{t_0}^t \left(v^{Nom}(\tau) - v(\tau)\right) d\tau = 0 \tag{6.3}$$
$$\left(\Lambda + \tfrac{d}{dt}\right)^2 \int_{t_0}^t \left(r^{Nom}(\tau) - r(\tau)\right) d\tau = 0$$

with $\Lambda = 12/s$.

6.1.2.3 The Effects of Even Parameter Errors and External Perturbations

In the control signal *throttle* considerable disturbance (Fig. 6.13) was introduced to test the adaptive version while the model parameters were exactly set. Due to the significant difference in the order of magnitude of the two components of the controlled quantities (in both the longitudinal and the lateral controlled variables) before applying (6.25) the smaller components were multiplied by a factor of 50. Figure 6.14 reveals that for a simple PID and PI tracking strategy as the tracking error in u well mirrors the disturbances. The results of the adaptive version with $B_{c_{long}} = 1$, $K_{c_{long}} = -10^6$, $A_{c_{long}} = 10^{-7}$, $B_{c_{lat}} = 1$, $K_{c_{lat}} = -5 \times 10^4$, and varying $A_{c_{lat}}$ are given in Figs. 6.15 and 6.16. The longitudinal tracking error decreased more than an order of magnitude. The trajectories to be tracked are given in Fig. 6.17. The control signals are given in Fig. 6.18 [A. 13].
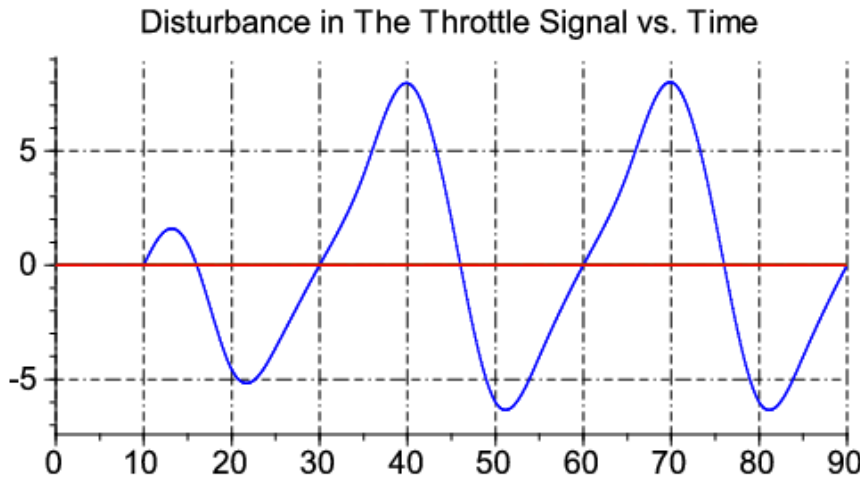
Figure 6.13: The disturbance signal in the *throttle* control signal (time in [s] units) [A. 13]
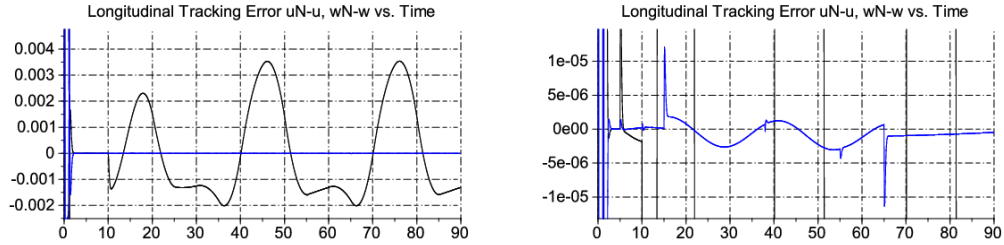
Figure 6.14: The tracking error in $[m/s]$ of the longitudinal subsystem for the non-adaptive case (time in $[s]$ units, u: black, w: blue lines) [A. 13]
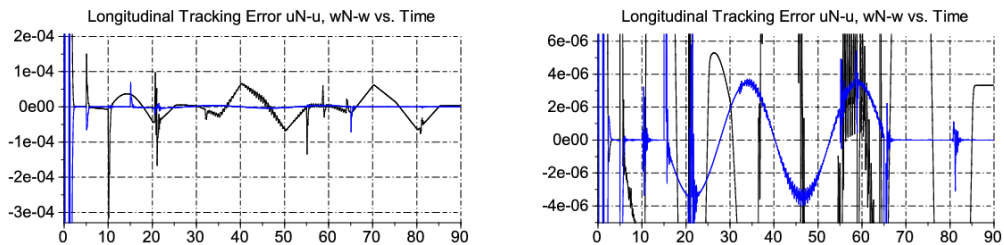
Figure 6.15: The tracking error in $[m/s]$ of the longitudinal subsystem for the adaptive case (time in $[s]$ units, u: black, w: blue lines) [A. 13]
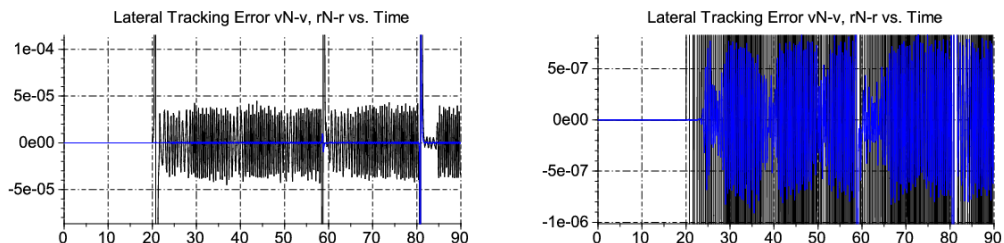
Figure 6.16: The tracking error in $[m/s]$ and $[rad/s]$ of the lateral subsystem for the adaptive case (time in $[s]$ units, v: black, r: blue lines) [A. 13]
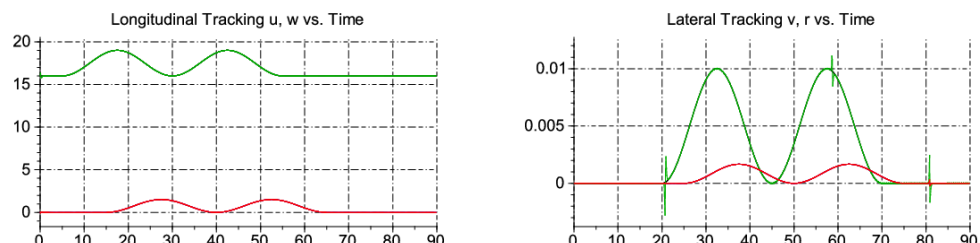
Figure 6.17: The longitudinal (u: green, w: red lines) and lateral (v: green, r: red lines) tracking in $[m/s]$ and $[rad/s]$ units for the adaptive case (time in $[s]$ units) [A. 13]
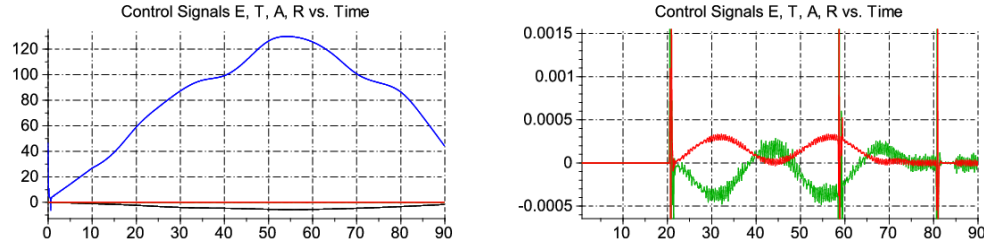
Figure 6.18: The control signals (elevator: black, throttle: blue, aileron: green, and rudder: red lines) and lateral (v: green, r: red lines) for the adaptive case (time in [s] units) [A. 13]

The details of adaptation are revealed by Fig. 6.19. While the *desired* (black) and *realized* (purple) values for $\ddot{u}$ are in each other's vicinity, they considerably differ from the *adaptively deformed* (green) values. For $\dot{w}$, in the lack of significant external disturbance these values are in each other's close vicinity (the blue, red, and ochre lines). Since no extra disturbance was introduced for the lateral subsystem, its adaptation shows similar behavior (Fig. 6.20). Figure 6.21 reveals the presence of *precursor oscillations* in strong correlation with the fast decrease in $A_{c_{lat}}$ about 20, 60, and 80 [s] [A. 13].
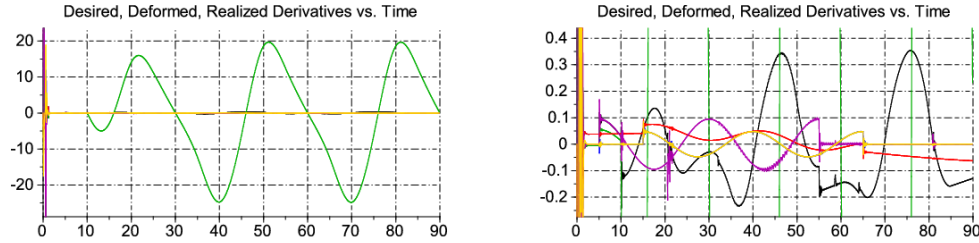
Figure 6.19: The longitudinal adaptive deformation: *desired* ($\ddot{u}$: black, $\dot{w}$: blue), the *deformed* signals (for $\ddot{u}$: green, $\dot{w}$: red), and the *realized* values ($\ddot{u}$: purple, $\dot{w}$: ochre) (time in [s] units) [A. 13]
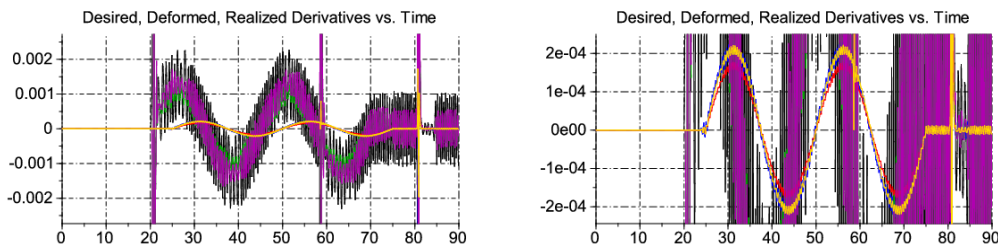
Figure 6.20: The lateral adaptive deformation: *desired* ($\dot{v}$: black, $\dot{r}$: blue), the *deformed* signals (for $\dot{v}$: green, $\dot{r}$: red), and the *realized* values ($\dot{v}$: purple, $\dot{r}$: ochre) (time in [s] units) [A. 13]
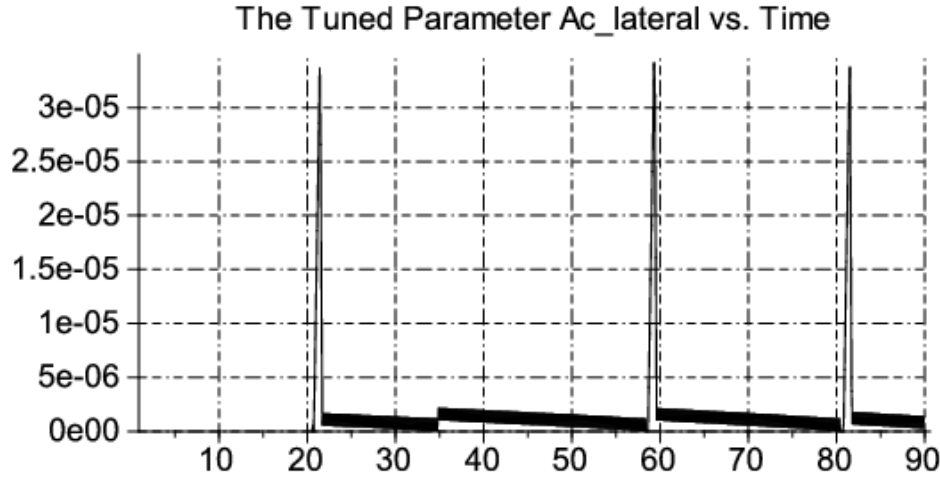
Figure 6.21: The tuned parameter $A_{c_{lat}}$ vs. time in $[s]$ units [A. 13]

6.1.2.4   The Effects of Uneven Modeling Errors and External Perturbations

In this case the same external perturbations in the *throttle signal* were considered as in the previous investigations but the control parameters were set as follows: $\Lambda = 6/s$, $A_{c_{long}} = 10^{-8}$, $K_{c_{long}} = -10^7$, $B_{c_{long}} = 1$, $A_{c_{lat}} = 10^{-7}$, $K_{c_{lat}} = -5 \times 10^4$, $B_{c_{lat}} = 1$. The results are shown in Figs. 6.22, 6.23, 6.24, 6.25, 6.26, and 6.27 [A. 13].
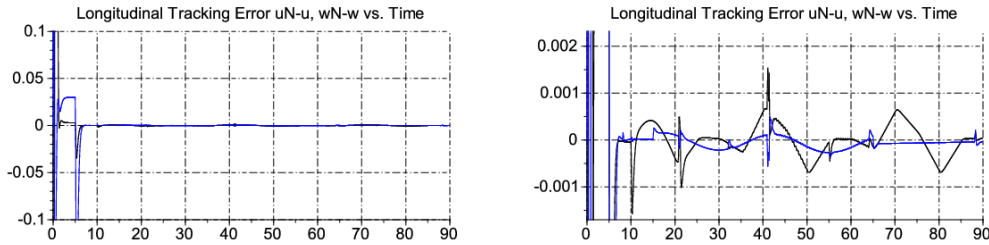
Figure 6.22: The tracking error in $[m/s]$ of the longitudinal subsystem for the adaptive case (time in $[s]$ units, u: black, w: blue lines) [A. 13]
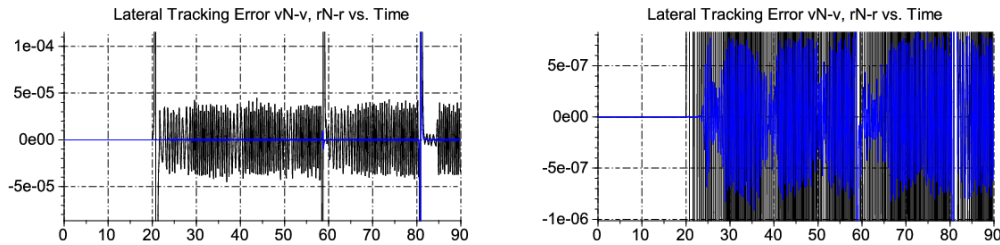
Figure 6.23: The tracking error in $[m/s]$ and $[rad/s]$ of the lateral subsystem for the adaptive case (time in $[s]$ units, v: black, r: blue lines) [A. 13]
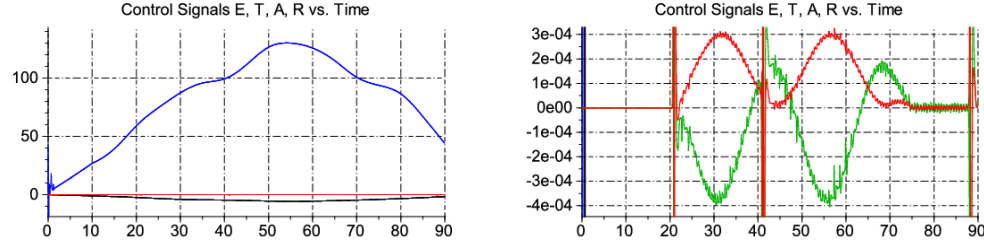
Figure 6.24: The control signals (elevator: black, throttle: blue, aileron: green, and rudder: red lines) and lateral (v: green, r: red lines) for the adaptive case (time in $[s]$ units) [A. 13]
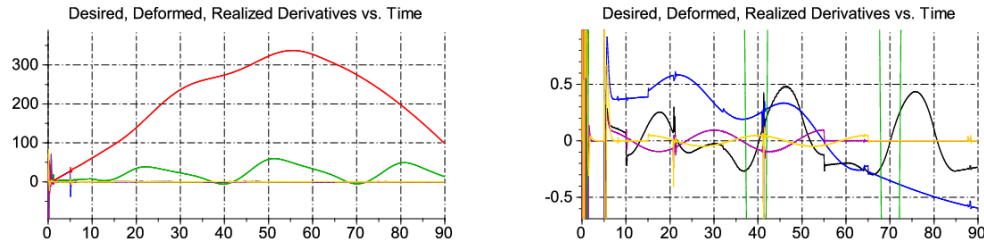
Figure 6.25: The longitudinal adaptive deformation: *desired* ($\ddot{u}$: black, $\dot{w}$: blue), the *deformed* signals (for $\ddot{u}$: green, $\dot{w}$: red), and the *realized* values ($\ddot{u}$: purple, $\dot{w}$: ochre) (time in $[s]$ units) [A. 13]
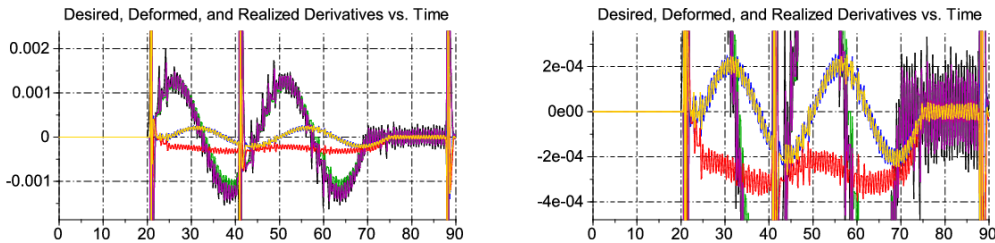
Figure 6.26: The lateral adaptive deformation: *desired* ($\dot{v}$: black, $\dot{r}$: blue), the *deformed* signals (for $\dot{v}$: green, $\dot{r}$: red), and the *realized* values ($\dot{v}$: purple, $\dot{r}$: ochre) (time in $[s]$ units) [A. 13]
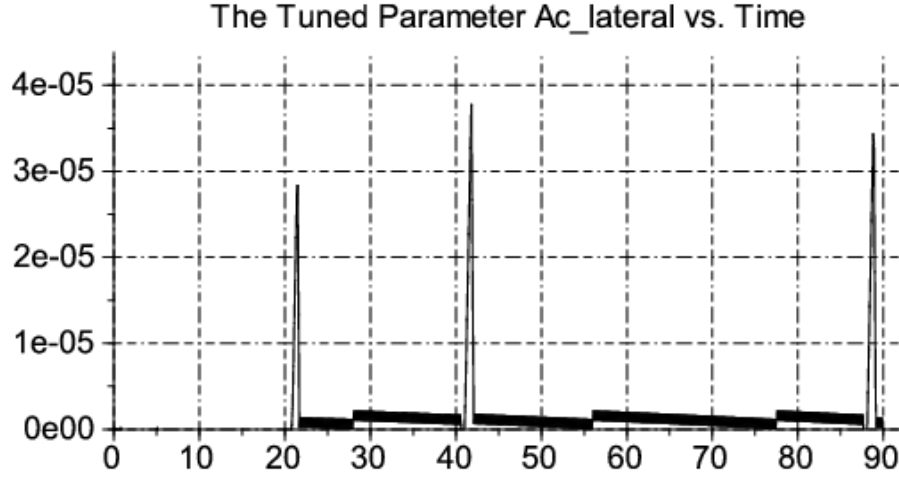
Figure 6.27: The tuned parameter $A_{c_{lat}}$ vs. time in $[s]$ units [A. 13]

It can well be seen that the controller worked similarly as in the first case considered. Due to the uneven parameter errors the *deformed* $\dot{w}$ (red line) signal in Fig. 6.25 also very significantly was modified [A. 13].

6.2 Novel application for order reduction in the control of a WMR

6.2.1 The Kinematic Model

The kinematic model was taken from [76]. Assuming that no skidding occurs the (x, y, θ) coordinates of the frame fixed on the road, i.e. the time-derivatives of the position of the center of the cart on the (x, y) plane with Cartesian coordinates and that of its rotational orientation θ are unique functions of the rotational velocities of the wheel axles as [A. 14]

$$\begin{aligned}
\dot{x} &= \tfrac{r}{2}(\dot{q}_r + \dot{q}_l)\cos(\theta), \\
\dot{y} &= \tfrac{r}{2}(\dot{q}_r + \dot{q}_l)\sin(\theta), \\
\dot{\theta} &= \tfrac{r}{2D}(\dot{q}_r - \dot{q}_l),
\end{aligned} \tag{6.4}$$

in which $r = 0.1\,m$ denotes the radii of the wheels, $D = 1\,m$ means the distances between the wheels and the center of the cart that is assumed to be on the line connection the centers of the wheels, and q_r and q_l denote the rotation angles of the wheels at the *right* and the *left sides* of the cart, respectively. (This system is a non-holonomic device in which the pair of variables (q_r, q_l) cannot be used as *generalized coordinates* of the mechanical system.) Via further derivation of (6.4) the *acceleration data* can be obtained that are utilized in the *dynamic model* of the system [A. 14]:

$$\begin{aligned}
\ddot{x} &= \tfrac{r}{2}(\ddot{q}_r + \ddot{q}_l)\cos(\theta) - \tfrac{r}{2}(\dot{q}_r + \dot{q}_l)\sin(\theta)\dot{\theta}, \\
\ddot{y} &= \tfrac{r}{2}(\ddot{q}_r + \ddot{q}_l)\sin(\theta) + \tfrac{r}{2}(\dot{q}_r + \dot{q}_l)\cos(\theta)\dot{\theta}, \\
\ddot{\theta} &= \tfrac{r}{2D}(\ddot{q}_r - \ddot{q}_l)
\end{aligned} \tag{6.5}$$

6.2.2 Kinematically Formulated Desired Trajectory Tracking for the Given Kinematic Constraints

Assume that the user of the cart should like to *kinematically prescribe* the trajectory tracking error relaxation by the formula $(\Lambda + \tfrac{d}{dt})^3 \int_{t_0}^{t} \left(X^N(\xi) - X(\xi) \right) d\xi \equiv 0$ ($\Lambda > 0$, $X^N(t)$ is the *nominal trajectory to*

be tracked, while $X(t) \overset{def}{=} (x, y, \theta)$ is the actual one). This prescription leads to the *desired 2nd time-derivative* that corresponds to a PID-type control as [A. 14]

$$\ddot{X}^{Des} \overset{def}{=} \ddot{X}^N + \Lambda^3 \int_{t_0}^t \left[X^N(\xi) - X(\xi) \right] d\xi \\ + 3\Lambda^2 \left[X^N(t) - X(t) \right] + 3\Lambda \left[\dot{X}^N(t) - \dot{X}(t) \right] \tag{6.6}$$

resulting exponential error-relaxation for $\Lambda > 0$. Due to the fact that for the *three quantities to be controlled*, i.e. for x, y, and θ we have only two control actions as T_r and T_l, (6.6) cannot be realized. Some compromise has to be introduced that somehow distributes the tracking error over these quantities. For this purpose a very simple approach was applied in this paper: in each control cycle the *quadratic error* [A. 14]

$$\Phi(\ddot{q}_r^{Des}, \ddot{q}_l^{Des}) \overset{def}{=} \\ = \left(\ddot{x}^{Des} - \ddot{x} \right)^2 + \left(\ddot{y}^{Des} - \ddot{y} \right)^2 + \kappa \left(\ddot{\theta}^{Des} - \ddot{\theta} \right)^2 \\ \text{in which} \\ \kappa > 0, \\ \ddot{x} = \ddot{x}(q_r, q_l, \dot{q}_r, \dot{q}_l, \ddot{q}_r^{Des}, \ddot{q}_l^{Des}), \\ \ddot{y} = \ddot{y}(q_r, q_l, \dot{q}_r, \dot{q}_l, \ddot{q}_r^{Des}, \ddot{q}_l^{Des}), \text{ and} \\ \ddot{\theta} = \ddot{\theta}(q_r, q_l, \dot{q}_r, \dot{q}_l, \ddot{q}_r^{Des}, \ddot{q}_l^{Des}) \tag{6.7}$$

was minimized according to the variables $(\ddot{q}_r^{Des}, \ddot{q}_l^{Des})$. In this manner the appearance of complicated Riccati equations that are typical in *optimal control* was simply evaded. By the use of the kinematic equations (6.34) led to the inversion of a simple $\mathbb{R}^2$ matrix that was solved "by hand". In the use of the dynamic model the *kinematically realizable* $(\ddot{q}_r^{Des}, \ddot{q}_l^{Des})$ quantities were taken into consideration [A. 14].

6.2.3   The Dynamic Model of the Cart

The dynamic model can directly be deduced from the laws of Classical Mechanics: the acceleration of the *mass center point of the cart with respect to the inertial road-system* is proportional to the inertia of the whole system, $M = 20 \, kg$, and its acceleration. The *angular acceleration of the rotation around the mass center point* multiplied by the momentum of the system $I = 10 \, kg \cdot m^2$ must yield the rotary torque. (It was assumed that M and I cannot be exactly known if the cart carries some work-load. In the simulations their approximate counterparts $\hat{M} = 25 \, kg$, and $\hat{I} = 15 \, kg \cdot m^2$ were used for the calculation of the control forces and the exact values we applied for the calculation of the motion of the cart.) Regarding the *scaling rules for the motor-wheel axles*, if a wheel of radius $r \, [m]$ exerts the torque $T \, [N \cdot m]$ the *contact force at the road* must be $F = \frac{T}{r} \, [N]$, that with the *arm length $D \, [m]$* exerts $FD = \frac{TD}{r} \, [N \cdot m]$ torque that rotates around the mass center point. Therefore it can be written that [A. 14]

$$I\ddot{\theta} = \frac{Ir}{2D} (\ddot{q}_r - \ddot{q}_l) = \frac{D}{r}(T_r - T_l), \\ M \begin{pmatrix} \ddot{x} \\ \ddot{y} \end{pmatrix} = \begin{pmatrix} \cos(\theta) \\ \sin(\theta) \end{pmatrix} \frac{T_r + T_l}{r}. \tag{6.8}$$

Via making the *scalar product* of the 2nd equation in (6.35) with $(\cos(\theta), \sin(\theta))^T$ and utilizing (6.5) it is easy to obtain that [A. 14]

$$\frac{Mr^2}{2} (\ddot{q}_r + \ddot{q}_l) = T_r + T_l, \\ \frac{Ir^2}{2D^2} (\ddot{q}_r - \ddot{q}_l) = T_r - T_l \tag{6.9}$$

from which it is easy to determine the necessary torques for a given pair $(\ddot{q}_r, \ddot{q}_l)$ [A. 14].

6.2.4 The Model of The DC Motors

In this case it is assumed that the *rotary axles of the DC motors* are rigidly connected to that of the wheels by the *gear reduction ratio* $\nu = 0.1$ as $q_{rl}^{Mot} = \frac{q_{rl}}{\nu}$, $\dot{q}_{rl}^{Mot} = \frac{\dot{q}_{rl}}{\nu}$, and $\ddot{q}_{rl}^{Mot} = \frac{\ddot{q}_{rl}}{\nu}$ (the rotational speed of the motor axles is higher than that of the wheels). Due to the conservation of the energy (in this case the *mechanical wok* in the coupling cog-wheels also determines the *scaling rule for the torques* as follows: the $\delta\varphi_1$ rotation of the axle of radius r_1 causes the displacement $\delta s = r_1\delta\varphi_1$ at the connecting cogs. The *same displacement* has to be done by the cog of the other wheel as $\delta s = r_2\delta\varphi_2$. If the *contact force* F_1 and its *reaction force* $F_2 = -F_1$ *in absolute value* has to make the *same mechanical work as transmitted energy*, i.e. $|F_1|r_1\delta\varphi_1 = |F_2|r_2\delta\varphi_2$ in which the *torques* $T_1 \overset{def}{=} |F_1|r_1$ and $T_2 \overset{def}{=} |F_2|r_2$ can be recognized. Therefore $\frac{\delta\varphi_1}{\delta\varphi_2} = \frac{r_2}{r_1} \overset{def}{=} \nu$, and $\frac{T_1}{T_2} = \frac{\delta\varphi_2}{\delta\varphi_1} = \frac{1}{\nu}$ can be written. By the use of the *wheel axles* in the motor model taken from [77] it can be written that [A. 14]

$$\begin{aligned} \nu\ddot{q}_{rl} &= \frac{Q_{rl}^e + \frac{Q_{rl}^{ext}}{\nu} - b\nu\dot{q}_{rl}}{\Theta}, \\ \dot{Q}_{rl}^e &= \frac{-RQ_{rl}^e - K^2\nu\dot{q}_{rl} + KU_{rl}}{L} \end{aligned} \tag{6.10}$$

where *identical motors* were assumed at the LHS and RHS with the variables and parameters as follows [A. 14]:

- $Q^e\,[N \cdot m]$ is the torque of electromagnetic origin exerted on the motor's axle (it is proportional to the motor current),

- $Q^{ext}\,[N \cdot m]$ is the torque of external origin acting on the wheel's axle, i.e. $Q_{rl}^{ext} = T_{rl}$ in (6.9),

- $R = 1\,[\Omega]$ is the Ohmic resistance of the motor's coil system,

- $L = 0.5\,[H]$ is its inductivity,

- $\Theta = 0.01\,[kg \cdot m^2]$ denotes the momentum of the rotary part of the motor,

- $b = 0.1\,[N \cdot m \cdot s/rad]$ describes the viscous friction of the motor's axle,

- $K = 0.01$ is the motor's torque coefficient, and

- $U\,[V]$ denotes the motor control voltage.

It is evident from (6.36) that an *abrupt variation in U* causes an *abrupt variation* only in $\dot{Q}^e$ therefore instead of Q^e only $\dot{Q}^e$ can directly be controlled by U. The "orthodox" way for developing a precise control would require the calculation of the time-derivative of the first equation in (6.36), in which $\dddot{q}$ could be directly related to U through the 2nd equation. That is the precise control should be developed for $\dddot{q}$, and therefore for $\dot{T}_{rl}$ instead of T_{rl} that directly can be calculated from the *mechanical model* in (6.9) [A. 14].

Instead following the "orthodox way" in this paper we develop an RFPT-based adaptive design for a 2nd order control as it is expounded in the next section [A. 14].

6.2.5 The RFPT-Based Design for Order Reduced Adaptive Controller

If we wish to avoid the development of a 3rd order control we have to apply some *order reduction technique*. In the realm of the "*Linear Time-Invariant (LTI)*" systems *that can be described in the frequency domain* by fractional polynomial expressions as "*Transfer Functions*" the Padé approximation theory [48] can widely be used for order reduction even in the case of fractional order systems of long memory (e.g. [78]). However, *in the case of nonlinear systems alternative approaches have to be chosen* [A. 14].

To avoid 3rd order control the *RFPT-based order reduction* can be formulated as follows: if $\dot{q}$ would be constant the 2nd equation of the group (6.36) could describe a *stable linear system* that exponentially could trace the abrupt jumps in U. If the electromagnetic components could work considerably faster than the mechanical ones group (6.36) could be used for designing abrupt changes in U_{rl} to realize $\ddot{q}_{rl}^{Des}$ in the control cycles. However, this is only an approximation. *The role of the RFPT-based adaptive design consist in correcting this preliminary design together with the effects of the modeling errors and unknown external disturbances.* In this approach $\ddot{q}_{rl}^{Des}$ is computed from (6.9), but instead of the "exact model" the same equations with the *approximate model parameters* can be used. By the use of the first equation of the group (6.36) Q_{rl}^{eDes} is calculated for $\ddot{q}_{rl}^{Des}$. Assuming that $\dot{Q}_{rl}^e \approx 0$ for a given constant $\dot{q}_{rl}$ *the stabilized value of the necessary* U_{rl}^{Des} *is estimated from the 2nd equation as* [A. 14]

$$U_{rl}^{Des} \stackrel{def}{=} \frac{R}{K} Q_{rl}^{eDes} + K v \dot{q}_{rl}. \tag{6.11}$$

The adaptivity is introduced in the above outlined argumentation when the $\ddot{q}^{Des} \stackrel{def}{=} (\ddot{q}_r^{Des}, \ddot{q}_l^{Des})^T \in \mathbb{R}^2$ value is replaced by *its adaptively deformed counterpart* for control cycle $(n+1)$ as [A. 14]

$$
\begin{aligned}
\mathbb{R}^2 \ni e_n &\stackrel{def}{=} \frac{\ddot{q}_n - \ddot{q}_{n+1}^{Des}}{\|\ddot{q}_n - \ddot{q}_{n+1}^{Des}\|}, \\
\tilde{B} &\stackrel{def}{=} B_c \sigma\left(A_c \|\ddot{q}_n - \ddot{q}_{n+1}^{Des}\|\right), \\
\ddot{q}_{n+1}^{Req} &\stackrel{def}{=} (1 + \tilde{B})\ddot{q}_n^{Req} + \tilde{B}K_c e_n
\end{aligned}
\tag{6.12}
$$

in which A_c, B_c, and K_c are adaptive control parameters, $\mathbb{R}^2 \ni \ddot{q}_n$ is the *observed response* at cycle n, and the function $\sigma(x)$ is defined as follows [A. 14]:

$$\sigma(x) \stackrel{def}{=} \frac{x}{1 + |x|}. \tag{6.13}$$

Evidently, if $\ddot{q}_n = \ddot{q}_{n+1}^{Des}$ i.e. when we found the appropriate deformation, $\ddot{q}_{n+1}^{Req} = \ddot{q}_n^{Req}$, that is the solution of the control task is the *fixed point* of the mapping defined in (6.12). For convergence this mapping must be made *contractive*. For this purpose normally $B_c = \pm 1$, a very big $|K_c|$, and an appropriately small $A_c > 0$ value has to be chosen (for the details see e.g. [28], and [A. 6]). In this paper this issue will not be considered in details. In the sequel simulation results will be presented [A. 14].

6.2.6 Simulation Results

The simulations were made by using the software SCILAB 5.4.1 for LINUX and its graphical tool called XCOS. These softwares can be down-loaded from the Web [79]. They were developed for the needs of *higher education* in France [80]. It also is a useful for solving optimization problems by providing interfaces to other, freely usable, very efficient softwares [81]. It offers various numerical integrators for *Ordinary Differential Equations*. In the simulations we used the "*Livermore Solver for solving Ordinary Differential Equations*", an option abbreviated as "*LSodar*" that applies an automatic switching for stiff and non-stiff problems. It also uses variable step size and combines the "*(Backward Differentiation Formula (BDF)*" and "*Adams*" integration methods. The stiffness detection is done by step size attempts in both cases. In (6.12) the element called *continuous time delay* was used to utilize the "past values" in the iteration. Normally the necessary time-delay depends on the dynamics of the motion to be tracked and it also directly influences the available tracking precision. The discrete time-resolution (i.e. the cycle-time of the controller) was $\delta t = 10^{-3} s$ [A. 14].

To achieve useful results the allowable step-size was limited to 10^{-2} in the simulations by setting the solver. One of the advantages of the RFPT-based methods is that they can work with relatively small Λ values. In our case $\Lambda = 1 s^{-1}$ and $\Lambda = 0.5 s^{-1}$ values were applied in (6.6).The adaptive control parameters were set as $B_c = -1$, $K_c = 10^8$, and $A_c = 5 \times 10^{-9}$, and no tuning for A_c was necessary. To

check the abilities of the controller a "slalom"-type nominal trajectory was chosen with an appropriate orientation θ^N that corresponded to that of the actual tangent of the trajectory [A. 14].

In Figs. 6.28 and 6.29 the results for the trajectory tracking can be seen for $\Lambda = 0.5\,s^{-1}$ and $\Lambda = 1\,s^{-1}$ values in (6.6). The *nominal trajectory* intentionally contained relatively sharp turns that are more appropriate to test the control method than the relatively smooth ones. As it was expected greater Λ caused "tighter", i.e. more precise tracking. The slow relaxation of the orientation error is quite illustrative. According to Fig. 6.30 that describes the rotary speeds of the wheels it is evident that significant differences between the values belonging to the greater and lesser Λ parameters are only in the initial transient phase. The appropriate control voltages are described in Fig. 6.31. It is well shown that following a hectic transient initial section the voltages vary quite "smoothly" depending on the needs of the nominal trajectory and the system's dynamics. As it could be expected, for greater Λ greater initial fluctuations pertain [A. 14].
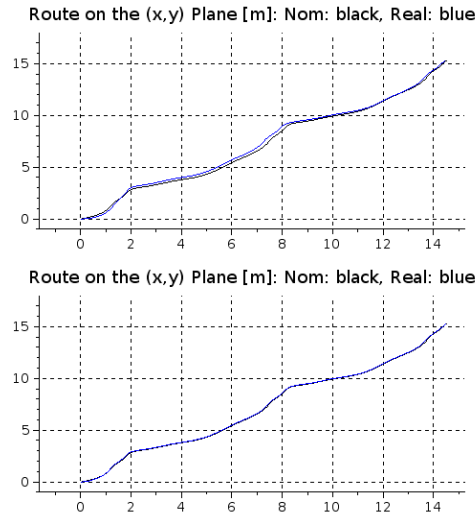
Figure 6.28: Tracking of the trajectory in the (x, y) plane for $\Lambda = 0.5\,s^{-1}$ (upper chart) and $\Lambda = 1\,s^{-1}$ (lower chart) [The nominal trajectory: black line, the simulated one: blue line] [A. 14]
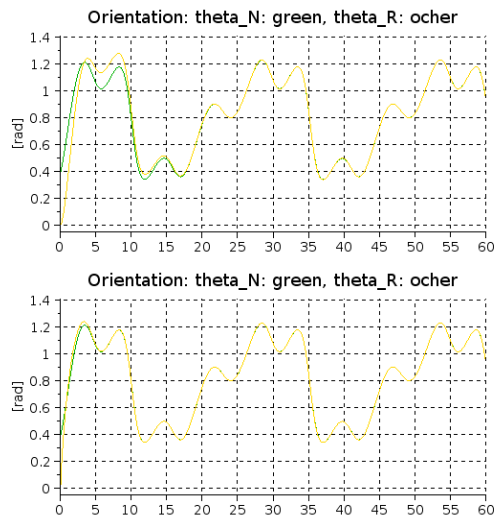
Figure 6.29: Tracking of the trajectory for the orientation θ for $\Lambda = 0.5\,s^{-1}$ (upper chart) and $\Lambda = 1\,s^{-1}$ (lower chart) [The nominal trajectory: green line, the simulated one: ocher line, time in $[s]$ units in the horizontal axes] [A. 14]
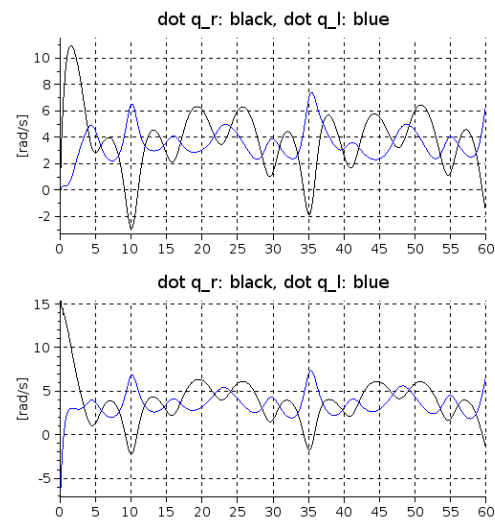
Figure 6.30: The rotary speed of the wheels for $\Lambda = 0.5\,s^{-1}$ (upper chart) and $\Lambda = 1\,s^{-1}$ (lower chart) [$\dot{q}_r$: black line, $\dot{q}_l$: blue line, time in $[s]$ units in the horizontal axes] [A. 14]
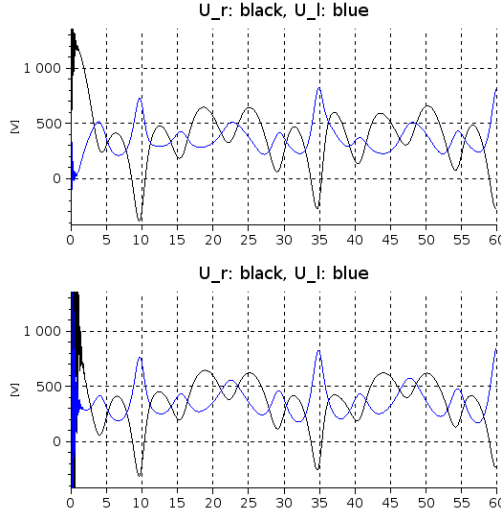
Figure 6.31: The control voltages versus time in $[s]$ units for $\Lambda = 0.5\,s^{-1}$ (upper chart) and $\Lambda = 1\,s^{-1}$ (lower chart) [U_r: black line, U_l: blue line] [A. 14]

To reveal the operation of the adaptive controller Figs. 6.32, 6.33, and 6.34 describe the kinematically calculated "Desired", the adaptively deformed "Required", and the simulated "Realized" values for $\ddot{q}_{rl}$. It is clearly visible that the extent of the adaptive deformation is quite significant, i.e. the "Desired" and the "Required" values are quite different, but the "Desired" values are precisely approximated by the "Realized" ones [A. 14].
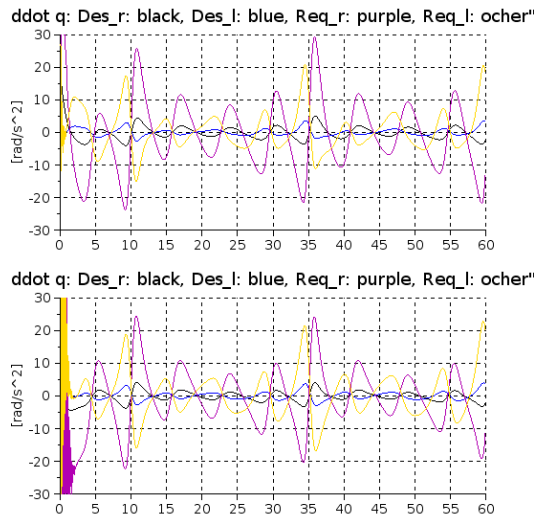
Figure 6.32: The *"Desired"* and the *adaptively deformed "Required"* second time-derivatives of the wheels' axles versus time in $[s]$ units for $\Lambda = 0.5\,s^{-1}$ (upper chart) and $\Lambda = 1\,s^{-1}$ (lower chart) [$\ddot{q}_r^{Des}$: black line, $\ddot{q}_r^{Req}$: purple line, $\ddot{q}_l^{Des}$: blue line, $\ddot{q}_l^{Req}$: ocher line] [A. 14]
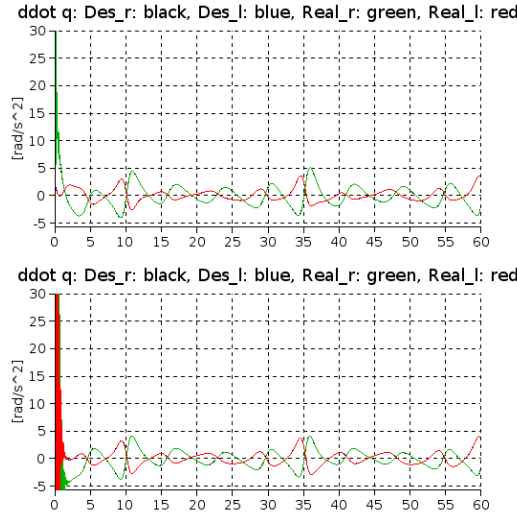
Figure 6.33: The *"Desired"* and the *simulated "Real"* second time-derivatives of the wheels' axles versus time in $[s]$ units for $\Lambda = 0.5\,s^{-1}$ (upper chart) and $\Lambda = 1\,s^{-1}$ (lower chart) [$\ddot{q}_r^{Des}$: black line, $\ddot{q}_r^{Real}$: green line, $\ddot{q}_l^{Des}$: blue line, $\ddot{q}_l^{Real}$: red line] [A. 14]
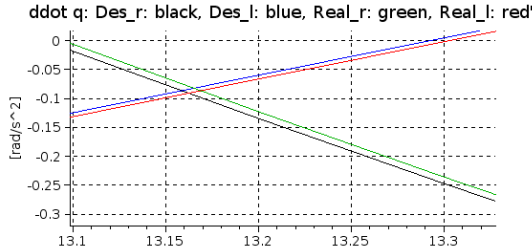
Figure 6.34: The *"Desired"* and the *simulated "Real"* second time-derivatives of the wheels' axles versus time in $[s]$ units for $\Lambda = 1\,s^{-1}$ [$\ddot{q}_r^{Des}$: black line, $\ddot{q}_r^{Real}$: green line, $\ddot{q}_l^{Des}$: blue line, $\ddot{q}_l^{Real}$: red line, zoomed excerpts] [A. 14]

6.3 Adaptive control for 4th order dynamic systems.

6.3.1 Dynamically coupled SISO systems

6.3.1.1 The Model of the 4th Order System

Consider two mass points m_1 and m_2 so coupled by a nonlinear spring that directly no any control force can be exerted on m_1. This mass-point can be "actuated" by the force of a spring that connects these mass points as $m_1\ddot{q}_1 = F_1(q_1, \dot{q}_1) + F_{spr}(q_1 - q_2)$. The 2nd mass point has similar equation of motion as $m_2\ddot{q}_2 = F_2(q_2, \dot{q}_2) - F_{spr}(q_1 - q_2) + F_{ctrl}$ in which near the reaction force of the interaction between the masses the *directly applicable control force* F_{ctrl} appears. If we wish to use F_{ctrl} for directly controlling q_1 we have to differentiate the first equation two times by the time to make F_{ctrl} directly appear in $\ddot{q}_2$, therefore it directly appears in $q_1^{(4)}$ as a control agent. This simple explanation highlights why we believe that controlling a Classical Mechanical system through some deformable component leads to 4th order differential equations as equations of motion. In the simulation examples considered in this paper we used the *exact system model* as [A. 15]

$$q^{(4)} = \left(-a_3 q^{(3)} - a_2 \ddot{q} - a_1 \dot{q} - a_0 q + F_{ctrl}\right)/m \qquad (6.14)$$

while the *approximate inverse model* was represented by the parameters

$$F_{ctrl} = \tilde{m} q^{(4)} + \tilde{a}_3 q^{(3)} + \tilde{a}_2 \ddot{q} + \tilde{a}_1 \dot{q} + \tilde{a}_0 q \qquad (6.15)$$

with $\Omega_{mod} = 2/s$, $\tilde{a}_0 = \Omega_{mod}^4$, $\tilde{a}_1 = 4\Omega_{mod}^3$, $\tilde{a}_2 = 6\Omega_{mod}^2$, $\tilde{a}_3 = 4\Omega_{mod}$, $\tilde{m} = 3$, $\Omega = 1$, $a_0 = \Omega^4$, $a_1 = 4\Omega^3$, $a_2 = 6\Omega^2$, $a_3 = 4\Omega$, and $m = 1$ [A. 15].

6.3.1.2 Simulation Problems in the Numerical Computation of Higher Order Derivatives

For simulation purposes we used the freely available software SCILAB 5.4 for Linux and its XCOS co-simulator. In the first experiment we calculated the first 4 time-derivatives of a sinusoidal signal generator of amplitude 1 and circular frequency $\omega = 2/s$ by chaining 4 numerical derivators of XCOS. According to the analytical rules of differentiation signals of amplitude 2, 4, 8, and 16 were expected in the 1st, 2nd, 3^{dr}, and 4th derivatives, respectively. The result displayed in Fig. 6.35 do not reveal any problem [A. 15].
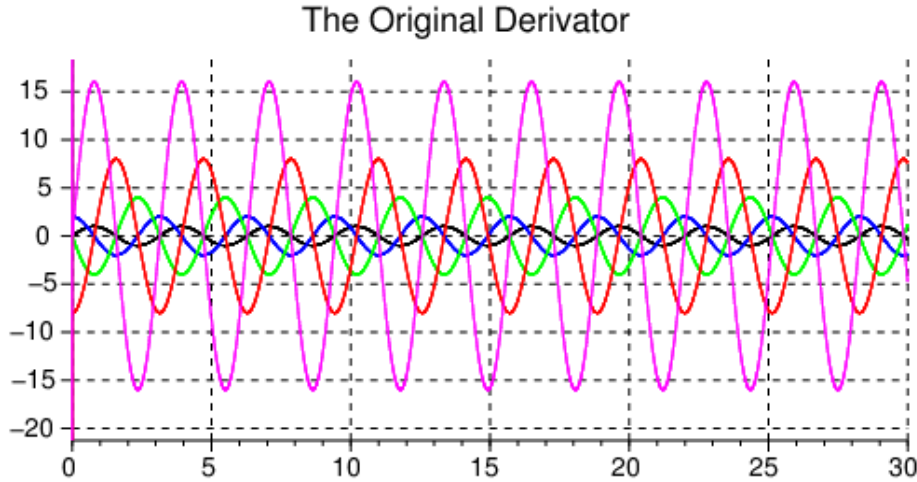
Figure 6.35: The results provided by SCILAB's chained built-in differentiators for the signal of a sinusoidal signal generator ($q^{(0)}$: black, $q^{(1)}$: blue, $q^{(2)}$: green, $q^{(3)}$:red, and $q^{(4)}$: magenta lines) [A. 15]

However, the situation drastically changes when this smooth signal is *numerically integrated* and after that is differentiated by the same chained structure. *The result obtained drastically depends on the type of numerical integration chosen.* In Fig. 6.36 the *"ADAMS-FUNCTIONAL"* option was chosen with arbitrary (i.e. to be automatically determined by the integrator) option, while Fig. 6.37 reveals the results obtained by the *"ADAMS-NEWTON"* option [A. 15].
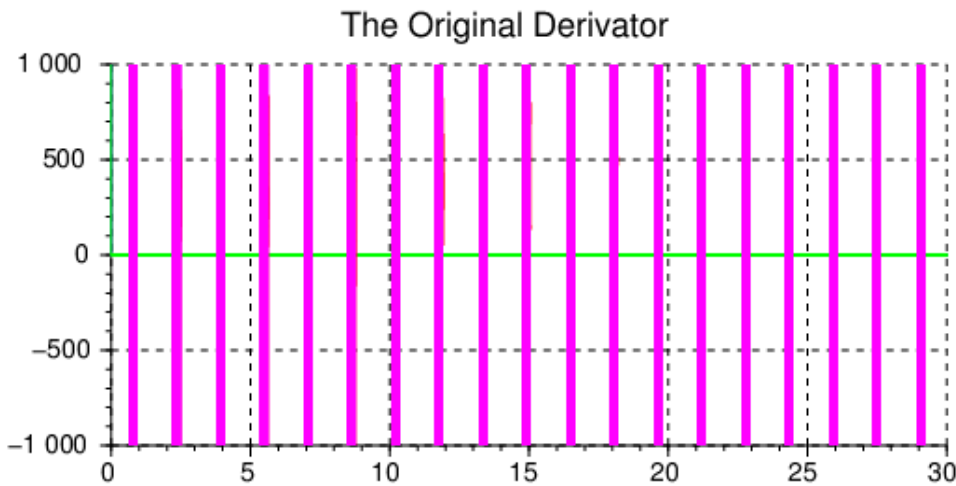
Figure 6.36: The results provided by SCILAB's chained built-in differentiators for the integrated signal of a sinusoidal signal generator using the "*ADAMS-FUNCTIONAL*" option ($q^{(0)}$: black, $q^{(1)}$: blue, $q^{(2)}$: green, $q^{(3)}$: red, and $q^{(4)}$: magenta lines) [A. 15]
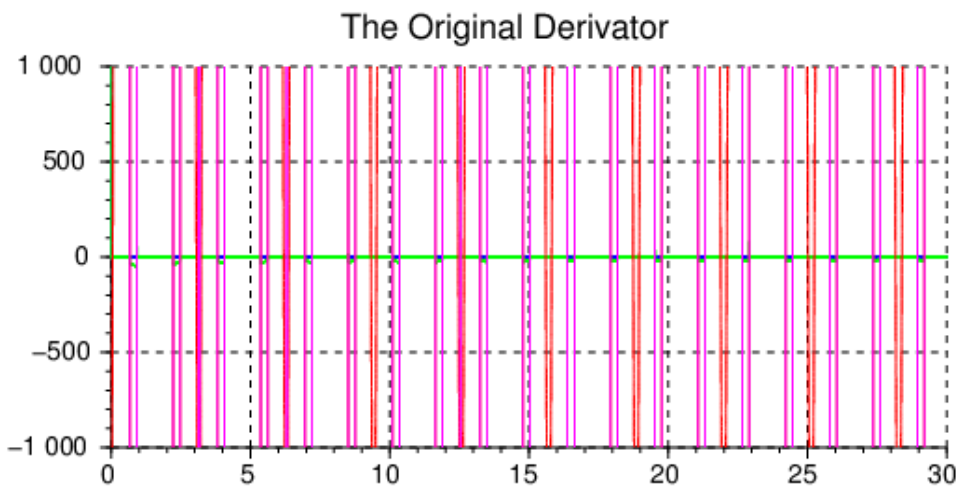
Figure 6.37: The results provided by SCILAB's chained built-in differentiators for the integrated signal of a sinusoidal signal generator using the "*ADAMS-NEWTON*" option ($q^{(0)}$: black, $q^{(1)}$: blue, $q^{(2)}$: green, $q^{(3)}$: red, and $q^{(4)}$: magenta lines) [A. 15]

Similar problems were observed for all the other implemented numerical integration methods. *These observations revealed that SCILAB's own derivators cannot be used in a chained manner for our purposes.* To solve this problem a simple *polynomial differentiator* was developed as follows [A. 15].

6.3.1.3 Polynomial Estimator for Higher Order Derivatives

The basic idea of the numerical differentiator is that in the case of a moving average over a fixed window size a zero order polynomial is fitted: the *mean value* is assumed to be that of the *constant function* while any deviation from the mean value is interpreted as noise or measurement error. For the approximation of trends the simplest approach is fitting the parameters of an *affine function* that corresponds to a 1st order polynomial. In this approach the information to be obtained is the mean value and the trend of

variation around this mean value, i.e. the coefficients of the fitted 1st order polynomial. All higher order variation is considered to be some noise or measurement error [A. 15].

By following this practice, if we wish to estimate the nth order derivative of a function we can fit an order n polynomial to this function within a moving window of fixed length. Since order $n+1$ derivative of this polynomial is zero, it means that any higher order variation is considered to be some noise or measurement error that must be dropped. The fitted polynomial can be evaluated at the latest point of the window and we obtain simultaneous estimations for the $\{0, 1, \ldots, n\}$ order derivatives [A. 15].

Regarding the realization of the idea we need *invertible (well conditioned) matrices* in the polynomial fitting process. If the function values to be fitted can be taken over the time-grid $\{t - 2N_P\Delta t, t + (-2N_P + 1)\Delta t, \ldots, t\}$ (altogether $2N_P + 1$ grid points), this grid can be mapped to the grid of integers as $\{-N_P, -N_P + 1, \ldots, N_P\}$ as the window of fitting varies (moves) in time. With the continuous variable ξ it can be written that $z := N_P - \xi$ and [A. 15]

$$f(t - \Delta t\xi) = g(z(\xi)) \approx \sum_{s=0}^{4} c_s z^s, \quad \frac{df}{d\xi} = \frac{dg}{dz}\frac{dz}{d\xi},$$
$$-f'(t - \Delta t\xi)\Delta t = -\frac{dg}{dz}, \tag{6.16}$$
$$\Rightarrow f'(t - \Delta t\xi) = \frac{1}{\Delta t}\frac{dg(z)}{dz}\Big|_{z=N_P-\xi}$$

in which $\frac{dg}{dz} = \sum_{s=0}^{4} s c_s z^{(s-1)}$ can be written for the first derivative, etc. This estimation can evidently be used only if the variation of $f^{(n)}$ is not significant in the interval $[t - 2N_P\Delta t, t]$. For maintaining the initial philosophy the derivatives can be estimated in the center of the interval, i.e. for $\xi = N_P$, i.e. $z = 0$. By the use of this idea the counterparts of Figs. 6.36 and 6.37 are give in Figs. 6.38 and 6.39. The time-resolution of the numerical derivation was $1\,ms$, and 17 grid points were taken into consideration in the numerical differentiation [A. 15].
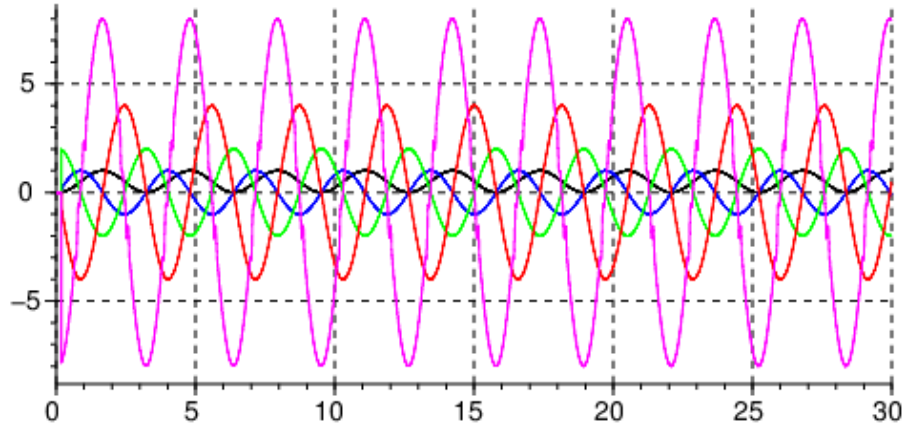
Figure 6.38: The results provided by the polynomial differentiators for the integrated signal of a sinusoidal signal generator using the *"ADAMS-FUNCTIONAL"* option ($q^{(0)}$: black, $q^{(1)}$: blue, $q^{(2)}$: green, $q^{(3)}$: red, and $q^{(4)}$: magenta lines) [A. 15]
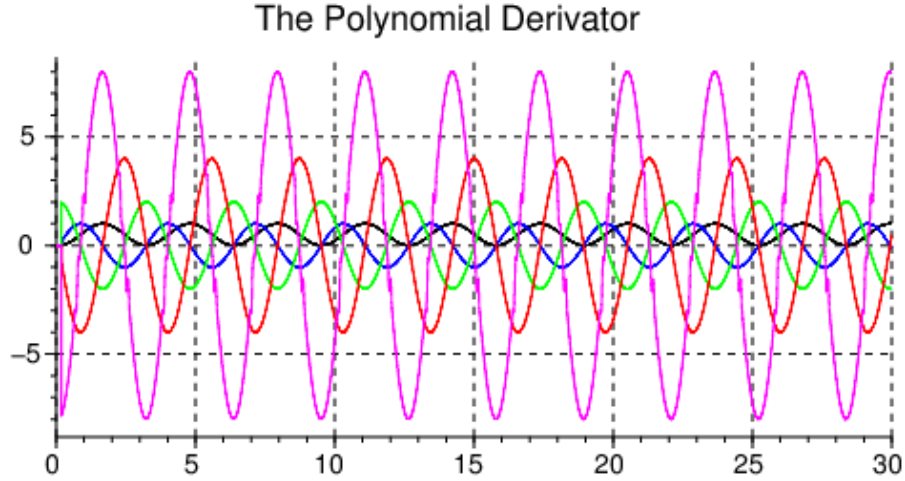
Figure 6.39: The results provided by the polynomial differentiators for the integrated signal of a sinusoidal signal generator using the "*ADAMS-NEWTON*" option ($q^{(0)}$: black, $q^{(1)}$: blue, $q^{(2)}$: green, $q^{(3)}$: red, and $q^{(4)}$: magenta lines) [A. 15]

The results reveal that the polynomial 4th order differentiator yielded much better results than the chained own differentiators of SCILAB. Similar results were obtained for each integrator option available in SCILAB 4.1 for Linux. In the possession of these promising results it made sense to check the operation of the RFPT-based adaptive controller for the control 4th order system defined in Section 6.3.1.1 [A. 15].

6.3.1.4   The RFPT-based Adaptive Control of the 4th Order System

The RFP-based approach always is started with a purely kinematic prescription for the relaxation tracking error. The aim of the adaptive dynamic controller is the realization of this tracking policy. In the simulation examples considered this tracking policy resulted in the *desired 4th time-derivative* [A. 15]

$$
\begin{aligned}
q^{(4)Des} = q^{(4)Nom} + a_{\Lambda_3}e^{(3)} + a_{\Lambda_2}e^{(2)} + \\
a_{\Lambda_1}\dot{e} + a_{\Lambda_0}e + a_{\Lambda_{int}}\int_0^t e(\xi)d\xi
\end{aligned}
\tag{6.17}
$$

in which $e(t) := q^{Nom}(t) - q(t)$, $a_{\Lambda_3} = 5\Lambda$, $a_{\Lambda_2} = 10\Lambda^2$, $a_{\Lambda_1} = 10\Lambda^3$, $a_{\Lambda_0} = 5\Lambda^4$, and $a_{\Lambda_{int}} = \Lambda^5$ with $\Lambda = 10/s$. The idea behind (6.17) was achieving an exponential relaxation for the integrated error as $\left(\Lambda + \frac{d}{dt}\right)^5 \int_0^t e(\xi)d\xi = 0$. The adaptive control parameters were as follows: $B_c = 1$, $K_c = -10^9$, $K_s = 3\times10^4$, $A_c = 10^{-10}$, the cycle time was $1\,ms$. For the numerical derivation a 9 points grid was applied. To simulate the "*common engineering practice*" it was assumed that the directly observable quantity is $q(t)$, therefore the realized $q^{(4)}$ derivative was integrated by 4 chained numerical integrators, and this result was differentiated 4 times by the polynomial differentiator. The trajectory tracking of the non-adaptive and the adaptive controllers are compared in Fig. 6.40. Figure 6.41 reveals that the 4th derivative of the *nominal* trajectory (black line) needed little kinematic correction as the *desired* value (ochre line) and the *realized* value (green line) remained in their vicinity while the *adaptively deformed* value (red line) was significantly different to them. This fact substantiate the effectiveness of the adaptive control [A. 15].
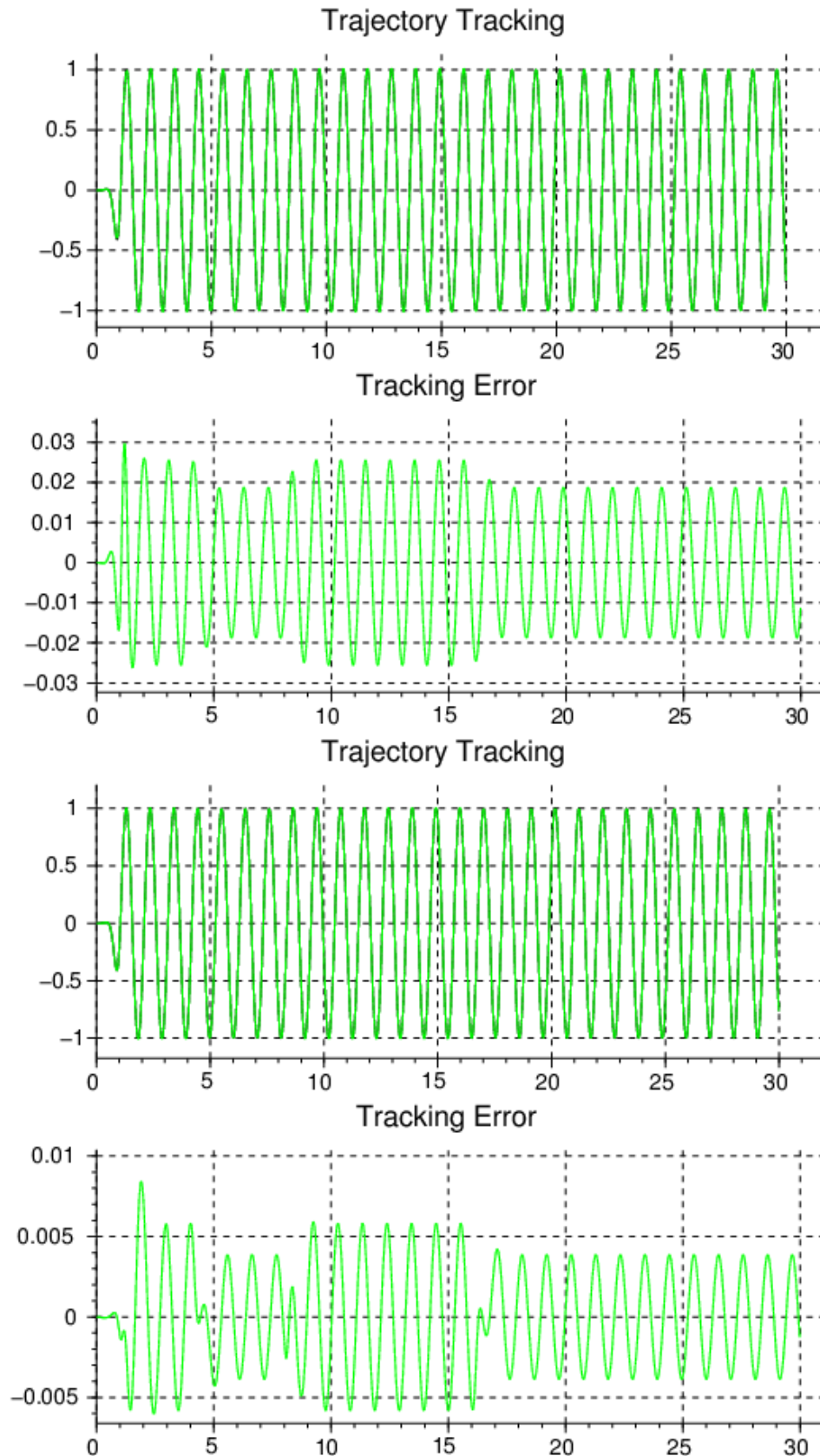
Figure 6.40: The trajectory tracking of the non-adaptive (top) and the adaptive (bottom) controllers (q^{Nom}: black, q: green lines, $q^{Nom} - q$: green line), time in s units [A. 15]
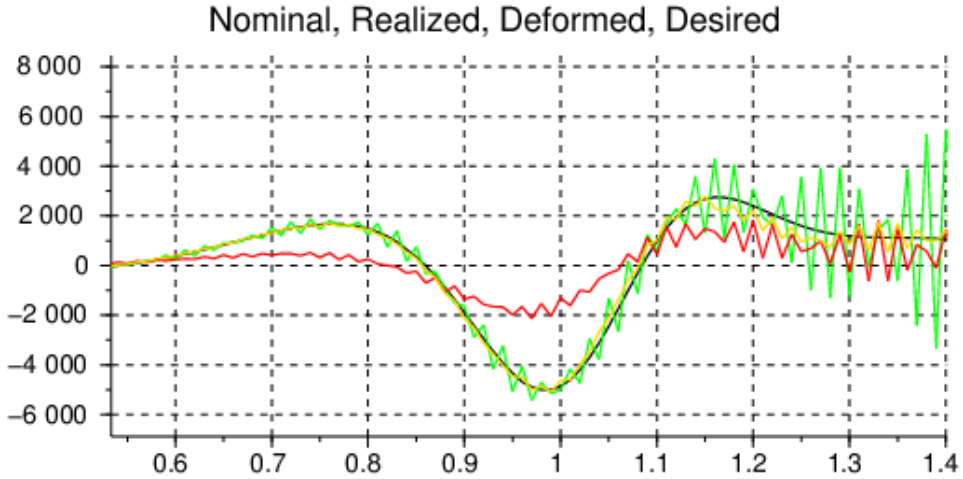
Figure 6.41: The nominal (black), simulated (green), adaptively deformed (red), and kinematically desired (ochre) 4th time-derivatives vs. time in s units [A. 15]

6.3.2 Dynamically coupled MIMO systems

6.3.2.1 The Dynamic Model of the System to be Controlled

Assume that we have two mass-points of masses m_x and m_y in the locations $\vec{x}$ and $\vec{y}$. These points are dynamically so coupled by a spring of L_0 zero force length that the spring is able to exert force only in its own direction, i.e. in the direction of the vector $\vec{y} - \vec{x}$. The mass-point m_y can directly be accelerated by the control force $\vec{F}$. Our aim is to control the motion of m_x to track the *nominal trajectory* $\vec{x}^N(t)$. The equations of motion of this system are:

$$
\begin{aligned}
m_x \ddot{\vec{x}} &= m_x \vec{g} + \vec{h}(\vec{x}, \vec{y}) + \vec{H}\left(\vec{x}, \vec{y}, \dot{\vec{x}}, \dot{\vec{y}}\right) \\
m_y \ddot{\vec{y}} &= m_y \vec{g} - \vec{h}(\vec{x}, \vec{y}) - \vec{H}\left(\vec{x}, \vec{y}, \dot{\vec{x}}, \dot{\vec{y}}\right) + \vec{F},
\end{aligned}
\tag{6.18}
$$

where in the motion of the mass-points the "action-reaction principle" by Newton is taken into consideration, $\vec{g}$ denotes the vector of the gravitational acceleration, and the contact force between the mass-points is determined by the properties of the spring as

$$
\begin{aligned}
\mathcal{N}(\vec{x}, \vec{y}) &:= \|\vec{y} - \vec{x}\|, \\
\vec{h} &:= k \frac{\vec{y} - \vec{x}}{\mathcal{N}} (\mathcal{N} - L_0), \\
\vec{H} &:= b \frac{\vec{y} - \vec{x}}{\mathcal{N}} \frac{(\vec{y} - \vec{x})^T (\dot{\vec{y}} - \dot{\vec{x}})}{\mathcal{N}},
\end{aligned}
\tag{6.19}
$$

in which $k > 0$ corresponds to a spring constant, $b > 0$ denotes a viscous friction coefficient, and the symbol $\mathcal{N}$ refers to the Frobenius norm. Regarding the viscous friction it is assumed that it is restricted in the direction of $\vec{y} - \vec{x}$ and its absolute value depends on the dilatation according to the factor $\frac{(\vec{y} - \vec{x})^T (\dot{\vec{y}} - \dot{\vec{x}})}{\mathcal{N}}$. It can be expected that the directional limitations of the force of the dynamic interaction between the mass-points needs a particular control that will be detailed in the next section.

6.3.2.2 The Controller Based on the Exact Model

At first a precise model-based controller will be suggested, then an adaptive one using only an approximate model. Assume that the viscous friction forces are negligible. Let us purely kinematically prescribe a tracking error relaxation for $\vec{x}$ as

$$\vec{\zeta}(t) := \int_0^t \left(\vec{x}^N(\xi) - \vec{x}(\xi) \right) d\xi$$
$$\left(\Lambda + \tfrac{d}{dt} \right)^3 \vec{\zeta} = 0 \Rightarrow$$
$$\ddot{\vec{x}}^{Des} = \ddot{\vec{x}}^N + \Lambda^3 \vec{\zeta} + 3\Lambda^2 \left(\vec{x}^N(t) - \vec{x}(t) \right) +$$
$$3\Lambda \left(\dot{\vec{x}}^N(t) - \dot{\vec{x}}(t) \right),$$

(6.20)

where $\ddot{\vec{x}}^{Des}$ denotes a *desired acceleration*. In the possession of the model it is possible to design for the nominal trajectory of $\vec{x}$ a nominal one for $\vec{y}$ so that the contact force $\vec{y} - \vec{x}$ can provide the force need of mass-point $\vec{x}$

$$m_x \left(\ddot{\vec{x}}^{Des} - \vec{g} \right) = k \frac{\vec{y}^N - \vec{x}}{\mathcal{N}} (\mathcal{N} - L_0)$$

(6.21)

where $\mathcal{N} = \|\vec{y}^N - \vec{x}\|$ also depends on $\vec{y}^N$. However, it is not difficult to explicitly determine $\vec{y}^N$. The equality of the vectors at the RHS and LHS of (6.21) assumes parallel vectors at the different sides. So let us seek the solution in the form of $\vec{c} := \ddot{\vec{x}}^{Des} - \vec{g}$, $\vec{y}^N - \vec{x} = \alpha \vec{c}$ in which α may be either positive or negative. By multiplying both sides with $\vec{c}^T$ we obtain the equality of two scalar products as

$$m_x \|\vec{c}\|^2 = k\alpha \frac{\|\vec{c}\|^2}{|\alpha| \|\vec{c}\|} (|\alpha| \|\vec{c}\| - L_0) \Rightarrow$$
$$m_x = k\alpha - \frac{kL_0}{\|\vec{c}\|} \frac{\alpha}{|\alpha|}.$$

(6.22)

If $\alpha < 0$ then $\frac{\alpha}{|\alpha|} = -1$. If $\alpha > 0$ then $\frac{\alpha}{|\alpha|} = 1$. By the use of these hypotheses we can obtain a solution for α as

$$\alpha = \left(m_x + \frac{kL_0}{\|\vec{c}\|} \right) \frac{1}{k} \text{ if } \alpha > 0,$$
$$\alpha = \left(m_x - \frac{kL_0}{\|\vec{c}\|} \right) \frac{1}{k} \text{ if } \alpha < 0 .$$

(6.23)

The sign of the solution is known due to physical reasons. To determine the appropriate sign the sign of the quantity $\left(m_x - \frac{kL_0}{\|\vec{c}\|} \right)$ has to be computed.

For the *"nominal trajectory"* $y^N(t)$ a PID-type trajectory tracking that is faster than that in (6.20) can be prescribed as

$$\vec{\zeta}_y(t) := \int_0^t \left(\vec{y}^N(\xi) - \vec{y}(\xi) \right) d\xi$$
$$\ddot{\vec{y}}^{Des} = \ddot{\vec{y}}^N + \Lambda_y^3 \vec{\zeta} + 3\Lambda_y^2 \left(\vec{y}^N(t) - \vec{y}(t) \right) +$$
$$3\Lambda_y \left(\dot{\vec{y}}^N(t) - \dot{\vec{y}}(t) \right)$$

(6.24)

since according to (6.18) the instant value of $\ddot{\vec{y}}$ can directly be influenced by the force $\vec{F}$. For this purpose $\ddot{\vec{y}}^{Des}$ can be substituted into the second equation of (6.18). This control is of approximate nature since it is formally based on neglecting the effect of the viscous friction term $\vec{H}$. If besides this approximation the available parameter values are imprecise and adaptive controller is needed.

6.3.2.3   The Adaptive Controller based on the Approximate Model

Let us assume that the reality is described by the *exact parameter values* as $m_x = 3\,kg$, $m_y = 1\,kg$, $b = 0.1\,N \cdot s/m$, $k = 100\,N/m$, $L_0 = 1\,m$ and $\vec{g} = [0, 0, -9.81]^T\,m/s^2$. Let the available *approximate model parameters* be $\hat{m}_x = 2\,kg$, $\hat{m}_y = 1.5\,kg$, $\hat{b} = 0.1\,N \cdot s/m$, $\hat{k} = 120\,N/m$, $\hat{L}_0 = 1.2\,m$ and $\hat{\vec{g}} = [0, 0, -10]^T\,m/s^2$. The desired $\ddot{\vec{x}}^{Des}$ can be computed from the variant of (6.21) in which instead of the exact parameters the approximate ones are written. For this the error-relaxation (6.24) ca be prescribed that results in the desired $\ddot{\vec{y}}^{Des}$. This value can be substituted into (6.18)(now containing the approximate parameters) the necessary contact force F can be estimated.

It is important to note hat since $\ddot{\vec{y}}^{Des}$ is derived from $\frac{d^2}{dt^2} \ddot{\vec{x}}^{Des}$, our system is a 4th relative order one. Since the double differentiation of the solution originating from (6.23) is complicated enough, instead

using analytical formulae we used a 4th order polynomial differentiator reported in [A. 15] for the calculation of $\ddot{\vec{y}}^N$. The effects of the model imprecisions and other approximations can be compensated by iterative learning outlined in e.g. [82] with $\delta t = 10^{-3}$ and

$$
\begin{aligned}
\vec{h} &:= \vec{f}(\ddot{\vec{x}}_n) - \ddot{\vec{x}}^{Des}, \quad \vec{e} := \vec{h}/\|\vec{h}\|, \\
\sigma(x) &:= \frac{x}{1+|x|}, \\
\tilde{B} &= B_{ctrl}\sigma(A_{ctrl}\|\vec{h}\|) \\
\ddot{\vec{x}}_{n+1} &= \vec{G}\left(\ddot{\vec{x}}_n, f(\ddot{\vec{x}}_n), \ddot{\vec{x}}^{Des}_{n+1}\right) := \\
&(1 + \tilde{B})\ddot{\vec{x}}_n + \tilde{B}K_{ctrl}\vec{e},
\end{aligned}
\tag{6.25}
$$

where the so-called "response function" $\vec{f}(\ddot{\vec{x}}_n) := \ddot{\vec{x}}(t_n)$ contains the system's response for the previous control section, and A_{ctrl}, B_{ctrl}, and K_{ctrl} are the adaptive control parameters.

It is evident that if there exists a $\ddot{\vec{x}}_\star$ control signal for which $\vec{f}(\ddot{\vec{x}}_\star) = \ddot{\vec{x}}^{Des}$ then $\ddot{\vec{x}}_\star = \vec{G}\left(\ddot{\vec{x}}_\star, f(\ddot{\vec{x}}_\star), \ddot{\vec{x}}^{Des}\right)$, i.e. $\ddot{\vec{x}}_\star$ is a fixed point of the problem. The idea of *"Fixed Point Transformations"* originates from this observation. If the function $\vec{G}\left(\ddot{\vec{x}}_n, f(\ddot{\vec{x}}_n), \ddot{\vec{x}}^{Des}_{n+1}\right)$ is flat enough according to $\ddot{\vec{x}}_n$ this iteration converges to its fixed point. It is relatively easy to meet this condition: let $B_{ctrl} = \pm 1$, $|K_{ctrl}| \gg |$ observable accelerations $|$, and A_{ctrl} a small positive number. No parameter tuning was necessary in the case of the forthcoming simulation results.

6.3.2.4 Simulation Results

The control parameters were set as follows: Λ faster than that in (6.20) $= 6/s$, $\Lambda_y = 12/s$, the adaptive parameters were $K_{ctrl} = -10^5$, $B_{ctrl} = 1$, $A_{ctrl} = 10^{-6}$. The task was to track a tilted ellipsoid trajectory. In the simulations the simple Euler integration was applied with the time-resolution of the controller $\delta t = 10^{-3}\,s$. Figure 6.42 clearly reveals that the adaptivity improved the trajectory tracking.
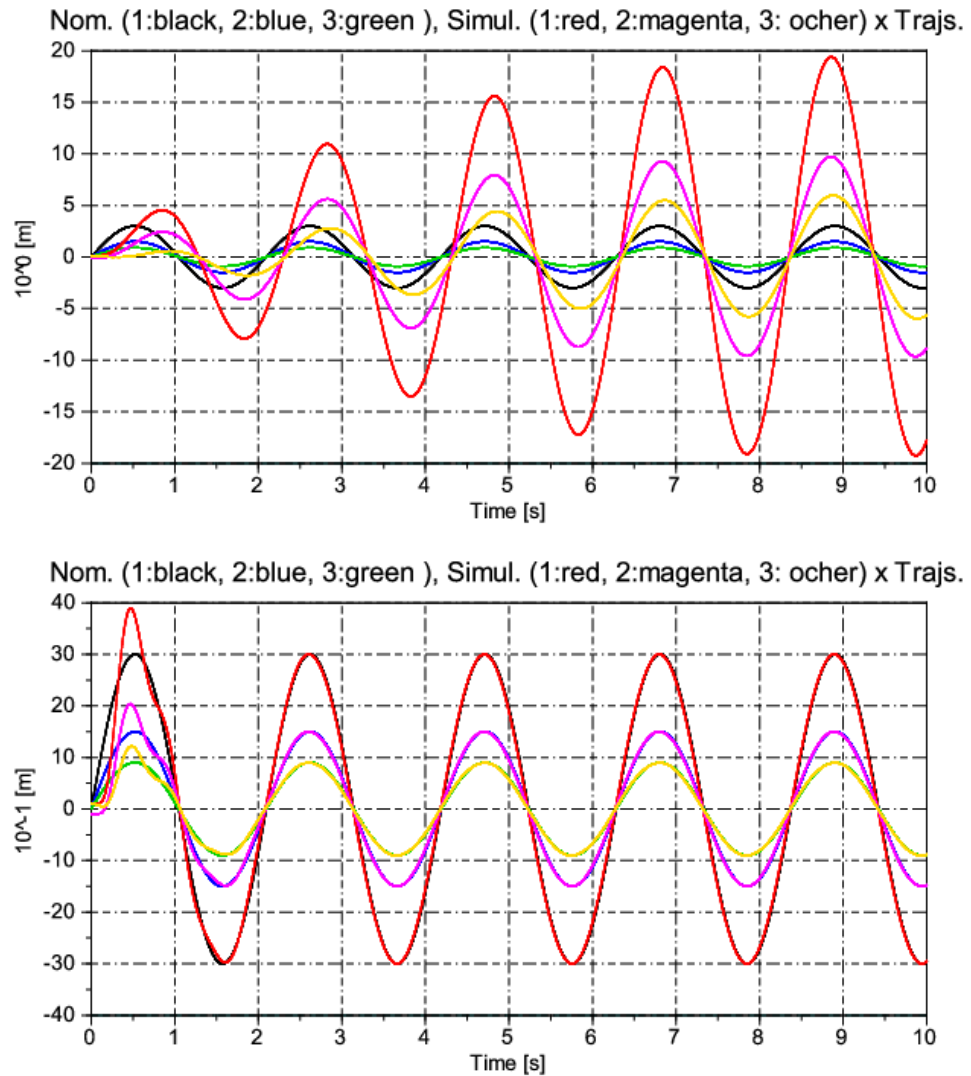
Figure 6.42: The trajectory tracking of the *non-adaptive* (upper) and the *adaptivev* (lower) controllers for $\vec{x}$

Figure 6.42 suggests that the non-adaptive controller slowly diverges while the adaptive one nicely converges. This expectation is reinforced by Fig. 6.43.
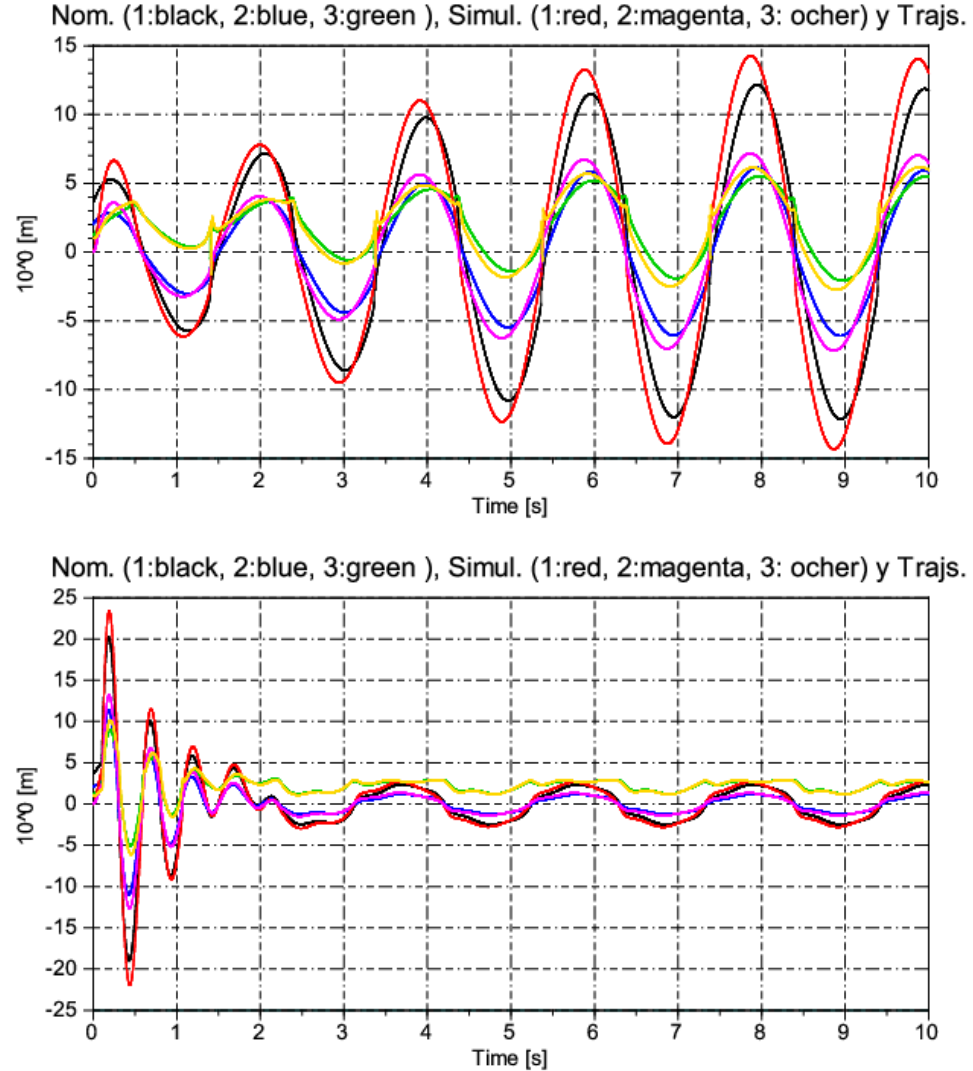
Figure 6.43: The trajectory tracking of the *non-adaptive* (upper) and the *adaptivev* (lower) controllers for $\vec{y}$

The operation of the adaptivity is revealed by Fig. 6.44. In the non-adaptive case the lines *red*, *magenta*, and *ocher* colors are *exactly covered* by the *brown*, *purple*, and *pink* ones. In the adaptive case these curves are well separated but the "desired" and the "simulated" ones are in each-other's close vicinity. Details are displayed by Fig. 6.45 in which the events that follow turning on the adaptivity are shown: then the formerly "identical" lines separate.

Sim(1:black 2:blue 3:green) DES(1:red 2:magenta 3:ocher) REQ(1:brown 2:purple 3:pink)

Sim(1:black 2:blue 3:green) DES(1:red 2:magenta 3:ocher) REQ(1:brown 2:purple 3:pink)

Figure 6.44: The 2nd time-derivatives of $\ddot{\vec{x}}$ in the non-adaptive (upper chart) and the adaptive (lower chart) controllers: simulated motion – black, blue, green lines, desired ones – red, magenta, ocher lines, and the adaptively deformed – brown, purple, pink lines
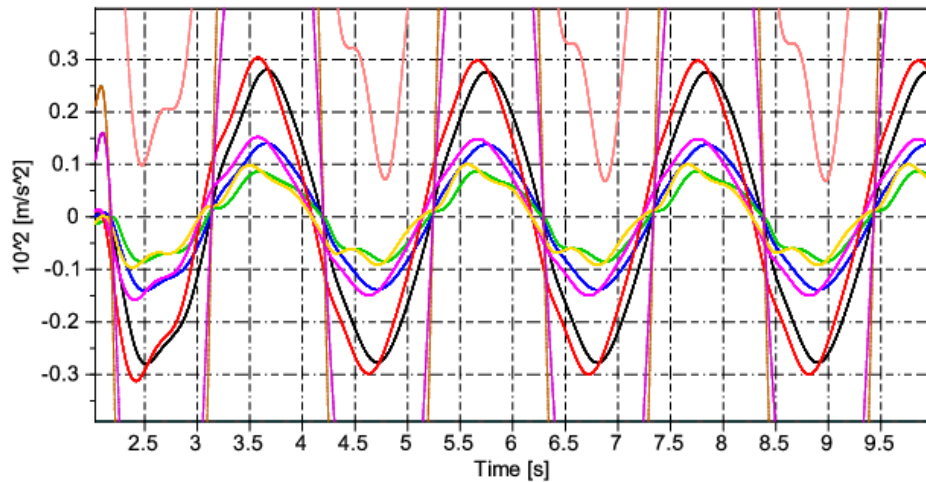
Figure 6.45: The 2nd time-derivatives of $\ddot{\tilde{x}}$ in the non-adaptive (upper chart) and the adaptive (lower chart) controllers: simulated motion – black, blue, green lines, desired ones – red, magenta, ocher lines, and the adaptively deformed – brown, purple, pink lines (zoomed in excerpts)

The exerted forces are revealed by Fig. 6.46. In the non-adaptive case hectic fluctuations appear in cyclic manner, while in the adaptive case, following the transient parts they disappear. Zooming in the details in Fig. 6.47 also testifies that faster than that in (6.20).
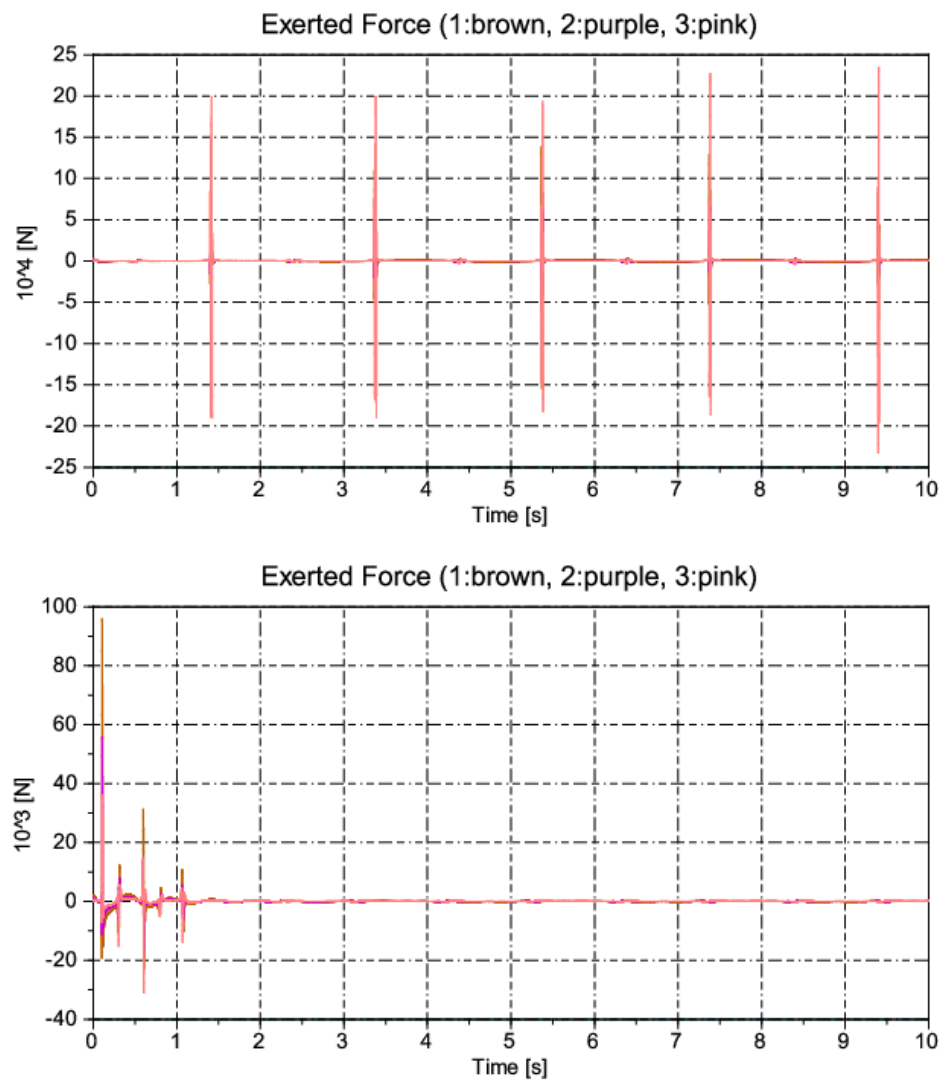
Figure 6.46: Exerted force in the non-adaptive case (upper chart) and in the adaptive case (lower chart)

$$\left(m_x - \frac{kL_0}{\|\vec{c}\|}\right)$$
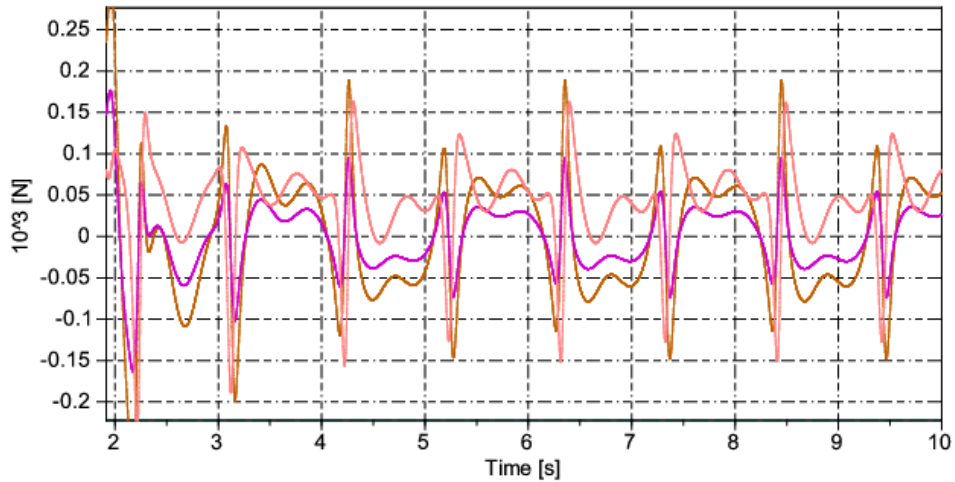
Figure 6.47: Exerted force in the non-adaptive case (upper chart) and in the adaptive case (lower chart) (zoomed in excerpts)

6.4 Application in vehicle control

6.4.1 Control of caster-supported carts with two driving wheels

In the past decade motion control of WMRs consisting of two actively driven wheels and a caster obtained considerable attention (e.g. [76, 83, 84]). These approaches used Lyapunov's 2nd method and normally were based on complicated mathematical details. Our aim is to show that the RFPT-based adaptive controller design allows the selection of *kinematically prescribed point of the WMR* for controlling its motion and the rotation of the cart around this point. This point may differ from the mass center point of the cart that was a very popular choice for tracking due to the fact that the equations of motion in this case appear as that of a simple LTI system. If the tracked point is different to the mass center point in the equations of motion strongly coupled nonlinear terms appear that makes the

controller design task very complicated. It is also shown that if the properties of the driving motors as Electrodynamic subsystems are also taken into consideration the control task becomes a third order one. It is also shown that by the use of this adaptive technique the order of the control task can be reduced from 3 to 2. In this way I made a step towards the elaboration of a more general order reduction technique in the case of nonlinear systems.

The main problem in the control of such systems [A. 17]:

1. Kinematic constraints 1: the cart must move on the surface of a plain ground, the *independent variables to be controlled* are the (x, y) coordinates of a particular point of the cart on this plain, and the rotational position around the horizontal axis θ.

2. Kinematic constraints 2: the above condition allows skidding/sliding/slipping of the cart on the ground. These effects must be excluded, i.e. *the system to be controlled is a non-holonomic device* in which *the rotational speeds of the wheels uniquely determine the speed of the motion over the ground*.

3. For solving this task we *have only two control agents*, the torques exerted by the driven wheels.

4. The dynamic model of the cart has simple equations *only if the the tracked point and the mass center point of the system are identical. This condition rarely can be met.*

5. Normally the dynamic parameters of the system are *only approximately known*.

6. On the basis of Classical Mechanics a 2nd order control can be formulated for the rotation of the wheels. *If the system is driven by electric DC motors the necessary torque components cannot be instantaneously set, only the time-derivatives of these torque values can be instantaneously prescribed.*

7. Consequently

   (a) *either a 3rd order controller can be designed for the rotation of the wheels*, or
   (b) *some order reduction technique must be elaborated for a nonlinear system*
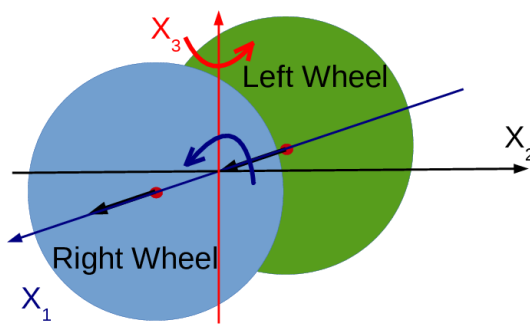
Figure 6.48: The kinematic structure of the two wheels model in which only the wheels must remain in contact with the ground (rotations and torque components are defined according to the "right handed convention") [A. 17]

The solution is to 1. Local Optimization without Riccati Equations.The general conditions allow two rotary degree of freedom. Let apply a *rotation of the cart around axle* $\hat{x}_1$ *by angle* q_u radian by the rotational matrix $U(q_u)$ generated by the generator $\hat{G}U$ as [A. 17]

$$U(q_u) \stackrel{def}{=} \begin{pmatrix} 1 & 0 & 0 \\ 0 & \cos q_u & -\sin q_u \\ 0 & \sin q_u & \cos q_u \end{pmatrix}, \hat{G}^{(U)} \stackrel{def}{=} \begin{pmatrix} 0 & 0 & 0 \\ 0 & 0 & -1 \\ 0 & 1 & 0 \end{pmatrix}. \tag{6.26}$$

If the axles of the wheels in the "basic position" were parallel with $\hat{x}_1$ this operation can be realized because it keeps the wheels in contact with the plane of motion that is perpendicular to $\hat{x}_3$ [A. 17].

Following that apply a *rotation around $\hat{x}_3$ with angle q_v* radians by the orthogonal matrix $V(q_v)$ generated by the generator $\hat{G}^{(V)}$ as [A. 17]

$$V(q_v) \stackrel{def}{=} \begin{pmatrix} \cos q_v & -\sin q_v & 0 \\ \sin q_v & \cos q_v & 0 \\ 0 & 0 & 1 \end{pmatrix}, \hat{G}^{(V)} \stackrel{def}{=} \begin{pmatrix} 0 & -1 & 0 \\ 1 & 0 & 0 \\ 0 & 0 & 0 \end{pmatrix}. \tag{6.27}$$

This operation is possible, too, since it moves the wheels on the surface of the horizontal plain. Therefore a two-parameters subgroup of the 3D rotational group was so found that its elements describe the possible motion of the cart if it remains in contact with the horizontal plain. $(q_v \equiv \theta)$ [A. 17].

From that fact cart is a Non-Holonomic device further constraints originate.

Since the rotation $U(q_u)$ around x_1 does not concern the position of the wheels on the ground only $V(q_v)$ is interesting that moves the wheels on the ground. (In the case of a caster $U \equiv I$.) [A. 17].

$$\begin{matrix} R_1^R = D\cos q_v + R_1 & R_1^L = -D\cos q_v + R_1 \\ R_2^R = D\sin q_v + R_2 & R_2^L = -D\sin q_v + R_2 \end{matrix}, \tag{6.28}$$

$$\begin{matrix} \dot{R}_1^R = -D\sin q_v \dot{q}_v + \dot{R}_1 & \dot{R}_1^L = D\sin q_v \dot{q}_v + \dot{R}_1 \\ \dot{R}_2^R = D\cos q_v \dot{q}_v + \dot{R}_2 & \dot{R}_2^L = -D\cos q_v \dot{q}_v + \dot{R}_2 \end{matrix} \tag{6.29}$$

So these relations are generally valid.

$$\begin{aligned} \frac{\dot{R}_1^R + \dot{R}_1^L}{2} &= \dot{R}_1 = r_w \frac{\dot{q}_r + \dot{q}_l}{2} \sin q_v \\ \frac{\dot{R}_2^R + \dot{R}_2^L}{2} &= \dot{R}_2 = -r_w \frac{\dot{q}_r + \dot{q}_l}{2} \cos q_v \\ \frac{\dot{R}_1^R - \dot{R}_1^L}{2} &= -D\sin q_v \dot{q}_v = r_w \frac{\dot{q}_r - \dot{q}_l}{2} \sin q_v \\ \frac{\dot{R}_2^R - \dot{R}_2^L}{2} &= D\cos q_v \dot{q}_v = -r_w \frac{\dot{q}_r - \dot{q}_l}{2} \cos q_v. \end{aligned} \tag{6.30}$$

The non-holonomic constraints originate form the next figure:
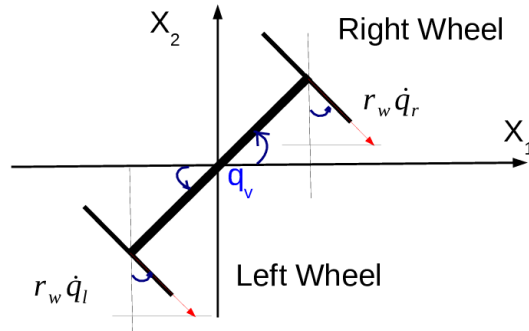
Figure 6.49: The nature of the kinematic constraints in the case of a non-holonomic device [A. 17]

$$\dot{R}_1 = r_w \frac{\dot{q}_r + \dot{q}_l}{2} \sin q_v, \dot{R}_2 = -r_w \frac{\dot{q}_r + \dot{q}_l}{2} \cos q_v$$
$$\dot{q}_v = -\frac{r_w}{D} \frac{\dot{q}_r - \dot{q}_l}{2}. \tag{6.31}$$

Apply a generally not realizable PID-type tracking policy by the use of the quantities to be controlled as [A. 17]

$$h_{int}(t) \stackrel{def}{=} \int_{t_0}^{t} \left(\xi^N(\zeta) - \xi(\zeta) \right) d\zeta, \quad \left(\frac{d}{dt} + \Lambda \right)^3 h_{int}(t) \equiv 0 \tag{6.32}$$

where $\xi \stackrel{def}{=} (q_v(t), R_1(t), R_2(t))^T$. This idea works because the solution of the differential equation $\left(\frac{d}{dt} + \Lambda \right) f(t) \equiv 0$ is $f(t) = f(t_0) \exp(-\Lambda(t - t_0)) \longrightarrow 0$ as $t \longrightarrow \infty$. Equation (6.42) simply leads to the *desired 2nd time-derivatives* as [A. 17]

$$\ddot{\xi}^{Des}(t) = \Lambda^3 h_{int}(t) + 3\lambda^2 \xi(t) + 3\Lambda \dot{\xi}(t) + \ddot{\xi}^N(t) \tag{6.33}$$

Then in each program cycle the *allowed* $\ddot{q}_r^{Des}$ and $\ddot{q}_l^{Des}$ values that yield the best approximation of the desired 2nd derivatives if a quadratic goal function

$$\Phi(\ddot{q}_r^{Des}, \ddot{q}_l^{Des}) \stackrel{def}{=}$$
$$= \left(\ddot{x}^{Des} - \ddot{x} \right)^2 + \left(\ddot{y}^{Des} - \ddot{y} \right)^2 + \kappa \left(\ddot{\theta}^{Des} - \ddot{\theta} \right)^2$$

$$\kappa > 0, \tag{6.34}$$
$$\ddot{x} = \ddot{x}(q_r, q_l, \dot{q}_r, \dot{q}_l, \ddot{q}_r^{Des}, \ddot{q}_l^{Des}),$$
$$\ddot{y} = \ddot{y}(q_r, q_l, \dot{q}_r, \dot{q}_l, \ddot{q}_r^{Des}, \ddot{q}_l^{Des}),$$
$$\ddot{\theta} = \ddot{\theta}(q_r, q_l, \dot{q}_r, \dot{q}_l, \ddot{q}_r^{Des}, \ddot{q}_l^{Des})$$

is used [A. 17].

Suggested solution for simultaneous compensation of the modeling imprecisions and nonlinear order reduction.

Use the analytical form and the numerical parameters of the best available model for the cart's dynamics! In our case it is [A. 17]:

$$I\ddot{\theta} = \frac{Ir}{2D} (\ddot{q}_r - \ddot{q}_l) = \frac{D}{r}(T_r - T_l),$$
$$M \begin{pmatrix} \ddot{x} \\ \ddot{y} \end{pmatrix} = \begin{pmatrix} \cos(\theta) \\ \sin(\theta) \end{pmatrix} \frac{T_r + T_l}{r}. \tag{6.35}$$

Consider the model of the DC motor as follows:

$$v\ddot{q}_{rl} = \frac{Q_{rl}^e + \frac{Q_{rl}^{ext}}{v} - bv\dot{q}_{rl}}{\Theta},$$
$$\dot{Q}_{rl}^e = \frac{-RQ_{rl}^e - K^2 v\dot{q}_{rl} + KU_{rl}}{L} \tag{6.36}$$

where *identical motors* were assumed at the LHS and RHS with the variables and parameters as follows [A. 17]:

- $Q^e [N \cdot m]$ is the torque of electromagnetic origin exerted on the motor's axle (it is proportional to the motor current),

- $Q^{ext} [N \cdot m]$ is the torque of external origin acting on the wheel's axle, i.e. $Q_{rl}^{ext} = T_{rl}$,

- $R = 1 [\Omega]$ is the Ohmic resistance of the motor's coil system,

- $L = 0.5 [H]$ is its inductivity,

- $\Theta = 0.01 [kg \cdot m^2]$ denotes the momentum of the rotary part of the motor,

- $b = 0.1 [N \cdot m \cdot s/rad]$ describes the viscous friction of the motor's axle,

- $K = 0.01$ is the motor's torque coefficient, and

- $U\,[V]$ denotes the motor control voltage,

- $\nu = 1/5$ is the gear ratio regarding the motor and the wheel axles

By the use of the first equation of the motor's equation of motion $Q_{rl}^{e^{Des}}$ is calculated for $\ddot{q}_{rl}^{Des}$. Assuming that $\dot{Q}_{rl}^{e} \approx 0$ for a given constant $\dot{q}_{rl}$ *the stabilized value of the necessary U_{rl}^{Des} is estimated from* the 2nd equation of (6.36) as [A. 17]

$$U_{rl}^{Des} \overset{def}{=} \frac{R}{K}Q_{rl}^{e^{Des}} + K\nu\dot{q}_{rl}. \tag{6.37}$$

This approximate estimation has to be adaptively deformed.

6.4.1.1   Simulation Results

The above described model was used, both adaptive RFPT and RFPT based MRAC cases.
    The adaptive RFPT case:
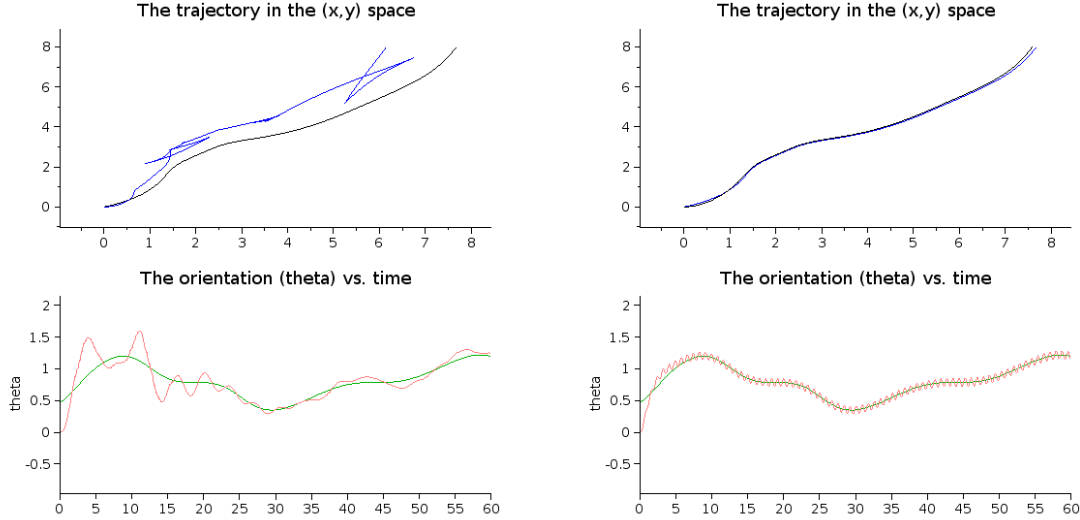
Figure 6.50: The trajectory tracking: non-adaptive control (LHS), adaptive control (RHS) $[x^N, y^N$: black $,\theta^N$: green, x, y: blue, θ: pink] [A. 17]
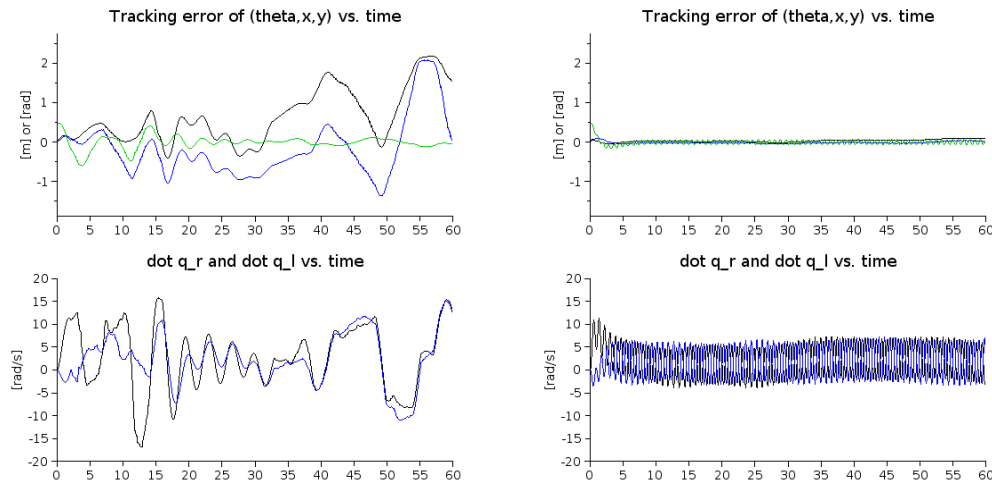
Figure 6.51: The tracking error (upper) and the wheels' rotational speeds (lower): non-adaptive control (LHS), adaptive control (RHS) [$x^N - x$: black, $y^N - y$: blue, $\theta^N - \theta$: green, $\dot{q}_r$: black, $\dot{q}_l$: blue] [A. 17]

The MRAC case:
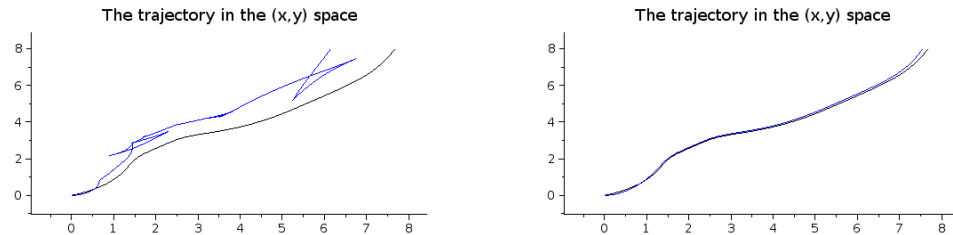
Figure 6.52: The trajectories: Non Adaptive case (LHS), MRAC case (RHS) (Nominal: black, Simulated: blue)[A. 18]
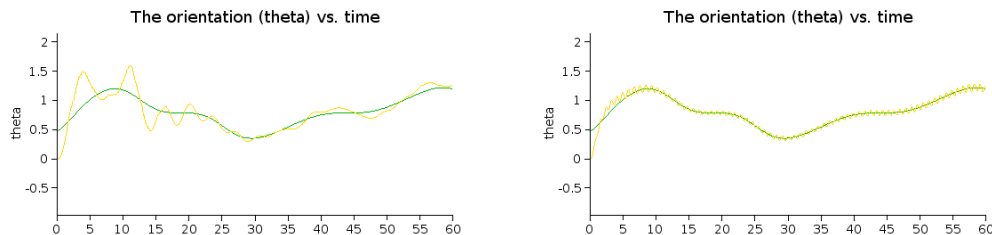
Figure 6.53: The rotation of the Cart: Non Adaptive case (LHS), MRAC case (RHS) (Nominal: green, Simulated: ocher) [A. 18]
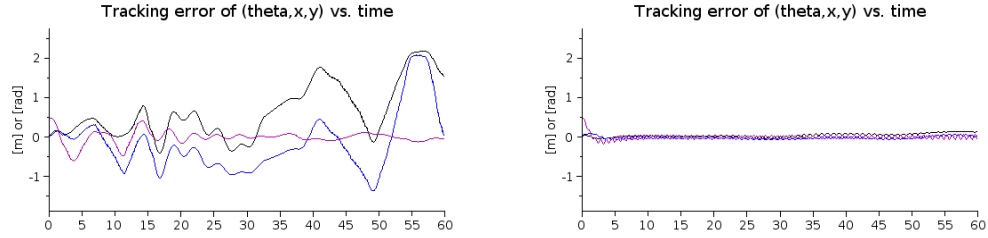
Figure 6.54: Tracking Error: Non Adaptive case (LHS), MRAC case (RHS) (x: black, y: blue, θ: magenta) [A. 18]
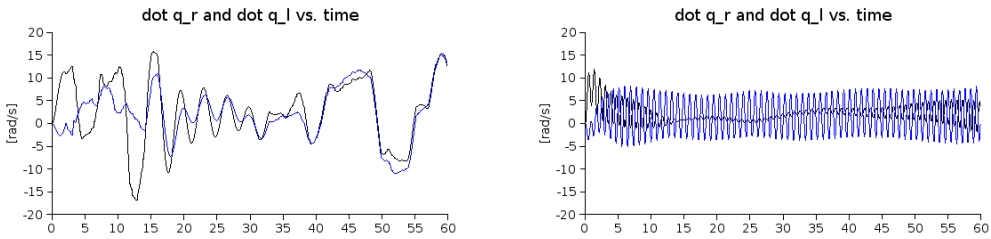
Figure 6.55: Rotational speed of the wheels: Non Adaptive case (LHS), MRAC case (RHS) (wheel left: blue, wheel right: black) [A. 18]

6.4.2 Nonlinear Order Reduction based on an Adaptive Controller Using Approximate Dynamical Model

The approach I suggested is not based on these antecedents. With the assumption that the operation of the electromagnetic subsystem is considerably faster than that of the mechanical parts it seems to be a realistic approach to apply constant torque values during the cycles of the digital controllers. Between the cycles this results in step functions. It is assumed that the necessary torque or force values quickly reach the stationary states and remain almost constant. The possibility for that is generally guaranteed by the the stabilizing nature of the dissipative components as in the case of the *"Passivity Control"* [85, 86]. This approach as it is only a simple approximation that generates errors. My main idea was to compensate the consequences of these approximations together with that of other modeling imprecisions or external disturbances by an adaptive controller.

6.4.3 The Model of the Permanent Magnet DC Motor and the Unified Model

m I is assumed that both of the active wheels are driven by identical motors the model of which was taken from [77].

$$\dot{Q}_e = \frac{-RQ_e - K^2\dot{q} + KU}{L} \ .$$
(6.38)

The definition of the variables and parameters is given as follows:

- q is the rotational angle of the motor's shaftét,

- Q_e denotes the torque of electromagnetic origin,

- R is the dissipative Ohmic resistance of this coil,

- L denotes the inductivity of this coil,

- K the torque coefficient of the motor,

- U is the actual control voltage.

This model has to be combined with the dynamic model of the cart. The result is:

$$\left[\frac{\Theta^{\mathrm{Mot}}}{v}I + \frac{-vr_{\mathrm{w}}^2}{2D}\begin{pmatrix}\frac{1}{r_{\mathrm{w}}} & -\frac{D}{r_{\mathrm{w}}}\\ -\frac{1}{r_{\mathrm{w}}} & -\frac{D}{r_{\mathrm{w}}}\end{pmatrix}\tilde{H}\right]\times\begin{pmatrix}\ddot{q}_{\mathrm{r}}\\ \ddot{q}_{\mathrm{l}}\end{pmatrix} + \frac{b}{v}\begin{pmatrix}\dot{q}_{\mathrm{r}}\\ \dot{q}_{\mathrm{l}}\end{pmatrix} + \frac{-vr_{\mathrm{w}}^2}{2D}\begin{pmatrix}\frac{1}{r_{\mathrm{w}}} & -\frac{D}{r_{\mathrm{w}}}\\ -\frac{1}{r_{\mathrm{w}}} & -\frac{D}{r_{\mathrm{w}}}\end{pmatrix}B = \begin{pmatrix}Q_{\mathrm{r}}^{\mathrm{eMot}}\\ Q_{\mathrm{l}}^{\mathrm{eMot}}\end{pmatrix}, \text{ where}$$

$$\tilde{H}_{11} = \frac{r_{\mathrm{w}}}{2D}(\Theta_{11} + \Theta_{22})+$$
$$\frac{Mr_{\mathrm{w}}}{2}(S_2 sq_{\mathrm{v}} + S_1 cq_{\mathrm{v}}) \ ,$$
$$\tilde{H}_{12} = -\frac{r_{\mathrm{w}}}{2D}(\Theta_{11} + \Theta_{22})+$$
$$\frac{Mr_{\mathrm{w}}}{2}(S_2 sq_{\mathrm{v}} + S_1 cq_{\mathrm{v}}) \ ,$$
$$\tilde{H}_{21} = \frac{Mr_{\mathrm{w}}}{2D}(S_2 sq_{\mathrm{v}} + S_1 cq_{\mathrm{v}})+$$
$$\frac{Mr_{\mathrm{w}}}{2} \ ,$$
$$\tilde{H}_{22} = \frac{Mr_{\mathrm{w}}}{2} - \frac{Mr_{\mathrm{w}}}{2D}\times$$
$$(S_2 sq_{\mathrm{v}} + S_1 cq_{\mathrm{v}})$$

$$(6.39)$$

in which the more condensed form was used with the definitions $cq_{\mathrm{v}} \stackrel{def}{=} \cos q_{\mathrm{v}}$ and $sq_{\mathrm{v}} \stackrel{def}{=} \sin q_{\mathrm{v}}$ wile $I \in \mathrm{IR}^{2\times 2}$ denotes a unit matrix.

Via comparing (6.39) with (6.35) the increase in the formal model-complexity becomes evident. Even if on symmetry reasons the sum $(\Theta_{11} + \Theta_{22})$ remains constant as well as Ξ if $\hat{S} \neq 0$ (and consequently $S \neq 0$), (6.39) cannot be LTI-type: the matrix elements of $\tilde{H}$ will depend on the rotational orientation q_{v} and the term defined in the array B of (6.39), besides the nonlinearities caused by the occurrence of $\sin q_{\mathrm{v}}$ and $\cos q_{\mathrm{v}}$ quadratic terms in $\dot{q}_{\mathrm{r}}$ és $\dot{q}_{\mathrm{l}}$ also appear. On this reason the formal properties of the model in (6.39) do not allow the simple design that is possible in the case of (6.35). The nonlinearities require the use either Lyapunov's 2nd method or one of its alternatives. In my contribution I developed and RFPT-based adaptive controller that separates the dynamics of the system from the purely kinematically formulated desired trajectory tracking properties. On this reason it is expedient to consider the *kinematically possible trajectory tracking properties* in the sequel.

6.4.4 Possible Trajectory Tracking Prescriptions Allowed by the Kinematic Constraints

$$\dot{R}_1 = r_{\mathrm{w}}\frac{\dot{q}_{\mathrm{r}}+\dot{q}_{\mathrm{l}}}{2}\sin q_{\mathrm{v}}$$
$$\dot{R}_2 = -r_{\mathrm{w}}\frac{\dot{q}_{\mathrm{r}}+\dot{q}_{\mathrm{l}}}{2}\cos q_{\mathrm{v}} \qquad (6.40)$$
$$\dot{q}_{\mathrm{v}} = -\frac{r_{\mathrm{w}}}{D}\frac{\dot{q}_{\mathrm{r}}-\dot{q}_{\mathrm{l}}}{2} \ .$$

A kinematikailag megengedhető 2. deriváltak a csúszástól mentes speciális esetben (6.40)-ból származtathatók a következőképp:

$$\ddot{R}_1 = r_{\mathrm{w}}\frac{\ddot{q}_{\mathrm{r}}+\ddot{q}_{\mathrm{l}}}{2}\sin q_{\mathrm{v}} + r_{\mathrm{w}}\frac{\dot{q}_{\mathrm{r}}+\dot{q}_{\mathrm{l}}}{2}\cos q_{\mathrm{v}}\dot{q}_{\mathrm{v}}$$
$$\ddot{R}_2 = -r_{\mathrm{w}}\frac{\ddot{q}_{\mathrm{r}}+\ddot{q}_{\mathrm{l}}}{2}\cos q_{\mathrm{v}} + r_{\mathrm{w}}\frac{\dot{q}_{\mathrm{r}}+\dot{q}_{\mathrm{l}}}{2}\sin q_{\mathrm{v}}\dot{q}_{\mathrm{v}} \qquad (6.41)$$
$$\ddot{q}_{\mathrm{v}} = -\frac{r_{\mathrm{w}}}{D}\frac{\ddot{q}_{\mathrm{r}}-\ddot{q}_{\mathrm{l}}}{2} \ .$$

Assume that we have some nominal trajectory expressed as $\xi^{\mathrm{N}} \stackrel{def}{=} \left(q_{\mathrm{v}}^{\mathrm{N}}(t), R_1^{\mathrm{N}}(t), R_2^{\mathrm{N}}(t)\right)^T$ that has to be tracked by the controller *as precisely as it is possible*. (It is not assumed that this trajectory would be exactly realizable. It may origin from a driver who does not mind the problem of kinematic limitations.) A purely kinematic design for the tracking can be a PID-type tracking error relaxation given by (6.42) with $\mathrm{IR} \ni \Lambda > 0$:

$$h(t) \stackrel{def}{=} \xi^{\mathrm{N}}(t) - \xi(t) \; ,$$
$$h_{\mathrm{int}}(t) \stackrel{def}{=} \int_{t_0}^{t} \left(\xi^{\mathrm{N}}(\zeta) - \xi(\zeta) \right) d\zeta \; , \tag{6.42}$$
$$\left(\tfrac{d}{dt} + \Lambda \right)^3 h_{\mathrm{int}}(t) \equiv 0$$

in which $\xi \stackrel{def}{=} (q_v(t), R_1(t), R_2(t))^T$. This idea is based on the observation that the solution of the differential equation $\left(\tfrac{d}{dt} + \Lambda \right) f(t) \equiv 0$ for an arbitrary initial value converges to 0 as $t \to \infty$. The equation (6.42) leads to the following *"desired 2nd time- derivatives"*:

$$\ddot{\xi}^{\mathrm{Des}}(t) = \Lambda^3 h_{\mathrm{int}}(t) + 3\Lambda^2 h(t) +$$
$$3\Lambda \dot{h}(t) + \ddot{\xi}^{\mathrm{N}}(t) \; . \tag{6.43}$$

In the case of a PD-type tracking strategy we may prescribe $\left(\Lambda + \tfrac{d}{dt} \right)^2 \left(\xi^{\mathrm{N}}(t) - \xi(t) \right) \equiv 0$ that leads to the feedback terms in (6.44) and the desired 2nd time-derivatives

$$\ddot{\xi}^{\mathrm{Des}}(t) = 2\Lambda^2 h(t) + 2\Lambda \dot{h}(t) + \ddot{\xi}^{\mathrm{N}}(t) \; . \tag{6.44}$$

In the lack of skidding, due to the non-holonomic constraints neither (6.43) nor (6.44) can be exactly realized. This may result in a continuously increasing integrated error that cannot be compensated, therefore the appropriate tracking prescription may result even in divergence. A plausible "remedy" may be the limitation of the effect of the error integral with a limiting factor $w > 0$ as

$$\ddot{\xi}^{\mathrm{Des}}(t) = \Lambda^3 w \tanh\left(\tfrac{h_{\mathrm{int}}(t)}{w} \right) +$$
$$3\Lambda^2 h(t) + 3\Lambda \dot{h}(t) + \ddot{\xi}^{\mathrm{N}}(t) \; . \tag{6.45}$$

(*"truncated PID strategy"*).

If in spite of that remains some little tracking error remains its relaxation can be sped by the equation:

$$\dot{h} = -\alpha \operatorname{sign}(h) |h|^{\beta_{\mathrm{kin}}} \; ,$$
$$h(t) = \left[h(0)^{1-\beta_{\mathrm{kin}}} \right.$$
$$\left. -\alpha(1-\beta_{\mathrm{kin}})t \right]^{\frac{1}{1-\beta_{\mathrm{kin}}}} \tag{6.46}$$
$$\alpha > 0 \text{ és } \beta_{\mathrm{kin}} \in (0,1), \, h \geq 0, \, t \geq 0 \; ,$$

in which a little initial error could be relaxed much faster than in the case of a linear feedback. On this reason I refer to this strategy as *"greedy error relaxation"*. Since this feedback is considerably for small errors and its significance fades as the error increases it may be expedient to combine it with the linear feedback by the use of a *"balancing factor"* $b_{\mathrm{bal}} \in (0,1)$ and modify the original PID- and PD-type strategies as

$$\ddot{\xi}^{\mathrm{Des}}(t) = \Lambda^3 w \tanh\left(\tfrac{h_{\mathrm{int}}(t)}{w} \right) +$$
$$3\Lambda^2 \big[b_{\mathrm{bal}} h(t) +$$
$$(1 - b_{\mathrm{bal}}) \operatorname{sign}(h) |h(t)|^{\beta_{\mathrm{kin}}} \big] +$$
$$3\Lambda \dot{h}(t) + \ddot{\xi}^{\mathrm{N}}(t) \; , \tag{6.47}$$

and

$$\ddot{\xi}^{\mathrm{Des}}(t) = 2\Lambda^2 \big[b_{\mathrm{bal}} h(t) +$$
$$(1 - b_{\mathrm{bal}}) \operatorname{sign}(h) |h(t)|^{\beta_{\mathrm{kin}}} \big] +$$
$$2\Lambda \dot{h}(t) + \ddot{\xi}^{\mathrm{N}}(t) \; . \tag{6.48}$$

Our expectation is a faster relaxation for both the small and the big errors.

A urther possibility is the application of a little sinusoidal modulation of the original nominal trajectory. The Ackermann-type steering systems have the feature that they allow only simultaneous modification of the rotational pose and the location. This behavior can be experienced by the drivers whenever the car must be "inserted" into a narrow parking place or it has to be moved out from such places. In the latter case at first the orientation has to be set in an iterative manner step-by-step compensating the little translations. In the possession of the desired orientation already greater translations can be allowed. The suggested sinusoidal modulation allows a similar compromise between orientation and position during the whole trip.

A simple possibility for finding a viable compromise to distribute the tracking error between the three components is the minimization of the sum of their weighted squares according to $\ddot{q}_r$ and $\ddot{q}_l$ in each considered time-instant. Due to that only possible desired motion is considered. According to (6.41)

$$\Phi(\ddot{q}_r, \ddot{q}_l) := \kappa_1 \left[\ddot{\xi}_1(t) - \ddot{\xi}_1^{\text{Des}}(t)\right]^2 +$$
$$\kappa_2 \left[\ddot{\xi}_2(t) - \ddot{\xi}_2^{\text{Des}}(t)\right]^2 +$$
$$\kappa_3 \left[\ddot{\xi}_3(t) - \ddot{\xi}_3^{\text{Des}}(t)\right]^2 \tag{6.49}$$

in which κ_1, κ_2, $\kappa_3 > 0$ are positive weights concern the *orientation error*, the *position error according to coordinate x*, and the *position error according to coordinate y*, respectively. The case $\kappa_2 \neq \kappa_3$ means a on-isotropic error sensitivity. It is easy to find the minimum of the goal function since

$$0 = \frac{\partial \Phi}{\partial \ddot{q}_r} =$$
$$2\kappa_1 \left[\ddot{\xi}_1(t) - \ddot{\xi}_1^{\text{Des}}(t)\right]\frac{\partial \ddot{\xi}_1}{\partial \ddot{q}_r} + 2\kappa_2 \left[\ddot{\xi}_2(t) - \ddot{\xi}_2^{\text{Des}}(t)\right]\frac{\partial \ddot{\xi}_2}{\partial \ddot{q}_r} + 2\kappa_3 \left[\ddot{\xi}_3(t) - \ddot{\xi}_3^{\text{Des}}(t)\right]\frac{\partial \ddot{\xi}_3}{\partial \ddot{q}_r} \ ,$$
$$0 = \frac{\partial \Phi}{\partial \ddot{q}_l} =$$
$$2\kappa_1 \left[\ddot{\xi}_1(t) - \ddot{\xi}_1^{\text{Des}}(t)\right]\frac{\partial \ddot{\xi}_1}{\partial \ddot{q}_l} + 2\kappa_2 \left[\ddot{\xi}_2(t) - \ddot{\xi}_2^{\text{Des}}(t)\right]\frac{\partial \ddot{\xi}_2}{\partial \ddot{q}_l} + 2\kappa_3 \left[\ddot{\xi}_3(t) - \ddot{\xi}_3^{\text{Des}}(t)\right]\frac{\partial \ddot{\xi}_3}{\partial \ddot{q}_l} \tag{6.50}$$

in which according to (6.41)

$$\frac{\partial \ddot{\xi}_1}{\partial \ddot{q}_r} = \frac{\partial \ddot{q}_v}{\partial \ddot{q}_r} = -\frac{r_w}{2D},$$
$$\frac{\partial \ddot{\xi}_2}{\partial \ddot{q}_r} = \frac{\partial \ddot{R}_1}{\partial \ddot{q}_r} = \frac{r_w \sin q_v}{2},$$
$$\frac{\partial \ddot{\xi}_3}{\partial \ddot{q}_r} = \frac{\partial \ddot{R}_2}{\partial \ddot{q}_r} = -\frac{r_w \cos q_v}{2},$$
$$\frac{\partial \ddot{\xi}_1}{\partial \ddot{q}_l} = \frac{\partial \ddot{q}_v}{\partial \ddot{q}_l} = \frac{r_w}{2D},$$
$$\frac{\partial \ddot{\xi}_2}{\partial \ddot{q}_l} = \frac{\partial \ddot{R}_1}{\partial \ddot{q}_l} = \frac{r_w \sin q_v}{2},$$
$$\frac{\partial \ddot{\xi}_3}{\partial \ddot{q}_l} = \frac{\partial \ddot{R}_2}{\partial \ddot{q}_l} = -\frac{r_w \cos q_v}{2}, \tag{6.51}$$

that is

$$0 = -\kappa_1 \left[\ddot{\xi}_1(t) - \ddot{\xi}_1^{\text{Des}}(t)\right]\frac{r_w}{2D} + \kappa_2 \left[\ddot{\xi}_2(t) - \ddot{\xi}_2^{\text{Des}}(t)\right]\frac{r_w \sin q_v}{2} \kappa_3 \left[\ddot{\xi}_3(t) - \ddot{\xi}_3^{\text{Des}}(t)\right]\frac{r_w \cos q_v}{2}$$
$$0 = \kappa_1 \left[\ddot{\xi}_1(t) - \ddot{\xi}_1^{\text{Des}}(t)\right]\frac{r_w}{2D} + \kappa_2 \left[\ddot{\xi}_2(t) - \ddot{\xi}_2^{\text{Des}}(t)\right]\frac{r_w \sin q_v}{2} - \kappa_3 \left[\ddot{\xi}_3(t) - \ddot{\xi}_3^{\text{Des}}(t)\right]\frac{r_w \cos q_v}{2} \ . \tag{6.52}$$

Furthermore, according to (6.41) these expressions are linear in $\ddot{q}_r$ and $\ddot{q}_l$, therefore the solution can easily be obtained as

$$
0 = -\kappa_1\left[-\frac{r_\mathrm{w}}{D}\frac{\ddot{q}_\mathrm{r}-\ddot{q}_\mathrm{l}}{2} - \ddot{\xi}_1^{\mathrm{Des}}(t)\right]\frac{r_\mathrm{w}}{2D} +
$$
$$
\kappa_2\left[r_\mathrm{w}\frac{\ddot{q}_\mathrm{r}+\ddot{q}_\mathrm{l}}{2}\sin q_\mathrm{v} + r_\mathrm{w}\frac{\dot{q}_\mathrm{r}+\dot{q}_\mathrm{l}}{2}\cos q_\mathrm{v}\dot{q}_\mathrm{v}\right.
$$
$$
\left.-\ddot{\xi}_2^{\mathrm{Des}}(t)\right]\frac{r_\mathrm{w}\sin q_\mathrm{v}}{2}
$$
$$
-\kappa_3\left[-r_\mathrm{w}\frac{\ddot{q}_\mathrm{r}+\ddot{q}_\mathrm{l}}{2}\cos q_\mathrm{v} + r_\mathrm{w}\frac{\dot{q}_\mathrm{r}+\dot{q}_\mathrm{l}}{2}\sin q_\mathrm{v}\dot{q}_\mathrm{v}\right.
$$
$$
\left.-\ddot{\xi}_3^{\mathrm{Des}}(t)\right]\frac{r_\mathrm{w}\cos q_\mathrm{v}}{2} \ ,
$$

$$
0 = \kappa_1\left[-\frac{r_\mathrm{w}}{D}\frac{\ddot{q}_\mathrm{r}-\ddot{q}_\mathrm{l}}{2} - \ddot{\xi}_1^{\mathrm{Des}}(t)\right]\frac{r_\mathrm{w}}{2D} +
$$
$$
\kappa_2\left[r_\mathrm{w}\frac{\ddot{q}_\mathrm{r}+\ddot{q}_\mathrm{l}}{2}\sin q_\mathrm{v} + r_\mathrm{w}\frac{\dot{q}_\mathrm{r}+\dot{q}_\mathrm{l}}{2}\cos q_\mathrm{v}\dot{q}_\mathrm{v}\right.
$$
$$
\left.-\ddot{\xi}_2^{\mathrm{Des}}(t)\right]\frac{r_\mathrm{w}\sin q_\mathrm{v}}{2}
$$
$$
-\kappa_3\left[-r_\mathrm{w}\frac{\ddot{q}_\mathrm{r}+\ddot{q}_\mathrm{l}}{2}\cos q_\mathrm{v} + r_\mathrm{w}\frac{\dot{q}_\mathrm{r}+\dot{q}_\mathrm{l}}{2}\sin q_\mathrm{v}\dot{q}_\mathrm{v}\right.
$$
$$
\left.-\ddot{\xi}_3^{\mathrm{Des}}(t)\right]\frac{r_\mathrm{w}\cos q_\mathrm{v}}{2} \ .
$$

(6.53)

This is a set of linear equations that easily can be solved with a variable transformation for $\ddot{q}_- \overset{def}{=} (\ddot{q}_\mathrm{r} - \ddot{q}_\mathrm{l})$ and $\ddot{q}_+ \overset{def}{=} (\ddot{q}_\mathrm{r} + \ddot{q}_\mathrm{l})$ in (6.55). Via comparing the two equations it is obtained that

$$
\begin{pmatrix} \frac{\kappa_1 r_\mathrm{w}^2}{4D^2} & \frac{r_\mathrm{w}^2(\kappa_2 sq_\mathrm{v}^2 + \kappa_3 cq_\mathrm{v}^2)}{4} \\ -\frac{\kappa_1 r_\mathrm{w}^2}{4D^2} & \frac{r_\mathrm{w}^2(\kappa_2 sq_\mathrm{v}^2 + \kappa_3 cq_\mathrm{v}^2)}{4} \end{pmatrix}\begin{pmatrix} \ddot{q}_- \\ \ddot{q}_+ \end{pmatrix}
$$
$$
= \begin{pmatrix} -\kappa_1\ddot{\xi}_1^{\mathrm{Des}}\frac{r_\mathrm{w}}{2D} + \kappa_2\ddot{\xi}_2^{\mathrm{Des}}\frac{r_\mathrm{w} sq_\mathrm{v}}{2} \\ \kappa_1\ddot{\xi}_1^{\mathrm{Des}}\frac{r_\mathrm{w}}{2D} + \kappa_2\ddot{\xi}_2^{\mathrm{Des}}\frac{r_\mathrm{w} sq_\mathrm{v}}{2} \end{pmatrix} +
$$
$$
\begin{pmatrix} -\kappa_3\ddot{\xi}_3^{\mathrm{Des}}\frac{r_\mathrm{w} cq_\mathrm{v}}{2} \\ -\kappa_3\ddot{\xi}_3^{\mathrm{Des}}\frac{r_\mathrm{w} cq_\mathrm{v}}{2} \end{pmatrix} +
$$
$$
\begin{pmatrix} (\kappa_3-\kappa_2)r_\mathrm{w}^2\frac{\dot{q}_\mathrm{r}+\dot{q}_\mathrm{l}}{4}cq_\mathrm{v} sq_\mathrm{v}\dot{q}_\mathrm{v} \\ (\kappa_3-\kappa_2)r_\mathrm{w}^2\frac{\dot{q}_\mathrm{r}+\dot{q}_\mathrm{l}}{4}cq_\mathrm{v} sq_\mathrm{v}\dot{q}_\mathrm{v} \end{pmatrix}
$$

(6.54)

$$
\begin{pmatrix} \frac{\kappa_1 r_\mathrm{w}^2}{4D^2} & \frac{r_\mathrm{w}^2(\kappa_2\sin^2 q_\mathrm{v} + \kappa_3\cos^2 q_\mathrm{v})}{4} \\ -\frac{\kappa_1 r_\mathrm{w}^2}{4D^2} & \frac{r_\mathrm{w}^2(\kappa_2\sin^2 q_\mathrm{v} + \kappa_3\cos^2 q_\mathrm{v})}{4} \end{pmatrix}\begin{pmatrix} \ddot{q}_- \\ \ddot{q}_+ \end{pmatrix} =
$$
$$
\begin{pmatrix} -\kappa_1\ddot{\xi}_1^{\mathrm{Des}}\frac{r_\mathrm{w}}{2D} + \kappa_2\ddot{\xi}_2^{\mathrm{Des}}\frac{r_\mathrm{w}\sin q_\mathrm{v}}{2} - \kappa_3\ddot{\xi}_3^{\mathrm{Des}}\frac{r_\mathrm{w}\cos q_\mathrm{v}}{2} + (\kappa_3-\kappa_2)r_\mathrm{w}^2\frac{\dot{q}_\mathrm{r}+\dot{q}_\mathrm{l}}{4}\cos q_\mathrm{v}\sin q_\mathrm{v}\dot{q}_\mathrm{v} \\ \kappa_1\ddot{\xi}_1^{\mathrm{Des}}\frac{r_\mathrm{w}}{2D} + \kappa_2\ddot{\xi}_2^{\mathrm{Des}}\frac{r_\mathrm{w}\sin q_\mathrm{v}}{2} - \kappa_3\ddot{\xi}_3^{\mathrm{Des}}\frac{r_\mathrm{w}\cos q_\mathrm{v}}{2} + (\kappa_3-\kappa_2)r_\mathrm{w}^2\frac{\dot{q}_\mathrm{r}+\dot{q}_\mathrm{l}}{4}\cos q_\mathrm{v}\sin q_\mathrm{v}\dot{q}_\mathrm{v} \end{pmatrix} .
$$

(6.55)

$$
\ddot{q}_+^{\mathrm{Des}} = \frac{2\left(\kappa_2\ddot{\xi}_2^{\mathrm{Des}} sq_\mathrm{v} - \kappa_3\ddot{\xi}_3^{\mathrm{Des}} cq_\mathrm{v} + (\kappa_3-\kappa_2)r_\mathrm{w}^2\frac{\dot{q}_\mathrm{r}+\dot{q}_\mathrm{l}}{2}cq_\mathrm{v} sq_\mathrm{v}\dot{q}_\mathrm{v}\right)}{r_\mathrm{w}^2(\kappa_2 sq_\mathrm{v}^2 + \kappa_3 cq_\mathrm{v}^2)}
$$

(6.56)

Via subtracting the 2nd equation from the 1st one we obtain that

$$
\ddot{q}_-^{\mathrm{Des}} = -\frac{2D^2}{\kappa_1 r_\mathrm{w}^2}\frac{\kappa_1 r_\mathrm{w}}{D}\ddot{\xi}_1^{\mathrm{Des}} = -\frac{2D}{r_\mathrm{w}}\ddot{\xi}_1^{\mathrm{Des}}
$$

(6.57)

from which it follows that

$$
\ddot{q}_\mathrm{r}^{\mathrm{Des}} = \frac{\ddot{q}_+^{\mathrm{Des}} + \ddot{q}_-^{\mathrm{Des}}}{2}, \text{ és}
$$
$$
\ddot{q}_\mathrm{l}^{\mathrm{Des}} = \frac{\ddot{q}_+^{\mathrm{Des}} - \ddot{q}_-^{\mathrm{Des}}}{2} \ .
$$

(6.58)

It is interesting that κ_1 is cancelled but κ_2 and κ_3 remain present in the equations.

From physical point of view −based on symmetry considerations− we could be apt to insist on the isotropic prescription $\kappa_2 = \kappa_3$. However, in the case of two actively driven wheels such an idea in not necessarily expedient. To explain this idea consider Fig. 6.51 and the constraint equations in (6.41). If $q_\mathrm{v} = 0$ or $q_\mathrm{v} = \pi$ $\ddot{q}_\mathrm{r}$ and $\ddot{q}_\mathrm{l}$ do not ave any effect on $\ddot{R}_1$.

In similar manner if $q_v = \pm\frac{\pi}{2}$, $\ddot{q}_r$ and $\ddot{q}_l$ do not have any effect on $\ddot{R}_2$. In the vicinity of these special points the kinematically prescribed $\ddot{R}_1^{Des}$ or $\ddot{R}_2^{Des}$ values have only little influence on $\ddot{q}_+$. These effects can be well tracked in (6.56) that can well be utilized in the following manner: if an effect is very small, e.g. there is no way to efficiently influence the value of $\ddot{x}$ let us neglect the prescription for it and let modify efficiently the value of $\ddot{y}$ that is easy in the given pose. Such a strategy can easily be realized by the application of *dynamically varying weight factors* in the goal function as $\kappa_2 \overset{def}{=} \kappa_{20}\left(1 - \cos^2 q_v\right)$ and $\kappa_3 \overset{def}{=} \kappa_{30}\left(1 - \sin^2 q_v\right)$ with the new parameters $\kappa_{20} > 0$ and $\kappa_{30} > 0$. The symmetric choice $\kappa_{20} = \kappa_{30}$ may be expedient due to symmetry reasons.

6.4.5 Simulation Results

The nominal trajectory was circle on the plain with continuous increase in the orientation angle q_v. The kinematic parameters of the carts and its approximation were the same but the dynamic parameters were different. The approximate model assumed that the center point of the two wheels (this poin was tracked by the controller) is identical with the mass center point. In the actually driven system there was an offset.

6.4.5.0.1 Exact model parameters

- The inertial momentum tensor in the "initial position" had the following elements: $\hat{\Theta}_{11}^{Exact} = 5\,kg\,m^2$, $\hat{\Theta}_{22}^{Exact} = 6\,kg\,m^2$;

- The ofset of the mass center point in the initial position was: $\hat{S}_1^{Exact} = 0.3\,m$, and $\hat{S}_2^{Exact} = 0.4\,m$;

- Full mass of the cart: $M^{Exact} = 2\,kg$;

- The viscous coefficient of the motor shaft: $b^{Exact} = 0.1\,Nm\,s\,rad^{-1}$;

- Gear ratio at the drives: $\nu^{Exact} = 0.1$,non-dimensional ;

- Ohmic resistance of the coils: $R^{Exact} = 1\,Ohm$;

- Inductance of the coils: $L^{Exact} = 0.5\,H$;

- Torque coefficient of the motor: $K^{Exact} = 0.01\,Nm\,A^{-1}$

- Momentum of the rotary part of the motor: $\Theta^{MotExact} = 0.01\,kg\,m^2$;

- The radii of the wheels: $r_w^{Exact} = 0.1\,m$;

- Half distance between the wheels: $D^{Exact} = 1\,m$;

6.4.5.0.2 Approximate model parameters

- The inertial momentum tensor in the "initial position": $\hat{\Theta}_{11}^{Approx} = 7\,kg\,m^2$, $\hat{\Theta}_{22}^{Approx} = 8\,kg\,m^2$;

- The offset of the mass center point in the initial position: $\hat{S}_1^{Approx} = 0\,m$, and $\hat{S}_2^{Approx} = 0\,m$;

- Full mass of the cart: : $M^{Approx} = 2.5\,kg$;

- The viscous coefficient of the motor shaft: $b^{Approx} = 0.05\,Nm\,s\,rad^{-1}$;

- Gear ratio at the drives: $\nu^{Approx} = \nu^{Exact}$;

- Ohmic resistance of the coils: $R^{Approx} = 1.5\,Ohm$;

- Inductance of the coils: $L^{\text{Approx}} = 0.55\,\text{H}$;

- Torque coefficient of the motor: $K^{\text{Approx}} = 0.02\,\text{N}\,\text{m}\,\text{A}^{-1}$;

- Momentum of the rotary part of the motor: $\Theta^{\text{MotApprox}} = \Theta^{\text{MotExact}}$;

- The radii of the wheels:: $r_{\text{w}}^{\text{Approx}} = r_{\text{w}}^{\text{Exact}}$;

- Half distance between the wheels: $D^{\text{Approx}} = D^{\text{Exact}}$;

The cycle time of the controller was $1\,\text{ms}$. The control parameters were as follows: $b_{\text{bal}} = 0.5$, $\beta_{\text{kin}} = 0.5$, $w = 5 \times 10^{-2}$, $B_c = -1$, $K_c = 10^4$, $\Lambda = 3\,\text{s}^{-1}$, A_c was tuned.

The PID-type and the truncated PID controllers' tracking error in the case of lacking sinusoidal modulation and fixed isotropic weighting ($\kappa_2 = \kappa_3 \equiv 1$) is displayed in Fig. 6.56. It is clear that in contrast to the non-constrained systems in which the application of the integrating term normally used to decrease the error, in our case the error increased. This was also found true for the truncated PID controller.
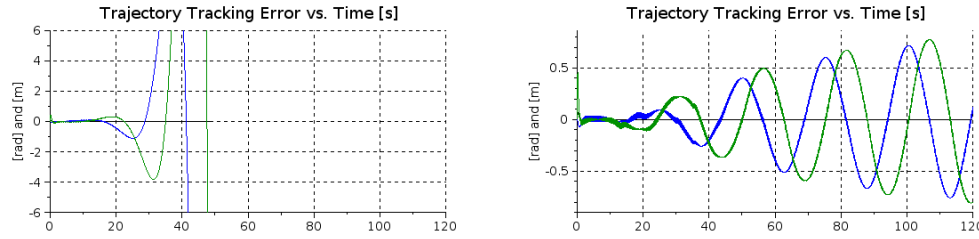
Figure 6.56: The trajectory tracking error of the PID (LHS) and the "truncated PID" (RHS) controllers without modulation in the static ($\kappa_2 = \kappa_3 \equiv 1$ case); Trajectory tracking error of the adaptive controller: PID case (LHS), "truncated PID" case (RHS) [θ: black, x: blue, y: green lines]

The trajectory tracking of the PD and "greedy PD" static controllers for sinusoidal modulation and modulation-free cases are shown in Fig. 6.57. It is evident that the "greedy PD" controller yields more precise tracking than the common PD controller. Figure 6.58 displays the the trajectory tracking in the (x, y) plane in the case of the same simulations.
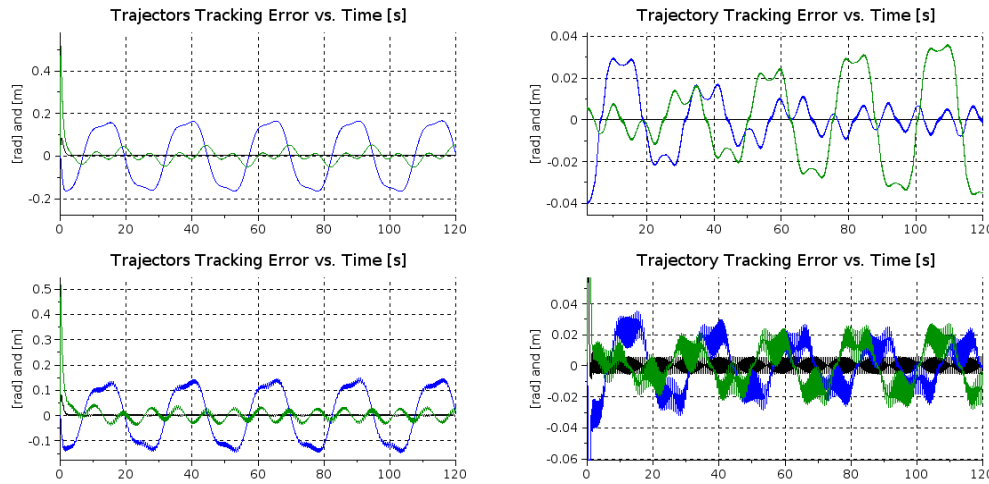
Figure 6.57: Trajectory tracking of the PD (LHS) and the "greedy PD" (RHS) controllers in the static, isotropic ($\kappa_2 = \kappa_3 \equiv 1$) case: without modulation: upper charts, modulated nominal motion: lower charts [θ: black, x: blue, y: green lines]
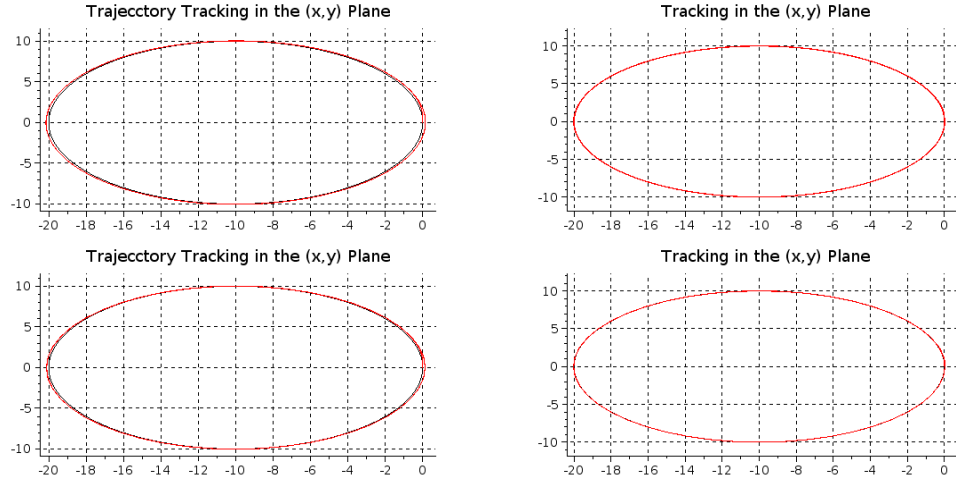
Figure 6.58: Trajectory tracking of the PD (LHS) and the "greedy PD" (RHS) controllers in the static, isotropic ($\kappa_2 = \kappa_3 \equiv 1$) case: without modulation: upper charts, modulated nominal motion: lower charts [nominal trajectory: black, simulated trajectory: red]

In Fig. 6.59 the $\dot{q}_{\mathrm{r}}$ and $\dot{q}_{\mathrm{l}}$ rotational speeds are revealed for the "greedy PD" controller. It reveals the mechanism according to which the modulation improves the tracking precision. The highest frequency variation is the consequence of the RFPT-based technique, the lower frequency pertains to the modulation.
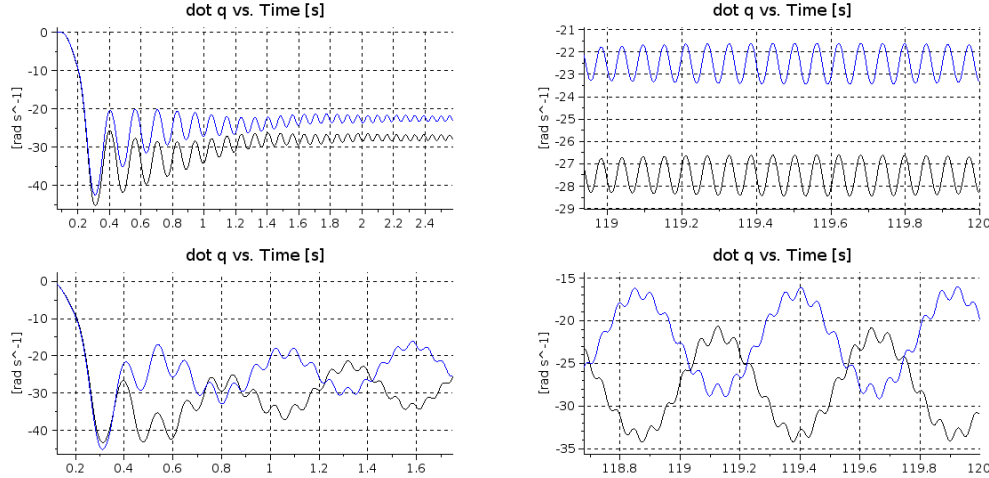
Figure 6.59: The $\dot{q}$ values for the static and isotropic ($\kappa_2 = \kappa_3 \equiv 1$) adaptive controller: without modulation (upper charts), with modulation (lower charts); "greedy PD" at the beginning of the trajectory (LHS) and at its end (RHS) [$\dot{q}_{\mathrm{r}}$: black, $\dot{q}_{\mathrm{l}}$: blue lines]

To substantiate that the RFPT-based adaptivity plays important role in the precise trajectory tracking Figs. 6.60 and 6.61 were created. The comparison with Figs. 6.57 and 6.58 make this statement evident.
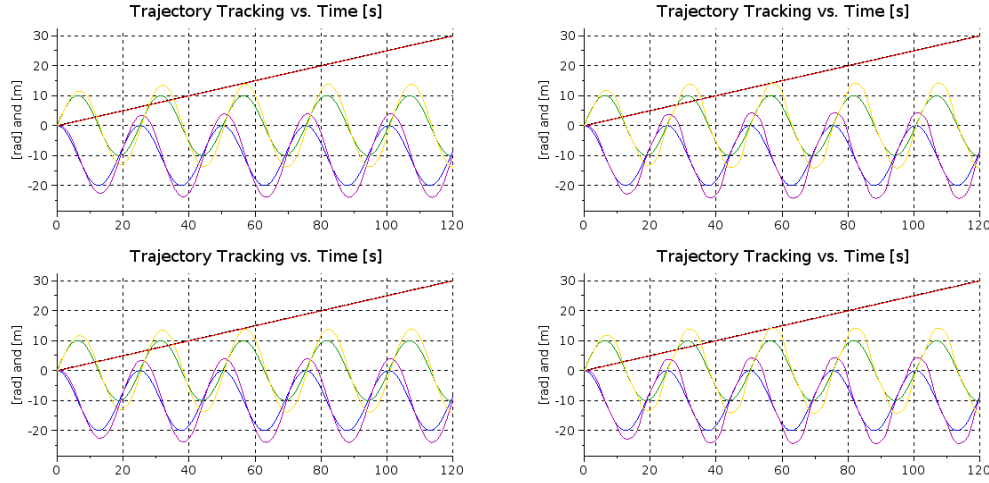
Figure 6.60: The behavior of the non-adaptive "greedy PD" with non-dynamic tracking (LHS) and dynamic tracking (RHS) without modulation (upper charts) and with modulation (lower charts) [θ^N: black, x^N: blue, y^N: green lines, θ: red, x: purple, y: ocher lines]
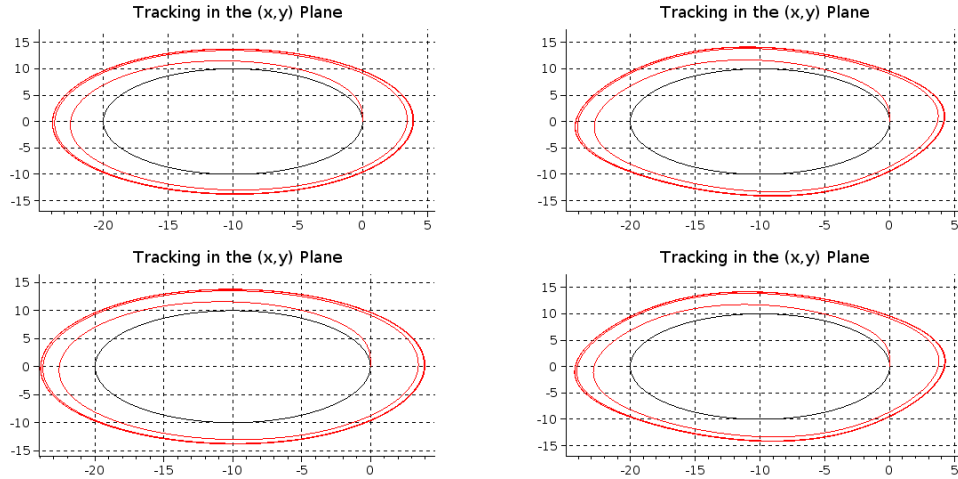
Figure 6.61: The trajectory tracking of the non-adaptive "greedy PD" controller in the (x, y) plane without modulation (upper charts), with modulation (lower charts) with static tracking (LHS) and dynamic tracking (RHS) [nominal trajectory: black, simulated trajectory: red lines]

The essence of the adaptive learning is revealed by Fig. 6.62. While the "desired" and "simulated" values are in each other's vicinity, the adaptively "deformed" signal considerably differs from them. It is also evident that the adaptive learning better works in the case of modulated nominal trajectory.
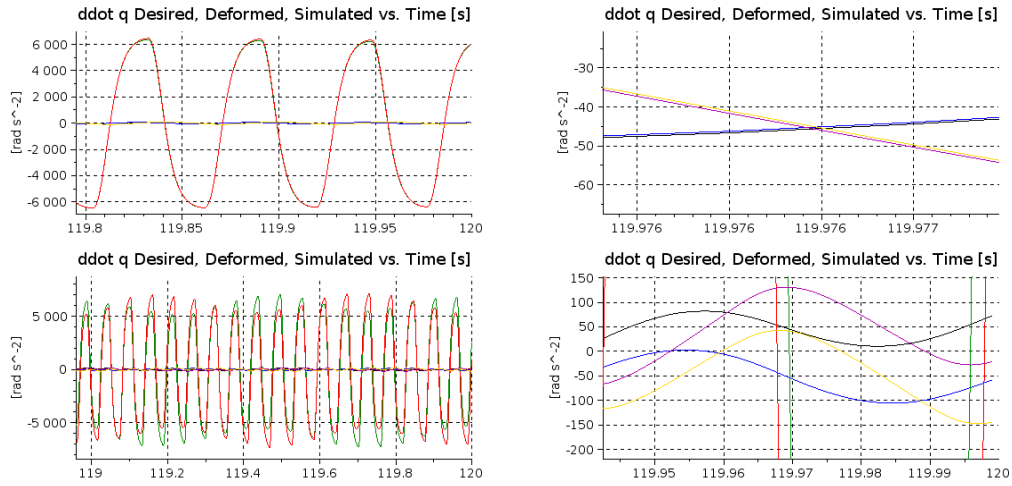
Figure 6.62: The $\ddot{q}$ values for the static adaptive controller without modulation (upper charts) and with modulation (lower charts) for the "greedy PD" option (LHS) (zoomed in excerpts are given in the RHS): [$\ddot{q}_{\mathrm{r}}^{\mathrm{Des}}$: black, $\ddot{q}_{\mathrm{l}}^{\mathrm{Des}}$: blue lines, $\ddot{q}_{\mathrm{r}}^{\mathrm{Def}}$: green, $\ddot{q}_{\mathrm{l}}^{\mathrm{Def}}$: red lines, $\ddot{q}_{\mathrm{r}}$: purple, $\ddot{q}_{\mathrm{l}}$: ocher lines]

6.5 Further research plans: Cognitive Control (CoCo)

The Cognitive Control (CoCo) is a new field of control theory [A. 23]. The Definition of Cognitive Control was:

"(Cognitive control (CoCo)). Cognitive control theory (CoCo) is an interdisciplinary branch of engineering, mathematics, informatics, control theory and the cognitive/social sciences. CoCo deals with the dynamics of individual and/or collective cognitive phenomena. The theories and methodologies of CoCo give control theoretical interpretations of such dynamics in order to explain and control cognitive phenomena, as well as to apply them in system control design, without necessarily distinguishing between biological and artificial aspects." [A. 23]

Remarks [A. 23]:

1. It is important to note that the definition of CoCo engenders systems which function in ways similar to cognitive phenomena, as well as systems which focus on the control of cognitive phenomena.

2. An important aspect of CoCo is that it deals with the dynamics of both individual and collective cognitive phenomena. This means that not only the perception and reasoning of individual living systems (i.e., a single person) are under focus, but also the collective tendencies and behaviors of systems comprised of a large number of animals, humans, etc.

3. The fact that CoCo does not necessarily distinguish between biological and artificial aspects implies that CoCo generally aims to create unified theories which reflect the tendency of merging between natural cog- nitive systems (e.g., humans) and artificial cognitive systems (e.g., infocommunications devices, ICT)

In the practice we must normally be content with very approximate models that do not promise any possibility for making them perfect via learning or parameter tuning. In this regard, the foundations of a novel control approach were laid down in and in related publications. This control approach can be largely equated with cognitive control, and it outlines the following major characteristics [A. 23]:

1. Instead of exerting efforts to identify a permanent, precise, complete, environment-independent model of the phenomenon under control, we can make do with temporal, imprecise, incomplete,

situation-dependent models. These models can correspond either to the usual universal approximators or may be taken from simple Lie groups (e.g. the Rotational Group, Lorentz Group, Symplectic Group) that are also able to provide us with uniform model structures having very limited number of independent parameters. These Lie groups do not belong to the phenomenology of the controlled systems: they are used only because they offer very convenient and lucid, geometrically interpreted possibilities for dealing with subspaces for which no actual information is available for the controller.

2. The temporal and situation dependent nature of these models allows great simplification: no need is generated for creating very sophisticated models. Instead of that frequent correcting actions are needed.

3. Besides the simple fact that these models need correcting feedback signals, their iterative nature worths especial emphasis. These controllers operate with simple Cauchy sequences obtained by contractive maps so these sequences have to converge to the solution of the control task. In this manner the control of fractional order systems –that generally have long term memory– can easily be attempted. Since the derivation rules for fractional order derivatives do not inherit that of the integer order ones we have extreme difficulties in dealing with the Lyapunov functions and their derivatives. All of these difficulties are elegantly evaded in this manner.

4. Due to temporal and situation dependent nature of the models this approach applies neither asymptotic nor global stability can be the general goal of such controllers. Due to the principle of causality the modeling insufficiencies at first can be observed, and the correcting action may happen only afterwards. (Asymptotic stability is generally possible only if the controller possesses an analytically exact model with approximate parameters. After precisely tuning the parameters the results of further observations are not used for correcting actions.) Also, in the lack of exact model we cannot give any statement on the exact limits of the stability of the so developed controllers: guaranteeing global stability is hopeless (and in the most of the practical applications is also unnecessary).

5. Due to the lack of reliable complete model any effort for developing model-based state estimators as Kalman filters is hopeless. Simulation examples indicate that this approach can work without taking the numerical burden of any state estimation.

6. Though global stability cannot be guaranteed simple complementary tuning strategies were invented that help keeping the controlled system in the region of convergence. It have been also shown that quitting the region of convergence cannot result in catastrophic aftermaths: the controller can still work with considerable chattering that can be reduced and evaded.

7. Finally, these controllers can behave in a cognitive way that besides applying iterative corrections to a given approximate model they can select various approximate models by observing the behavior of the controlled systems. These observers seriously differ from the classic state observers. Normally they can be realized by simple forgetting integrators that observe certain simple signals as e.g. certain aftermaths of the excitation of the not modeled internal degrees of freedom as in.

Thesis 1: Studying and improving the operation of the RFPT-based adaptive controller outside of its convergent regime

I conducted systematic investigations for the behavior of the RFPT-based controller's operation outside of the region of convergence in the case of single (SISO) and multiple (MIMO) dimensional systems.

I have proved that whenever the response function of the controlled SISO system can be approximated by affine expressions, and the initial signal of the iterative control sequence is between the trivial fixed point and the fixed point that is the solution of the control task the controller produces chaotic, bounded fluctuation in the control signal. This fluctuation corresponds to a "bouncing" motion between two repulsive fixed points.

I have observed that the controller's operation in this case is similar to that of a Sliding Mode/Variable Structure controller with great chattering.

I have illustrated the same qualitative behavior in the case of a 2 DoF and a 3 DoF system via simulations. On the basis of these simulation results I have revealed that the consequences of this chattering are not necessarily fatal from the point of view of the control.

I have successfully generalized the chattering reduction technique first announced in [29] for SISO systems to MIMO systems. I referred to the so obtained controller as "Bounded RFPT"-based design.

I have shown that if the initial signal is outside of this region the sequence diverges. I have shown it, too, that this case does not have practical significance because it can be avoided easily by properly setting the control parameters.

The publications strictly related to this thesis are: [A. 1], [A. 2].

Thesis 2: Application of the RFPT-based adaptive control for the special nonlinearities and phenomenological limitations in chemical reactions

I systematically studied the typical nonlinearities occurring in chemical systems. I have identified two types of significant classes: a) the nonlinear equations of motion that typically contain the multiplications of various powers of the concentrations, due to the "Mass Action Law"; b) the phenomenological limitations of the control signals, and that of the concentrations.

While the multiplicative nonlinearities has the usual consequences that the time-derivatives of the state variables nonlinearly depend on these variables, the phenomenological limitations have far more drastic aftermaths: by the use of dense reagents at the input side the concentration of the components within a stirred tank reactor can be selectively increased by the controller, but it cannot be selectively decreased: either each ingredient has to be diluted or the input rate has to be truncated at zero. During such periods the concentration of this component cannot be controlled according to the needs of the prescribed control law. The controller has to wait while this concentration decreases by the internal reactions within the tank.

The other limiting factor is that whenever a concentration achieves the value of zero, its time-derivative can be only non-negative. This nonlinearity is similar to the saturation effects.

I have illustrated the above effects in the case of the Brusselator model that was a significant paradigm of the autocatalytic phenomena. I have shown that in the case of a conventional PID-type control based on the reaction equations without applying the necessary phenomenological limitations nice tracking of the prescribed nominal motion is possible. However, in this case the solution partly lays within the physically not interpretable region.

By the use of the same paradigm I have shown that a carefully designed RFPT-based adaptive controller efficiently can solve the same task so that its solution remains always physically interpretable.

To extend the application field of the RFPT-based adaptive control approach I have studied a more precise model of the chemical reactions in which I took it into consideration that the addition of a given reagent dilutes the other ones, i.e. the concentration of the various ingredients cannot completely separately manipulated. (In the mainstream of the literature this effect normally is neglected.) I have called this effect "input coupling" and have shown that the RFPT-based design can be applied to this model in a contradiction-free manner at the cost of increasing the order of the control task. I have run numerical simulations to illustrate this ability of the RFPT-based design.

I have shown via simulations that this RFPT-based solution can be improved by the application of fractional order derivatives that gives the controller certain robustness with respect to the measurement noises and also allows some increase in the cycle time of the control that may have practical significance in the case of slow sensors.

The publications strictly related to this thesis are: [A. 3], [A. 4], [A. 5].

Thesis 3: Improving the parameter tuning possibilities for the RFPT-based design: the discovery and application of the "Precursor Oscillations"

Based on the observations related to the phenomenon of chaos formation of the RFPT-based control I have proven that if the response function of the controlled system can be approximated by an affine expression, by fixing the adaptive control parameters in the RFPT-based scheme, namely K_c and B_c, the following situation can be created: if the parameter A_c is slowly increased from zero, at the beginning the controller works with monotonic convergence in the "iterative learning". The speed of this convergence increases with increasing A_c till achieving its maximal value. Following that the controller still remains convergent with further increasing A_c but this convergence has non-monotonic, oscillating nature. I called these oscillations "Precursor Oscillations" because further increase in A_c decreases the speed of convergence and finally ends up in the non-convergent regime of bounded chaotic oscillations.

I have designed a model-independent observer to monitor the occurrence of the Precursor Oscillations and have shown that this observer can be efficiently used in the adaptive tuning of the control parameter A_c. In this manner I made a significant step in the direction of widening the applications of the RFPT-based design that originally suffered from the limitations of the bounded region of conver-

gence.

I have illustrated the applicability of the "Precursor Oscillations"-based technique via simulations for an underactuated mechanical system.

I have also shown the occurrence of the Precursor Oscillations in the case of the Bounded RFPT-based design and illustrated its use via simulations for a 1 DoF mechanical system.

The publications strictly related to this thesis are: [A. 6], [A. 7].

Thesis 4: Practical modification of the original RFPT-based design

In the original RFPT-based design the saturated nature of a sigmoid function was of essential significance: it determined the width of the slot within which the response error's details are taken into consideration.

I have shown that this component can be replaced by a truncated linear function that from mathematical point of view is not a sigmoid function (it is not monotone increasing because having constant parts at ±1), but it is a very good practical approximation that is easy to realize even by analog circuits. Furthermore its slope can easily be tuned.

The applicability of the so modified adaptive controller was shown via simulations for a fully driven and an underactuated 2 DoF mechanical system.

The publications strictly related to this thesis are: [A. 8], [A. 9].

Thesis 5: Combination of the RFPT-based control with the traditional Luenberger Observer

The traditional adaptive control results partly originate from the field of the adaptive control of robots. In this special application area the mechanical state of the controlled system ab ovo is measured by appropriate sensors the use of which do not require the use of "state observers". State observers normally have to be used when certain state variables cannot be directly measured. In this case some other measurable quantities are available that are in functional relationship with certain components of the state variables. In the realm of the LTI systems for this purpose a "canonical formulation" is available.

In this Thesis I have shown how the RFPT-based adaptive design can be combined with the classical Luenberger observer in the case of a nonlinear system under control. For the illustrative simulations the model of a nonlinear oscillator was used.

The publications strictly related to this thesis are: [A. 10].

Thesis 6: Novel RFPT-based order reduction technique for nonlinear systems

Whenever the system to be controlled consists of a great number of dynamically coupled subsystems the order of the appropriate model and that of the control task is inconveniently high. The drawbacks are the ample dimension of the initial states as well as the sensitivity of the differentiation to the measurement noises. In such cases it is practical to apply reduced order controllers. The traditional antecedents tackle this problem from the theoretical background of the LTI systems.

In this thesis I have shown that for the control of stable systems the RFPT-based adaptive technique allows a far simpler approach to the problem of order reduction in which the consequences of the order reduction are compensated by that of the other modeling errors without the need for the identification of the various effects. The considered simulations were made for a DC motor driven cart.

The publications strictly related to this thesis are: [A. 14], [A. 21].

Thesis 7: Application of the RFPT-based technique for the control of higher order systems

In certain applications that do not need too high order approach, instead of order reduction the application of higher order controller may be advantageous.

In this thesis I have shown that via completing the RFPT-based design with a polynomial higher order differentiator the method can efficiently solve 4th order control tasks. The basic idea of the applied numerical derivator is the application of a scaling for the time-variable to a scale in which the polynomial fitting yield stable result. Following this calculation the result can be scaled back to the real time scale.

The applicability of the method was shown via simulations for a swinging problem and a more or less artificial paradigm just developed for the purposes of this research (mass-points coupled by nonlinear springs).

The publications strictly related to this thesis are: [A. 15], [A. 16].

Thesis 8: Further applications of the RFPT-based adaptive control design

In the current control literature various modern solutions are in use. The aim of this thesis is to reveal novel applications for which alternative solutions were already found in the literature.

The first example was the control of an aeroelastic wing component based on the antecedents in [87, 88]. For this paradigm I have developed a basic RFPT-based method in [A. 11], and an RFPT-based MRAC solution in [A. 11].

The second example was the adaptive dynamic control of a small airplane model that normally serves as a "benchmarking object" in the control literature in [A. 13].

The other application paradigm that extensively was investigated the adaptive dynamic control of a caster supported WMR driven by two actively driven wheels. In this task the underactuation caused by the non-holonomic constraints and the complexity of the dynamic model in the case in which the location of the mass center point is not a priori known mean the main challenges. The publications strictly related to this part of the thesis are: [A. 14], [A. 17], [A. 18], [A. 19], [A. 20], [A. 21], [A. 22].

8.1   Own publications strictly related to the Thesis

[A. 1] K. Kósi; S. Hajdu; J. F. Bitó; J. K. Tar, "Chaos formation and reduction in robust fixed point transformations based adaptive control," Nonlinear Science and Complexity (NSC), 2012 IEEE 4th International Conference , pp.211,216, 6-11 Aug. 2012

[A. 2] K. Kósi; A. Breier; J. K. Tar, "Chaos patterns in a 3 Degree of Freedom control with Robust Fixed Point Transformation," Computational Intelligence and Informatics (CINTI), 2012 IEEE 13th International Symposium , pp.131,135, 20-22 Nov. 2012

[A. 3] K. Kósi; J. F. Bitó; J. K. Tar, "On the effects of strong asymmetries on the adaptive controllers based on Robust Fixed Point Transformations," Intelligent Systems and Informatics (SISY), 2012 IEEE 10th Jubilee International Symposium , pp.259,264, 20-22 Sept. 2012

[A. 4] J. K. Tar; I.J. Rudas; Nadai, L.; K. Kósi, "Adaptive controllability of the brusselator model with input coupling," Logistics and Industrial Informatics (LINDI), 2012 4th IEEE International Symposium, pp.157,162, 5-7 Sept. 2012

[A. 5] K. Kósi; A. Dineva; J. K. Tar, "Increased cycle time achieved by fractional derivatives in the adaptive control of the Brusselator model," Applied Machine Intelligence and Informatics (SAMI), 2013 IEEE 11th International Symposium , pp.65,70, Jan. 31 2013-Feb. 2 2013

[A. 6] K. Kósi; J. K. Tar; I.J. Rudas, "Improvement of the stability of RFPT-based adaptive controllers by observing "precursor oscillations"," Computational Cybernetics (ICCC), 2013 IEEE 9th International Conference, pp.267,272, 8-10 July 2013

[A. 7] K. Kósi, J. K. Tar, I.J. Rudas, J. F. Bitó: Stabilization by Suppressing Emerging Oscillations in Bounded RFPT-based Adaptive Control, LINDI 2013: 5th IEEE International Symposium on Logistics and Industrial Informatics. Wildau: IEEE Communications Society, pp. 73-78. , 2013.

[A. 8] K. Kósi; J. F. Bitó; J. K. Tar, "Fine tuning with sigmoid functions in robust fixed point transformation," Applied Computational Intelligence and Informatics (SACI), 2013 IEEE 8th International Symposium , pp.411,416, 23-25 May 2013

[A. 9] K. Kósi, Bitó J.F., Tar J.K.: Application of Truncated Linear Sigmoid Functions in Adaptive Controllers Based on Robust Fixed Point Transformations, BULETINUL STIINTIFIC AL UNIVERSITATI POLITEHNICA DIN TIMISOARA ROMANIA SERIA AUTOMATICA SI CALCULATORAE = SCIENTIFIC BULLETIN OF POLITECHNICA UNIVERSITY OF TIMISOARA TRANSACTIONS ON AUTOMATIC CONTROL AND COMPUTER SCIENCE 58(72): (2-4) pp. 119-124. (2013)

[A. 10] K. Kósi; J. K. Tar; T. Haidegger, "Application of Luenberger's observer in RFPT-based adaptive control — A case study," Computational Intelligence and Informatics (CINTI), 2013 IEEE 14th International Symposium, pp.365,369, 19-21 Nov. 2013

[A. 11] J. K. Tar, I.J. Rudas, J. F. Bitó, K. Kósi: Iterative Adaptive Control of a Three Degrees-of-Freedom Aeroelastic Wing Model, APPLIED MECHANICS AND MATERIALS 300-301: pp. 1593-1599. (2013)

[A. 12] J. K. Tar, I.J. Rudas, J. F. Bitó, K. Kósi: Robust Fixed Point Transformations in the Model Reference Adaptive Control of a Three DoF Aeroelastic Wing, APPLIED MECHANICS AND MATERIALS 300-301: pp. 1505-1512. (2013)

[A. 13] K. Kósi; J. K. Tar; I.J. Rudas, "RFPT-based adaptive control of a small aeroplane model," Intelligent Engineering Systems (INES), 2013 IEEE 17th International Conference, pp.97,102, 19-21 June 2013

[A. 14] Tar J.K., Haidegger T, Kovács L, K. Kósi, B. Botka, I.J. Rudas.J., Nonlinear Order-Reduced Adaptive Controller for a DC Motor Driven Electric Cart 18th International Conference on Intelligent Engineering Systems (INES 2014),(ISBN:978-1-4799-4616-7),pp. 73-78, Tihany, Hungary, 2014

[A. 15] K. Kósi; T.A Várkonyi.; J. K. Tar; I.J. Rudas; J. F. Bitó, "On the simulation of RFPT-based adaptive control of systems of 4th order response," Intelligent Systems and Informatics (SISY), 2013 IEEE 11th International Symposium , pp.259,264, 26-28 Sept. 2013

[A. 16] K Kósi, T. A. Várkonyi, J. K. Tar, Deformálható elemen keresztül hajtott dinamikai rendszer RFPT alapú adaptív szabályozása, Innováció és Fenntartható Felszíni Közlekedés konferencia (IFFK 2013) , 2013

[A. 17] J.K. Tar, K. Kósi, T. Haidegger, B. Kurtán, Resolution of Kinematic Constraints via Local Optimization in an Adaptive Dynamic Control of an Electric Cart, Workshop on Design, Simulation, Optimization and Control of Green Vehicles and Transportation, (lecture), Gyor, 2014

[A. 18] K. Kósi, T. Haidegger, B. Kurtán, J.K. Tar, A Novel Type Model Reference Adaptive Controller for the Dynamic Control of a WMR, Workshop on Design, Simulation, Optimization and Control of Green Vehicles and Transportation, (lecture), Gyor, 2014

[A. 19] T. Haidegger, K. Kósi, J.K. Tar, Kinematic Design of Traceable Trajectories for Caster Supported WMRs Having Two Active Wheels, 2nd Workshop on Design, Simulation, Optimization, and Control of Green Vehicles,(lecture), Gyor, 2014

[A. 20] K. Kósi, T. Haidegger, J.K. Tar, Simulation Tests of an RFPT-Based MRAC Controller for an Electric Cart for Various Trajectory Tracking Approaches, 2nd Workshop on Design, Simulation, Optimization, and Control of Green Vehicles,(lecture), Gyor, 2014

[A. 21] J.K. Tar, K. Kósi, T. Haidegger, Generalized Dynamic Model of DC Motors Driven WMRs for RFPT-Based Order Reduced Adaptive Control, 2nd Workshop on Design, Simulation, Optimization, and Control of Green Vehicles,(lecture), Gyor, 2014

[A. 22] Tar József, K. Kósirisztián, Haidegger Tamás, Elektromos DC motorral hajtott kerekes járművek szabályozásának új adaptív megoldásai, Innováció és fenntartható felszíni közlekedés (IFFK 2014), pp. 206-22, 25-27 Aug. 2014

[A. 23] J.K. Tar I.J. Rudas, K. Kósi,Á. Csapó, P. Baranyi, Cognitive Control Initiative, 3rd IEEE International Conference on Cognitive Infocommunications (CogInfoCom 2012), (ISBN:978-1-4673-5188-1), pp. 579-584, Kosice, Slovakia, 2012

8.2   Other own publications

[B. 1] K. Kósi, Method of Data Center Classifications, Acta Polytechnica Hungarica,Vol. 9, No. 5, pp. 127-137, 2012

[1] Tjalling J. Ypma. Historical development of the Newton-Raphson method. *SIAM Review*, 37(4):531–551, 1995.

[2] J.M. Ortega and W.C. Rheinboldt. *Iterative Solution of Nonlinear Equations in Several Variables*. SIAM, 2000.

[3] C.T. Kelley. *Solving Nonlinear Equations with Newton's Method, no 1 in Fundamentals of Algorithms*. SIAM, 2003.

[4] P. Deuflhard. *Newton Methods for Nonlinear Problems. Affine Invariance and Adaptive Algorithms, Springer Series in Computational Mathematics, Vol. 35*. Springer, Berlin, 2004.

[5] S. Banach. Sur les opérations dans les ensembles abstraits et leur application aux équations intégrales (About the Operations in the Abstract Sets and Their Application to Integral Equations). *Fund. Math.*, 3:133–181, 1922.

[6] A. Aitken. On Bernoulli's numerical solution of algebraic equations. *Proceedings of the Royal Society of Edinburgh*, 46:289–305, 1926.

[7] L.W. Johnson and D.R. Scholz. On Steffensen's method. *SIAM Journal on Numerical Analysis*, 5(2):296–302, 1968.

[8] S. Arimoto, S. Kawamura, and F. Miyazaki. Bettering operation of robots by learning. *Journal of Robotic Systems*, 1(2):123–140, 1984.

[9] S. Gunnarsson and M. Norrlöf. On the design of ILC algorithms using optimization. *Automatica*, 37:2011–2016, 2001.

[10] D.H. Owens and J. Hätönen. Iterative learning control – An optimization paradigm. *Annual Reviews in Control*, 29:57–70, 2005.

[11] Y. Wang, F. Gao, and F.J. Doyle III. Survey on iterative learning control, repetitive control, and run-to-run control. *Journal of Process Control*, 19:1589–1600, 2009.

[12] M. Deniša, A. Ude, and A. Gams. Adaptation of motor primitives to the environment through learning and statistical generalization. *Proc. of the 24th International Workshop on Robotics in Alpe Adria Danube Region (RAAD 2015), May 27-29 2015, Bucharest, Romania*, pages 1–8, 2015.

[13] A.M. Lyapunov. *A general task about the stability of motion. (in Russian)*. Ph.D. Thesis, University of Kazan, Tatarstan (Russia), 1892.

[14] A.M. Lyapunov. *Stability of motion*. Academic Press, New-York and London, 1966.

[15] Jean-Jacques E. Slotine and W. Li. *Applied Nonlinear Control*. Prentice Hall International, Inc., Englewood Cliffs, New Jersey, 1991.

[16] R. Isermann, K.H. Lachmann, and D. Matko. *Adaptive Control Systems*. Prentice-Hall, New York DC, USA, 1992.

[17] C.C. Nguyen, S.S. Antrazi, Zhen-Lei Zhou, and C.E. Campbell Jr. Adaptive control of a stewart platform-based manipulator. *Journal of Robotic Systems*, 10(5):657–687, 1993.

[18] R. Kamnik, D. Matko, and T. Bajd. Application of model reference adaptive control to industrial robot impedance control. *Journal of Intelligent and Robotic Systems*, 22:153–163, 1998.

[19] J. Somló, B. Lantos, and P.T. Cát. *Advanced Robot Control*. Akadémiai Kiadó, Budapest, 2002.

[20] L. Kovács. Modern robust control in patophysiology from theory to application. *In Proc. of the IEEE 11th Intl. Symp. on Applied Machine Intelligence and Informatics (SAMI 2013)*, page 13, 2013.

[21] I. Sekaj and V. Veselý. Robust output feedback controller design: Genetic Algorithm approach. *IMA J Math Control Info*, 22(3):257–265, 2005.

[22] J.L. Chen and Wei-Der Chang. Feedback linearization control of a two-link robot using a Multi-Crossover Genetic Algorithm. *Expert Systems with Applications*, 2(2 Part 2):4154–4159, 2009.

[23] J.K. Tar. *Adaptive Control of Smooth Nonlinear Systems Based on Lucid Geometric Interpretation (DSc Dissertation)*. Hungarian Academy of Sciences, Budapest, Hungary, 2012.

[24] J.K. Tar, J.F. Bitó, L. Nádai, and J.A. Tenreiro Machado. Robust Fixed Point Transformations in adaptive control using local basin of attraction. *Acta Polytechnica Hungarica*, 6(1):21–37, 2009.

[25] J.K. Tar and I.J. Rudas. Adaptive optimal dynamic control for nonholonomic systems. *COMPUTING AND INFORMATICS*, 28(3):339–351, 2009.

[26] J.K. Tar, L. Nádai, I.J. Rudas, and T.A. Várkonyi. Adaptive emission control of freeway traffic using quasi-stationary solutions of an approximate hydrodynamic model. *Journal of Applied Nonlinear Dynamics*, 1(1):29–50, 2012.

[27] J.K. Tar. Towards replacing Lyapunov's 'direct' method in adaptive control of nonlinear systems (invited plenary lecture). *In Proc. of the Mathematical Methods in Engineering Intl. Symp. (MME), Coimbra, Portugal*, 2010.

[28] J.K. Tar, L. Nádai, I.J. Rudas, and T.A. Várkonyi. RFPT-based adaptive control stabilized by fuzzy parameter tuning. *In Proc. of the 9th European Workshop on Advanced Control and Diagnosis (ACD 2011), Budapest, Hungary*, pages 1–8, 2011.

[29] T.A. Várkonyi, J.K. Tar, I.J. Rudas, and I. Krómer. Vs-type stabilization of mrac controllers using robust fixed point transformations. *In Proc. of the 7th IEEE Intl. Symp. on Applied Computational Intelligence and Informatics, Timişoara, Romania*, pages 389–394, 2012.

[30] R.M. Murray, Z. Li, and S.S. Sastry. *A mathematical introduction to robotic manipulation*. CRC Press, New York, 1994.

[31] Pi-Cheng Tung, Sun-Run Wang, and Fu-Yee Hong. Application of mrac theory for adaptive control of a constrained robot manipulator. *International Journal of Machine Tools & Manufacture*, 40:2083–2097, 2000.

[32] C.J. Khoh and K.K. Tan. Adaptive robust control for servo manipulators. *Neural Comput & Applic*, 12:178–184, 2003.

[33] K. Hosseini-Suny, H. Momeni, and F. Janabi-Sharifi. Model Reference Adaptive Control design for a teleoperation system with output prediction. *J Intell Robot Syst*, DOI 10.1007/s10846-010-9400-4:1–21, 2010.

[34] B. Mirkin, P.-O. Gutman, and Y. Shtessel. Robust adaptive tracking with an additional plant identifier for a class of nonlinear systems. *Journal of the Franklin Institute*, 347:974–987, 2010.

[35] I. Sekaj and V. Veselý. Robust output feedback controller design: Genetic algorithm approach. *IMA J Math Control Info*, 22(3):257–265, 2005.

[36] A. Dineva, A.R. Várkonyi-Kóczy, and J.K. Tar. Combination of RFPT-based adaptive control and classical model identification. *In Proc. of the IEEE 12th Intl. Symp. on Applied Machine Intelligence and Informatics (SAMI 2014), 2014, Herla'ny, Slovakia*, pages 35–40, 2014.

[37] J.K. Tar, I.J. Rudas, A. Dineva, and A. Várkonyi-Kóczy. Stabilization of a Modified Slotine-Li Adaptive Robot Controller by Robust Fixed Point Transformations. *In Proc. of Recent Advances in Intelligent Control, Modelling and Simulation, 2014, Cambridge, MA, USA*, pages 35–40, 2014.

[38] J.K. Tar, J.F. Bitó, I.J. Rudas, and K. Eredics. Comparative analysis of a traditional and a novel approach to Model Reference Adaptive Control. 11th *Intl. Symp. of Hungarian Researchers on Computational Intelligence and Informatics, Budapest, Hungary*, pages 93–98, 2010.

[39] S.V. Emelyanov, S.K. Korovin, and L.V. Levantovsky. Higher order sliding regimes in the binary control systems. *Soviet Physics*, 31:291–293, 1986.

[40] V.I. Utkin. *Sliding Modes in Optimization and Control Problems*. Springer Verlag, New York, 1992.

[41] A. Levant. Arbitrary-order sliding modes with finite time convergence. *In Proc. of the 6th IEEE Mediterranean Conference on Control and Systems, June 9-11, 1998, Alghero, Sardinia, Italy*, 1998.

[42] J.K. Tar L. Nádai I.J. Rudas T.A. Várkonyi. Rfpt-based adaptive control stabilized by fuzzy parameter tuning. *Proc. of the 9th European Workshop on Advanced Control and Diagnosis, ACD 2011. Budapest, Hungary*, pages 1–8, 2011.

[43] J. A. Tenreiro Machado. Fractional calculus and dynamical systems. *invited plenary lecture at the IEEE International Conference on Computational Cybernetics (ICCC 2006), Tallinn, Estonia*, 2006.

[44] Z. Bai. Krylov subspace techniques for reduced-order modeling of large-scale dynamical systems. *Applied Numerical Mathematics*, 43:9–44, 2002.

[45] F. Constantinescu. *Distributions and Their Applications in Physics*. Pergamon Press, Oxford, UK, 1980.

[46] B. Davies. *Integráltranszformációk és alkalmazásaik (in Hungarian)*. Műszaki Könyvkiadó, Budapest, Hungary, 1983.

[47] B. Davies. *Integral Transforms and Their Applications*. Springer Science & Business Media, 2002.

[48] H. Padé. *Sur la répresentation approchée d'une fonction par des fractions rationelles (Thesis)*. Ann. École Nor. (3), 9, 1892, pp. 1–93 supplement, 1892.

[49] A. Bultheel and M. van Barvel. Padé techniques for model reduction in linear system theory: A survey. *J. Comput. Appl. Math.*, 14:401–438, 1986.

[50] B. Salimbahrami and B. Lohmann. *Krylov Subspace Methods in Linear Model Order Reduction: Introduction and Invariance Properties. Scientific report, 2002.* http://www.iat.uni-bremen.de/mitarbeiter/salimbahrami/
Invariance properties.pdf, 2002.

[51] J.A. Tenreiro Machado, Alexandra M. Galhano, Anabela M. Oliveira, and J.K. Tar. Optimal approximation of fractional derivatives through discrete-time fractions using genetic algorithms. *Commun Nonlinear Sci Numer Simulat*, 6:482–490, 2009.

[52] C. Lanczos. An iteration method for the solution of the eigenvalue problem of linear differential and integral operators. *J. Res. Nat. Bureau Stan.*, 45:255–282, 1950.

[53] W.E. Arnoldi. The principle of minimized iterations in solution of the matrix eigenvalue problem. *Quart. Appl. Math.*, 9:17–29, 1951.

[54] W.J. Rugh. *Nonlinear System Theory*. The John Hopkins University Press, Baltimore, MA, USA, 1981.

[55] S. Sastry. *Nonlinear Systems: Analysis, Stability and Control*. Springer, New York, 1999.

[56] S. Lall, J.E. Marsden, and S. Glavaski. *Empirical model reduction of controlled nonlinear systems*. Technical Reports CIT/CDS 98-008, California Institute of Technology, 1998.

[57] B. Lohmann. Order reduction and determination of dominant state variables of nonlinear systems. *Mathematical Modelling of Systems*, 1(2):77–90, 1995.

[58] B. Salimbahrami and B. Lohmann. *A Simulation Free Nonlinear Model Order Reduction Approach and Comparison Study*. In Proc. 4th Mathmod, pages 429–435, Vienna, 2003., 2003.

[59] J.K. Tar J.F. Bitó I.J. Rudas K. Eredics. Comparative analysis of a traditional and a novel approach to model reference adaptive control. *In Proc. of the 11th International Symposium of Hungarian Researchers on Computational Intelligence and Informatics (CINTI 2010), Budapest*, pages 93–98, 2010.

[60] I. Prigogine R. Lefever. Symmetry breaking instabilities in dissipative systems ii. *J. Chem. Phys.*, 48:1695–1700, 1968.

[61] J.J. Tyson. The belousov-zhabotinskii reaction. *Lecture Notes in Biomathematics 10, (Springer-Verlag, Heidelberg)*, 1976.

[62] D. Kondepudi and I. Prigogine. Modern thermodynamics. *John Wiley & Sons, Chichester*, 1998.

[63] T.A. Várkonyi J.K. Tar I.J. Rudas. Fuzzy parameter tuning in the stabilization of an rfpt-based adaptive control for an underactuated system. *Proc. of the 2011 IEEE 12th International Symposium on Computational Intelligence and Informatics (CINTI), Budapest*, pages 591–596, 2011.

[64] J.A. Tenreiro Machado Alexandra M. Galhano Anabela M. Oliveira J. K. Tar. Optimal approximation of fractional derivatives through discrete-time fractions using genetic algorithms. *Commun Nonlinear Sci Numer Simulat*, pages 482–490, 2009.

[65] J.K. Tar, I.J. Rudas, and J.F. Bitó. Fixed point stabilization in a novel MRAC control for MIMO systems. *Proc. Proceedings of the 8th IEEE International Symposium on Intelligent Systems and Informatics (SISY 2010), Subotica, Serbia, 2010.09.10–2010.09.11.*, pages 377–382, 2010.

[66] R.T. Bupp, D.S Bernstein, and V.T. Coppola. A benchmark problem for nonlinear control design: Problem statement, experiment testbed and passive nonlinear compensation. *Proc. of the American Control Conference, Seattle, US*, pages 4363–4376, 1995.

[67] M. Jankovic, D. Fontanie, and P.V. Kokotovic. TORA example: Cascade- and passivity based control designs. *IEEE Transaction on Control System Technologies*, 4:292–297, 2006.

[68] P. Baranyi, Z. Petres, P. Várlaki, and P. Michelberger. Observer and control law design to the TORA system via TPDC framework. *WSEAS Transactions on Systems*, 1(5):156–163, 2006.

[69] B. Van der Pol. Forced oscillations in a circuit with non-linear resistance (reception with reactive triode). *The London, Edinburgh, and Dublin Philosophical Magazine and Journal of Science*, 7(3):65–80, 1927.

[70] Tar J.K. Bito J.F. Rudas I.J. Kozlowski K.R. and Tenreiro Machado J.A. Possible adaptive control by tangent hyperbolic fixed point transformations used for controlling the ϕ^6-type van der pol oscillator. *Proc. of the 6th IEEE International Conference on Computational Cybernetics (ICCC 2008), Stara Lesna, Slovakia,*, pages 15–20, 2008.

[71] A. Isidori. *Nonlinear Control Systems (Third Edition)*. Springer-Verlag London Limited, 1995.

[72] Z. Petres, B. Reskó, and P. Baranyi. TP model transformation based control of the TORA system. *Production Systems and Information Engineering*, 2:159–175, 2004.

[73] D.G. Luenberger. *Introduction to Dynamic Systems: Theory, Models, and Applications*. John Wiley & Sons, New York, 1979.

[74] B. Takarics. *TP model transformation based sliding mode control and friction compensation*. Ph.D. dissertation at Computer and Automation Research Institute of the Hungarian Academy of Sciences and Budapest University of Technology and Economics, Budapest, Hungary, (2011) p. 95., 2011.

[75] Aerosim Blockset. *AEROSIM BLOCKSET Version 1.01 User's Guide*. Unmanned Dynamics, LLC, No.8 Fourth St., Hood River, OR 97031 http://www.u-dynamics.com, 2013.

[76] G. Oriolo, A. De Luca, and M. Vendittelli. WMR control via dynamic feedback linearization: Design, implementation, and experimental validation. *IEEE Transactions on Control Systems Technology*, 10(6):835–852, 2002.

[77] *http://ctms.engin.umich.edu/CTMS/ index.php?example= MotorSpeed&section=SystemModeling*. Last time chechked: Feb. 1 2014.

[78] R.S. Barbosa and J.A. Tenreiro Machado. Implementation of discrete-time fractional-order controllers based on LS approximations. *Acta Polytechnica Hungarica*, 3(4):5–22, 2006.

[79] *http://www.scilab.org*. Last time chechked: Feb. 1 2014.

[80] *http://www.scilab.org/education/higher_education*.

[81] M. Baudin[1], V. Couvert[1], and S. Steer[2]. *Optimization in SCILAB*. [1]Scilab Consortium, [2]INRIA Paris - Rocquencourt, 2010.

[82] J.K. Tar. Application of local deformations in adaptive control; a comparative survey. *Computational Cybernetics, 2009. ICCC 2009. IEEE International Conference on*, pages 25–38, Jan 2009.

[83] S. LeBel and L. Rodrigues. Piecewise-affine parameter-varying control of wheeled mobile robots. *In Proc. of the American Control Conference, 2008, Seattle, WA, USA*, [WeA05.3]:195–200, 2008.

[84] V.M. Ojleska. *Control and Computational Synergy of Switched-Fuzzy and Fuzzy-Neural Nonlinear Systems*. Ph.D. Thesis, Ss. Cyril and Methodius University in Skopje, Faculty of Electrical Engineering and Information Technologies, Republic of Macedonia, 2013.

[85] I. D. Landau and R. Horowitz. Applications of the passive systems approach to the stability analysis of adaptive controllers for robot manipulators. *Int. J. Adaptive Control and Signal Processing*, 3:22–38, 1989.

[86] Jee-Wan Ryu, B. Hannaford, C. Preusche, and G. Hirzinger. Time domain passivity control with reference energy behavior. *In: Proc. of the 2003 IEEE/RSJ Intl. Conference on Intelligent Robots and Sytems, October 2003, Las Vegas, Nevada, USA*, pages 2932–2937, 2003.

[87] P. Baranyi. Tensor product model-based control of two-dimensional aeroelastic system. *Journal of Guidance, Control, and Dynamics*, 29:391–400, 2006.

[88] Z. Prime, B. Cazzolato, C. Doolan, and T. Strganac. Linear-Parameter-Varying control of an improved Three-Degree-of-Freedom aeroelastic model. *Journal of Guidance, Control, and Dynamics*, 33:615–619, 2010.